

Modelling single cell dynamics with trajectories and gene regulatory networks

Robrecht Cannoodt

Thesis submitted in fulfilment of the requirements for the degree of
Doctor in Computer Science, 2019

Supervisors:

Prof. Dr. Yvan Saeys
Prof. Dr. Kathleen De Preter



Vakgroep Toegepaste Wiskunde, Informatica, en Statistiek
Faculteit Wetenschappen, Universiteit Gent
Krijgslaan 281 - S2, 9000 Gent

Contents

1 Introduction	1
1.1 The cell	2
1.1.1 The origin of life and the RNA world	2
1.1.2 Central dogma	3
1.1.3 Cell types	4
1.1.4 Cell dynamics and gene regulation	4
1.1.5 Profiling single cells	5
1.2 Computational tools	7
1.2.1 Dimensionality reduction	8
1.2.2 Clustering	10
1.2.3 Trajectory inference	10
1.2.4 Differential expression	11
1.2.5 Network inference	12
1.3 Research context and objectives	13
2 Paper 1: Benchmarking with <i>in silico</i> single cells	15
2.1 Introduction	16
2.2 Results	16
2.3 Discussion	17
2.4 Methods	19
2.4.1 Defining the backbone: modules and states	19
2.4.2 Generating the gene regulatory network	23
2.4.3 Convert gene regulatory network to a set of reactions	24
2.4.4 Compute average expression along backbone transitions	25
2.4.5 Simulate single cells	25
2.4.6 Simulate experiment	25
2.5 References	27
3 Paper 2: A comparison of single-cell trajectory inference methods	29
3.1 Introduction	30
3.2 Results	31

3.2.1	Trajectory inference methods	31
3.2.2	Accuracy	33
3.2.3	Scalability	36
3.2.4	Stability	36
3.2.5	Usability	38
3.3	Discussion	40
3.4	Methods	44
3.4.1	Trajectory inference methods	44
3.4.2	Method wrappers	45
3.4.3	Trajectory types	48
3.4.4	Real datasets	48
3.4.5	Synthetic datasets	49
3.4.6	Dataset filtering and normalization	54
3.4.7	Benchmark metrics	55
3.4.8	Method execution	56
3.4.9	Complementarity	57
3.4.10	Scalability	57
3.4.11	Stability	58
3.4.12	Usability	58
3.4.13	Guidelines	59
3.4.14	Reporting Summary	59
3.5	Supplementary Note 1: Metrics to compare two trajectories	59
3.5.1	Metric characterisation and testing	60
3.5.2	Metric conformity	68
3.5.3	Score aggregation	69
3.6	References	75
4	Paper 3: A toolkit for inferring and interpreting trajectories	81
4.1	Introduction	82
4.2	Results	82
4.2.1	Preparing the dataset	82
4.2.2	Selecting the best methods for a dataset	83
4.2.3	Inferring trajectories	83
4.2.4	Execution details	84
4.2.5	Visualising trajectories	85
4.2.6	Manipulating the trajectory	87
4.2.7	Differentially expressed genes along the trajectory	87
4.3	Discussion	89
4.4	References	91
5	Paper 4: Fast, accurate, and robust single-cell pseudotime	93
5.1	Introduction	94
5.2	Results	94
5.2.1	SCORPIUS outperforms existing TI tools in inferring linear trajectories	94
5.2.2	Functional modules in dendritic cell development	95
5.3	Discussion	97
5.4	Methods	98

5.4.1	Sparse Spearman Rank Correlation	99
5.4.2	Landmark Multi-Dimensional Scaling	99
5.4.3	Approximated Principal Curves	99
5.4.4	Gene Importances	100
5.4.5	Datasets and benchmark results	100
5.4.6	Measurement of protein synthesis	100
5.4.7	Code availability	101
5.5	References	102
6	Paper 5: Inferring single cell regulatory networks	103
6.1	Introduction	104
6.2	Results	105
6.2.1	Hematopoietic cells from Tabula Muris	105
6.2.2	The Cancer Genome Atlas	105
6.3	Discussion	105
6.4	Methods	108
6.4.1	Inferring case-wise GRNs	108
6.4.2	Predicting the effect of an interaction	109
6.4.3	Clustering of case-wise GRNs	110
6.4.4	Visualising clustered GRNs	110
6.5	References	111
7	Paper 6: Optimising regulatory networks	113
7.1	Introduction	114
7.2	Materials and methods	115
7.2.1	Incremental graphlet counting	115
7.2.2	Timing experiments	116
7.2.3	Gene regulatory network optimisation experiments	117
7.3	Results and discussion	118
7.3.1	Execution time is reduced by orders of magnitude	119
7.3.2	IncGraph allows for better regulatory network optimisation	119
7.4	Conclusion	120
7.5	Supporting information	121
7.6	References	125
8	Paper 7: Self-assessment in trajectory inference	129
8.1	Introduction	130
8.2	Problem definition	130
8.3	Benchmarking datasets	131
8.4	Metrics	133
8.5	Guidelines for performing self-assessments	134
8.6	References	137
9	Paper 8: Essential guidelines for computational method benchmarking	143
9.1	Introduction	144
9.2	Ten essential guidelines	144
9.2.1	Defining the purpose and scope	144
9.2.2	Selection of methods	146

9.2.3	Selection (or design) of datasets	146
9.2.4	Parameters and software versions	147
9.2.5	Evaluation criteria: key quantitative performance metrics	148
9.2.6	Evaluation criteria: secondary measures	150
9.2.7	Interpretation, guidelines, and recommendations	151
9.2.8	Publication and reporting of results	151
9.2.9	Enabling future extensions	152
9.2.10	Reproducible research best practices	152
9.3	Discussion	153
9.4	References	156
10	Discussion	165
10.1	Benchmarking with <i>in silico</i> single cells	166
10.2	Comparing 45 trajectory inference methods	166
10.3	A toolkit to infer, visualise and interpret single-cell trajectories	166
10.4	Fast, accurate, and robust single-cell pseudotime	167
10.5	Inferring single cell regulatory networks	167
10.6	Optimising regulatory networks	167
10.7	A life without Git, Travis CI, or tidyverse	168
10.8	References	170
A	Curriculum Vitae	173
A.1	Personalia	173
A.2	Professional Experience	173
A.3	Education	173
A.4	First-author publications	174
A.5	Co-author publications	174
A.6	Open-source software	175
A.7	Sources of funding	175

Nomenclature

<i>k</i> NN	<i>k</i> -nearest-neighbour
CART	Classification And Regression Trees
DE	Differential Expression
DNA	Deoxyribonucleic Acid
DR	Dimensionality Reduction
GRN	Gene Regulatory Network
HCA	Human Cell Atlas
LDMS	Landmark Multi-Dimensional Scaling
MDS	Multi-Dimensional Scaling
mRNA	Messenger RNA
NI	Network Inference
PCA	Principal Component Analysis
RF	Random Forests
RNA	Ribonucleic Acid
t-SNE	t-distributed Stochastic Neighbor Embedding
TCGA	The Cancer Genome Atlas
TDE	Trajectory Differential Expression
TF	Transcription Factor
TI	Trajectory Inference
UMAP	Uniform Manifold Approximation and Projection

Summary

Recent technological developments triggered a major milestone in cellular biology by being able to profile and monitor biomolecular contents of single cells at a genome-wide level. The rapid advancements in single-cell omics allow for new types of analyses that fundamentally redefine our understanding of cellular heterogeneity and dynamic processes. Even now, there are even more exciting advancements on the horizon, with the Human Cell Atlas aiming to create a biomolecular and spatial map of all the different cell types in the body.

Throughout this doctoral project, I did not only get to follow these inspiring advancements first hand, but was able to make scientific contributions to the field by extensively reviewing novel computational tools, and developing several tools and algorithms of my own. More specifically, my efforts have resulted in the following contributions.

A common problem of pioneering computational tools is that during their development, there are rarely sufficient datasets available for adequately quantitatively assessing its performance. We developed a simulator of *in silico* single cells aimed at being flexible and extendible enough to be used to help kick-start emerging computational sub-domains (Chapter 2).

We performed a comprehensive comparison of 45 trajectory inference methods (Chapter 3). Trajectory inference is a new type of computational analysis whose aim is to identify and study transitions between main cellular states. While trajectory inference is one of the most rapidly growing new fields in single-cell omics tools, a quantitative study of the advantages and disadvantages was hitherto lacking.

We developed four new software tools ourselves. These methods include an extensive toolkit for inferring, visualising and interpreting trajectories (Chapter 4), a robust tool for inferring linear trajectories (Chapter 5), a novel way for studying gene regulation at a single-cell or single-sample level (Chapter 6), and tool for quantifying the topological changes resulting from minor perturbations in a network (Chapter 7).

We reflect on current challenges within the field, by providing guidelines for how to self-assess trajectory inference methods (Chapter 8) and, more generally, how to perform large-scale benchmarking experiments of computational methods (Chapter 9).

Throughout this project I particularly enjoyed working in an open-source ecosystem, collaborating with scientists around the world to tackle unsolved problems, whilst learning best practices by inspecting the source code of exemplary software projects.

Samenvatting

Recente technologische ontwikkelingen hebben geleid tot significante ontwikkelingen in celbiologie die ons toelieten om de biomoleculaire inhoud van individuele cellen op een genoomwijde manier te observeren. Dankzij snelle ontwikkelingen in *single-cell omics* technologieën wordt ons verstaan van cellulaire heterogeniteit en dynamische processen voortdurend gewijzigd. Inmiddels zijn er nieuwe spannende ontwikkelingen onderweg, zoals het *Human Cell Atlas* project, die mikt om alle celtypen in het menselijke lichaam op biomoleculaire en spatiële wijze in kaart te brengen.

Gedurende dit doctoraatsproject heb ik deze inspirerende ontwikkelingen niet alleen van heel dichtbij kunnen volgen, maar ik heb ook wetenschappelijke bijdragen aan het veld kunnen leveren door nieuwe analytische programma's extensief te onderzoeken, en door zelf verscheidene algoritmes te ontwikkelen. Meer specifiek heeft mijn onderzoek geleid tot de volgende bijdragen.

Een recurrent probleem van baanbrekende computationele algoritmes is dat gedurende hun ontwikkeling er helaas vaak onvoldoende datasets beschikbaar zijn om de performantie op een kwantitatieve wijze te kunnen beoordelen. We ontwikkelden een programma om individuele cellen te simuleren, dat flexibel en uitbreidbaar genoeg is om toekomstige computationele onderzoeksvalden te ondersteunen (Hoofdstuk 2).

We voerden een comprehensieve studie van 45 trajectvoorspellende methoden uit (Hoofdstuk 3). Trajectvoorspellende methoden is een nieuwe soort van computationele analyse waarbij het doel is om transities tussen verscheidene celtypen te identificeren en bestuderen. Terwijl deze klasse van methoden een van de snelst groeiende subdomeinen binnen *single-cell omics* was, was er tot op dat moment nog geen kwantitatieve studie van de voor- en nadelen van dergelijke methoden uitgevoerd.

We ontwikkeld ook zelf vier nieuwe computer programma's, waaronder een uitgebreide toolkit om trajecten te voorspellen, visualiseren en interpreteren (Hoofdstuk 4), een robuust programma om lineaire trajecten te voorspellen (Hoofdstuk 5), een nieuwe manier om gen regulatie op het niveau van een individuele cel of staal te bestuderen (Hoofdstuk 6), en een programma om topologische veranderingen te kwantificeren ten gevolge van kleine veranderingen in een netwerk (Hoofdstuk 7).

We reflecteren op huidige uitdagingen binnen het veld, door richtlijnen aan te bieden over hoe je je eigen trajectvoorspellende methode kan evalueren (Hoofdstuk 8) en, in het algemeen, hoe je grootschalige beoordelingen van computationele methoden kan uitvoeren (Hoofdstuk 9).

Tijdens het verloop van dit project heb ik bijzonder genoten van te werken in een *open-source* omgeving, waarbij ik wereldwijd collaboraties kon aangaan met onderzoekers. Hierbij heb ik bijgeleerd door naar de broncode van voorbeeldige softwareprojecten te kunnen kijken.

CHAPTER 1

Introduction

1.1 The cell

1

The cell is the smallest unit of life, of which all known living organisms are composed. Every cell houses a plethora of biomolecular processes that allows it to continuously adapt to changes in its environment. Due to the dynamic nature of these processes, it can be very challenging to comprehend the cellular response to a signal. A reductionist approach to understanding a complex biological system is to study the biochemical components of which it is comprised [1].

Recent advances in experimental technologies are playing a crucial role in reductionist biology, allowing to measure the abundance of thousands of different biochemical molecules in tens of thousands of individual cells. With it comes the challenge of analysing large amounts of data that are not easily interpretable by hand. The sheer volume of the data generated from such highly-integrative and high-throughput experiments are not the only reason why they are so challenging to interpret. For instance, the generated data contains high levels of noise arising from inherent biomolecular stochasticity in the cells and from the experimental profiling techniques used, as well as batch effects arising from differences between donors and labs [2]. Biologists thus turn to computer scientists to develop new tools to tackle these problems and help them to extract meaningful biological insights from the data. In this work, incremental contributions were made to the field in order to be able to address the aforementioned problems in a more comprehensive context.

Observing the biomolecular insides of cells can ultimately provide fundamental understanding into the processes that govern these cells and help uncover novel approaches for disease diagnosis, prognosis, and treatment. For example, the Human Cell Atlas (HCA) consortium [3] has set out to develop a comprehensive reference map of all the different types of cells in the human body. Experts in the field often metaphorically describe the HCA initiative as aiming to develop a 'Google Maps' of the human body. Even in its infancy, the HCA has profiled 3.8 million cells from 248 donors across 42 labs [4], and this number is likely to increase well above one hundred million.

The next part of the chapter highlights several key concepts in both cell biology and computer science, upon which the remainder of this work relies.

1.1.1 The origin of life and the RNA world

The discovery of the double helix shape of deoxyribonucleic acid (DNA) [5] is often considered the pivot point in our understanding of the origin of life and evolution. By now, it is well known that DNA serves as a medium for storing the genetic information required to reproduce a whole organism. With other words, the DNA of an organism contains the complete set of instructions required to build all of the biomolecular machinery present in its body.

Life (or cells) did not originate from DNA, however. A widely-accepted hypothesis states that life originates from its lesser-known cousin, ribonucleic acid (RNA). According to the RNA world hypothesis [6], the very first primitive cells used RNA both to store genetic information and to perform the chemical reactions required to sustain themselves (Figure 1.1). Only later did cells develop the ability to use the more chemically stable DNA molecules to self-sustain in a process commonly referred to as the central dogma.

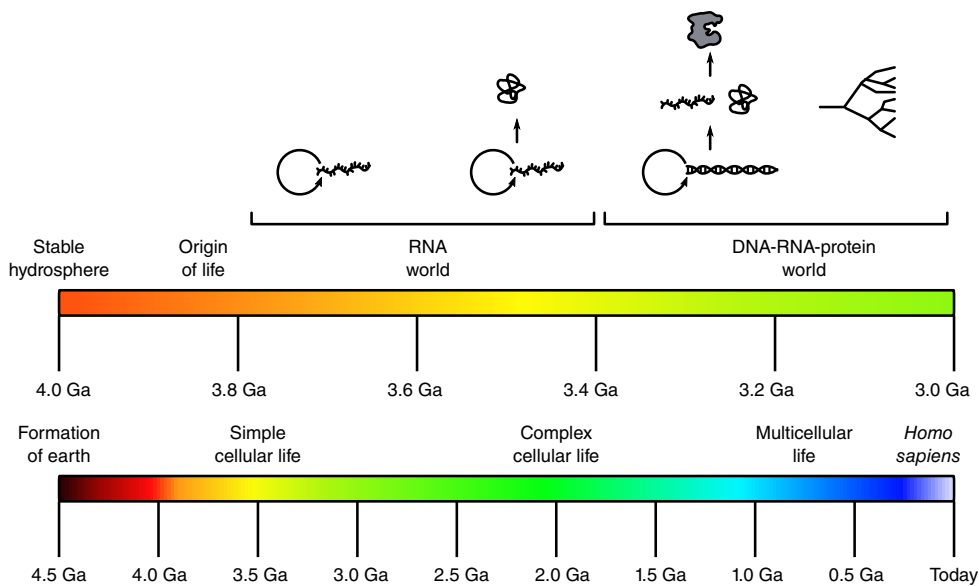


Figure 1.1: RNA world. The postulated rise and fall of the RNA world during the evolution of life, from early self-replicating RNA to complex, RNA-controlled metabolism, to the invention of translation, followed by diversification of all modern branches of life. Adapted from Horning (2011) [7].

1.1.2 Central dogma

The central dogma describes the general flow of genetic information in almost all existing living cells: DNA is decoded to RNA, which in turn encodes proteins [8]. Main processes involved in the central dogma are **transcription**, **splicing**, and **translation** (Figure 1.2).

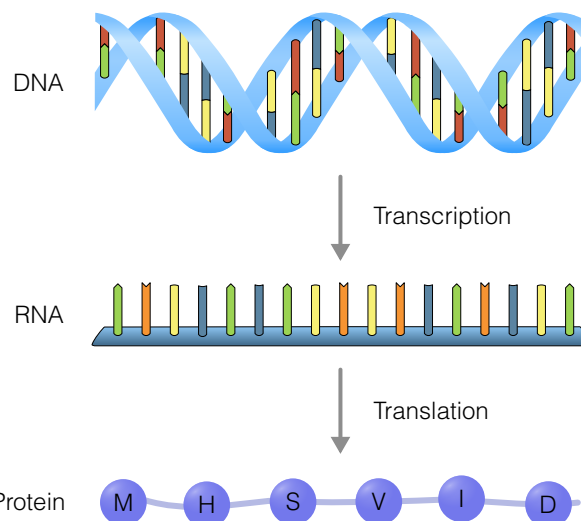


Figure 1.2: The central dogma of molecular biology explains the flow of genetic information, from DNA to RNA, to protein.

During the process of **transcription** that takes place in the cell nucleus, a complementary RNA copy is transcribed from the template DNA. The initial RNA transcript is a precursor messenger RNA (pre-mRNA) that needs to undergo series of maturation steps to ultimately form the mature messenger RNA (mRNA). This maturation includes pre-mRNA **splicing** to remove non-protein coding intervening sequences (the introns) and to join the neighbouring protein-coding sequences (the exons). A single pre-mRNA can be alternatively spliced to generate multiple forms of mRNAs that will result in the production of multiple protein isoforms. This process of alternative splicing is essential to generate

more than 100'000 different proteins starting from just 20'000 genes [9].

The mature mRNA is then transported to the cytoplasm, where it engages with ribosomes to initiate **translation**. During this highly evolutionary conserved process, a chain of amino acids, known as the protein building blocks, is being synthesised. Each amino acid is specified by three nucleotides (a codon) in the mRNA, according to a nearly universal genetic code. After being released by the ribosomes, the translation product undergoes a variety of chemical modifications to form the final folded protein, the structure of which is determined by the sequence of different amino acids in the chain. In addition, polypeptides may be cleaved to yield more than one active polypeptide product. The structure of a protein determines its functionality, which includes catalysing biochemical reactions, providing structure, and transportation of molecules.

1.1.3 Cell types

Ever since Robert Hook first described the different structures of cells in 1665, biologists have been classifying cells by form and function. The human body is said to contain more than 210 different cell types that are classified into four groups: epithelial, connective, muscle, and nervous. This however, is a major underestimation of the real number of cell types. Neurons, for instance, that are known to be extremely diverse, are estimated to reach numbers above 10,000 different types [8].

The concept of cell types eases reasoning and our understanding about many aspects of biology (e.g. the process of cell differentiation, cell-cell communication, cellular response to certain stimuli). Some cells are known to be highly specialised toward performing a particular function (e.g. memory B cells accelerate immune response by remembering previously encountered pathogens), or they can maintain a strong ability to differentiate into other cell types.

One common approach for understanding the functionality of a particular cell is to observe which molecules are present in the cell and to associate those set of molecules with functionality. Taking a snap shot of the protein or RNA transcript content in a particular cell, might already provide us with major insights into its functionality. However, in order to fulfil a particular task, the biochemical machinery of the cell gradually changes over time. Therefore it is highly informative to also consider the transition states between cell types and the dynamic processes involved therein.

1.1.4 Cell dynamics and gene regulation

Cells are dynamic entities that can gradually produce the molecules needed to acquire new functionality. The naturally occurring cell-to-cell variability happens at the level of gene expression. Gene expression itself can be controlled at different levels (Figure 1.3), one of which is gene regulation by transcription.

According to the needs of a cell, different genes are being transcribed. Housekeeping genes are being expressed in essentially every cell, while other genes are cell type or tissue specific or may be expressed in response to developmental and environmental signals [8].

Transcription factors (TFs) modulate the rate of gene transcription by binding and recruiting the transcriptional machinery to *cis*-regulatory regions (enhancers, and silencers) that are typically located in the promotor region of target genes. These bindings may result in increased or decreased gene expression. There are several TF families of which members share structural characteristics (e.g. zinc finger, helix-loop-helix).

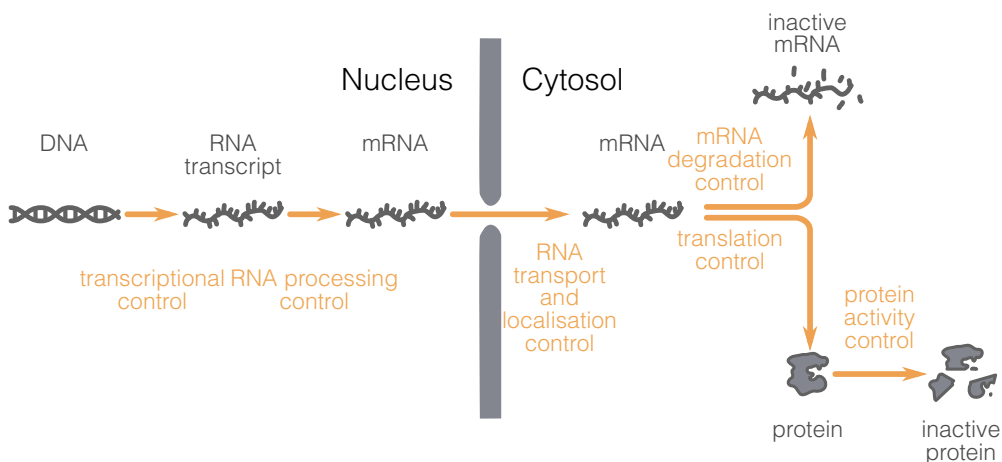


Figure 1.3: Levels of controlling gene expression can happen at the level of transcription, RNA processing (i.e. splicing), RNA transport and localization, mRNA translation, mRNA degradation and protein activity [10].

Many TFs are commonly present in virtually all cell types (e.g. NF- κ B), while others are specific for cells and developmental stages [11]. Typically, the same TF can regulate the rate of transcription of many target genes in different cell types, indicating that these gene regulatory networks (GRNs) are dynamic. Moreover, the production of a specific molecule might require several gene regulatory cascades. Studying the active parts of a cell's GRN can thus reveal which dynamic processes are taking place within a cell.

1.1.5 Profiling single cells

Several technologies are now available to profile (i.e. observe) biomolecular components, allowing us to gain better understanding in the biological processes that take place within a cell. The single-cell "omics" technologies originated from the convergence of two different fields, "*single-cell*" and "*omics*".

Single-cell

The earliest approach for measuring the abundance of a particular molecule in *single cells* is the microscope. Since its development by Coons et al. (1941), immunohistochemistry (IHC) has been instrumental in visualising proteins. [12]. A cell can present a particular type of protein, also called an antigen, on its cell surface. In many multicellular organisms, antigens can stimulate the immune system to produce antibodies. IHC realises the visualisation of proteins by exploiting the principle of antibodies binding to specific antigens.

IHC (and many other biotechnologies) visualises antigen-antibody reactions by attaching particular molecules to the antibody, such as an enzyme that catalyses a colour-producing reaction, or a fluorescent chemical compound that can re-emit light upon excitation. The use of several colours (wavelengths) allows measuring expression levels of different antibodies simultaneously. Characterising cells in a semi-quantifiable way is labour intensive, however; since it involves acquiring an image of many cells and drawing a contour around each cell (called cell segmentation). Modern implementations of IHC improve the throughput drastically by using robots and computer software to provide semi-automated image acquisition and cell segmentation [13].

Flow cytometry [14] circumvents imaging and segmentation issues by measuring fluorescently labelled proteins as cells pass through a fluidic system. Since cells need to be suspended in a buffer, flow cytometry is particularly useful for analysing non-adherent cells such as the many different immune cells in blood. However, many protocols already exist to extract viable single cells from tissues and tumours [15]. Conventional flow cytometry devices enable to measure protein expression levels of millions of cells using up to eight different antibody fluorochromes simultaneously, while state-of-the-art instrumentation allows detection of up to 27 biomarkers simultaneously [16].

Besides IHC and flow cytometry, many new technologies have been developed which allow quantifying expression levels of molecules in single cells (e.g. mass cytometry, single-cell quantitative polymerase chain reaction, fluorescence *in situ* hybridization). All of these single-cell (non-omics) technologies are limited by the number of different molecules they measure, however. Selecting molecules of interest prior to analysis, makes the experiment biased towards the preconceptions of the experimenter.

Omics

On the other side of the spectrum are the so-called "omics" technologies. "Omics"¹ is a collective term for profiling all molecules of a particular type in a high-throughput manner. There are at least ten types of "omics". In this work, we mostly consider genomics, transcriptomics, proteomics, and regulomics. Genomics studies the complete DNA sequence of an organism's genome, while transcriptomics and proteomics study the RNA transcripts and proteins, respectively. Regulomics studies the regulatory molecules (e.g. genes, RNAs, proteins) which play a role in determining gene regulation.

Specific examples of omics technologies are whole genome sequencing to determine the DNA sequence of an organism, and RNA sequencing to profiles the sequence of RNA transcripts, both using next-generation sequencing technologies. A gene expression profile can be obtained by mapping the sequences of RNA transcripts to the genome.

Several high-throughput technologies have been developed to investigate proteomes in depth. The most commonly applied are mass spectrometry-based and gel-based techniques (e.g. differential in-gel electrophoresis).

Typically for these methods, to capture enough material to generate a profile, numerous cells need to be pooled and lysed together, thereby granting the technology's name "bulk" omics. Bulk omics is a major workhorse in molecular genetics and has applications in cancer research and in diagnostic screening of inheritable disorders.

Increasing evidence shows that cells are biomolecularly heterogeneous, even in very similar cell types [18] (Figure 1.4A). Since a bulk profile is a population average (or rather, a summation), important cell-to-cell variability is not discernible (Figure 1.4B).

Single-cell omics

Comparing single-cell technologies with omics technologies shows that they have both clear advantages but also significant drawbacks (Figure 1.5A). Single-cell biology allows profiling thousands or even millions of cells, but only for a select number of genes. On the other hand, omics biology

¹The etymology of "omics" is quite interesting [17].

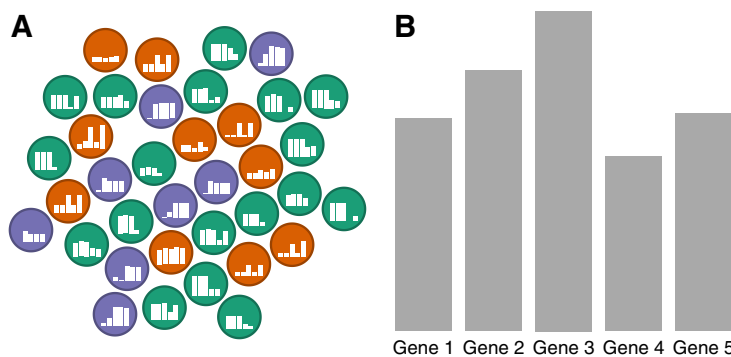


Figure 1.4: The 'masking' effect of bulk omics. **A:** Cells from several subpopulations are incorrectly assumed to be homogeneous and are profiled with a single bulk omics experiment. **B:** The signals from the different subpopulations are masked. The resulting profile is dissimilar from the majority of cells it is supposed to represent.

provides a broader view – since genes do not need to be selected beforehand – but is a profile of ensemble of cells and thus masks important cellular heterogeneity.

Advances in microvolume sequencing allowed profiling the transcriptome at single-cell resolution, thereby bringing single-cell biology and omics together to create single-cell omics. During the decade that followed, the number of single-cell omics technologies has sky-rocketed, allowing to profile >100'000 cells [19] and measuring other levels of information (e.g. protein abundance and spatial location) [20].

In this work, unless noted otherwise, we will be working with transcriptomics data resulting from a single-cell RNA-sequencing experiment (scRNA-seq). The workflow of generating scRNA-seq profiles is as follows. Same as other single-cell (non-omics) profiling methods, cells first need to be isolated (Figure 1.5B). Different sampling techniques yield different levels of information about cellular state. By now, many protocols for extracting and tagging RNA from single cells have been developed [19], the most popular of which are based on microfluidics or droplets (Figure 1.5C). By sequencing the transcripts and the attached unique cell identifier tags, each read can be mapped and tallied up. scRNA-seq data can thus be summarised in a matrix, where each column represent a single cell, each row a gene, and each value represents the number of transcripts that were sequenced for that gene and cell.

The rapidly advancing field of single-cell omics harbours exceptional opportunities to discover new aspects of biology and redefine existing knowledge. Some of these opportunities lie in efforts like the HCA consortium [3]. They have set out to redefine all human cell types in both terms of their gene expression and location, and as well as the developmental trajectories connecting the different cell types. As part of this endeavour, the consortium will likely profile the whole transcriptomes of tens or even hundreds of millions of cells [4].

1.2 Computational tools

Whole-genome profiling at single-cell level allows new types of analyses with which to study cellular heterogeneity at a hitherto unseen throughput. The new types of analyses permitted by single-cell omics present several computational challenges [21, 22, 23]. This necessitates the development of novel computational tools, either because the problem statement of the performed analysis is completely novel, or to adapt existing methodology to new data characteristics – dimensionality and noise.

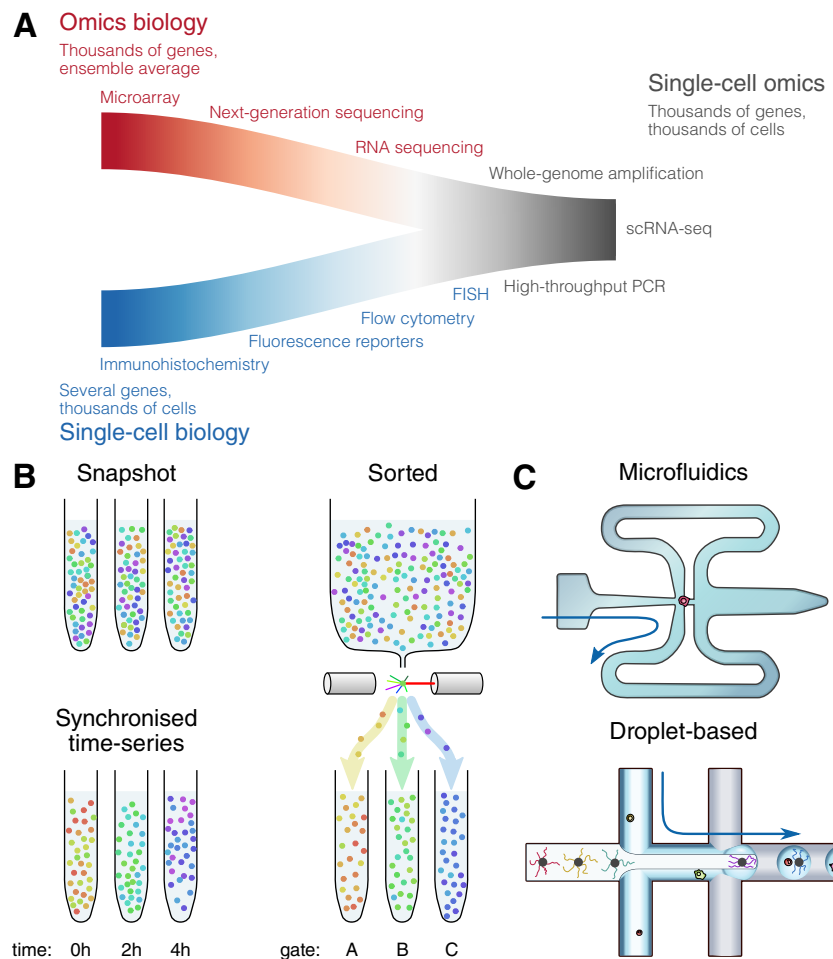


Figure 1.5: **A:** Convergence of single-cell and omics biology. **B:** Different approaches for sampling cells with decreasing levels of cellular heterogeneity within the different sub-populations: snapshot, time-series, sorted. **C:** Two common single-cell RNA sequencing technologies. Microfluidics systems let cells travel through nanometer scale tubing, capturing individual cells at intersections. Droplet-based systems encapsulate individual cells in droplets.

scRNA-seq data is typically very sparse – while the human genome has more than 20'000 genes, they only contain non-zero values of a few thousand genes (typically <4'000). This is partially due to cells being specialised in particular functions and thus they do not need proteins of every time, but also due to RNA transcription occurring in bursts rather than continuously [24]. This contributes to the high levels of noise seen in scRNA-seq data: no two cells have the same set of non-zero genes.

Over the past five years, already 450 new tools have been developed to perform various analyses of single-cell omics data [25], taking into account the specific noise characteristics. The most frequent types of analyses are detailed in the following subsections.

1.2.1 Dimensionality reduction

Single-cell omics datasets are usually one or more high-dimensional matrices, containing between $M = 10^3$ to 10^5 cells and typically about $N = 10^3$ to 10^4 genes (Figure 1.6A). The dimensionality of such datasets is typically too high for humans to interpret manually and for most modelling algorithms to tackle directly. Moreover, in reality, the intrinsic dimensionality of biological systems is probably much lower. For example, a differentiating hematopoietic cell could be described by just three dimensions: the first two dimensions lay out the hematopoietic lineage tree, and a third dimension allows for

reprogramming between branches to occur.

Dimensionality reduction (DR) methods transform high-dimensional data into a meaningful low-dimensional representation. DR methods have two main target audiences; computers – to construct a K-dimensional (with $K \ll M$) representation of the data such that pairwise distances between different samples are retained as well as possible (Figure 1.6B); and humans – to obtain a visual overview of the data (Figure 1.6C).

Each dimension frequently corresponds to one or more modules of co-expressed genes. The reduced space can be interpreted in way analogous to Waddington’s epigenetic landscapes [26, 27, 28], where the landscape dictates the possible states a cell can reside in, and transitions between states correspond to dynamic cellular processes, such as cell differentiation.

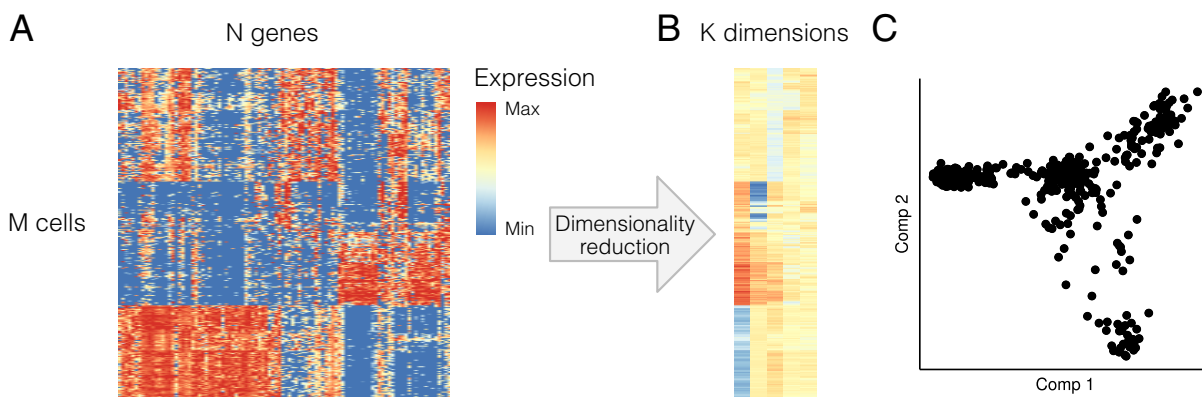


Figure 1.6: Dimensionality reduction for single-cell omics data. **A:** A heatmap visualisation of an scRNA-seq expression dataset of fibroblasts being reprogrammed to neuron cells [29]. Only the most variable **B:** The reduced space is a $M \times K$ -dimensional matrix which attempts to conserve the cellular heterogeneity of the original space as well as possible. **C:** A dot plot of the first two components of the reduced space provides a global overview of the cells in the dataset. Colouring the dots according to prior information (e.g. cell type) or gene expression provides insight into the cellular heterogeneity within the dataset.

DR methods can be classified into two main categories, feature projection-based and manifold learning [30].

Projection-based DR methods aim to perform a transformation of the data while preserving the pairwise distances between samples as much as possible. Examples of commonly used projection-based DR methods in single-cell omics are Principal Component Analysis [31] (PCA) and Multi-Dimensional Scaling [32] (MDS).

Manifold learning DR methods reconstruct a higher-order structure in the original space (e.g. a graph or a grid), visualising the structure in a lower-dimensional space, and mapping the original samples to the lower-dimensional space. Manifold learning can be an iterative optimisation process using a predefined criterion. Examples of manifold learning techniques are t-distributed Stochastic Neighbor Embedding [33] (t-SNE), Diffusion Maps [34, 35] and Uniform Manifold Approximation and Projection [36] (UMAP).

For scalability reasons, this work mostly makes use of Landmark MDS [37, 38] (LMDS) with a Spearman rank correlation distance metric. LMDS is an extension of classical MDS, but rather than calculating a complete distance matrix between all pairs of cells, a set of landmark cells is sampled, only the distances between a set of landmarks and the samples are calculated.

1.2.2 Clustering

To learn about the different cellular states within a population of cells, clustering methods divide up the cells into separate groups of highly similar cells (Figure 1.7A). By visualising gene expression of known genes involved in the cell types of interest, the clusters can be annotated (Figure 1.7B).

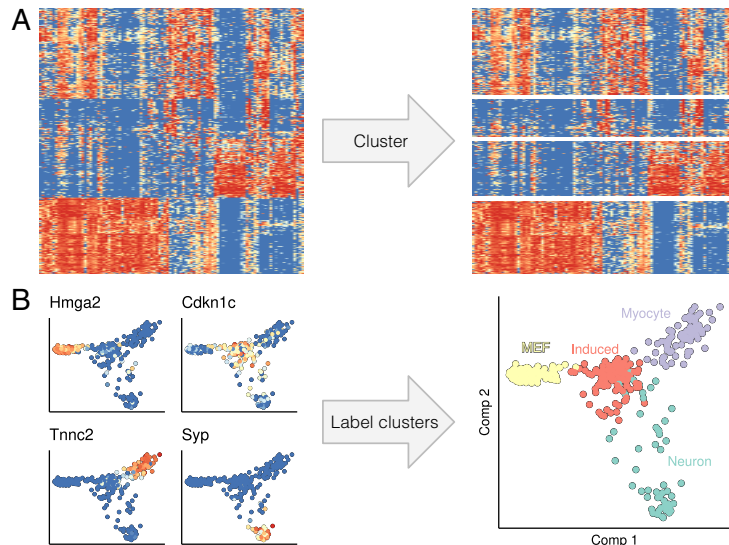


Figure 1.7: Clustering for single-cell omics data. **A:** Clustering methods group cells with similar omics profiles together. **B:** By overlaying gene expression levels on a dimensionality reduction, the clusters can be annotated to allow better interpretation of the cellular heterogeneity.

Usually, the number of clusters is determined by the user, either as a direct parameter (e.g. k -means [39]) or an indirect parameter (e.g. a height cutoff in hierarchical clustering). In some exceptional cases, the number of clusters is strictly determined by the data itself and cannot be altered with a parameter (e.g. Louvain clustering [40]).

Clustering methods used in this work are mostly restricted to k -Means for clustering low-dimensional spaces and Louvain for clustering networks, since both are highly scalable with respect to the number of cells.

1.2.3 Trajectory inference

While clustering methods divide cells into distinct groups, trajectory inference (TI) methods acknowledge that cells are dynamic entities which transition from one cellular state to another via various dynamic processes. Rather than making distinct groups, TI methods allow studying dynamic processes by reconstructing the topology of a dynamic process as a trajectory, and map the cells onto that trajectory. A trajectory is a graph where the nodes represent noteworthy cellular states, and each cell is predicted to be progressing along transitions between the different states (Figure 1.8A).

A trajectory can be visualised as a graph to better highlight the topology of the trajectory (Figure 1.8A middle), as a heatmap to better depict the changes in gene expression along the different transitions (Figure 1.8A right), or may be embedded in a dimensionality reduction of the cells to better demonstrate cellular heterogeneity along the trajectory (Figure 1.8B right). Similar to clustering, by colouring the cells according to the expression of genes known to be involved in the dynamic process of interest, the milestones in the trajectory can be annotated (Figure 1.7B).

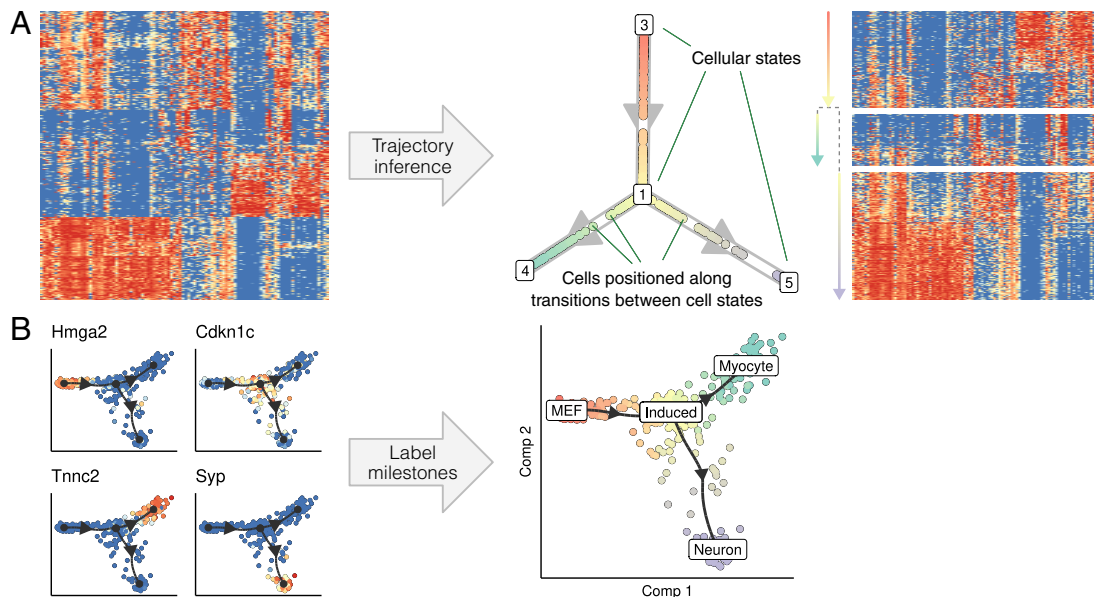


Figure 1.8: Trajectory inference for single-cell omics data. **A:** During a dynamic process cells pass through several transitional states, characterized by different waves of transcriptional, morphological, epigenomic and/or surface marker changes [41]. TI methods provide an unbiased approach to identifying and correctly ordering different transitional stages. **B:** By overlaying gene expression levels on a dimensionality reduction, the milestones can be annotated to allow better interpretation of the cellular heterogeneity.

A lot of TI methods use similar algorithms to be able to infer a trajectory. By breaking down each method into its set of core algorithms, we can create a map of TI methodology [42] (Figure 1.9A), which is divided into two major classes. In the first step, dimensionality reduction techniques such as manifold learning, clustering, or graph-based methods are used to convert the dataset to a more simplified representation. This representation of the data then allows the trajectory itself to be more easily modelled in a second step. In this second step, the trajectory is modelled within the data using graph-based or curve-based approaches, after which the cells themselves can be ordered using a variety of methods.

A common way to classify TI methods is by the types of trajectories they can infer [43] (Figure 1.9B). About half of TI methods specialise in inferring linear or cyclic trajectories (i.e. they order the cells). Others model the trajectory as a rooted tree, allowing for one or more bifurcations to occur. Only a few methods are able to infer more generalised trajectories containing disconnected subgraphs or cycles.

1.2.4 Differential expression

Given that cells are split up into groups differential expression (DE) methods ranks genes based on whether their expression is significantly higher or lower in one group in comparison to the others. This grouping can be based on prior information or an upstream clustering method. DE methods are useful for summarising the main differences between different groups of cells more compactly (Figure 1.10A) in comparison to when groups are compared without gene prioritisation (Figure 1.7A).

Trajectory differential expression (TDE) is an extension of DE where instead genes are prioritised according to whether their gene expression changes smoothly but significantly along a parts of a trajectory (Figure 1.10).

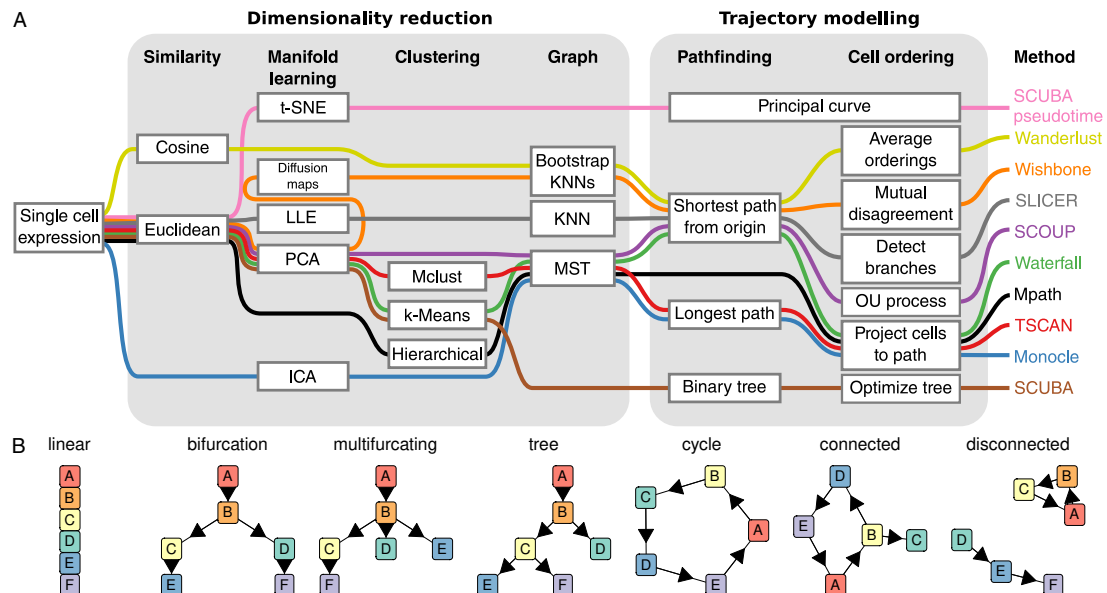


Figure 1.9: TI methods use several common building blocks and can be organized in a unifying modular framework. **A:** Most TI methods consist of two major steps, dimensionality reduction and trajectory modelling. TI methods require some form of dimensionality reduction in order to summarise cell heterogeneity in a lower dimensional space. Subsequently, a trajectory modelling step then operates in this reduced space, aiming to identify cell states, constructing a trajectory through the different states, and projecting the cells back on to the trajectory. **B:** TI methods can be classified according to the trajectory topologies they can infer.

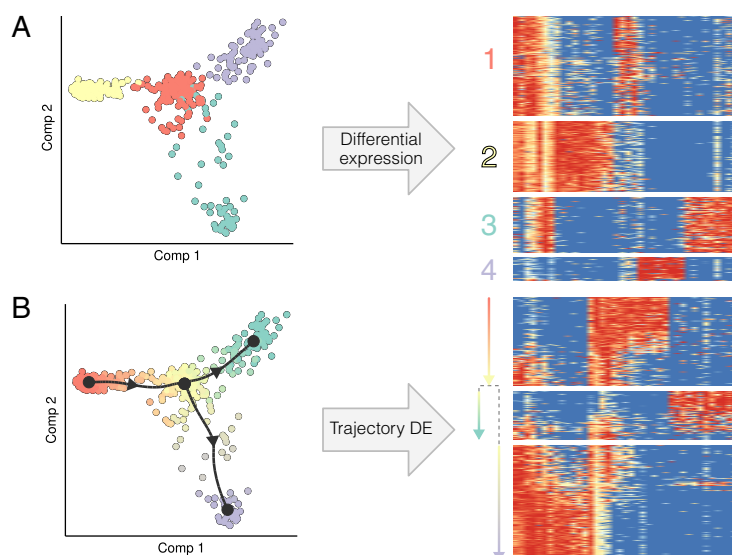


Figure 1.10: Differential expression for single-cell omics data. **A:** Differential expression methods prioritises genes that are expressed significantly higher or lower in particular given groups. **B:** Trajectory differential expression prioritises genes that change smoothly but significantly along particular transitions in a trajectory.

1.2.5 Network inference

One of the central cellular processes underlying development is transcriptional regulation. Modeling the dynamics of gene regulation is therefore essential to better understand why a cellular dynamic processes progresses through several steps, and what goes wrong in the case of disease.

Network inference (NI) methods predict which genes are regulated by which transcription factors (Figure 1.11). The output of a network inference is thus a graph, where nodes represent genes and edges denote a regulatory interaction between a regulator and a target gene. Interactions typically have

two properties: its regulatory strength (a positive real value) and its effect (promoting or repressing).

Before single-cell omics, these methods rely on multiple experiments, amongst which perturbation and time-series experiments, to predict the effect each transcription factor has on the up- or down-regulation of a gene. One of the main advantages of single-cell omics is the heterogeneity between cells caused by naturally occurring biological randomness [44] can be exploited to infer regulatory interactions between TFs and their target genes at much lower costs.

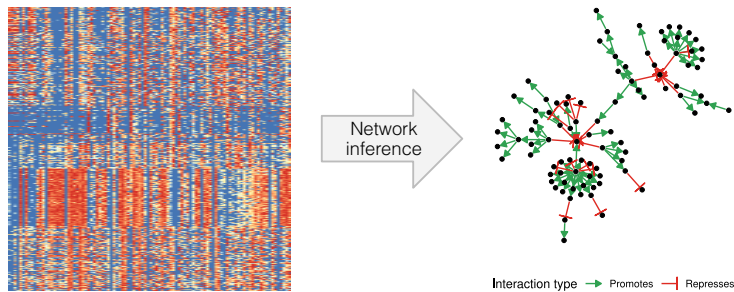


Figure 1.11: Network inference for single-cell omics data.

1.3 Research context and objectives

Recent technological advancements in profiling single cells are having significant repercussions in many fields of biology. Profiling thousands of individual cells in a genome-wide manner provides opportunities to study cell heterogeneity and dynamics, for example inferring mechanisms for cellular development or intercellular communication. Hundreds of new software tools were developed [25] to perform these new types of analyses, or to fit existing analytical tools to deal with new data characteristics (e.g. differential expression, dimensionality reduction, normalisation).

One major shortcoming during the advent of single-cell omics was that the majority of newly developed computational tools were not quantitatively and comparatively evaluated. Rather, they relied on anecdotal evidence to demonstrate its usefulness. This issue is not the result of the tool developer's malevolence, but instead of the lack of data required to perform such comprehensive benchmarks.

Uncontrolled development of software tools without comprehensive benchmarking poses serious problems. For one, it slows down scientific progress. Every end-user needs to make a large commitment researching the domain in order to make an informed decision of which tool to use, or risk a higher incidence of false positive discoveries (either way, valuable resources are being wasted). In addition, it also negatively impacts the credibility of the field, thus discouraging potential users or researchers from entering.

In this work, we aim to speed up scientific progress in single-cell omics by providing tools both for end-users and developers alike. For developers of computational approaches, we provide tools and guidelines for benchmarking their method on real and synthetic data. For end-users we develop new tools and guidelines for analysing dynamic processes by inferring trajectories and gene regulatory networks. Our specific scientific objectives are discussed in the following chapters.

- We **develop benchmarking strategies** for assessing the performance of computational tools constrained by low availability of novel types of real single-cell data (Chapter 2). *In silico* simulations of individual cells are used to help kick-start emerging domains much more safely and

allow anticipation of future technological developments by already developing computational tools.

- We apply this strategy to **perform a comparison of TI methods** (Chapter 3). Trajectory inference is one of the largest categories of all the novel single-cell omics tools, yet a comprehensive and quantitative study of the advantages and disadvantages of the numerous tools was hitherto lacking. We provide a set of guidelines for end-users wishing to infer trajectories. Our pipeline, datasets, metrics, and containerised wrappers of TI methods are made publicly available for developers to use.
- We develop **a toolkit to infer, visualise and interpret single-cell trajectories** using more than 50 different TI methods (Chapter 4). dyno provides downstream analysis such as: visualising a trajectory in a low-dimensional space or a heatmap, detecting genes differentially expressed at different stages of the trajectory, comparing multiple trajectories in a common dimensionality reduction, and manipulating the trajectory (e.g. adding directionality or adding annotation).
- We introduce a TI method specialised in **inferring linear trajectories** (Chapter 5). Despite linear TI being the most simple but commonly used form of trajectory inference, the benchmark demonstrated that most TI methods are not capable of producing accurate models of linear datasets.
- We explore a novel algorithm for **inferring gene regulatory interactions at a single-cell level** (Chapter 6). We demonstrate our NI methodology by inferring regulatory interactions for 22'122 hematopoietic cells, as well as for 14'963 bulk profiles of cancer tumours.
- We provide a tool for **analysing the topological properties of large, evolving networks** and use this to iteratively optimise GRN predictions (Chapter 7).
- We reflect on **challenges in performing self-assessments of TI methods** (Chapter 8). Reproducibility problems of TI methods are partially due to low rates of quantitative self-assessment. We look at 75 manuscripts of TI methods and identify key challenges the authors had in benchmarking their tool. For each of these challenges, we provide a summary of how we and others have successfully tackled these challenges, in order to spur developers to perform more self-assessments.
- Finally, we **summarise our experience in benchmarking computational methods** by providing a list of essential guidelines in benchmarking computational tools (Chapter 9).

CHAPTER 2

Paper 1: Benchmarking with *in silico* single cells

Abstract

Purpose: A common problem of pioneering computational tools is that during their development, there are rarely sufficient datasets available for adequately quantitatively assessing its performance.

Results: We developed `dyngen`, a multi-modality simulator of single cells. In `dyngen`, the biomolecular state of an *in silico* cell changes over time according to a set of reactions defined by the cell's gene regulatory network. By simulating single cells in terms of its biomolecular state and reactions, the simulator is easily extendible for adding new modalities or experimental procedures. We demonstrate `dyngen`'s flexibility by simulating snapshot, time-series and perturbation experiments.

Conclusion: `dyngen` lays the foundations for benchmarking a wide variety of computational single-cell tools, and can be used to help kick-start the development of future types of analyses.

Publication status

Manuscript in preparation.

Cannoodt R*, Saelens W*, and Saeys Y.

* Equal contribution

Author contributions

- R.C. and W.S. designed the study.
- R.C. and W.S. performed the experiments and analysed the data.
- R.C. and W.S. implemented software packages.
- R.C. wrote the original manuscript.
- R.C. and W.S. reviewed and edited the manuscript.
- Y.S. supervised the project.

2.1 Introduction

Continuous technological advancements to single-cells omics are having profound effects on how researchers can validate biological hypotheses. Early experimental technologies typically only allowed profiling a single modality (e.g. DNA sequence, RNA or protein expression). However, recent developments permit profiling multiple modalities simultaneously, and every modality added allows for new types of analyses that can be performed.

This presents method developers with a problem. The majority of the 250+ peer-reviewed computational tools for analysing single cell omics data were published without a quantitative assessment of the accuracy of the tool. This is partially due to low availability of suitable benchmarking datasets; even if there are sufficient suitable input datasets available, these are often not accompanied by the necessary metadata to serve as ground-truth for a benchmark.

Here, synthetic data plays a crucial role in asserting minimum performance requirements for novel tools in anticipation of adequate real data. Generators of scRNA-seq data (e.g. splatter [1], powsimR [2], PROSSTT [3] and SymSim [4]) have already been widely used to explore the strengths and weakness of computational tools, both by method developers [5, 6, 7, 8] and independent benchmarkers [9, 10, 11]. However, a limitation of scRNA-seq profiles generators is that they would require significant methodological alterations to add additional modalities.

An ideal experiment would be able to observe all aspects of a cell, including a full history of its molecular states, spatial positions and environmental interactions [12]. While this falls outside the reach of current experimental technologies, generating synthetic data in anticipation of new experimental technologies would allow already developing the next wave of computational tools.

We introduce `dyngen`, a multi-modality simulator of single cells and their dynamics (Figure 2.1A). A cell is simulated using Gillespie's Stochastic Simulation Algorithm (SSA) [13] where a cell consists of a set of molecules. Throughout a simulation, reactions (e.g. transcription, splicing) modify the abundance of these molecules, and the likelihood of a reaction occurring is again dependent on molecule abundance.

By simulating a cell over time in terms of its molecular state and the reactions that are allowed to occur, the simulator is more extendible to new modalities or experimental procedures (Figure 2.1B). We demonstrate `dyngen`'s flexibility by simulating snapshot, time-series and perturbation experiments, allowing to benchmark a wide variety of computational tools such as trajectory alignment and differential network inference methods.

2.2 Results

A cell consists of a set of molecules, the abundance of which are affected by a set of reactions: transcription, splicing, translation, and degradation (Figure 2.2A). A gene regulatory network (GRN) define the reactions that are allowed to occur (Figure 2.2B), and is constructed such that a cell will develop over time (Figure 2.2C–D). The likelihood of a reaction occurring is a function of the abundance of key molecules involved in each reaction (Figure 2.2E).

`dyngen` returns many modalities throughout the whole simulation: molecular abundance, cellular state, number of reaction firings, reaction likelihoods, and regulation activations (Figure 2.2C–F). These modalities can serve both as input data and ground truth for benchmarking many types of

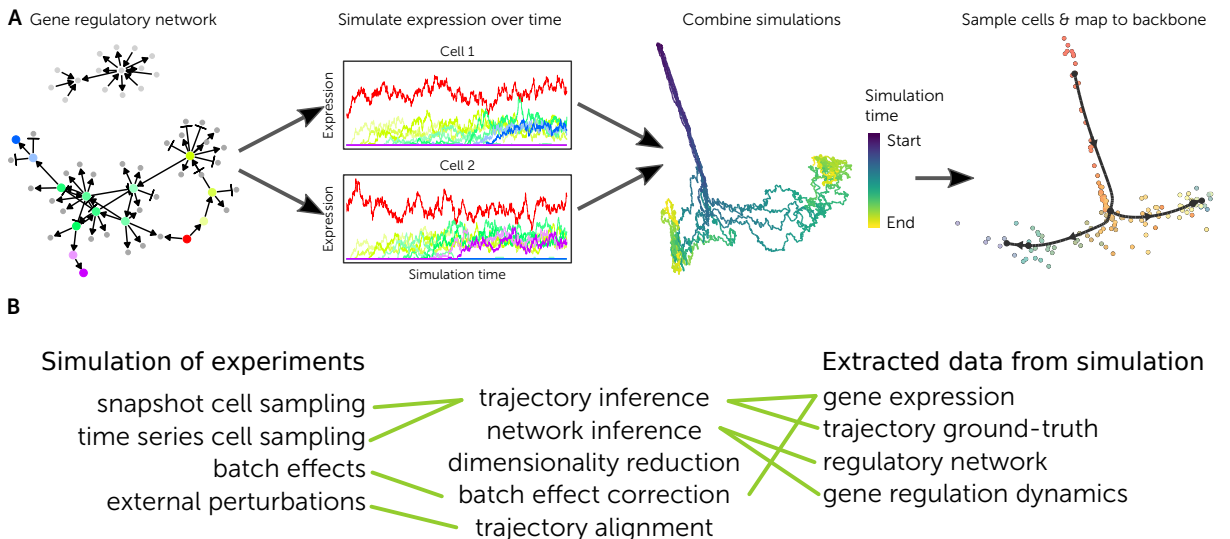


Figure 2.1: Showcase of dyngen functionality. **A:** Evaluating different types of computational tools requires simulating different types of experiments and extracting different layers of information from the simulation.

computational approaches. For example, a network inference method could use mRNA abundance and cellular states as inputs, and its output could be benchmarked against the gold standard GRN.

Depending on how the GRN is designed, different cellular developmental processes can be simulated. dyngen includes generators of GRNs which result in many different developmental topologies (Figure 2.3), including branching, converging, cyclic and even disconnected.

Custom-defined GRNs offer more fine-grained control over the simulation. Aside from simulating topologies currently not supported by dyngen, this has several other important use-cases. Simulations of the same GRN with small perturbations allow to emulate batch effects or perturbation experiments (Figure 2.4). Simulating perturbed GRNs allow evaluating trajectory alignment methods – which attempt to map two or more trajectories onto each other – or differential network inference methods – which infer differential regulatory interactions between two or more groups of profiles.

dyngen can be used to simulate different experimental conditions. By default, dyngen supports snapshot experiments (uniformly sampling from an asynchronous dynamic process) and time-series experiments (sampling cells from different intervals in the simulation). However, it is possible to imagine and implement other sampling strategies, such as sampling a cell at a certain time point and once more at a later time point. This would allow evaluating the performance of RNA velocity approaches – which predict the future state of a cell by looking at differences in pre-mRNA and mRNA abundance levels.

2.3 Discussion

As is, dyngen’s single cell simulations can be used to evaluate common single-cell omics computational methods such as clustering, batch correction, trajectory inference and network inference. However, the combined effect of these advantages results in a framework that is flexible enough to adapt to a broad range of applications. This may include methods that integrate clustering, network inference and trajectory inference. In this respect, dyngen may promote the development of new tools in the single-cell field similarly as other simulators have done in the past [14, 15].

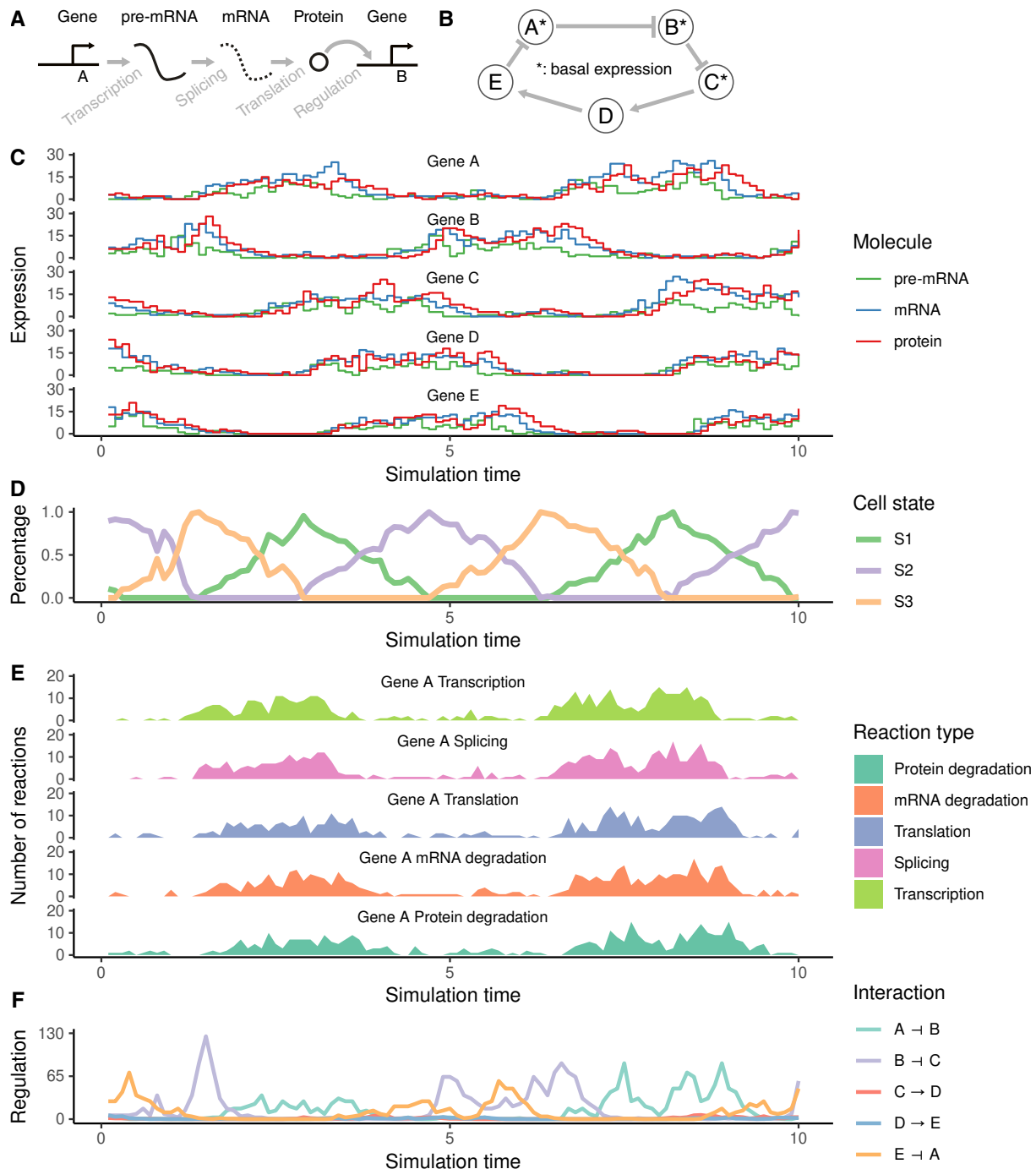


Figure 2.2: Key features of dyngen are illustrated using a cyclic toy example. While this example comprises only of a single cell and 5 genes, dyngen is able to simulate thousands of cells with GRNs containing thousands of genes.

dyngen ultimately allows anticipating technological developments in single-cell multi-omics. In this way, it is possible to design and evaluate the performance and robustness of new types of computational analyses before experimental data becomes available. In addition, it could also be used to compare which experimental protocol is the most cost-effective in producing the qualitative and robust results in downstream analysis.

Currently, dyngen focuses on simulating cells as standalone entities that are well mixed. Splitting up the simulation space into separate subvolumes could pave the way to better study key cellular processes such as cell division, intercellular communication and migration [16].

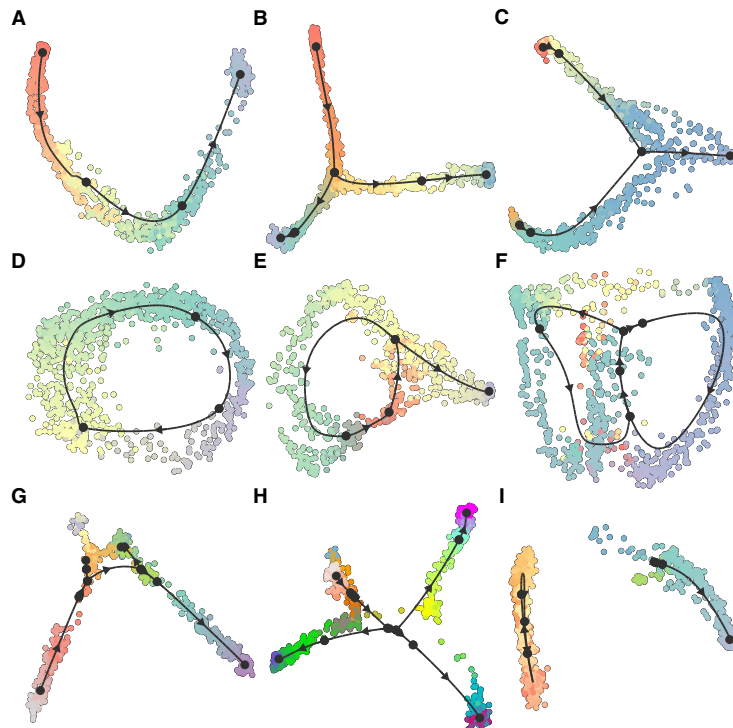


Figure 2.3: Multiple executions of dyngen with different predefined backbones. From each simulation of about 200 genes, 1000 cells were sampled. **A:** Linear. **B:** Bifurcating. **C:** Converging. **D:** Cyclic. **E:** Bifurcating loop. **F:** Bifurcating converging. **G:** Consecutive branching. **H:** Binary tree. **I:** Disconnected.

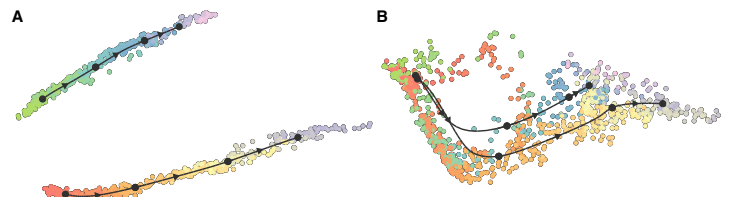


Figure 2.4: Examples of simulations with perturbed GRNs. **A:** The cells in the top half were simulated with the same GRN as the cells on the bottom half, except that all parameters (e.g. strength of the interaction) were randomised. **B:** Only 10 interactions in the GRN were randomised. In this example, the effect of the GRN perturbation is more subtle.

2.4 Methods

The workflow to generate *in silico* single cell data consists of six main steps (Figure 2.5).

2.4.1 Defining the backbone: modules and states

One of the main processes involved in cellular dynamic processes is gene regulation, where regulatory cascades and feedback loops lead to progressive changes in expression and decision making. The exact way a cell chooses a certain path during its differentiation is still an active research field, although certain models have already emerged and been tested *in vivo*. One driver of bifurcation seems to be mutual antagonism, where two genes strongly repress each other [17, 18], forcing one of the two to become inactive [19]. Such mutual antagonism can be modelled and simulated [20, 21]. Although the two-gene model is simple and elegant, the reality is frequently more complex, with multiple genes (grouped into modules) repressing each other [22].

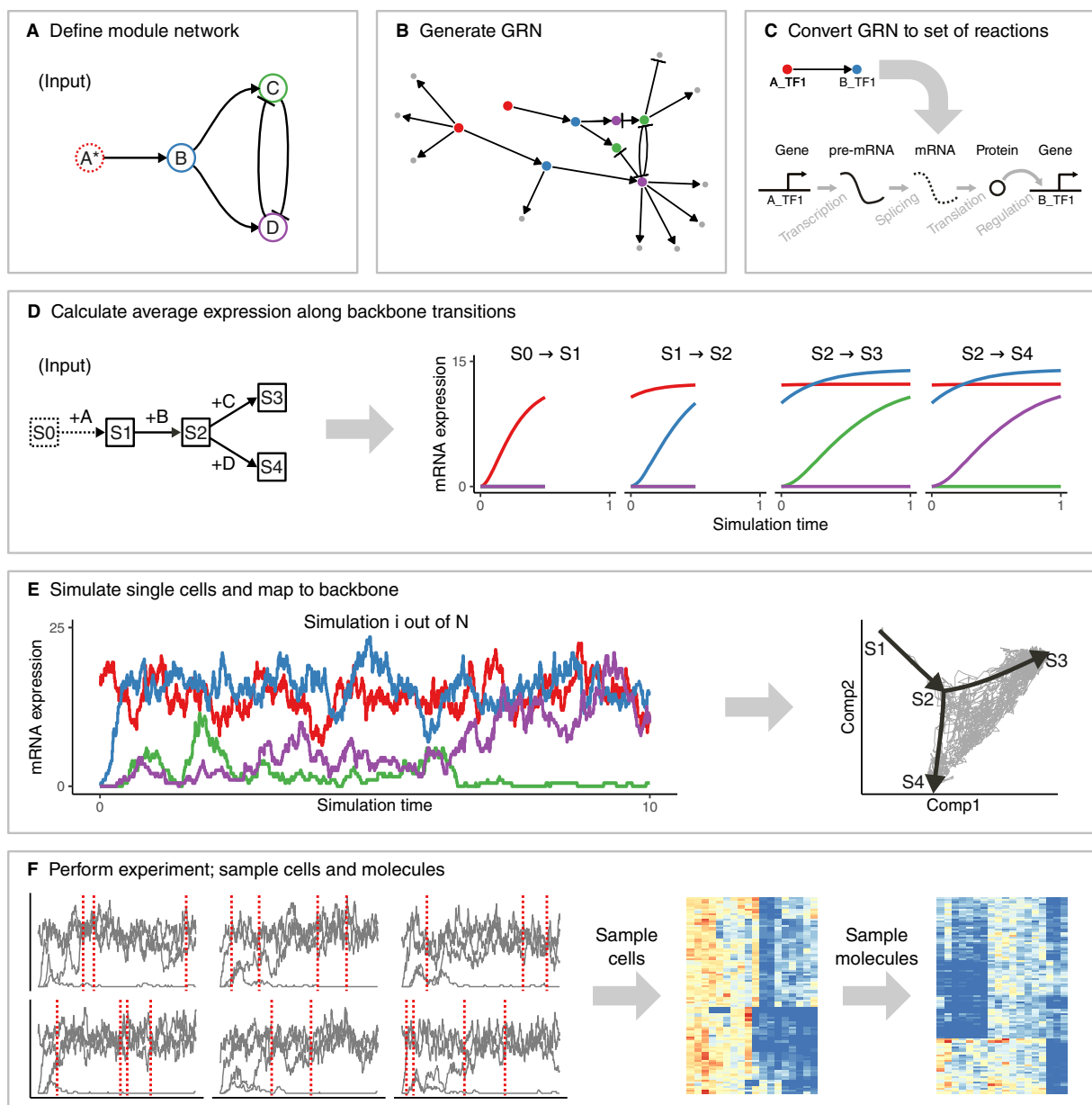


Figure 2.5: The workflow of dyngen is comprised of six main steps. **A:** The user needs to specify the desired module network or use a predefined module network. **B:** Each gene in a module is regulated by one or more transcription factors from the upstream module. Additional target genes are generated. **C:** Each gene regulatory interaction in the GRN is converted to a set of biochemical reactions. **D:** Along with the module network, the user also needs to specify the backbone structure of expected cell states. The average expression of each edge in the backbone is simulated by activating a restricted set of genes for each edge. **E:** Multiple Gillespie SSA simulations are run using the reactions defined in step C. The counts of each of the molecules at each time step are extracted. Each time step is mapped to a point in the backbone. **F:** Multiple cells are sampled from each simulation. Molecules are sampled from each cell.

In dyngen, the user defines the behaviour of the simulation by defining how sets of genes, called modules, are regulating each other. A module may have basal expression, which means that pre-mRNA of the genes in this module will be transcribed without the presence of transcription factor molecules. A module marked as “active during the burn phase” means that this module will be allowed to generate expression of its genes during an initial warm-up phase (See section 2.4.5). At the end of the dyngen process, cells will not be sampled from the burn phase simulations. Interactions between modules have a strength (which is a positive integer) and an effect (+1 for upregulating, -1 for downregulating).

Several examples of module networks are given (Figure 2.6). A simple chain of modules (where one module upregulates the next) results in a *linear* process. By having the last module repress the first module, the process becomes *cyclic*. Two modules repressing each other is the basis of a *bifurcating* process, though several chains of modules have to be attached in order to achieve progression before and after the bifurcation process. Finally, a *converging* process has a bifurcation occurring during the burn phase, after which any differences in module regulation is removed.

Note that these examples represent the bare minimum in terms of number of modules used. Using longer chains of modules is typically desired. In addition, the fate decisions made in this example of a bifurcation is reversible, meaning cells can be reprogrammed to go down a different differentiation path. If this effect is undesirable, more safeguards need to be put in place to prevent reprogramming from occurring (Section 2.4.1).

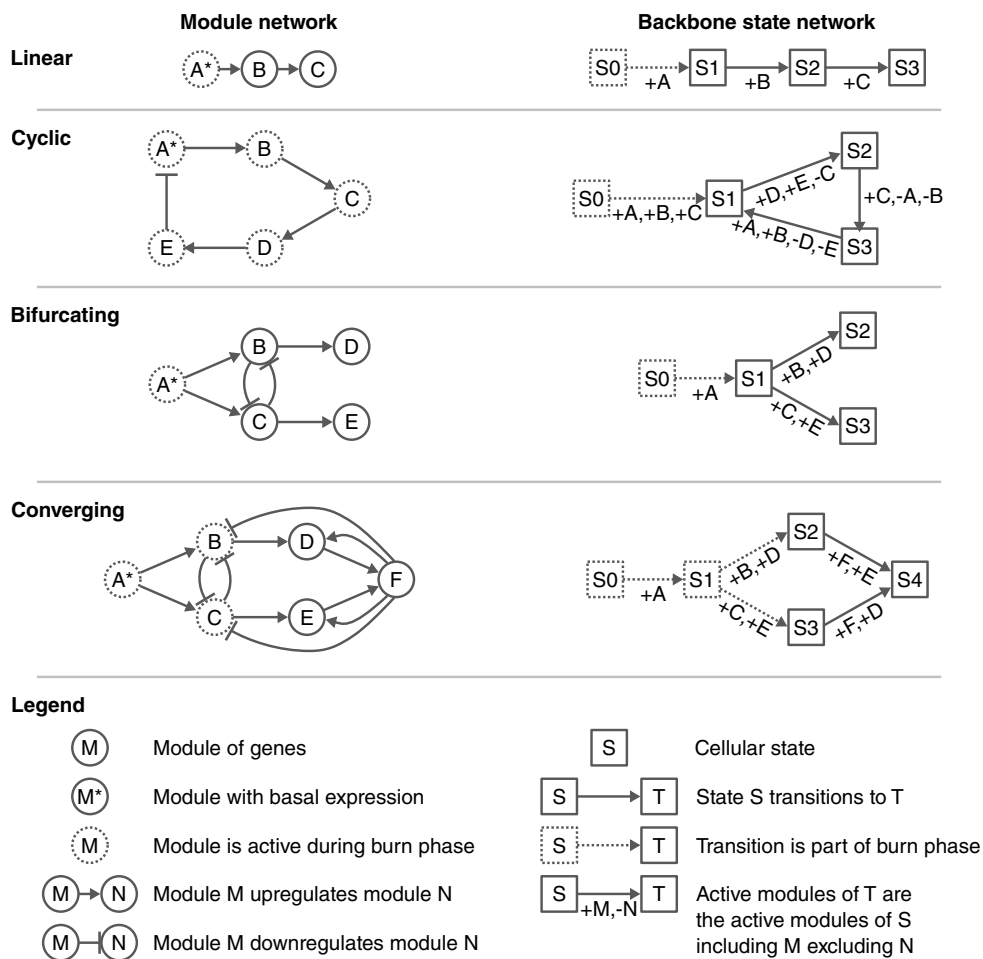


Figure 2.6: Example module networks

In addition to the module network, the user also needs to define a network of cellular states called the "backbone". Before simulating any cells, each transition in the backbone is simulated separately to obtain the average changes in expression along that transition (Figure 2.5D). As part of the backbone, the user needs to specify which modules are allowed to alter its expression from one state to another. For example, in order to transition from state S0 to S1 in the cyclic example, gene modules A, B and C are turned on and a simulation is allowed to run. To transition from S1 to S2, gene modules D and E are turned on, and expression of gene module C is kept constant. To transition from S2 to S3, C is turned on again and now A and B are fixed. Finally, to transition from S3 to S1 again, A and B are turned on again and D and E are fixed again. Demonstrations of the backbone will be explained in

more detail in section 2.4.4.

2

Backbone lego

The backbone can make use of one or more "backbone lego" (BBL) pieces (Figure 2.7). A BBL consists of one or more modules which regulate each other such that the output modules present a specific behaviour, depending on the input module (Figure 2.7A). Parameters allow determining the number of modules involved in the process and the number of outputs. Multiple BBLs can be chained together in order to intuitively create milestone networks and corresponding state networks (Figure 2.7B). Note that not all dynamic processes can be represented by a combination of BBLs, but they can serve as common building blocks to aid the construction of the backbone.

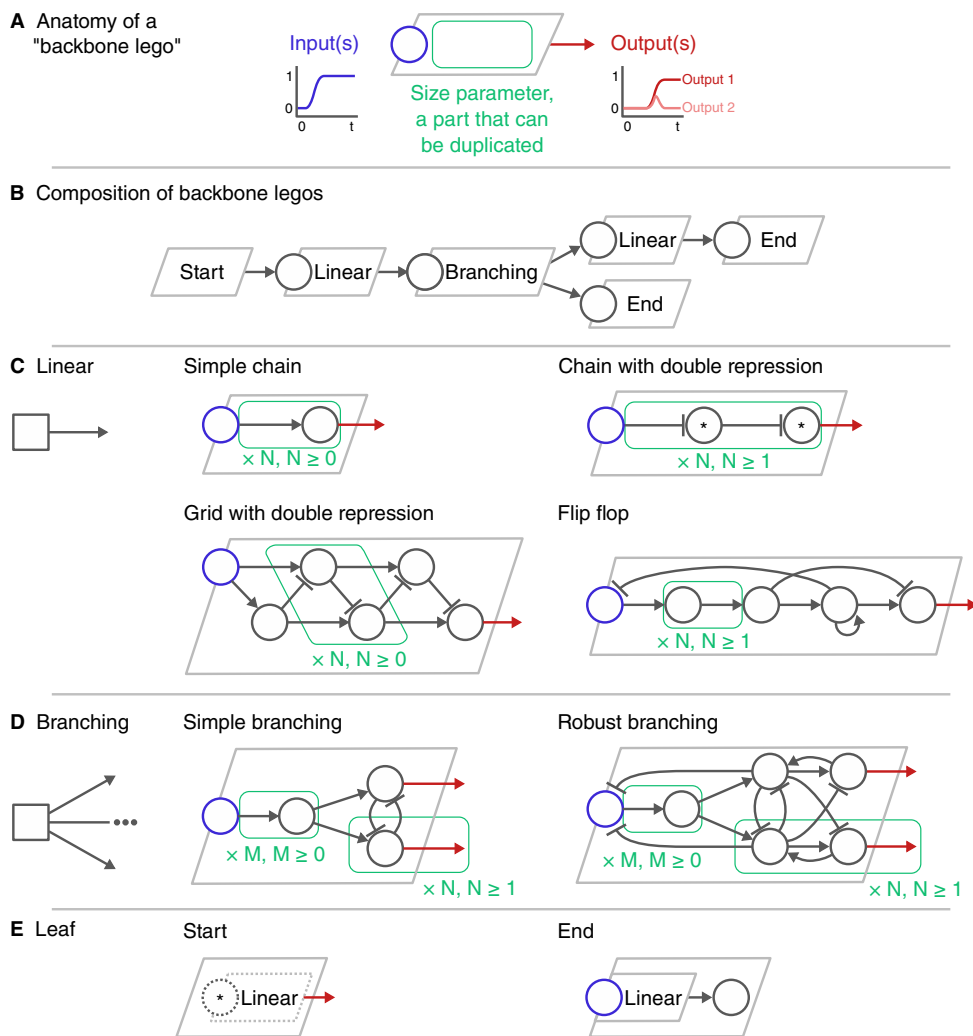


Figure 2.7: Backbone lego

When the input node of a **linear BBL** (Figure 2.7C) is upregulated, the module the BBL is connected to will be upregulated. A *simple chain* is a set of modules where a module upregulates the next. A *chain with double repression* has an uneven number of modules forming a chain where each module downregulates the next but all modules (except the input) have basal expression. A *grid with double repression* is similar; except that modules do not have basal expression but instead get upregulated by an upstream module in the chain. Finally, a *flip flop* consists of a simple chain where first the modules (except the last) are upregulated. Once the second to last module is upregulated, that module upreg-

ulates itself and the first module is strongly repressed, causing all other modules to lose expression and finally the last module to be upregulated. The *flip flop* retains this output state, even when the input changes.

When the input node of a **branching BBL** (Figure 2.7D) is upregulated, a subset of its output modules will eventually be upregulated. A *simple branching* uses reciprocal inhibition to drive the upregulation of one of the output modules. Due to its simplicity, however, multiple output modules might be upregulated simultaneously, and over long periods of simulation time it might be possible that the choice of upregulated module changes. A *robust branching* improves upon the simple branching by preventing upregulation of output modules until an internal branching decision has been made, and by repressing the decision mechanism to avoid other output modules being upregulated other than the one that has been chosen.

A **leaf BBL** (Figure 2.7E) is a linear BBL that has either no inputs or no outputs. A **start BBL** is a linear BBL where the first module has basal expression, and all modules in this module will be active during the burn-in phase of the simulation (Section 2.4.4). An **end BBL** is also a linear BBL with its output regulating one final module.

2.4.2 Generating the gene regulatory network

The GRN is generated based on the given backbone in four main steps (Figure 2.8).

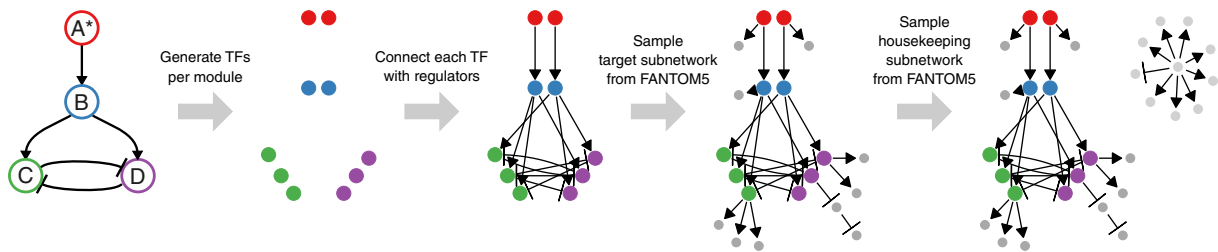


Figure 2.8: Generating the feature network from a backbone consists of four main steps.

Step 1, sampling the transcription factors (TF). The TFs are the main drivers of the molecular changes in the simulation. The user provides a backbone and the number of TFs to generate. Each TF is assigned to a module such that each module has at least x parameters (default $x = 1$). A TF inherits the ‘burn’ and ‘basal expression’ from the module it belongs to.

Step 2, generating the TF interactions. Let each TF be regulated according to the interactions in the backbone. These interactions inherit the effect, strength, and cooperativity parameters from the interactions in the backbone. A TF can only be regulated by other TFs or itself.

Step 3, sampling the target subnetwork. A user-defined number of target genes are added to the GRN. Target genes regulated by a TF or another target gene, but is always downstream of at least one TF. To sample the interactions between target genes, one of the many FANTOM5 [23] GRNs is sampled. The currently existing TFs are mapped to regulators in the FANTOM5 GRN. The targets are drawn from the FANTOM5 GRN, weighted by their page rank value. For each target, at most x regulators are sampled from the induced FANTOM5 GRN (default $x = 5$). The interactions connecting a target gene and its regulators are added to the GRN.

Step 4, sampling the housekeeping subnetwork. Housekeeping genes are completely separate from any TFs or target genes. A user-defined set of housekeeping genes are also sampled from the FANTOM5 GRN. The interactions of the FANTOM5 GRN are first subsampled such that the maximum in-degree of each gene is x (default $x = 5$). A random gene is sampled, and a breadth-first-search is performed to sample the desired number of housekeeping genes.

2.4.3 Convert gene regulatory network to a set of reactions

For every gene G in the GRN, the simulation will keep track of the abundance levels of three molecules, a pre-mRNA, a mature mRNA and a protein. These abundance levels are represented as w_G , x_G and y_G respectively.

Throughout a simulation, the abundance levels of molecules are affected by five reactions, namely transcription, splicing, mRNA degradation, translation, and protein degradation. Each reaction consists of its propensity – a formula to calculate the probability of the reaction occurring during an infinitesimal time interval – and the effect – how it will affect the current state if triggered. The effects and propensity functions of these reactions are defined in Table 2.1.

Table 2.1: Reactions affecting the abundance levels of pre-mRNA w_G , mRNA x_G and proteins y_G of gene G .
Define the set of regulators of G as R_G , the set of upregulating regulators of G as R_G^+ , and the set of downregulating regulators of G as R_G^- . Parameters used in the propensity formulae are defined in Table 2.2.

Reaction	Effect	Propensity
Transcription	$\emptyset \rightarrow w_G$	$wpr_G \times \frac{ba_G - ind_G^{R_G^+} + \prod_{H \in R_G^+} (ind_G + reg_{G,H})}{\prod_{H \in R_G} (1 + reg_{G,H})}$
Splicing	$w_G \rightarrow x_G$	$wsr_G \times w_G$
mRNA degradation	$x_G \rightarrow \emptyset$	$xdr_G \times x_G$
Translation	$x_G \rightarrow w_G + y_G$	$ypr_G \times x_G$
Protein degradation	$y_G \rightarrow \emptyset$	$ydr_G \times y_G$

Table 2.2: Default parameters defined for the calculation of reaction propensity functions.

Parameter	Symbol	Definition
Transcription rate	wpr_G	$\in N(100, 20), \geq 10$
Splicing rate	wsr_G	$\in N(10, 2), \geq 2$
mRNA degradation rate	xdr_G	$\in N(5, 1), \geq 2$
Translation rate	ypr_G	$\in N(5, 1), \geq 2$
Protein degradation rate	ydr_G	$\in N(3, 0.5), \geq 1$
Interaction strength	$str_{G,H}$	$\in 10^{U(0,2)} *$
Interaction cooperativity	$co_{G,H}$	$\in U(0.5, 2) *$
Independence factor	ind_G	$\in [0, 1] *$
TF concentration at half-maximal binding	hmy_H	$= 0.5 \times \frac{wpr_H \times ypr_H}{xdr_H \times ydr_H}$
Regulation activity	$reg_{G,H}$	$= \left(str_{G,H} \times \frac{y_H}{hmy_H} \right)^{co_{G,H}}$
Basal expression	ba_G	$= \begin{cases} 1 & \text{if } R_G^+ = \emptyset \\ 0.0001 & \text{if } R_G^- = \emptyset \text{ and } R_G^+ \neq \emptyset \\ 0.5 & \text{otherwise} \end{cases} *$

*: unless G is a TF, then the value is determined by the backbone.

2.4.4 Compute average expression along backbone transitions

When simulating the developmental backbone, we go through the edges of the backbone state network defined in an earlier step (Section 2.4.1), starting from the root state. It is assumed the root state has no modules active and has no expression of any molecules. To get to the next state, we follow a transition starting from the root state, activate and deactivate the modules as indicated by the transition, and compute the average molecule abundance along the transition. To compute the average abundance, we perform small time steps $t = 0.001$ and let each reaction (Section 2.4.3) occur t times its propensity.

2.4.5 Simulate single cells

`dyngen` uses Gillespie's stochastic simulation algorithm (SSA) [13] to simulate dynamic processes. An SSA simulation is an iterative process where at each iteration one reaction is triggered.

Each reaction consists of its propensity – a formula to calculate the probability of the reaction occurring during an infinitesimal time interval – and the effect – how it will affect the current state if triggered. Each time a reaction is triggered, the simulation time is incremented by $\tau = \frac{1}{\sum_j prop_j} \ln(\frac{1}{r})$, with $r \in U(0, 1)$ and $prop_j$ the propensity value of the j th reaction for the current state of the simulation.

`GillespieSSA2` is an optimised library for performing SSA simulations. The propensity functions are compiled to C++, and SSA approximations can be used which allow to trigger many reactions simultaneously at each iteration. The framework also allows to store the abundance levels of molecules only after a specific interval has passed since the previous census. By setting the census interval to 0, the whole simulation's trajectory is retained but many of these time points will contain very similar information. In addition to the abundance levels, also the propensity values and the number of firings of each of the reactions at each of the time steps can be retained, as well as specific sub-calculations of the propensity values, such as the regulator activity level $reg_{G,H}$.

Map SSA simulations to backbone

We compute the Pearson correlation between the state vectors in the simulation and the average expression levels along a transition in the backbone. Each timepoint in the SSA simulation is mapped to the point in the backbone that has the highest correlation value.

2.4.6 Simulate experiment

From the SSA simulation we obtain the abundance levels of all the molecules at the different time points. We need to replicate technical effects introduced by experimental protocols in order to obtain data that is similar to real data. For this, the cells are sampled from the simulations, and molecules are sampled for each of the cells. Real datasets are used in order to achieve similar data characteristics.

Sample cells

Cells can be sampled from an unsynchronised population of single cells (snapshot) or at multiple time points in a synchronised population (time series).

Snapshot Cells are sampled uniformly from the different time points in the simulation.

2

Time series The timeline of the simulations is divided into multiple chunks. From several of these chunks, cells are sampled. For each cell it is known at which time point it was sampled.

Sample molecules

Molecules are sampled from the simulation to replicate how molecules are experimentally sampled. A real dataset is downloaded from a repository of single-cell RNA-seq datasets [24]. For each *in silico* cell i , draw its library size ls_i from the distribution of transcript counts per cell in the real dataset. The capture rate cr_j of each *in silico* molecule type j is drawn from $N(1, 0.05)$. Finally, for each cell i , draw ls_i molecules from the multinomial distribution with probabilities $cr_j \times ab_{i,j}$ with $ab_{i,j}$ the molecule abundance level of molecule j in cell i .

2.5 References

- [1] Luke Zappia, Belinda Phipson, and Alicia Oshlack. "Splatter: Simulation of Single-Cell RNA Sequencing Data". In: *Genome Biology* 18 (Sept. 2017), p. 174. ISSN: 1474-760X. DOI: [10.1186/s13059-017-1305-0](https://doi.org/10.1186/s13059-017-1305-0).
- [2] Beate Vieth et al. "powsimR: Power Analysis for Bulk and Single Cell RNA-Seq Experiments". In: *Bioinformatics* 33.21 (Nov. 1, 2017), pp. 3486–3488. ISSN: 1367-4803. DOI: [10.1093/bioinformatics/btx435](https://doi.org/10.1093/bioinformatics/btx435).
- [3] Nikolaos Papadopoulos, Rodrigo Gonzalo Parra, and Johannes Soeding. "PROSSTT: Probabilistic Simulation of Single-Cell RNA-Seq Data for Complex Differentiation Processes". In: *bioRxiv* (Jan. 2018), p. 256941. DOI: [10.1101/256941](https://doi.org/10.1101/256941).
- [4] Xiuwei Zhang, Chenling Xu, and Nir Yosef. "Simulating Multiple Faceted Variability in Single Cell RNA Sequencing". In: *Nature Communications* 10.1 (June 13, 2019), pp. 1–16. ISSN: 2041-1723. DOI: [10.1038/s41467-019-10500-w](https://doi.org/10.1038/s41467-019-10500-w).
- [5] Kelly Street et al. "Slingshot: Cell Lineage and Pseudotime Inference for Single-Cell Transcriptomics". In: *BMC Genomics* 19.1 (June 2018), p. 477. ISSN: 1471-2164. DOI: [10.1186/s12864-018-4772-0](https://doi.org/10.1186/s12864-018-4772-0).
- [6] R Gonzalo Parra et al. "Reconstructing Complex Lineage Trees from scRNA-Seq Data Using MERLoT". In: *bioRxiv* (Feb. 2018), p. 261768. DOI: [10.1101/261768](https://doi.org/10.1101/261768).
- [7] Edroaldo Lummertz da Rocha et al. "Reconstruction of Complex Single-Cell Trajectories Using CellRouter". In: *Nature Communications* 9.1 (Mar. 1, 2018), p. 892. ISSN: 2041-1723. DOI: [10.1038/s41467-018-03214-y](https://doi.org/10.1038/s41467-018-03214-y).
- [8] Yingxin Lin et al. "scClassify: Hierarchical Classification of Cells". In: *bioRxiv* (Jan. 1, 2019), p. 776948. DOI: [10.1101/776948](https://doi.org/10.1101/776948).
- [9] Angelo Duò, Mark D. Robinson, and Charlotte Soneson. "A Systematic Performance Evaluation of Clustering Methods for Single-Cell RNA-Seq Data". In: *F1000Research* 7 (2018), p. 1141. ISSN: 2046-1402. DOI: [10.12688/f1000research.15666.2](https://doi.org/10.12688/f1000research.15666.2). pmid: [30271584](#).
- [10] Wouter Saelens et al. "A Comparison of Single-Cell Trajectory Inference Methods". In: *Nature Biotechnology* 37 (May 2019). ISSN: 15461696. DOI: [10.1038/s41587-019-0071-9](https://doi.org/10.1038/s41587-019-0071-9).
- [11] Charlotte Soneson and Mark D. Robinson. "Bias, Robustness and Scalability in Single-Cell Differential Expression Analysis". In: *Nature Methods* 15.4 (Apr. 2018), pp. 255–261. ISSN: 1548-7105. DOI: [10.1038/nmeth.4612](https://doi.org/10.1038/nmeth.4612). pmid: [29481549](#).
- [12] Tim Stuart and Rahul Satija. "Integrative Single-Cell Analysis". In: *Nature Reviews Genetics* 20.5 (May 2019), pp. 257–272. ISSN: 1471-0064. DOI: [10.1038/s41576-019-0093-7](https://doi.org/10.1038/s41576-019-0093-7).
- [13] Daniel T. Gillespie. "Exact Stochastic Simulation of Coupled Chemical Reactions". In: *The Journal of Physical Chemistry* 81.25 (Dec. 1, 1977), pp. 2340–2361. ISSN: 0022-3654. DOI: [10.1021/j100540a008](https://doi.org/10.1021/j100540a008).
- [14] Thomas Schaffter, Daniel Marbach, and Dario Floreano. "GeneNetWeaver: In Silico Benchmark Generation and Performance Profiling of Network Inference Methods." In: *Bioinformatics* 27.16 (Aug. 2011), pp. 2263–2270. ISSN: 1367-4811. DOI: [10.1093/bioinformatics/btr373](https://doi.org/10.1093/bioinformatics/btr373). pmid: [21697125](#).
- [15] Adam D. Ewing et al. "Combining Tumor Genome Simulation with Crowdsourcing to Benchmark Somatic Single-Nucleotide-Variant Detection". In: *Nature Methods* 12.7 (July 2015), pp. 623–630. ISSN: 1548-7105. DOI: [10.1038/nmeth.3407](https://doi.org/10.1038/nmeth.3407).

- [16] Stephen Smith and Ramon Grima. "Spatial Stochastic Intracellular Kinetics: A Review of Modelling Approaches". In: *Bulletin of Mathematical Biology* 81.8 (Aug. 1, 2019), pp. 2960–3009. ISSN: 1522-9602. DOI: [10.1007/s11538-018-0443-1](https://doi.org/10.1007/s11538-018-0443-1).
- [17] N. Rekhtman et al. "Direct Interaction of Hematopoietic Transcription Factors PU.1 and GATA-1: Functional Antagonism in Erythroid Cells". In: *Genes & Development* 13.11 (June 1, 1999), pp. 1398–1411. ISSN: 0890-9369. DOI: [10.1101/gad.13.11.1398](https://doi.org/10.1101/gad.13.11.1398). pmid: [10364157](#).
- [18] Heping Xu et al. "Regulation of Bifurcating {B} Cell Trajectories by Mutual Antagonism between Transcription Factors {IRF4} and {IRF8}". In: *Nat. Immunol.* 16.12 (Dec. 2015), pp. 1274–1281.
- [19] Thomas Graf and Tariq Enver. "Forcing Cells to Change Lineages". In: *Nature* 462.7273 (Dec. 2009), p. 587. ISSN: 1476-4687. DOI: [10.1038/nature08533](https://doi.org/10.1038/nature08533).
- [20] Jin Wang et al. "Quantifying the Waddington Landscape and Biological Paths for Development and Differentiation". In: *Proceedings of the National Academy of Sciences* 108.20 (May 2011), pp. 8257–8262. ISSN: 0027-8424, 1091-6490. DOI: [10.1073/pnas.1017017108](https://doi.org/10.1073/pnas.1017017108). pmid: [21536909](#).
- [21] James E Ferrell. "Bistability, Bifurcations, and Waddington's Epigenetic Landscape". In: *Current Biology* 22.11 (June 2012), R458–R466. ISSN: 0960-9822. DOI: [10.1016/j.cub.2012.03.045](https://doi.org/10.1016/j.cub.2012.03.045).
- [22] Nir Yosef et al. "Dynamic Regulatory Network Controlling {TH17} Cell Differentiation". In: *Nature* 496.7446 (2013), pp. 461–468.
- [23] Marina Lizio et al. "Gateways to the FANTOM5 Promoter Level Mammalian Expression Atlas". In: *Genome Biology* 16.1 (Jan. 5, 2015), p. 22. ISSN: 1465-6906. DOI: [10.1186/s13059-014-0560-6](https://doi.org/10.1186/s13059-014-0560-6).
- [24] Robrecht Cannoodt et al. "Single-Cell -Oomics Datasets Containing a Trajectory". In: *Zenodo* (Oct. 2018). DOI: [10.5281/zenodo.1211532](https://doi.org/10.5281/zenodo.1211532).

CHAPTER 3

Paper 2: A comparison of single-cell trajectory inference methods

Abstract

Purpose: Trajectory inference approaches analyse genome-wide omics data from thousands of single cells and computationally infer the order of these cells along developmental trajectories. Although more than 75 trajectory inference tools have already been developed, it is challenging to compare their performance because the input they require and output models they produce vary substantially.

Results: Here, we benchmark 45 of these methods on 110 real and 229 synthetic datasets for cellular ordering, topology, scalability and usability. Our results highlight the complementarity of existing tools, and that the choice of method should depend mostly on the dataset dimensions and trajectory topology. We develop a set of guidelines to help users select the best method for their dataset.

Conclusion: Our freely available data and evaluation pipeline will aid in the development of improved tools designed to analyse increasingly large and complex single-cell datasets.

Publication status

Published in Nature Biotechnology 37, 5 (2019). doi:[10.1038/s41587-019-0071-9](https://doi.org/10.1038/s41587-019-0071-9).

Saelens W*, **Cannoodt R***, Todorov H, and Saeys Y.

* Equal contribution

Author contributions

- R.C., W.S., H.T. and Y.S. designed the study.
- R.C. and W.S. performed the experiments and analysed the data.
- R.C., W.S., and H.T. implemented software packages.
- R.C. and W.S. wrote the original manuscript.
- R.C., W.S., H.T., and Y.S. reviewed and edited the manuscript.
- Y.S. supervised the project.

3.1 Introduction

3

Single-cell omics data, including transcriptomics, proteomics and epigenomics data, provide new opportunities for studying cellular dynamic processes, such as the cell cycle, cell differentiation and cell activation [1, 2]. Such dynamic processes can be modeled computationally using trajectory inference (TI) methods, also called pseudotime analysis, which order cells along a trajectory based on similarities in their expression patterns [3, 4, 5]. The resulting trajectories are most often linear, bifurcating or tree-shaped, but more recent methods also identify more complex trajectory topologies, such as cyclic [6] or disconnected graphs [7]. TI methods offer an unbiased and transcriptome-wide understanding of a dynamic process [1], thereby allowing the objective identification of new (primed) subsets of cells [8], delineation of a differentiation tree [9, 10] and inference of regulatory interactions responsible for one or more bifurcations [11]. Current applications of TI focus on specific subsets of cells, but ongoing efforts to construct transcriptomic catalogs of whole organisms [12, 13, 14] underline the urgency for accurate, scalable [11, 15] and user-friendly TI methods.

A plethora of TI methods has been developed over the past few years and even more are being created every month (Supplementary Table 1). Indeed, in several repositories listing single-cell tools, such as [omictools.org](#) [16], the ‘awesome-single-cell’ list [17] and [scRNA-tools.org](#) [18], TI methods are one of the largest categories. While each method has its own unique set of characteristics in terms of underlying algorithm, required prior information and produced outputs, two of the most distinctive differences between TI methods are whether they fix the topology of the trajectory and what type(s) of graph topologies they can detect. Early TI methods typically fixed the topology algorithmically (for example, linear [19, 8, 20, 21] or bifurcating trajectories [22, 23]) or through parameters provided by the user [24, 25]. These methods therefore mainly focus on correctly ordering the cells along the fixed topology. More recent methods also infer the topology [26, 27, 7], which increases the difficulty of the problem at hand, but allows the unbiased identification of both the ordering inside a branch and the topology connecting these branches.

Given the diversity in TI methods, it is important to quantitatively assess their performance, scalability, robustness and usability. Many attempts at tackling this issue have already been made [22, 28, 29, 25, 30, 4, 31, 32, 7], but a comprehensive comparison of TI methods across a large number of different datasets is still lacking. This is problematic, as new users to the field are confronted with an overwhelming choice of TI methods, without a clear idea of which would optimally solve their problem. Moreover, the strengths and weaknesses of existing methods need to be assessed, so that new developments in the field can focus on improving the current state-of-the-art.

In this study, we evaluated the accuracy, scalability, stability and usability of 45 TI methods (Figure 3.1a). We found substantial complementarity between current methods, with different sets of methods performing most optimally depending on the characteristics of the data. For method users, we created an interactive set of guidelines (available at [guidelines.dynverse.org](#)), which gives context-specific recommendations for method usage. Our evaluation also highlights some challenges for current methods, and our evaluation strategy can be useful to spearhead the development of new tools that accurately infer trajectories on ever more complex use cases.

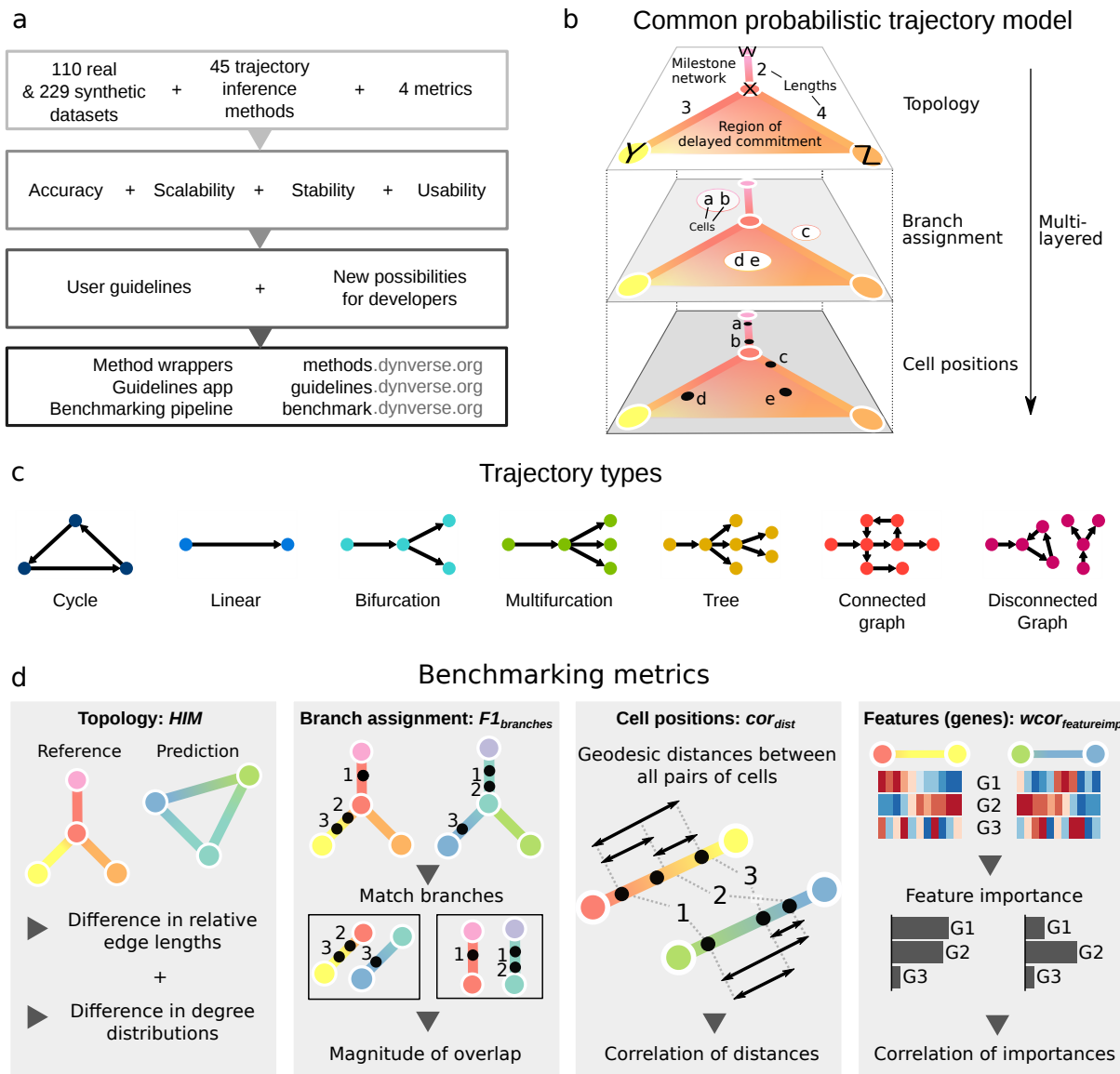


Figure 3.1: Overview of several key aspects of the evaluation. **a**, A schematic overview of our evaluation pipeline. **b**, To make the trajectories comparable to each other, a common trajectory model was used to represent reference trajectories from the real and synthetic datasets, as well as any predictions of TI methods. **c**, Trajectories are automatically classified into one of seven trajectory types, with increasing complexity. **d**, We defined four metrics, each assessing the quality of a different aspect of the trajectory. The HIM score assesses the similarity between the two topologies, taking into account differences in edge lengths and degree distributions. The $F1_{branches}$ assesses the similarity of the assignment of cells onto branches. The cor_{dist} quantifies the similarity in cellular positions between two trajectories, by calculating the correlation between pairwise geodesic distances. Finally, $wcor_{featureimp}$ quantifies the agreement between trajectory differentially expressed features from the known trajectory and the predicted trajectory.

3.2 Results

3.2.1 Trajectory inference methods

To make the outputs from different methods directly comparable to each other, we developed a common probabilistic model for representing trajectories from all possible sources (Figure 3.1b). In this model, the overall topology is represented by a network of ‘milestones’, and the cells are placed within the space formed by each set of connected milestones. Although almost every method returned a

unique set of outputs, we were able to classify these outputs into seven distinct groups (Figure 3.2) and we wrote a common output converter for each of these groups (Figure 3.3a). When strictly required, we also provided prior information to the method. These different priors can range from weak priors that are relatively easy to acquire, such as a start cell, to strong priors, such as a known grouping of cells, that are much harder to know a priori, and which can potentially introduce a large bias into the analysis (Figure 3.3a).

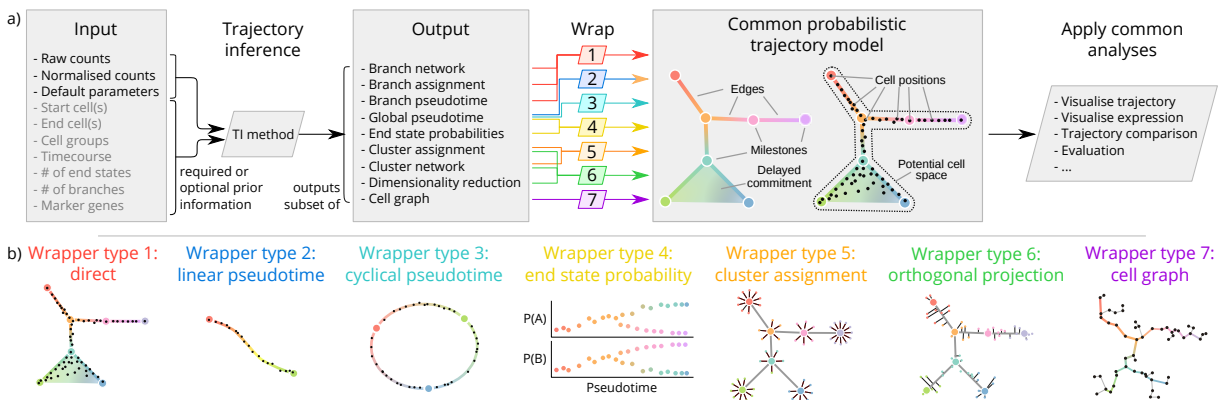


Figure 3.2: A common interface for TI methods. **a** The input and output of each TI method is standardized. As input, each TI method receives either raw or normalized counts, several parameters, and a selection of prior information. After its execution, a method uses one of the seven wrapper functions to transform its output to the common trajectory model. This common model then allows to perform common analysis functions on trajectory models produced by any TI method. **b** Illustrations of the specific transformations performed by each of the wrapper functions.

The largest difference between TI methods is whether a method fixes the topology and, if it does not, what kind of topology it can detect. We defined seven possible types of topology, ranging from very basic topologies (linear, cyclical and bifurcating) to the more complex ones (connected and disconnected graphs). Most methods either focus on inferring linear trajectories or limit the search to tree or less complex topologies, with only a selected few attempting to infer cyclic or disconnected topologies (Figure 3.3a).

We evaluated each method on four core aspects: (1) accuracy of a prediction, given a gold or silver standard on 110 real and 229 synthetic datasets; (2) scalability with respect to the number of cells and features (for example, genes); (3) stability of the predictions after subsampling the datasets; and (4) the usability of the tool in terms of software, documentation and the manuscript. Overall, we found a large diversity across the four evaluation criteria, with only a few methods, such as PAGA, Slingshot and SCORPIUS, performing well across the board (Figure 3.3b). We will discuss each evaluation criterion in more detail (Figure 3.4 and Supplementary Fig. 2), after which we conclude with guidelines for method users and future perspectives for method developers.

3.2.2 Accuracy

We defined several metrics to compare a prediction to a reference trajectory (Section 3.5). Based on an analysis of their robustness and conformity to a set of rules (Section 3.5), we chose four metrics each assessing a different aspect of a trajectory (Figure 3.1d): the topology (Hamming–Ipsen–Mikhailov, HIM), the quality of the assignment of cells to branches (F1branches), the cell positions (cordist) and the accuracy of the differentially expressed features along the trajectory (wcorfeatures). The data compendium consisted of both synthetic datasets, which offer the most exact reference trajectory, and real datasets, which provide the highest biological relevance. These real datasets come from a variety of single-cell technologies, organisms and dynamic processes, and contain several types of trajectory topologies (Supplementary Table 2). Real datasets were classified as ‘gold standard’ if the reference trajectory was not extracted from the expression data itself, such as via cellular sorting or cell mixing [33]. All other real datasets were classified as ‘silver standard’. For synthetic datasets we used several data simulators, including a simulator of gene regulatory networks using a thermodynamic model of gene regulation [34]. For each simulation, we used a real dataset as a reference, to match its dimensions, number of differentially expressed genes, drop-out rates and other statistical properties [35].

We found that method performance was very variable across datasets, indicating that there is no ‘one-size-fits-all’ method that works well on every dataset (Figure 3.5a). Even methods that can detect most of the trajectory types, such as PAGA, RacelD/StemID and SLICER were not the best methods across all trajectory types (Figure 3.4b). The overall score between the different dataset sources was moderately to highly correlated (Spearman rank correlation between 0.5–0.9) with the scores on real datasets containing a gold standard (Figure 3.5b), confirming both the accuracy of the gold standard trajectories and the relevance of the synthetic data. On the other hand, the different metrics frequently disagreed with each other, with Monocle and PAGA Tree scoring better on the topology scores, whereas other methods, such as Slingshot, were better at ordering the cells and placing them into the correct branches (Figure 3.4b).

The performance of a method was strongly dependent on the type of trajectory present in the data (Figure 3.4b). Slingshot typically performed better on datasets containing more simple topologies, while PAGA, pCreode and RacelD/StemID had higher scores on datasets with trees or more complex trajectories (Figure 3.5c). This was reflected in the types of topologies detected by every method, as those predicted by Slingshot tended to contain less branches, whereas those detected by PAGA, pCreode and Monocle DDRTree gravitated towards more complex topologies (Figure 3.5d). This analysis therefore indicates that detecting the right topology is still a difficult task for most of these methods, because methods tend to be either too optimistic or too pessimistic regarding the complexity of the topology in the data.

The high variability between datasets, together with the diversity in detected topologies between methods, could indicate some complementarity between the different methods. To test this, we calculated the likelihood of obtaining a top model when using only a subset of all methods. A top model in this case was defined as a model with an overall score of at least 95% as the best model. On all datasets, using one method resulted in getting a top model about 27% of the time. This increased up to 74% with the addition of six other methods (Figure 3.6a). The result was a relatively diverse set of methods, containing both strictly linear or cyclic methods, and methods with a broad trajectory type range such as PAGA. We found similar indications of complementarity between the top methods on data containing only linear, bifurcation or multifurcating trajectories (Figure 3.6b), although in these cases less methods were necessary to obtain at least one top model for a given dataset. Altogether,

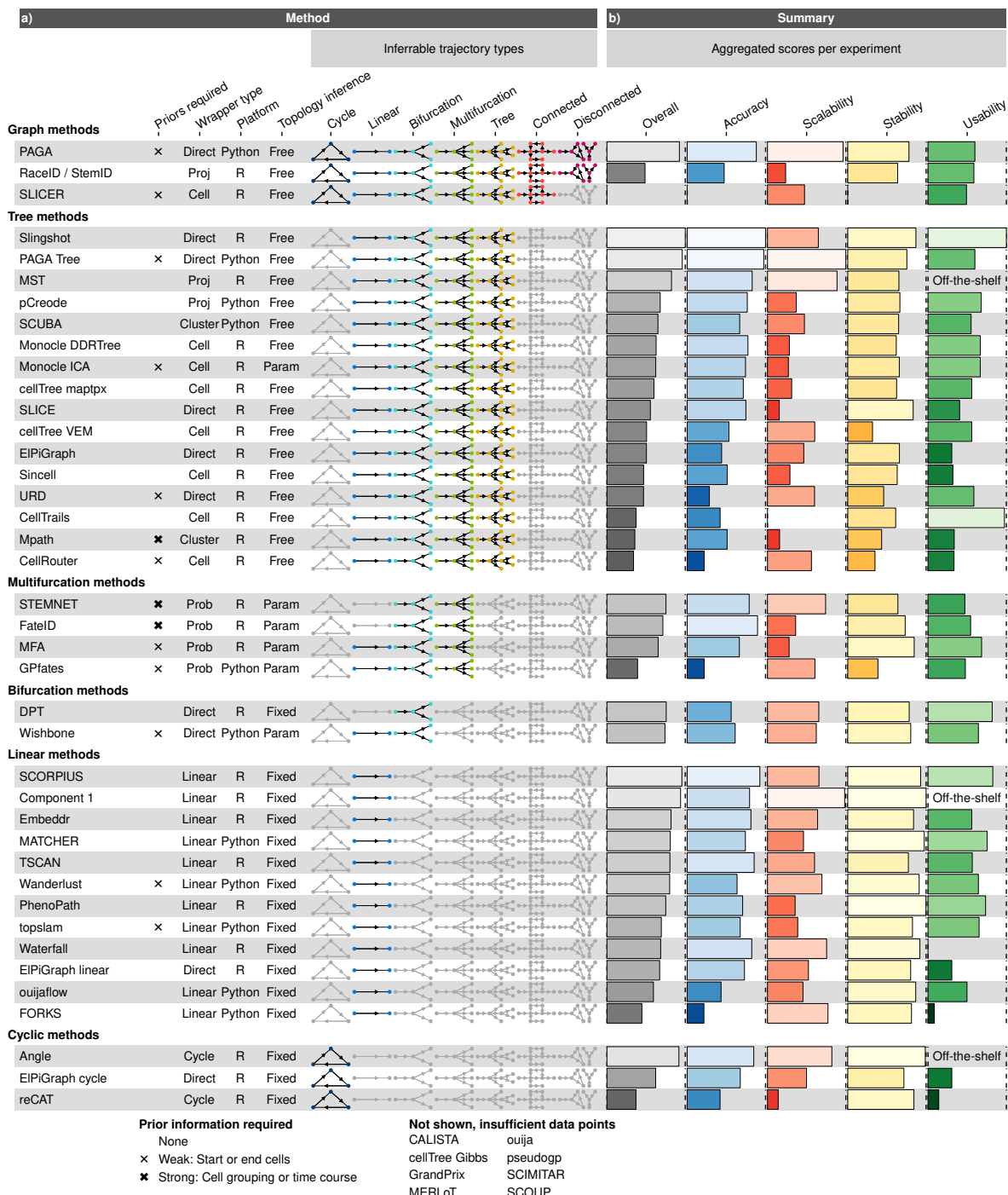


Figure 3.3: A characterization of the 45 methods evaluated in this study and their overall evaluation results. **a**, We characterized the methods according to the wrapper type, their required priors, whether the inferred topology is constrained by the algorithm (fixed) or a parameter (param), and the types of inferable topologies. The methods are grouped vertically based on the most complex trajectory type they can infer. **b**, The overall results of the evaluation on four criteria: accuracy using a reference trajectory on real and synthetic data, scalability with increasing number of cells and features, stability across dataset subsamples and quality of the implementation. Methods that errored on more than 50% of the datasets are not included in this figure and are shown instead in Supplementary Fig. 2.

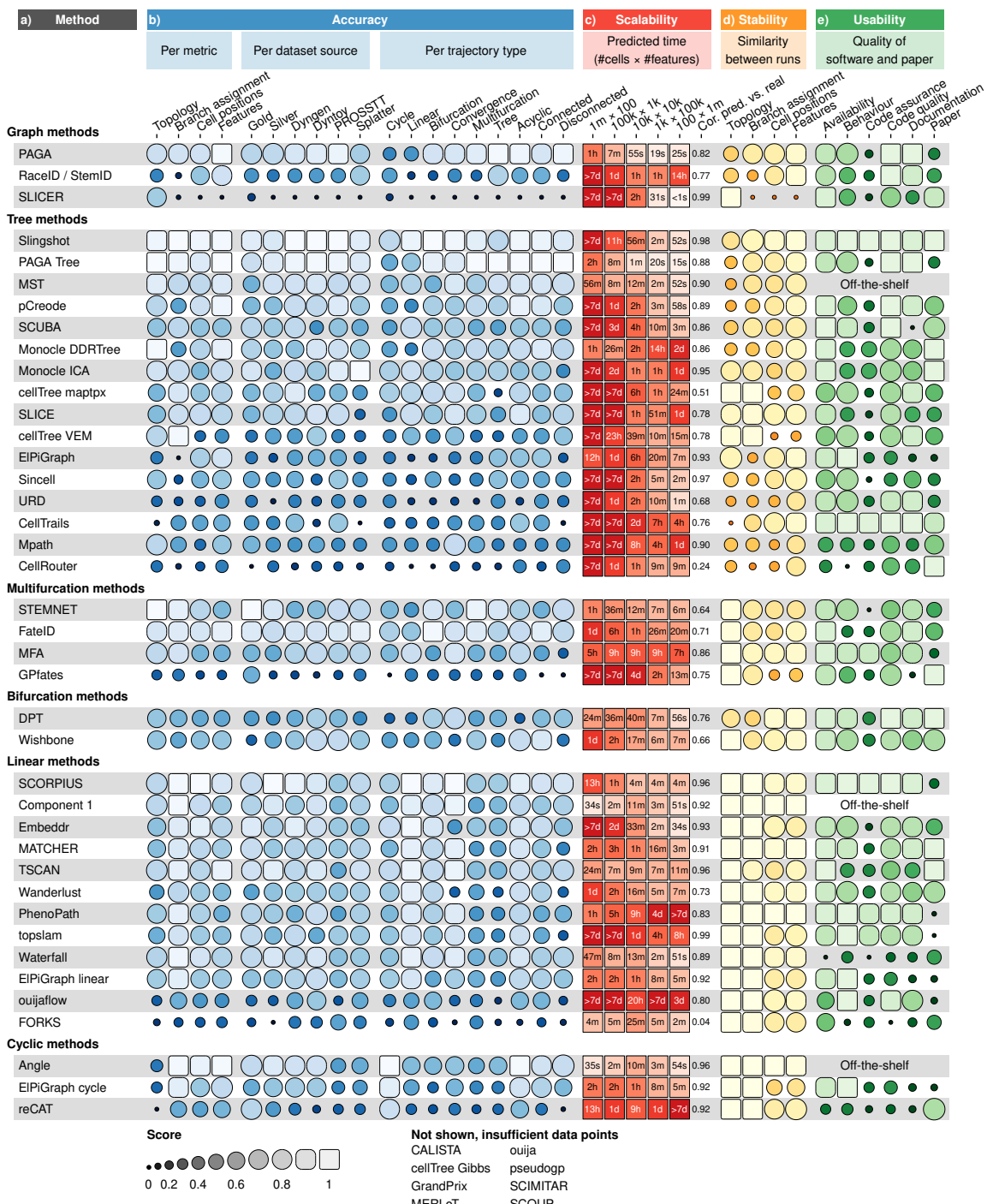


Figure 3.4: Detailed results of the four main evaluation criteria: accuracy, scalability, stability and usability. **a,** The names of the methods, ordered as in Figure 3.3. **b,** Accuracy of trajectory inference methods across metrics, dataset sources and dataset trajectory types. The performance of a method is generally more stable across dataset sources, but very variable depending on the metric and trajectory type. **c,** Predicted execution times for varying numbers of cells and features (no. of cells \times no. of features). Predictions were made by training a regression model after running each method on bootstrapped datasets with varying numbers of cells and features. k, thousands; m, millions; cor, correlation. **d,** Stability results by calculating the average pairwise similarity between models inferred across multiple runs of the same method. **e,** Usability scores of the tool and corresponding manuscript, grouped per category. Off-the-shelf methods were directly implemented in R and thus do not have a usability score.

this shows that there is considerable complementarity between the different methods and that users should try out a diverse set of methods on their data, especially when the topology is unclear a priori. Moreover, it also opens up the possibilities for new ensemble methods that utilize this complementarity.

3.2.3 Scalability

While early TI methods were developed at a time where profiling more than a thousand cells was exceptional, methods now have to cope with hundreds of thousands of cells, and perhaps soon with more than ten million [36]. Moreover, the recent application of TI methods on multi-omics single-cell data also showcases the increasing demands on the number of features [37]. To assess the scalability, we ran each method on up- and downscaled versions of five distinct real datasets. We modeled the running time and memory usage using a Shape Constrained Additive Model [38] (Figure 3.7a). As a control, we compared the predicted time (and memory) with the actual time (respectively memory) on all benchmarking datasets, and found that these were highly correlated overall (Spearman rank correlation >0.9 , Figure 3.8, and moderately to highly correlated (Spearman rank correlation of 0.5–0.9) for almost every method, depending to what extent the execution of a method succeeded during the scalability experiments (Figure 3.4c and Supplementary Fig. 2a).

We found that the scalability of most methods was overall very poor, with most graph and tree methods not finishing within an hour on a dataset with ten thousand cells and ten thousand features (Figure 3.4c), which is around the size of a typical droplet-based single-cell dataset [36]. Running times increased further with increasing number of cells, with only a handful of graph/tree methods completing within a day on a million cells (PAGA, PAGA Tree, Monocle DDRTree, Stemnet and GrandPrix). Some methods, such as Monocle DDRTree and GrandPrix, also suffered from unsatisfactory running times when given a high number of features.

Methods with a low running time typically had two defining aspects: they had a linear time complexity with respect to the features and/or cells, and adding new cells or features led to a relatively low increase in time (Figure 3.7b). We found that more than half of all methods had a quadratic or superquadratic complexity with respect to the number of cells, which would make it difficult to apply any of these methods in a reasonable time frame on datasets with more than a thousand cells (Figure 3.7b).

We also assessed the memory requirements of each method (Supplementary Fig. 2c). Most methods had reasonable memory requirements for modern workstations or computer clusters (≤ 12 GB) with PAGA and STEMNET in particular having a low memory usage with both a high number of cells or a high number of features. Notably, the memory requirements were very high for several methods on datasets with high numbers of cells (RaceID/StemID, pCreode and MATCHER) or features (Monocle DDRTree, SLICE and MFA).

Altogether, the scalability analysis indicated that the dimensions of the data are an important factor in the choice of method, and that method development should pay more attention to maintaining reasonable running times and memory usage.

3.2.4 Stability

It is not only important that a method is able to infer an accurate model in a reasonable time frame, but also that it produces a similar model when given very similar input data. To test the stability of

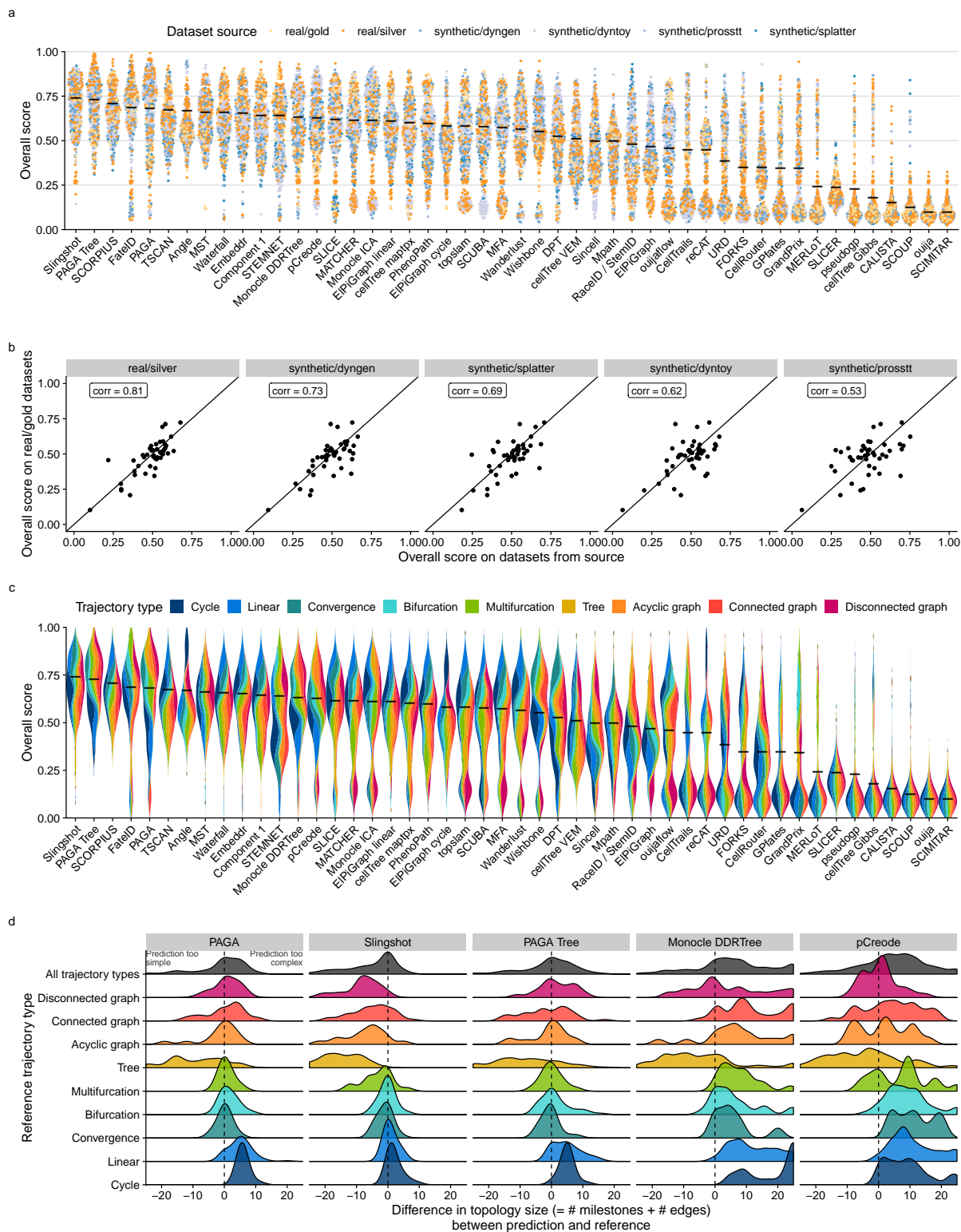


Figure 3.5: Accuracy of trajectory inference methods. **a** Overall score for all methods across 339 datasets, colored by the source of the datasets. Black line indicates the mean. **b** Similarity between the overall scores of all dataset sources, compared to real datasets with a gold standard, across all methods ($n = 46$, after filtering out methods that errored too frequently). Shown in the top left is the Pearson correlation. **c** Bias in the overall score towards trajectory types for all methods across 339 datasets. Black line indicates the mean. **d** Distributions of the difference in size between predicted and reference topologies. A positive difference means that the topology predicted by the method is more complex than the one in the reference.

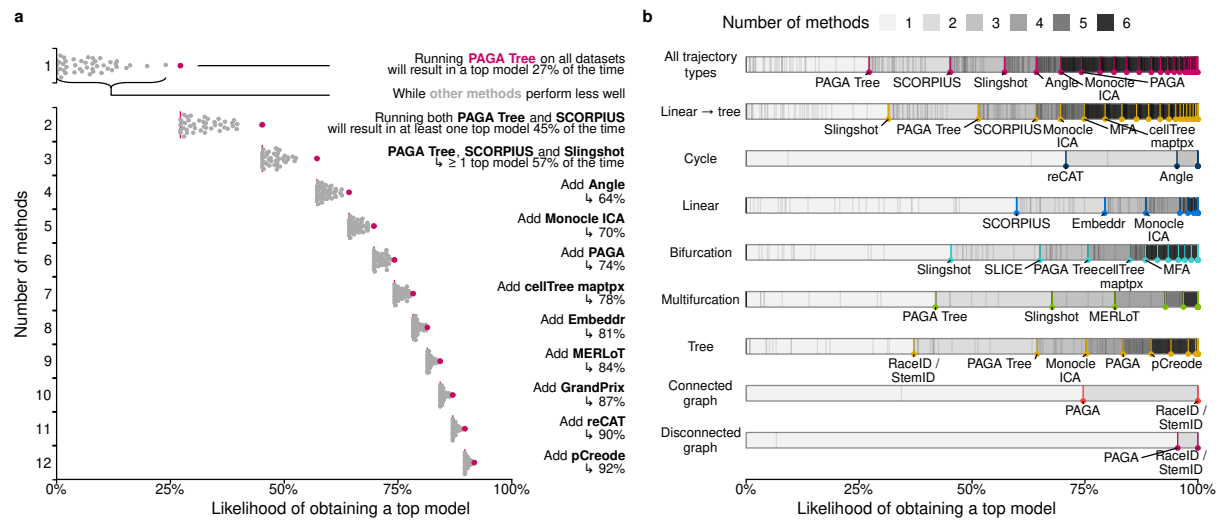


Figure 3.6: Complementarity between different trajectory inference methods. **a**, We assessed the likelihood for different combinations of methods to lead to a ‘top model’ (defined as a model with an overall score of at least 95% of the best model) when applied to all datasets. **b**, The likelihood for different combinations of methods to lead to a ‘top model’ was assessed separately on different trajectory types. For this figure, we did not include any methods requiring a cell grouping or a time course as prior information.

each method, we executed each method on ten different subsamples of the datasets (95% of the cells, 95% of the features), and calculated the average similarity between each pair of models using the same scores used to assess the accuracy of a trajectory (Figure 3.4d).

Given that the trajectories of methods that fix the topology either algorithmically or through a parameter are already very constrained, it is to be expected that such methods tend to generate very stable results. Nonetheless, some fixed topology methods still produced slightly more stable results, such as SCORPIUS and MATCHER for linear methods and MFA for multifurcating methods. Stability was much more diverse among methods with a free topology. Slingshot produced more stable models than PAGA (Tree), which in turn produced more stable results than pCreode and Monocle DDRTree.

3.2.5 Usability

While not directly related to the accuracy of the inferred trajectory, it is also important to assess the quality of the implementation and how user-friendly it is for a biological user [39]. We scored each method using a transparent checklist of important scientific and software development practices, including software packaging, documentation, automated code testing and publication into a peer-reviewed journal (Table 3.1). It is important to note that there is a selection bias in the tools chosen for this analysis, as we did not include a substantial set of tools due to issues with installation, code availability and executability on a freely available platform (which excludes MATLAB). The reasons for not including certain tools are all discussed on our repository (<https://github.com/dynverse/dynmethods/issues?q=label:unwrappable>). Installation issues seem to be quite general in bioinformatics [40] and the trajectory inference field is no exception.

We found that most methods fulfilled the basic criteria, such as the availability of a tutorial and elemental code quality criteria (Figure 3.4d and Figure 3.9). While recent methods had a slightly better quality score than older methods, several quality aspects were consistently lacking for the majority of the methods (Figure 3.9 right) and we believe that these should receive extra attention from developers. Although these outstanding issues covered all five categories, code assurance and documentation in

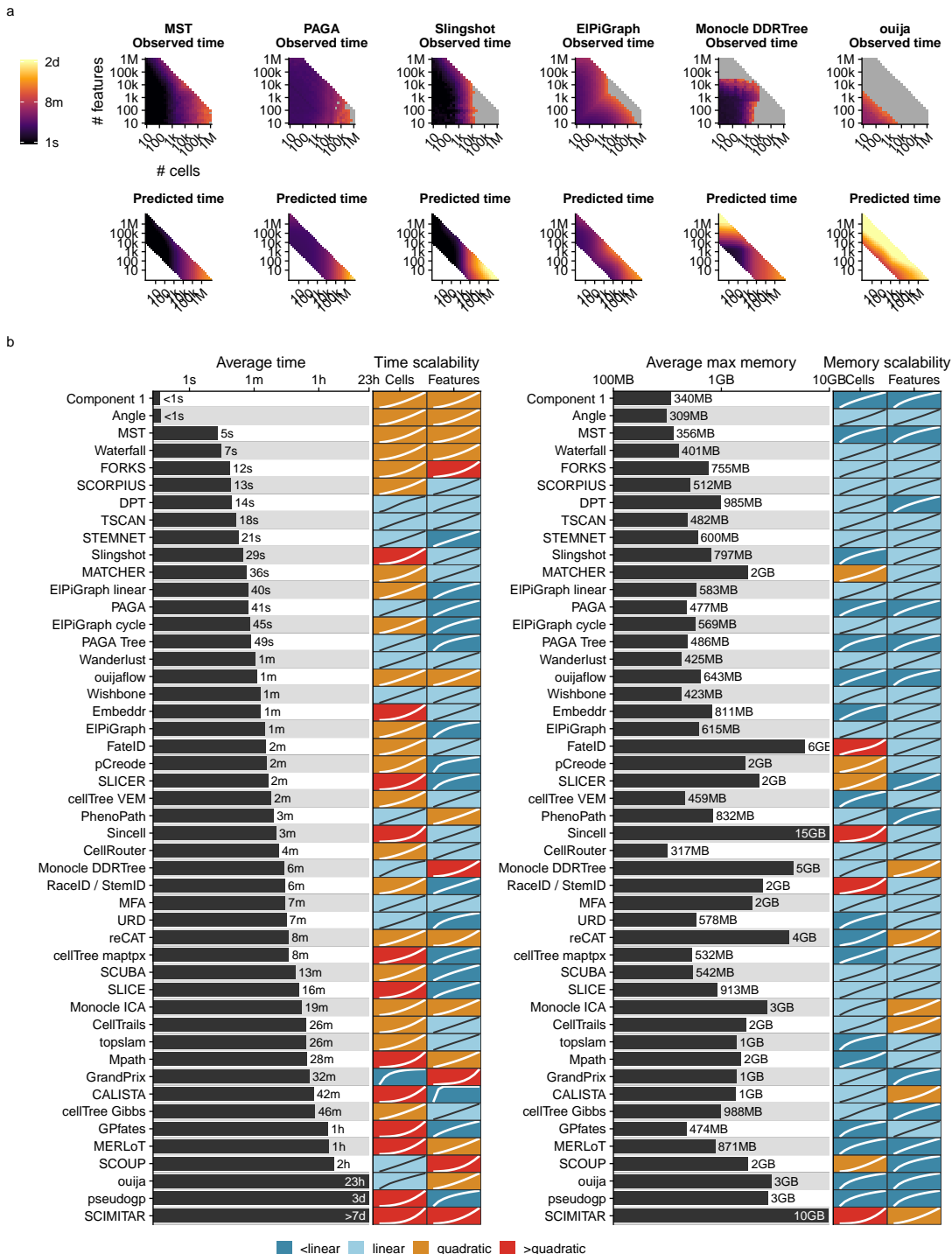


Figure 3.7: Scalability of trajectory inference methods. **a** Three examples of average observed running times across five datasets (left) and the predicted running time (right). **b** Overview of the scalability results of all methods, ordered by their average predicted running time from (a). We predicted execution times and memory usage for each method with increasing number of features or cells, and used these values to classify each method into sublinear, linear, quadratic and superquadratic based on the shape of the curve.

particular were problematic areas, notwithstanding several studies pinpointing these as good practices [41, 42]. Only two methods had a nearly perfect usability score (Slingshot and Celltrails), and these could be used as an inspiration for future methods. We observed no clear relation between usability and method accuracy or usability (Figure 3.3b).

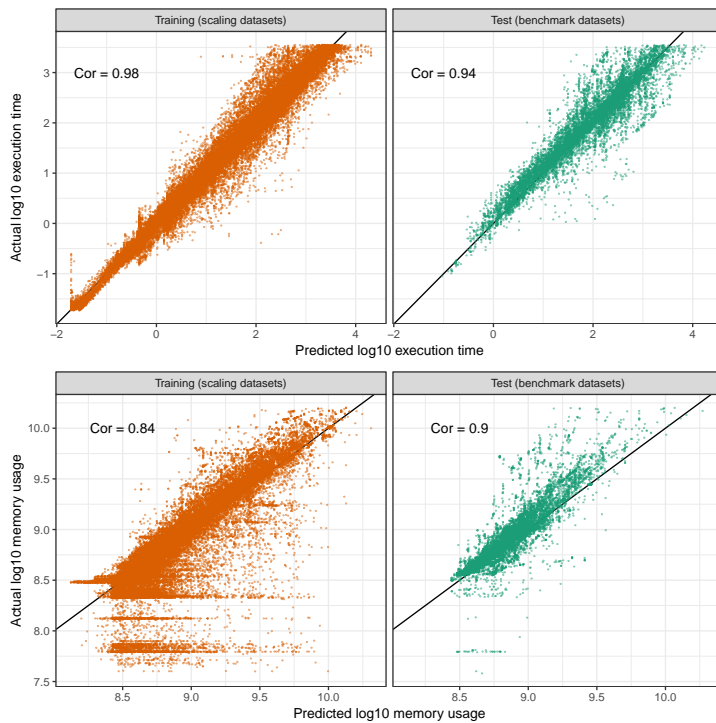


Figure 3.8: Agreement between actual values and predictions for execution times and memory usage. We created a predictive model of the running time and memory usage based on a set of scaling datasets (left), and validated this model based on the similarity of the predictions and actual values on all benchmark datasets (right). Shown are the values for each method and dataset ($n = 65618$ for training, $n = 11939$ for test). Top left indicates the Pearson correlation coefficient.

3.3 Discussion

In this study, we presented a large-scale evaluation of the performance of 45 TI methods. By using a common trajectory representation and four metrics to compare the methods' outputs, we were able to assess the accuracy of the methods on more than 200 datasets. We also assessed several other important quality measures, such as the quality of the method's implementation, the scalability to hundreds of thousands of cells and the stability of the output on small variations of the datasets.

Based on the results of our benchmark, we propose a set of practical guidelines for method users (Figure 3.10 and guidelines.dynverse.org). We postulate that, as a method's performance is heavily dependent on the trajectory type being studied, the choice of method should currently be primarily driven by the anticipated trajectory topology in the data. For most use cases, the user will know very little about the expected trajectory, except perhaps whether the data is expected to contain multiple disconnected trajectories, cycles or a complex tree structure. In each of these use cases, our evaluation suggests a different set of optimal methods, as shown in Figure 3.10. Several other factors will also impact the choice of methods, such as the dimensions of the dataset and the prior information that is available. These factors and several others can all be dynamically explored in our interactive app (guidelines.dynverse.org). This app can also be used to query the results of this evaluation, such as filtering the datasets or changing the importance of the evaluation metrics for the final ranking.

When inferring a trajectory on a dataset of interest, it is important to take two further points into account. First, it is critical that a trajectory, and the downstream results and/or hypotheses originating from it, are confirmed by multiple TI methods. This is to make sure that the prediction is not biased

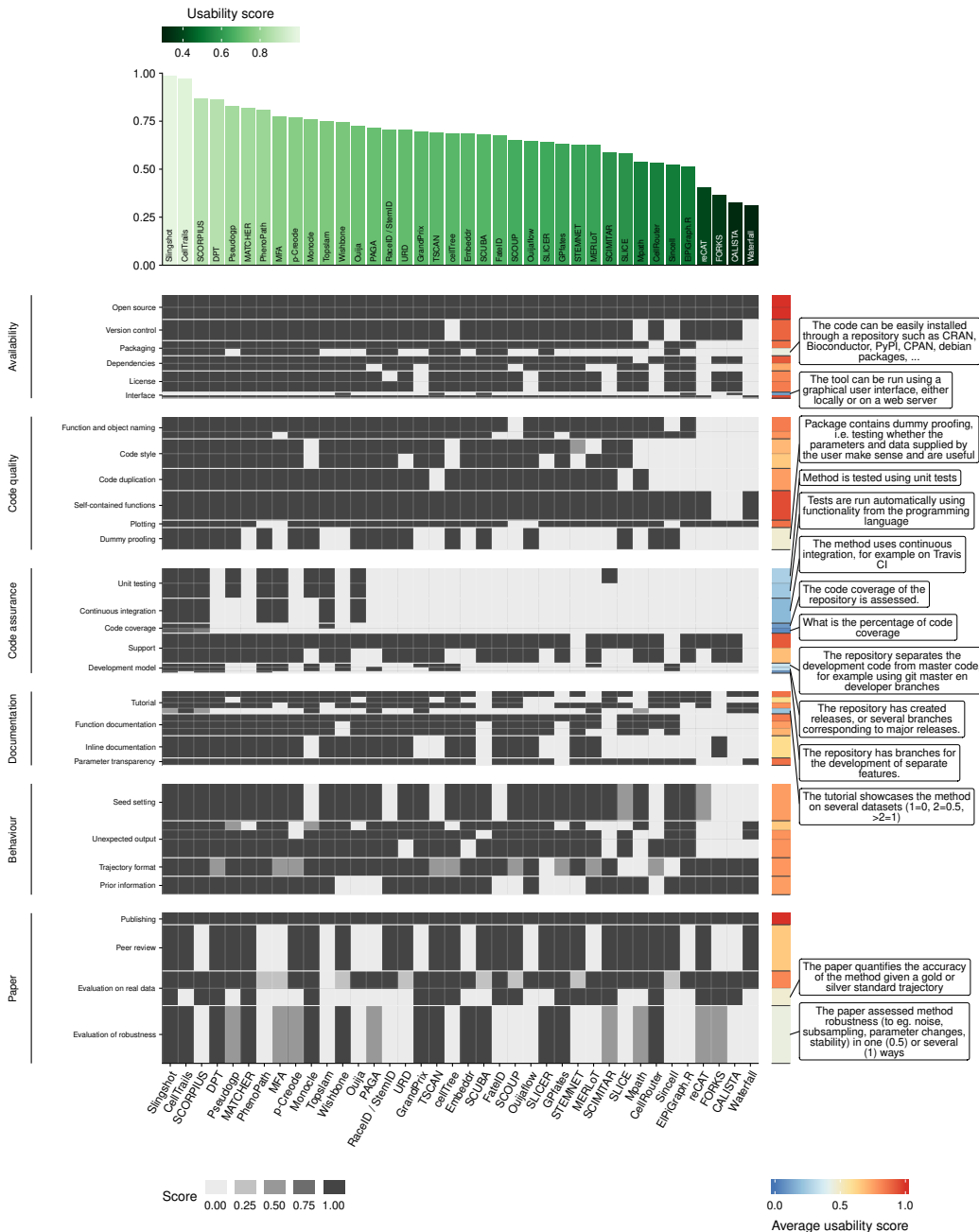


Figure 3.9: Usability of trajectory inference methods. Shown is the score given for each method on every item from the usability score sheet (Table 3.1). Each aspect of the quality control was part of a category, and each category was weighted so that it contributed equally to the final quality score. Within each category, each aspect also received a weight depending on how often it was mentioned in a set of papers discussing good practices in tool development and evaluation. This is represented in the plot as the height on the y-axis. Top: Average usability score for each method. Right: The average score of each quality control item. Shown into more detail are those items which had an average score lower than 0.5.

due to the given parameter setting or the particular algorithm underlying a TI method. The value of using different methods is further supported by our analysis indicating substantial complementarity between the different methods. Second, even if the expected topology is known, it can be beneficial to also try out methods that make less assumptions about the trajectory topology. When the expected topology is confirmed using such a method, it provides additional evidence to the user. When a more complex topology is produced, this could indicate that the underlying biology is much more complex than anticipated by the user.

Table 3.1: Scoring sheet for assessing usability of trajectory inference methods. Each quality aspect was given a weight based on how many times it was mentioned in a set of articles discussing best practices for tool development.

Aspect	Items	References
Availability		
Open source	(1) Method's code is freely available (2) The code can be run on a freely available platform	[43, 41, 39, 44, 42, 45, 46]
Version control	The code is available on a public version controlled repository, such as Github	[43, 41, 39, 44, 42, 45]
Packaging	(1) The code is provided as a "package", exposing functionality through functions or shell commands (2) The code can be easily installed through a repository such as CRAN, Bioconductor, PyPI, CPAN, debian packages, ...	[43, 44, 46, 45]
Dependencies	(1) Dependencies are clearly stated in the tutorial or in the code (2) Dependencies are automatically installed	[39, 44, 42, 47]
License	(1) The code is licensed (2) License allows academic use	[43, 39, 44, 42, 45, 46]
Interface	(1) The tool can be run using a graphical user interface, either locally or on a web server (2) The tool can be run through the command line or through a programming language	[45]
Code quality		
Function and object naming	(1) Functions/commands have well chosen names (2) Arguments/parameters have well chosen names	[41, 44]
Code style	(1) Code has a consistent style (2) Code follows (basic) good practices in the programming language of choice, for example PEP8 or the tidyverse style guide	[41, 44, 42]
Code duplication	Duplicated code is minimal	[41, 44]
Self-contained functions	The method is exposed to the user as self-contained functions or commands	[48, 39, 45]
Plotting	Plotting functions are provided for the final and/or intermediate results	
Dummy proofing	Package contains dummy proofing, i.e. testing whether the parameters and data supplied by the user make sense and are useful	[43, 47]
Code assurance		
Unit testing	Method is tested using unit tests	[43, 41, 48, 44, 45]
Unit testing	Tests are run automatically using functionality from the programming language	[43, 41, 48, 44, 45]
Continuous integration	The method uses continuous integration, for example on Travis CI	[49, 44, 42, 45]
Code coverage	(1) The code coverage of the repository is assessed. (2) What is the percentage of code coverage	
Documentation		
Support	(1) There is a support ticket system, for example on Github (2) The authors respond to tickets and issues are resolved within a reasonable time frame	[41, 44, 42, 45, 46]
Development model	(1) The repository separates the development code from master code, for example using git master en developer branches (2) The repository has created releases, or several branches corresponding to major releases. (3) The repository has branches for the development of separate features.	[50]
Tutorial	(1) A tutorial or vignette is available (2) The tutorial has example results (3) The tutorial has real example data (4) The tutorial showcases the method on several datasets ($1=0, 2=0.5, >2=1$)	[44, 45, 46, 47, 51]
Function documentation	(1) The purpose and usage of functions/commands is documented (2) The parameters of functions/commands are documented (3) The output of functions/commands is documented	[41, 39, 44, 45, 47]
Inline documentation	Inline documentation is present in the code	[41, 39, 44, 45, 47]
Parameter transparency	All important parameters are exposed to the user	[39]
Behaviour		
Seed setting	The method does not artificially become deterministic (1), for example by setting some (0.5) or a lot (0) of seeds	[52]
Unexpected output	(1) No unexpected output messages are generated by the method (2) No unexpected files, folders or plots are generated (3) No unexpected warnings during runtime or compilation are generated	[42]
Trajectory format	The postprocessing necessary to extract the relevant output from the method is minimal (1), moderate (0.5) or extensive (0)	
Prior information	Prior information is required (0), optional (1) or not required (1)	
Paper		
Publishing	The method is published	
Peer review	The paper is published in a peer-reviewed journal	[47, 53, 54]
Evaluation on real data	(1) The paper shows the method's usefulness on several (1), one (0.25) or no real datasets. (2) The paper quantifies the accuracy of the method given a gold or silver standard trajectory	[55, 56]
Evaluation of robustness	The paper assessed method robustness (to eg. noise, subsampling, parameter changes, stability) in one (0.5) or several (1) ways	[47, 55, 51, 56]

Critical to the broad applicability of TI methods is the standardization of the input and output interfaces of TI methods, so that users can effortlessly execute TI methods on their dataset of interest, compare different predicted trajectories and apply downstream analyses, such as finding genes important for the trajectory, network inference [11] or finding modules of genes [57]. Our framework

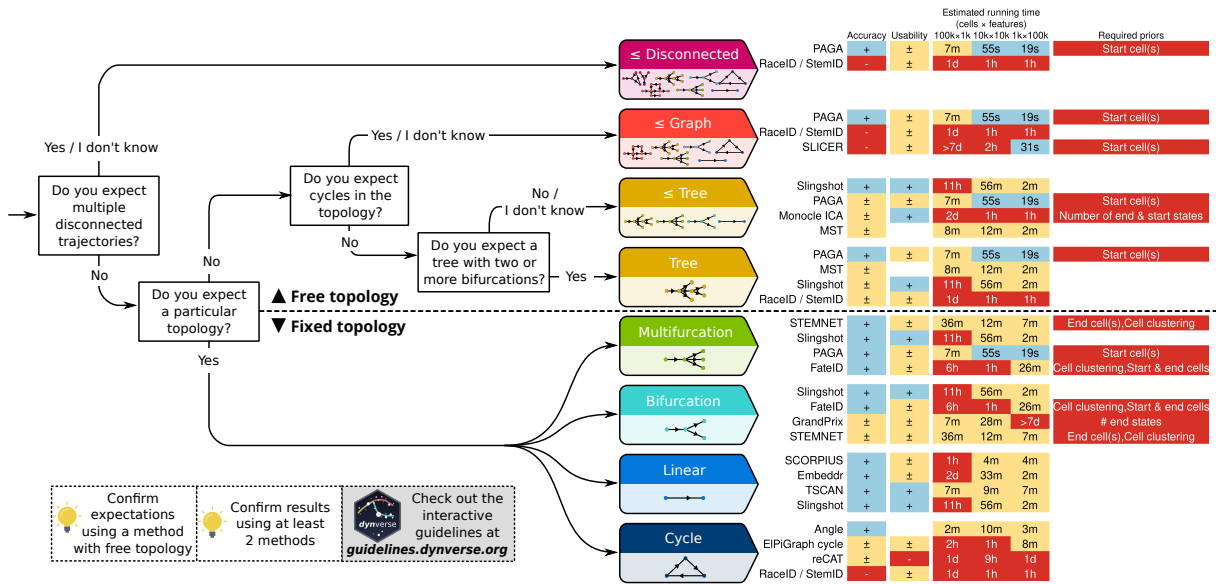


Figure 3.10: Practical guidelines for method users. As the performance of a method mostly depends on the topology of the trajectory, the choice of TI method will be primarily influenced by the user's existing knowledge about the expected topology in the data. We therefore devised a set of practical guidelines, which combines the method's performance, user friendliness and the number of assumptions a user is willing to make about the topology of the trajectory. Methods to the right are ranked according to their performance on a particular (set of) trajectory type. Further to the right are shown the accuracy (+: scaled performance ≥ 0.9 , \pm : >0.6), usability scores (+: ≥ 0.9 , \pm : >0.6), estimated running times and required prior information. k, thousands; m, millions.

is an initial attempt at tackling this problem, and we illustrate its usefulness here by comparing the predicted trajectories of several top-performing methods on datasets containing a linear, tree, cyclic and disconnected graph topology (Figure 3.11). Using our framework, this figure can be recreated using only a couple of lines of R code (<https://methods.dynverse.org>). In the future, this framework could be extended to allow additional input data, such as spatial and RNA velocity information [58], and easier downstream analyses. In addition, further discussion within the field is required to arrive at a consensus concerning a common interface for trajectory models, which can include additional features such as uncertainty and gene importance.

Our study indicates that the field of trajectory inference is maturing, primarily for linear and bifurcating trajectories (Figure 3.11a,b). However, we also highlight several ongoing challenges, which should be addressed before TI can be a reliable tool for analyzing single-cell omics datasets with complex trajectories. Foremost, new methods should focus on improving the unbiased inference of tree, cyclic graph and disconnected topologies, as we found that methods repeatedly overestimate or underestimate the complexity of the underlying topology, even if the trajectory could easily be identified using a dimensionality reduction method (Figure 3.11c,d). Furthermore, higher standards for code assurance and documentation could help in adopting these tools across the single-cell omics field. Finally, new tools should be designed to scale well with the increasing number of cells and features. We found that only a handful of current methods can handle datasets with more than 10,000 cells within a reasonable time frame. To support the development of these new tools, we provide a series of vignettes on how to wrap and evaluate a method on the different measures proposed in this study at <https://benchmark.dynverse.org>.

We found that the performance of a method can be very variable between datasets, and therefore included a large set of both real and synthetic data within our evaluation, leading to a robust overall

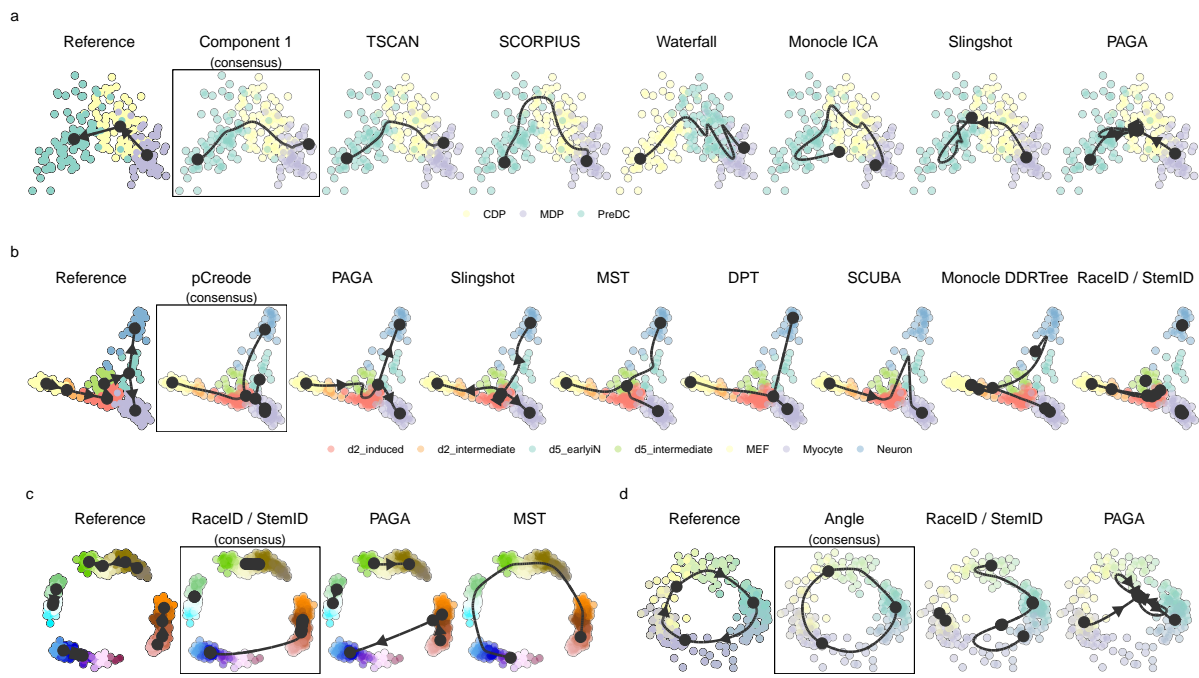


Figure 3.11: Demonstration of how a common framework for TI methods facilitates broad applicability using some example datasets. Trajectories inferred by each method were projected to a common dimensionality reduction using multidimensional scaling. For each dataset, we also calculated a ‘consensus’ prediction, by calculating the cordist between each pair of models and picking the model with the highest score on average. **a**, The top methods applied on a dataset containing a linear trajectory of differentiation dendritic cells, going from MDP, CDP to PreDC. **b**, The top methods applied on a dataset containing a bifurcating trajectory of reprogrammed fibroblasts. **c**, A synthetic dataset generated by dyntoy, containing four disconnected trajectories. **d**, A synthetic dataset generated by dyngen, containing a cyclic trajectory.

ranking of the different methods. However, ‘good-yet-not-the-best’ methods [59] can still provide a very valuable contribution to the field, especially if they make use of novel algorithms, return a more scalable solution or provide a unique insight in specific use cases. This is also supported by our analysis of method complementarity. Some examples for the latter include PhenoPath, which can include additional covariates in its model, ouija, which returns a measure of uncertainty of each cell’s position within the trajectory, and StemID, which can infer the directionality of edges within the trajectory.

3.4 Methods

3.4.1 Trajectory inference methods

We gathered a list of 71 trajectory inference tools (Supplementary Table 1) by searching the literature for ‘trajectory inference’ and ‘pseudotemporal ordering’, and based on two existing lists found online: [awesome-single-cell](#) [17] and [single-cell-pseudotime](#) [60]. We welcome any contributions by creating an issue at <https://methods.dynverse.org>.

Methods were excluded from the evaluation based on several criteria: (1) not freely available; (2) no code available; (3) superseded by another method; (4) requires data types other than expression; (5) no programming interface; (6) unresolved errors during wrapping; (7) too slow (requires more than 1 h on a 100×100 dataset); (8) does not return an ordering; and (9) requires additional user input during

the algorithm (other than prior information). The discussions on why these methods were excluded can be found at <https://github.com/dynverse/dynmethods/issues?q=label:unwrappable>. In the end, we included 45 methods in the evaluation.

3.4.2 Method wrappers

To make it easy to run each method in a reproducible manner, each method was wrapped within Docker and singularity containers (available at <https://methods.dynverse.org>). These containers are automatically built and tested using Travis continuous integration (<https://travis-ci.org/dynverse>) and can be ran using both Docker and Singularity. For each method, we wrote a wrapper script based on example scripts or tutorials provided by the authors (as mentioned in the respective wrapper scripts). This script reads in the input data, runs the method and outputs the files required to construct a trajectory. We also created a script to generate an example dataset, which is used for automated testing.

We used the Github issues system to contact the authors of each method, and asked for feedback on the wrappers, the metadata and the usability scores. About one-third of the authors responded and we improved the wrappers based on their feedback. These discussions can be viewed on Github: https://github.com/dynverse/dynmethods/issues?q=label:method_discussion

Method input

As input, we provided each method with either the raw count data (after cell and gene filtering) or normalized expression values, based on the description in the method documentation or from the study describing the method. A large portion of the methods requires some form of prior information (for example, a start cell) to be executable. Other methods optionally allow the exploitation of certain prior information. Prior information can be supplied as a starting cell from which the trajectory will originate, a set of important marker genes or even a grouping of cells into cell states. Providing prior information to a TI method can be both a blessing and a curse. In one way, prior information can help the method to find the correct trajectory among many, equally likely, alternatives. On the other hand, incorrect or noisy prior information can bias the trajectory towards current knowledge. Moreover, prior information is not always easily available, and its subjectivity can therefore lead to multiple equally plausible solutions, restricting the applicability of such TI methods to well-studied systems.

The prior information was extracted from the reference trajectory as follows:

- **Start cells:** the identity of one or more start cells. For both real and synthetic data, a cell was chosen that was the closest (in geodesic distance) to each milestone with only outgoing edges. For ties, one random cell was chosen. For cyclic datasets, a random cell was chosen.
- **End cells:** the identity of one or more end cells. This is similar to the start cells, but now for every state with only incoming edges.
- **No. of end states:** number of terminal states, i.e., the number of milestones with only incoming edges.
- **Grouping:** for each cell a label showing which state/cluster/branch it belongs to. For real data, the states were from the gold/silver standard. For synthetic data, each milestone was seen as one group and cells were assigned to their closest milestone.

- **No. of branches:** number of branches/intermediate states. For real data, this was the number of states in the gold/silver standard. For synthetic data, this was the number of milestones.
- **Discrete time course:** for each cell a time point from which it was sampled. If available, this was directly extracted from the reference trajectory; otherwise the geodesic distance from the root milestone was used. For synthetic data, the simulation time was uniformly discretized into four timepoints.
- **Continuous time course:** for each cell a time point from which it was sampled. For real data, this was equal to the discrete time course. For synthetic data, we used the internal simulation time of each simulator.

Common trajectory model

Due to the absence of a common format for trajectory models, most methods return a unique set of output formats with few overlaps. We therefore post-processed the output of each method into a common probabilistic trajectory model (Figure 3.2a). This model consisted of three parts. (1) The milestone network represents the overall network topology, and contains edges between different milestones and the length of the edge between them. (2) The milestone percentages contain, for each cell, its position between milestones and sums for each cell to one. (3) The regions of delayed commitment define connections between three or more milestones. These must be explicitly defined in the trajectory model and per region one milestone must be directly connected to all other milestones of the region.

Depending on the output of a method, we used different strategies to convert the output to our model (Figure 3.2b). Special conversions are denoted by an asterisk and will be explained in more detail in the second list below.

- **Type 1, direct:** CALISTA*, DPT*, ElPiGraph, ElPiGraph cycle, ElPiGraph linear, MERLoT, PAGA, SLICE*, Slingshot, URD* and Wishbone. The wrapped method directly returned a network of milestones, the regions of delayed commitment and for each cell it is given to what extent it belongs to a milestone. In some cases, this indicates that additional transformations were required for the method, not covered by any of the following output formats. Some methods returned a branch network instead of a milestone network and this network was converted by calculating the line graph of the branch network.
- **Type 2, linear pseudotime:** Component 1, Embeddr, FORKS, MATCHER, ouija, ouijaflow, PhenoPath, pseudogp, SCIMITAR, SCORPIUS, topslam, TSCAN, Wanderlust and Waterfall. The method returned a pseudotime, which is translated into a linear trajectory where the milestone network contains two milestones and cells are positioned between these two milestones.
- **Type 3, cyclical pseudotime:** Angle and reCAT. The method returned a pseudotime, which is translated into a cyclical trajectory where the milestone network contains three milestones and cells are positioned between these three milestones. These milestones were positioned at pseudotime 0, 1/3 and 2/3.
- **Type 4, end state probability:** FateID, GPfates, GrandPrix, MFA*, SCOUPE and STEMNET. The method returned a pseudotime and for each cell and end state a probability (Pr) for how likely a cell will end up in a certain end state. This was translated into a star-shaped milestone network, with one starting milestone (M_0) and several outer milestones (M_i), with regions of delayed commitment between all milestones. The milestone percentage of a cell to one of the outer

milestones was equal to pseudotime \times PrMi. The milestone percentage to the starting milestone was equal to $1 - \text{pseudotime}$.

- **Type 5, cluster assignment:** Mpath and SCUBA. The method returned a milestone network and an assignment of each cell to a specific milestone. Cells were positioned onto the milestones they are assigned to, with milestone percentage equal to 1.
- **Type 6, orthogonal projection:** MST, pCreode and RacelID/StemID. The method returned a milestone network, and a dimensionality reduction of the cells and milestones. The cells were projected to the closest nearest segment, thus determining the cells' position along the milestone network. If a method also returned a cluster assignment (type 5), we limited the projection of each cell to the closest edge connecting to the milestone of a cell. For these methods, we usually wrote two wrappers, one which included the projection and one without.
- **Type 7, cell graph:** CellRouter, CellTrails, cellTree Gibbs, cellTree maptpx, cellTree VEM, Monocle DDRTree, Monocle ICA, Sincell* and SLICER. The method returned a network of cells and which cell–cell transitions were part of the ‘backbone’ structure. Backbone cells with degree $\neq 2$ were regarded as milestones and all other cells were placed on transitions between the milestones. If a method did not return a distance between pairs of cells, the cells were uniformly positioned between the two milestones. Otherwise, we first calculated the distance between two milestones as the sum of the distances between the cells and then divided the distance of each pair of cells with the total distance to get the milestone percentages.

Special conversions were necessary for certain methods:

- **CALISTA:** We assigned the cells to the branch at which the sum of the cluster probabilities of two connected milestones was the highest. The cluster probabilities of the two selected milestones were then used as milestone percentages. This was then processed as a type 1, direct, method.
- **DPT:** We projected the cells onto the cluster network, consisting of a central milestone (this cluster contained the cells that were assigned to the ‘unknown’ branch) and three terminal milestones, each corresponding to a tip point. This was then processed as a type 1, direct, method.
- **Sincell:** To constrain the number of milestones this method creates, we merged two cell clusters iteratively until the percentage of leaf nodes was below a certain cutoff, with the default cutoff set to 25%. This was then processed as a type 7, cell graph, method.
- **SLICE:** As discussed in the vignette of SLICE (<https://research.cchmc.org/pbge/slice.html>), we ran principal curves one by one for every edge detected by SLICE. This was then processed as a type 1, direct, method.
- **MFA:** We used the branch assignment as state probabilities, which together with the global pseudotime were processed as a type 4, end state probabilities, method.
- **URD:** We extracted the pseudotime of a cell within each branch using the y positions in the tree layout. This was then further processed as a type 1, direct, method.

More information on how each method was wrapped can be found within the comments of each wrapper script, listed at <https://methods.dynverse.org>.

Off-the-shelf methods

For baseline performance, we added several ‘off-the-shelf’ TI methods that can be run using a few lines of code in R.

- **Component 1:** This method returns the first component of a principal component analysis (PCA) dimensionality reduction as a linear trajectory. This method is especially relevant as it has been used in a few studies already [61, 62].
- **Angle:** Similar to the previous method, this method computes the angle with respect to the origin in a two-dimensional PCA and uses this angle as a pseudotime for generating a cyclical trajectory.
- **MST:** This method performs PCA dimensionality reduction, followed by clustering using the R mclust package, after which the clusters are connected using a minimum spanning tree. The trees are orthogonally projected to the nearest segment of the tree. This baseline is highly relevant as many methods follow the same methodology: dimensionality reduction, clustering, topology inference and project cells to topology.

3.4.3 Trajectory types

We classified all possible trajectory topologies into distinct trajectory types, based on topological criteria (Figure 3.1c). These trajectory types start from the most general trajectory type, a disconnected graph, and move down (within a directed acyclic graph structure), progressively becoming more simple until the two basic types are reached: linear and cyclical. A disconnected graph is a graph in which only one edge can exist between two nodes. A (connected) graph is a disconnected graph in which all nodes are connected. An acyclic graph is a graph containing no cycles. A tree is an acyclic graph containing no convergences (no nodes with in-degree higher than 1). A convergence is an acyclic graph in which only one node has a degree larger than 1 and this same node has an in-degree of 1. A multifurcation is a tree in which only one node has a degree larger than 1. A bifurcation is a multifurcation in which only one node has a degree equal to 3. A linear topology is a graph in which no node has a degree larger than 3. Finally, a cycle is a connected graph in which every node has a degree equal to 2. In most cases, a method that was able to detect a complex trajectory type was also able to detect less complex trajectory types, with some exceptions shown in Figure 3.3a.

For simplicity, we merged the bifurcation and convergence trajectory type, and the acyclic graph and connected graph trajectory type in the main figures of the paper.

3.4.4 Real datasets

We gathered real datasets by searching for ‘single-cell’ at the Gene Expression Omnibus and selecting those datasets in which the cells are sampled from different stages in a dynamic process (Supplementary Table 2). The scripts to download and process these datasets are available on our repository (<https://benchmark.dynverse.org/tree/master/scripts/01-datasets>). Whenever possible, we preferred to start from the raw counts data. These raw counts were all normalized and filtered using a common pipeline, as discussed later. Some original datasets contained more than one trajectory, in which case we split the dataset into its separate connected trajectory, but also generated several combinations of connected trajectories to include some datasets with disconnected trajectories in the evaluation. In the end, we included 110 datasets for this evaluation.

For each dataset, we extracted a reference trajectory, consisting of two parts: the cellular grouping (milestones) and the connections between these groups (milestone network). The cellular grouping was provided by the authors of the original study, and we classified it as a gold standard when it was created independently from the expression matrix (such as from cell sorting, the origin of the sample, the time it was sampled or cellular mixing) or as a silver standard otherwise (usually by clustering the expression values). To connect these cell groups, we used the original study to determine the network that the authors validated or otherwise found to be the most likely. In the end, each group of cells was placed on a milestone, having a percentage of 1 for that particular milestone. The known connections between these groups were used to construct the milestone network. If there was biological or experimental time data available, we used this as the length of the edge; otherwise we set all the lengths equal to one.

3.4.5 Synthetic datasets

To generate synthetic datasets, we used four different synthetic data simulators:

- **dyngen**: simulations of gene regulatory networks, available at <https://github.com/dynverse/dyngen>
- **dyntoy**: random gradients of expression in the reduced space, available at <https://github.com/dynverse/dyntoy>
- **PROSTT**: expression is sampled from a linear model that depends on pseudotime [63]
- **Splatter**: simulations of non-linear paths between different expression states [35]

For every simulator, we took great care to make the datasets as realistic as possible. To do this, we extracted several parameters from all real datasets. We calculated the number of differentially expressed features within a trajectory using a two-way Mann–Whitney U test between every pair of cell groups. These values were corrected for multiple testing using the Benjamini-Hochberg procedure (FDR < 0.05) and we required that a gene was expressed in at least 5% of cells, and had at least a fold-change of 2. We also calculated several other parameters, such as drop-out rates and library sizes using the Splatter package [35]. These parameters were then given to the simulators when applicable, as described for each simulator below. Not every real dataset was selected to serve as a reference for a synthetic dataset. Instead, we chose a set of ten distinct reference real datasets by clustering all the parameters of each real dataset, and used the reference real datasets at the cluster centers from a pam clustering (with $k = 10$, implemented in the R cluster package) to generate synthetic data.

dyngen

The dyngen (<https://github.com/dynverse/dyngen>) workflow to generate synthetic data is based on the well established workflow used in the evaluation of network inference methods [34, 64] and consists of four main steps: network generation, simulation, gold standard extraction and simulation of the scRNA-seq experiment. At every step, we tried to mirror real regulatory networks, while keeping the model simple and easily extendable. We simulated a total of 110 datasets, with 11 different topologies.

Network generation

One of the main processes involved in cellular dynamic processes is gene regulation, where regulatory cascades and feedback loops lead to progressive changes in expression and decision making. The exact way a cell chooses a certain path during its differentiation is still an active research field, although certain models have already emerged and been tested *in vivo*. One driver of bifurcation seems to be mutual antagonism, where genes [65] strongly repress each other, forcing one of the two to become inactive [66]. Such mutual antagonism can be modelled and simulated [67, 68]. Although such a two-gene model is simple and elegant, the reality is frequently more complex, with multiple genes (grouped into modules) repressing each other [69].

To simulate certain trajectory topologies, we therefore designed module networks in which the cells follow a particular trajectory topology given certain parameters. Two module networks generated linear trajectories (linear and linear long), one generated a bifurcation, one generated a convergence, one generated a multifurcation (trifurcating), two generated a tree (consecutive bifurcating and binary tree), one generated an acyclic graph (bifurcating and converging), one generated a complex fork (trifurcating), one generated a rooted tree (consecutive bifurcating) and two generated simple graph structures (bifurcating loop and bifurcating cycle). The structure of these module networks is available at https://github.com/dynverse/dyngen/tree/master/inst/ext_data/modulenetworks.

From these module networks we generated gene regulatory networks in two steps: the main regulatory network was first generated, and extra target genes from real regulatory networks were added. For each dataset, we used the same number of genes as were differentially expressed in the real datasets. 5% of the genes were assigned to be part of the main regulatory network, and were randomly distributed among all modules (with at least one gene per module). We sampled edges between these individual genes (according to the module network) using a uniform distribution between 1 and the number of possible targets in each module. To add additional target genes to the network, we assigned every regulator from the network to a real regulator in a real network (from regulatory circuits [70]), and extracted for every regulator a local network around it using personalized pagerank (with damping factor set to 0.1), as implemented in the `page_rank` function of the `igraph` package.

Simulation of gene regulatory systems using thermodynamic models

To simulate the gene regulatory network, we used a system of differential equations similar to those used in evaluations of gene regulatory network inference methods [64]. In this model, the changes in gene expression (x_i) and protein expression (y_i) are modeled using ordinary differential equations [34] (ODEs):

$$\begin{aligned}\frac{dx_i}{dt} &= \underbrace{m \times f(y_1, y_2, \dots)}_{\text{production}} - \underbrace{\lambda \times x_i}_{\text{degradation}} \\ \frac{dy_i}{dt} &= \underbrace{r \times x_i}_{\text{production}} - \underbrace{\Lambda \times y_i}_{\text{degradation}}\end{aligned}$$

where m , λ , r and Λ represent production and degradation rates, the ratio of which determines the maximal gene and protein expression. The two types of equations are coupled because the production of protein y_i depends on the amount of gene expression x_i , which in turn depends on the amount of other proteins through the activation function $f(y_1, y_2, \dots)$.

The activation function is inspired by a thermodynamic model of gene regulation, in which the pro-

moter of a gene can be bound or unbound by a set of transcription factors, each representing a certain state of the promoter. Each state is linked with a relative activation α_j , a number between 0 and 1 representing the activity of the promoter at this particular state. The production rate of the gene is calculated by combining the probabilities of the promoter being in each state with the relative activation:

$$f(y_1, y_2, \dots, y_n) = \sum_{j \in \{0,1,\dots,n^2\}} \alpha_j \times P_j$$

The probability of being in a state is based on the thermodynamics of transcription factor binding. When only one transcription factor is bound in a state:

$$P_j \propto \nu = \left(\frac{y}{k}\right)^n$$

where the hill coefficient n represents the cooperativity of binding and k the transcription factor concentration at half-maximal binding. When multiple regulators are bound:

$$P_j \propto \nu = \rho \times \prod_j \left(\frac{y_j}{k_j}\right)^{n_j}$$

where ρ represents the cooperativity of binding between the different transcription factors.

P_i is only proportional to ν because ν is normalized such that $\sum_i P_i = 1$.

To each differential equation, we added an additional stochastic term:

$$\begin{aligned} \frac{dx_i}{dt} &= m \times f(y_1, y_2, \dots) - \lambda \times x_i + \eta \times \sqrt{x_i} \times \Delta W_t \\ \frac{dy_i}{dt} &= r \times x_i - \Lambda \times y_i + \eta \times \sqrt{y_i} \times \Delta W_t \end{aligned}$$

with $\Delta W_t \sim \mathcal{N}(0, h)$.

Similar to GeneNetWeaver [34], we sample the different parameters from random distributions, defined as follows. e defines whether a transcription factor activates (1) or represses (-1), as defined within the regulatory network network.

$$\begin{aligned}
r &= \mathcal{U}(10, 200) \\
d &= \mathcal{U}(2, 8) \\
p &= \mathcal{U}(2, 8) \\
q &= \mathcal{U}(1, 5) \\
a_0 &= \begin{cases} 1 & \text{if } |e| = 0 \\ 1 & \text{if } \forall x \in e, x = -1 \\ 0 & \text{if } \forall x \in e, x = 1 \\ 0.5 & \text{otherwise} \end{cases} \\
a_i &= \begin{cases} 0 & \text{if } \exists x \in e_i, x = -1 \\ 1 & \text{otherwise} \end{cases} \\
s &= \mathcal{U}(1, 20) \\
k &= y_{max}/(2 * s), \\
&\quad \text{where } y_{max} = r/d \times p/q \\
c &= \mathcal{U}(1, 4)
\end{aligned}$$

We converted each ODE to an SDE by adding a chemical Langevin equation, as described in [34]. These SDEs were simulated using the Euler–Maruyama approximation, with time-step $h = 0.01$ and noise strength $\eta = 8$. The total simulation time varied between 5 for linear and bifurcating datasets, 10 for consecutive bifurcating, trifurcating and converging datasets, 15 for bifurcating converging datasets and 30 for linear long, cycle and bifurcating loop datasets. The burn-in period was for each simulation 2. Each network was simulated 32 times.

Simulation of the single-cell RNA-seq experiment

For each dataset we sampled the same number of cells as were present in the reference real dataset, limited to the simulation steps after burn-in. These cells were sampled uniformly across the different steps of the 32 simulations. Next, we used the Splatter package [35] to estimate the different characteristics of a real dataset, such as the distributions of average gene expression, library sizes and dropout probabilities. We used Splatter to simulate the expression levels $\lambda_{i,j}$ of housekeeping genes i (to match the number of genes in the reference dataset) in every cell j . These were combined with the expression levels of the genes simulated within a trajectory. Next, true counts were simulated using $Y'_{i,j} \sim \text{Poisson}(\lambda_{i,j})$. Finally, we simulated dropouts by setting true counts to zero by sampling from a Bernoulli distribution using a dropout probability $\pi_{i,j}^D = \frac{1}{1+e^{-k(\ln(\lambda_{i,j})-x_0)}}$. Both x_0 (the midpoint for the dropout logistic function) and k (the shape of the dropout logistic function) were estimated by Splatter.

This count matrix was then filtered and normalised using the pipeline described below.

Gold standard extraction

Because each cellular simulation follows the trajectory at its own speed, knowing the exact position of a cell within the trajectory topology is not straightforward. Furthermore, the speed at which simulated

cells make a decision between two or more alternative paths is highly variable. We therefore first constructed a backbone expression profile for each branch within the trajectory. To do this, we first defined in which order the expression of the modules is expected to change, and then generated a backbone expression profile in which the expression of these modules increases and decreases smoothly between 0 and 1. We also smoothed the expression in each simulation using a rolling mean with a window of 50 time steps, and then calculated the average module expression along the simulation. We used dynamic time warping, implemented in the dtw R package [71, 72], with an open end to align a simulation to all possible module progressions, and then picked the alignment which minimised the normalised distance between the simulation and the backbone. In case of cyclical trajectory topologies, the number of possible milestones a backbone could progress through was limited to 20.

dyntoy

For more simplistic data generation ("toy" datasets), we created the dyntoy workflow (<https://github.com/dynverse/dyntoy>). We created 12 topology generators (described below), and with 10 datasets per generator, this lead to a total of 120 datasets.

We created a set of topology generators, were $B(n, p)$ denotes a binomial distribution, and $U(a, b)$ denotes a uniform distribution:

- Linear and cyclic, with number of milestones $\sim B(10, 0.25)$
- Bifurcating and converging, with four milestones
- Binary tree, with number of branching points $\sim U(3, 6)$
- Tree, with number of branching points $\sim U(3, 6)$ and maximal degree $\sim U(3, 6)$

For more complex topologies we first calculated a random number of "modifications" $\sim U(3, 6)$ and a $deg_{max} \sim B(10, 0.25) + 1$. For each type of topology, we defined what kind of modifications are possible: divergences, loops, convergences and divergence-convergence. We then iteratively constructed the topology by uniformly sampling from the set of possible modifications, and adding this modification to the existing topology. For a divergence, we connected an existing milestone to a number of new milestones. Conversely, for a convergence we connected a number of new nodes to an existing node. For a loop, we connected two existing milestones with a number of milestones in between. Finally for a divergence-convergence we connected an existing milestone to several new milestones which again converged on a new milestone. The number of nodes was sampled from $\sim B(deg_{max} - 3, 0.25) + 2$

- Looping, allowed loop modifications
- Diverging-converging, allowed divergence and converging modifications
- Diverging with loops, allowed divergence and loop modifications
- Multiple looping, allowed looping modifications
- Connected, allowed looping, divergence and convergence modifications
- Disconnected, number of components sampled from $\sim B(5, 0.25) + 2$, for each component we randomly chose a topology from the ones listed above

After generating the topology, we sampled the length of each edge $\sim U(0.5, 1)$. We added regions of delayed commitment to a divergence in a random half of the cases. We then placed the number of cells (same number as from the reference real dataset), on this topology uniformly, based on the length of the edges in the milestone network.

For each gene (same number as from the reference real dataset), we calculated the Kamada-Kawai layout in 2 dimensions, with edge weight equal to the length of the edge. For this gene, we then extracted for each cell a density value using a bivariate normal distribution with $\mu \sim U(x_{min}, x_{min})$ and $\sigma \sim U(x_{min}/10, x_{min}/8)$. We used this density as input for a zero-inflated negative binomial distribution with $\mu \sim U(100, 1000) \times \text{density}$, $k \sim U(\mu/10, \mu/4)$ and pi from the parameters of the reference real dataset, to get the final count values.

This count matrix was then filtered and normalised using the pipeline described below.

PROSSTT

PROSSTT is a recent data simulator [63], which simulates expression using linear mixtures of expression programs and random walks through the trajectory. We used 5 topology generators from dyntoy (linear, bifurcating, multifurcating, binary tree and tree), and simulated for each topology generator 10 datasets using different reference real datasets. However, due to frequent crashes of the tool, only 19 datasets created output and were thus used in the evaluation.

Using the `simulate_lineage` function, we simulated the lineage expression, with parameters $a \sim U(0.01, 0.1)$, $\text{branch-tol}_{\text{intra}} \sim U(0, 0.9)$ and $\text{branch-tol}_{\text{inter}} \sim U(0, 0.9)$. These parameter distributions were chosen very broad so as to make sure both easy and difficult datasets are simulated. After simulating base gene expression with `simulate_base_gene_exp`, we used the `sample_density` function to finally simulate expression values of a number of cells (the same as from the reference real dataset), with $\alpha \sim \text{Lognormal} (\mu = 0.3 \text{ and } \sigma = 1.5)$ and $\beta \sim \text{Lognormal} (\mu = 2 \text{ and } \sigma = 1.5)$. Each of these parameters were centered around the default values of PROSSTT, but with enough variability to ensure a varied set of datasets.

This count matrix was then filtered and normalised using the pipeline described below.

Splatter

Splatter [35] simulates expression values by constructing non-linear paths between different states, each having a distinct expression profile. We used 5 topology generators from dyntoy (linear, bifurcating, multifurcating, binary tree and tree), and simulated for each topology generator 10 datasets using different reference real datasets, leading to a total of 50 datasets.

We used the `splatSimulatePaths` function from Splatter to simulate datasets, with number of cells and genes equal to those in the reference real dataset, and with parameters `nonlinearProb`, `sigmaFac` and `skew` all sampled from $U(0, 1)$.

3.4.6 Dataset filtering and normalization

We used a standard single-cell RNA-seq preprocessing pipeline that applies parts of the scran and scater Bioconductor packages [73]. The advantages of this pipeline are that it works both with and

without spike-ins, and it includes a harsh cell filtering that looks at abnormalities in library sizes, mitochondrial gene expression and the number of genes expressed using median absolute deviations (which we set to 3). We required that a gene was expressed in at least 5% of the cells and that it should have an average expression higher than 0.02. Furthermore, we used the pipeline to select the most highly variable genes, using a false discovery rate of 5% and a biological component higher than 0.5. As a final filter, we removed both all-zero genes and cells until convergence.

3.4.7 Benchmark metrics

The importance of using multiple metrics to compare complex models has been stated repeatedly [59]. Furthermore, a trajectory is a model with multiple layers of complexity, which calls for several metrics each assessing a different layer. We therefore defined several possible metrics for comparing trajectories, each investigating different layers. These are all discussed in Section 3.5 along with examples and robustness analyses when appropriate.

Next, we created a set of rules to which we think a good trajectory metric should conform, and tested this empirically for each metric by comparing scores before and after perturbing a dataset (Section 3.5). Based on this analysis, we chose four metrics for the evaluation, each assessing a different aspect of the trajectory: (1) the HIM measures the topological similarity; (2) the F1branches compares the branch assignment; (3) the cordist assesses the similarity in pairwise cell–cell distances and thus the cellular positions; and (4) the wcorfeatures looks at whether similar important features (genes) are found in both the reference dataset and the prediction.

The Hamming–Ipsen–Mikhailov metric

The HIM metric [74] uses the two weighted adjacency matrices of the milestone networks as input (weighted by edge length). It is a linear combination of the normalized Hamming distance, which gives an indication of the differences in edge lengths, and the normalized Ipsen–Mikhailov distance, which assesses the similarity in degree distributions. The latter has a parameter γ , which was fixed at 0.1 to make the scores comparable between datasets. We illustrate the metric and discuss alternatives in Section 3.5.

The F1 between branch assignments

To compare branch assignment, we used an F1 score, also used for comparing biclustering methods [57]. To calculate this metric, we first calculated the similarity of all pairs of branches between the two trajectories using the Jaccard similarity. Next, we defined the ‘Recovery’ (respectively ‘Relevance’) as the average maximal similarity of all branches in the reference dataset (respectively prediction). The F1branches was then defined as the harmonic mean between Recovery and Relevance. We illustrate this metric further in Section 3.5.

Correlation between geodesic distances

When the position of a cell is the same in both the reference and the prediction, its relative distances to all other cells in the trajectory should also be the same. This observation is the basis for the cordist metric. To calculate the cordist, we first sampled 100 waypoint cells in both the prediction and the reference dataset, using stratified sampling between the different milestones, edges and regions of

delayed commitment, weighted by the number of cells in each collection. We then calculated the geodesic distances between the union of waypoint cells from both datasets and all other cells. The calculation of the geodesic distance depended on the location of the two cells within the trajectory, further discussed in Section 3.5, and was weighted by the length of the edge in the milestone network. Finally, the cordist was defined as the Spearman rank correlation between the distances of both datasets. We illustrate the metric and assess the effect of the number of waypoint cells in Section 3.5.

The correlation between important features

The wcorfeatures assesses whether the same differentially expressed features are found using the predicted trajectory as in the known trajectory. To calculate this metric, we used Random Forest regression (implemented in the R ranger package [75]), to predict expression values of each gene, based on the geodesic distances of a cell to each milestone. We then extracted feature importance values for each feature and calculated the similarity of the feature importances using a weighted Pearson correlation, weighted by the feature importance in the reference dataset to give more weight to large differences. As hyperparameters we set the number of trees to 10,000 and the number of features on which to split to 1% of all available features. We illustrate this metric and assess the effect of its hyperparameters in Section 3.5.

Score aggregation

To rank methods, we needed to aggregate the different scores on two levels: across datasets and across different metrics. This aggregation strategy is explained in more detail in Section 3.5.

To ensure that easy and difficult datasets have equal influence on the final score, we first normalized the scores on each dataset across the different methods. We shifted and scaled the scores to $\sigma = 1$ and $\mu = 0$, and then applied the unit probability density function of a normal distribution on these values to get the scores back into the [0,1] range.

Since there is a bias in dataset source and trajectory type (for example, there are many more linear datasets), we aggregated the scores per method and dataset in multiple steps. We first aggregated the datasets with the same dataset source and trajectory type using an arithmetic mean of their scores. Next, the scores were averaged over different dataset sources, using an arithmetic mean that was weighted based on how much the synthetic and silver scores correlated with the real gold scores. Finally, the scores were aggregated over the different trajectory types again using an arithmetic mean.

Finally, to get an overall benchmarking score, we aggregated the different metrics using a geometric mean.

3.4.8 Method execution

Each execution of a method on a dataset was performed in a separate task as part of a gridengine job. Each task was allocated one CPU core of an Intel(R) Xeon(R) CPU E5-2665 at 2.40 GHz, and one R session was started for each task. During the execution of a method on a dataset, if the time limit (>1 h) or memory limit (16 GB) was exceeded, or an error was produced, a zero score was returned for that execution.

3.4.9 Complementarity

To assess the complementarity between different methods, we first calculated for every method and dataset whether the overall score was equal to or higher than 95% of the best overall score for that particular dataset. We then calculated for every method the weighted percentage of datasets that fulfilled this rule, weighted similarly as in the benchmark aggregation, and chose the best method. We iteratively added new methods until all methods were selected. For this analysis, we did not include any methods that require any strong prior information and only included methods that could detect the trajectory types present in at least one of the datasets.

3.4.10 Scalability

To assess the scalability of each method, we started from five real datasets, selected using the centers from a k-medoids as discussed before. We up- and downscaled these datasets between 10 and 100,000 cells and 10 and 100,000 features, while never going higher than 1,000,000 values in total. To generate new cells or features, we first generated a 10-nearest-neighbor graph of both the cells and features from the expression space. For every new cell or feature, we used a linear combination of one to three existing cells or features, where each cell or feature was given a weight sampled from a uniform distribution between 0 and 1.

We ran each method on each dataset for maximally 1 h and gave each process 10 GB of memory. To determine the running time of each method, we started the timer right after data loading and the loading of any packages, and stopped the clock before postprocessing and saving of the output. Pre- and postprocessing steps specific to a method, such as dimensionality reduction and gene filtering, were included in the time. To estimate the maximal memory usage, we used the `max_vmem` value from the `qacct` command provided by a gridengine cluster. We acknowledge, however, that these memory estimates are very noisy and the averages provided in this study are therefore only rough estimates.

The relationship between the dimensions of a dataset and the running time or maximal memory usage was modeled using shape constrained additive models [38], with $\log_{10}|\text{cells}|$ and $\log_{10}|\text{features}|$ as predictor variables, and fitted this model using the `scam` function as implemented in the R `scam` package, with $\log_{10}\text{time}$ (or $\log_{10}\text{memory}$) as outcome.

To classify the time complexity of each method with respect to the number of cells, we predicted the running time at 10,000 features with increasing number of cells from 100 to 100,000, with steps of 100. We trained a generalized linear model with the following function: $y \approx \log x + \sqrt{x} + x + x^2 + x^3$ with y as running time and x as the number of cells or features. The time complexity of a method was then classified using the weights w from this model:

$$\left\{ \begin{array}{ll} \text{superquadratic} & \text{if } w_{x^3} > 0.25, \\ \text{quadratic} & \text{if } w_{x^2} > 0.25, \\ \text{linear} & \text{if } w_x > 0.25, \\ \text{sublinear} & \text{if } w_{\log(x)} > 0.25 \text{ or } w_{\sqrt{x}} > 0.25, \\ \text{case with highest weight} & \text{else.} \end{array} \right.$$

This process was repeated for classifying the time complexity with respect to the number of features,

and the memory complexity both with respect to the number of cells and features.

3

3.4.11 Stability

In the ideal case, a method should produce a similar trajectory, even when the input data is slightly different. However, running the method multiple times on the same input data would not be the ideal approach to assess its stability, given that a lot of tools are artificially deterministic by internally resetting the pseudorandom number generator (for example, using the ‘set.seed’ function in R or the ‘random.seed’ function in numpy). To assess the stability of each method, we therefore selected a number of datasets, which consisted of 25% of the datasets accounting for 15% of the total runtime, chosen such that after aggregation the overall scores still has > 0.99 correlation with the original overall ranking. We subsampled each dataset 10 times with 95% of the original cells and 95% of the original features. We ran every method on each of the bootstraps, and assessed the stability by calculating the benchmarking scores between each pair of subsequent models (run i is compared to run $i + 1$). For the cordist and F1branches, we only used the intersection between the cells of two datasets, while the intersection of the features was used for the wcorfeatures.

3.4.12 Usability

We created a transparent scoring scheme to quantify the usability of each method based on several existing tool quality and programming guidelines in the literature and online (Table 3.1). The main goal of this quality control is to stimulate the improvement of current methods, and the development of user- and developer-friendly new methods. The quality control assessed six categories, each looking at several aspects, which are further divided into individual items. The availability category checks whether the method is easily available, whether the code and dependencies can be easily installed, and how the method can be used. The code quality assesses the quality of the code both from a user perspective (function naming, dummy proofing and availability of plotting functions) and a developer perspective (consistent style and code duplication). The code assurance category is frequently overlooked, and checks for code testing, continuous integration [49] and an active support system. The documentation category checks the quality of the documentation, both externally (tutorials and function documentation) and internally (inline documentation). The behavior category assesses the ease by which the method can be run, by looking for unexpected output files and messages, prior information and how easy the trajectory model can be extracted from the output. Finally, we also assessed certain aspects of the study in which the method was proposed, such as publication in a peer-reviewed journal, the number of datasets in which the usefulness of the method was shown and the scope of method evaluation in the paper.

Each quality aspect received a weight depending on how frequently it was found in several papers and online sources that discuss tool quality (Table 3.1). This was to make sure that more important aspects, such as the open source availability of the method, outweighed other less important aspects, such as the availability of a graphical user interface. For each aspect, we also assigned a weight to the individual questions being investigated (Table 3.1). For calculating the final score, we weighed each of the six categories equally.

3.4.13 Guidelines

For each set of outcomes in the guidelines figure, we selected one to four methods, by first filtering the methods on those that can detect all required trajectory types, and ordering the methods according to their average accuracy score on datasets containing these trajectory types (aggregated according to the scheme presented in the section Accuracy).

We used the same approach for selecting the best set of methods in the guidelines app (<http://guidelines.dynverse.org>), developed using the R shiny package. This app will also filter the methods, among other things, depending on the predicted running time and memory requirements, the prior information available and the preferred execution environment (using the dynmethods package or standalone).

3.4.14 Reporting Summary

Further information on research design is available in the Nature Research Reporting Summary, available at <https://www.nature.com/articles/s41587-019-0071-9#MOESM2>.

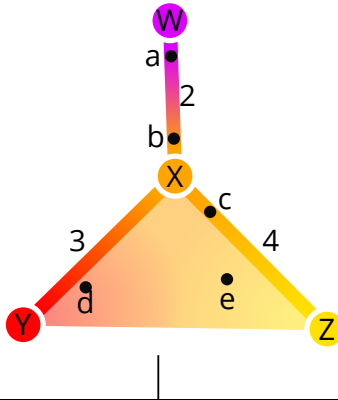
3.5 Supplementary Note 1: Metrics to compare two trajectories

A trajectory, as defined in our evaluation, is a model with multiple abstractions. The top abstraction is the topology which contains information about the paths each cell can take from their starting point. Deeper abstractions involve the mapping of each cell to a particular branch within this network, and the position (or ordering) of each cells within these branches. Internally, the topology is represented by the milestone network and regions of delayed commitment, the branch assignment and cellular positions are represented by the milestone percentages (Figure 3.12).

Given the multilayered complexity of a trajectory model, it is not trivial to compare the similarity of two trajectory models using only one metric. We therefore sought to use different comparison metrics, each serving a different purpose:

- **Specific metrics** investigate one particular aspect of the trajectory. Such metrics make it possible to find particular weak points for methods, e.g. that a method is very good at ordering but does not frequently find the correct topology. Moreover, having multiple individual metrics allow personalised rankings of methods, for example for users which are primarily interested in using the method correct topology.
- **Application metrics** focus on the quality of a downstream analysis using the trajectory. For example, it measures whether the trajectory can be used to find accurate differentially expressed genes.
- **Overall metrics** should capture all the different abstractions, in other words such metrics measure whether the resulting trajectory has a good topology, that the cells belong to similar branches and that they are ordered correctly.

Here, we first describe and illustrate several possible specific, application and overall metrics. Next, we test these metrics on several test cases, to make sure they robustly identify "wrong" trajectory predictions.



Milestone network	Regions of delayed commitment	Branch assignment	Cell positions
from to length	region to is_begin	Represented by the milestone percentages	
W X 2	XYZ X TRUE	cell milestone percentage	
X Y 3	XYZ Y FALSE	a W 0.9	
X Z 4	XYZ Z FALSE	a X 0.1	
		b W 0.2	
		b X 0.8	
		c X 0.8	
		c Z 0.2	
		d X 0.2	
		d Y 0.7	
		d Z 0.1	
		e X 0.3	
		e Y 0.2	
		e Z 0.5	

Figure 3.12: An example trajectory that will be used throughout this section. It contains four milestones (W to Z) and five cells (a to e).

All metrics described here were implemented within the dyneval R package (<https://github.com/dynverse/dyneval>).

3.5.1 Metric characterisation and testing

isomorphic, *edgeflip* and *HIM*: Edit distance between two trajectory topologies

We used three different scores to assess the similarity in the topology between two trajectories, regardless of where the cells were positioned.

For all three scores, we first simplified the topology of the trajectory to make both graph structures comparable:

- As we are only interested in the main structure of the topology without start or end, the graph was made undirected.
- All milestones with degree 2 were removed. For example in the topology $A \Rightarrow B \Rightarrow C \Rightarrow D$, $C \Rightarrow D$, the B milestone was removed
- A linear topology was converted to $A \Rightarrow B \Rightarrow C$
- A cyclical topology such as $A \Rightarrow B \Rightarrow C \Rightarrow D$ or $A \Rightarrow B \Rightarrow A$ were all simplified to $A \Rightarrow B \Rightarrow C \Rightarrow A$
- Duplicated edges such as $A \Rightarrow B$, $A \Rightarrow B$ were decoupled to $A \Rightarrow B$, $A \Rightarrow C \Rightarrow B$

The *isomorphic* score returns 1 if two graphs are isomorphic, and 0 if they were not. For this, we used the BLISS algorithm [76], as implemented in the R **igraph** package.

The *edgeflip* score was defined as the minimal number of edges which should be added or removed to convert one network into the other, divided by the total number of edges in both networks. This problem is equivalent to the maximum common edge subgraph problem, a known NP-hard problem without a scalable solution [77]. We implemented a branch and bound approach for this problem, using several heuristics to speed up the search:

- First check all possible edge additions and removals corresponding to the number of different edges between the two graphs.
- For each possible solution, first check whether:
 1. The maximal degree is the same
 2. The minimal degree is the same
 3. All degrees are the same after sorting
- Only then check if the two graphs are isomorphic as described earlier.
- If no solution is found, check all possible solutions with two extra edge additions/removals.

The *HIM* metric (Hamming-Ipsen-Mikhailov distance) [74] which was adopted from the R nettools package (<https://github.com/filosi/nettools>). It uses an adjacency matrix which was weighted according to the lengths of each edges within the milestone network. Conceptually, *HIM* is a linear combination of:

- The normalised Hamming distance [78], which calculates the distance between two graphs by matching individual edges in the adjacency matrix, but disregards overall structural similarity.
- The normalised Ipsen-Mikhailov distance [79], which calculates the overall distance of two graphs based on matches between its degree and adjacency matrix, while disregarding local structural similarities. It requires a γ parameter, which is usually estimated based on the number of nodes in the graph, but which we fixed at 0.1 so as to make the score comparable across different graph sizes.

We compared the three scores on several common topologies (Figure 3.13a). While conceptually very different, the *edgeflip* and *HIM* still produce similar scores (Figure 3.13b). The *HIM* tends to punish the detection of cycles, while the *edgeflip* is more harsh for differences in the number of bifurcations (Figure 3.13b). The main difference however is that the *HIM* takes into account edge lengths when comparing two trajectories, as illustrated in (Figure 3.13c). Short "extra" edges in the topology are less punished by the *HIM* than by the *edgeflip*.

To summarise, the different topology based scores are useful for different scenarios:

- If the two trajectories should only be compared when the topology is exactly the same, the *isomorphic* should be used.
- If it is important that the topologies are similar, but not necessarily isomorphic, the *edgeflip* is most appropriate.
- If the topologies should be similar, but shorter edges should not be punished as hard as longer edges, the *HIM* is most appropriate.

3

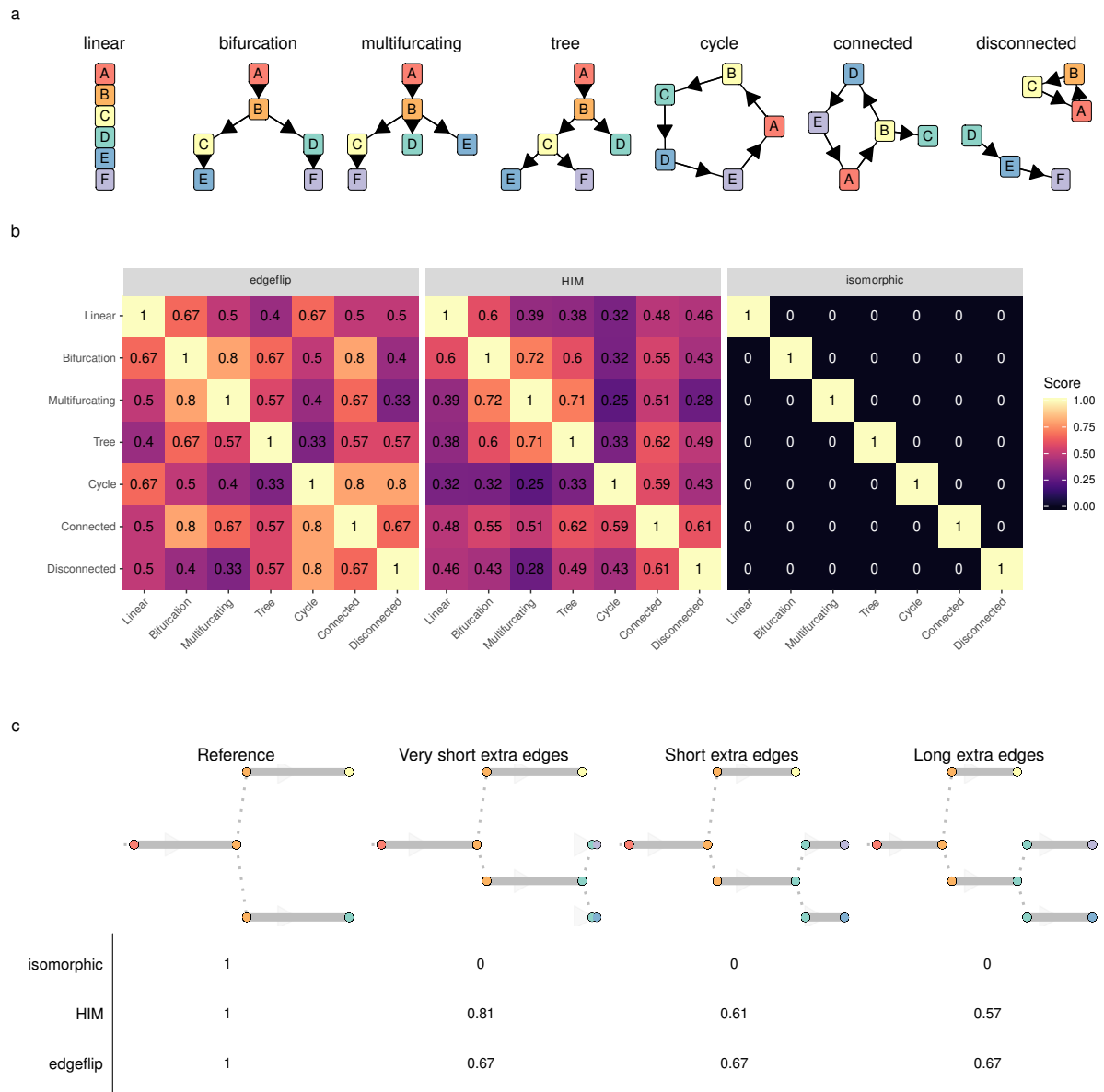


Figure 3.13: Showcase of three metrics to evaluate topologies: *isomorphic*, *edgeflip* and *HIM* (a) The used topologies. (b) The scores when comparing each pair of trajectory types. (c) Four datasets in which an extra edge is added and made progressively longer. This shows how the HIM can take into account edge lengths.

F1_{branches} and F1_{milestones}: Comparing how well the cells are clustered in the trajectory

Perhaps one of the simplest ways to calculate the similarity between the cellular positions of two topologies is by mapping each cell to its closest milestone or branch 3.14. These clusters of cells can then be compared using one of the many external cluster evaluation measures [57]. When selecting a cluster evaluation metric, we had two main conditions:

- Because we allow methods to filter cells in the trajectory, the metric should be able to handle "non-exhaustive assignment", where some cells are not assigned to any cluster.
- The metric should give each cluster equal weight, so that rare cell stages are equally important as large stages.

The *F1* score between the *Recovery* and *Relevance* is a metric which conforms to both these conditions. This metric will map two clustersets by using their shared members based on the Jaccard

similarity. It then calculates the *Recovery* as the average maximal Jaccard for every cluster in the first set of clusters (in our case the reference trajectory). Conversely, the *Relevance* is calculated based on the average maximal similarity in the second set of clusters (in our case the prediction). Both the *Recovery* and *Relevance* are then given equal weight in a harmonic mean ($F1$). Formally, if C and C' are two cell clusters:

$$\text{Jaccard}(c, c') = \frac{|c \cap c'|}{|c \cup c'|}$$

$$\text{Recovery} = \frac{1}{|C|} \sum_{c \in C} \max_{c' \in C'} \text{Jaccard}(c, c')$$

$$\text{Relevance} = \frac{1}{|C'|} \sum_{c' \in C'} \max_{c \in C} \text{Jaccard}(c, c')$$

$$F1 = \frac{2}{\frac{1}{\text{Recovery}} + \frac{1}{\text{Relevance}}}$$

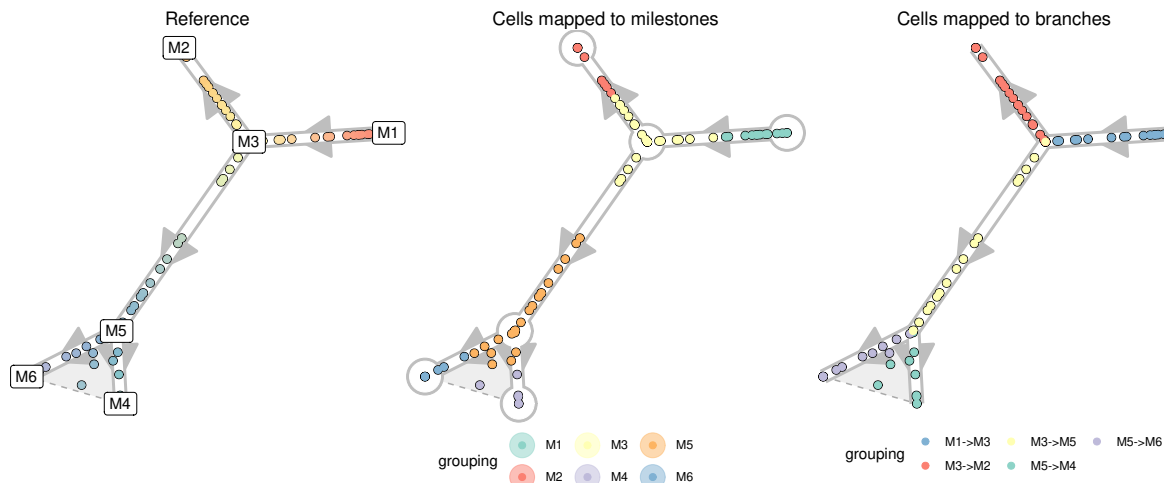


Figure 3.14: Mapping cells to their closest milestone or branch for the calculation of the $F1_{\text{milestones}}$ and $F1_{\text{branches}}$. To calculate the $F1_{\text{milestones}}$, cells are mapped towards the nearest milestone, i.e. the milestone with the highest milestone percentage. For the $F1_{\text{branches}}$, the cells are mapped to the closest edge.

cor_{dist} : Correlation between geodesic distances

When the position of a cell is the same in both the reference and the prediction, its *relative* distances to all other cells in the trajectory should also be the same. This observation is the basis for the cor_{dist} metric.

The geodesic distance is the distance a cell has to go through the trajectory space to get from one position to another. The way this distance is calculated depends on how two cells are positioned, showcased by an example in Figure 3.15:

- **Both cells are on the same edge in the milestone network.** In this case, the geodesic distance is defined as the product of the difference in milestone percentages and the length of their shared edge. For cells a and b in the example, $d(a, b)$ is equal to $1 \times (0.9 - 0.2) = 0.7$.
- **Cells reside on different edges in the milestone network.** First, the distance of the cell to all

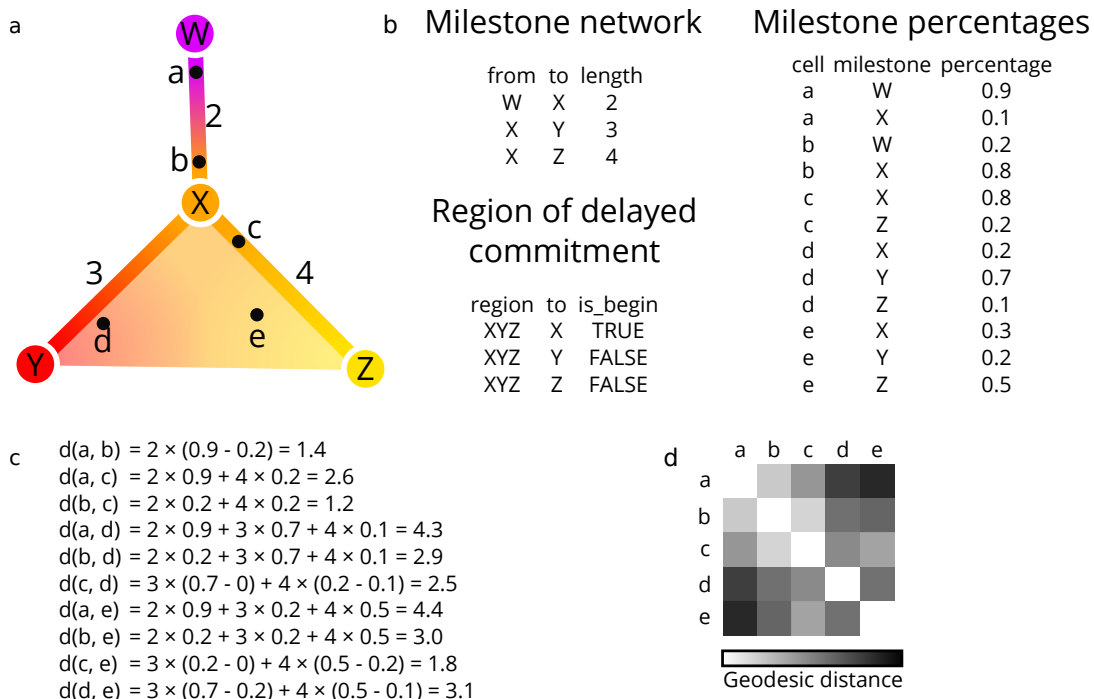


Figure 3.15: The calculation of geodesic distances on a small example trajectory. a) A toy example containing four milestones (W to Z) and five cells (a to e). **b)** The corresponding milestone network, milestone percentages and regions of delayed commitment, when the toy trajectory is converted to the common trajectory model. **c)** The calculations made for calculating the pairwise geodesic distances. **d)** A heatmap representation of the pairwise geodesic distances.

its nearby milestones is calculated, based on its percentage within the edge and the length of the edge. These distances in combination with the milestone network are used to calculate the shortest path distance between the two cells. For cells a and c in the example, $d(a, X) = 1 \times 0.9$ and $d(c, X) = 3 \times 0.2$, and therefore $d(a, c) = 1 \times 0.9 + 3 \times 0.2$.

The geodesic distance can be easily extended towards cells within regions of delayed commitment. When both cells are part of the same region of delayed commitment, the geodesic distance was defined as the manhattan distances between the milestone percentages weighted by the lengths from the milestone network. For cells d and e in the example, $d(d, e)$ is equal to $0 \times (0.3 - 0.2) + 2 \times (0.7 - 0.2) + 3 \times (0.4 - 0.1) = 1.9$. The distance between two cells where only one is part of a region of delayed commitment is calculated similarly to the previous paragraph, by first calculating the distance between the cells and their neighbouring milestones first, then calculating the shortest path distances between the two.

Calculating the pairwise distances between cells scales quadratically with the number of cells, and would therefore not be scaleable for large datasets. For this reason, a set of waypoint cells are defined *a priori*, and only the distances between the waypoint cells and all other cells is calculated, in order to calculate the correlation of geodesic distances of two trajectories (Figure 3.16a). These cell waypoints are determined by viewing each milestone, edge and region of delayed commitment as a collection of cells. We do stratified sampling from each collection of cells by weighing them by the total number of cells within that collection. For calculating the cor_{dist} between two trajectories, the distances between all cells and the union of both waypoint sets is computed.

To select the number of cell waypoints, we need to find a trade-off between the accuracy versus the time to calculate cor_{dist} . To select an optimal number of cell waypoints, we used the synthetic dataset

with the most complex topology, and determined the cor_{dist} at different levels of both cell shuffling and number of cell waypoints (Figure 3.16a). We found that using cell waypoints does not induce a systematic bias in the cor_{dist} , and that its variability was relatively minimal when compared to the variability between different levels of cell shuffling when using 100 or more cell waypoints.

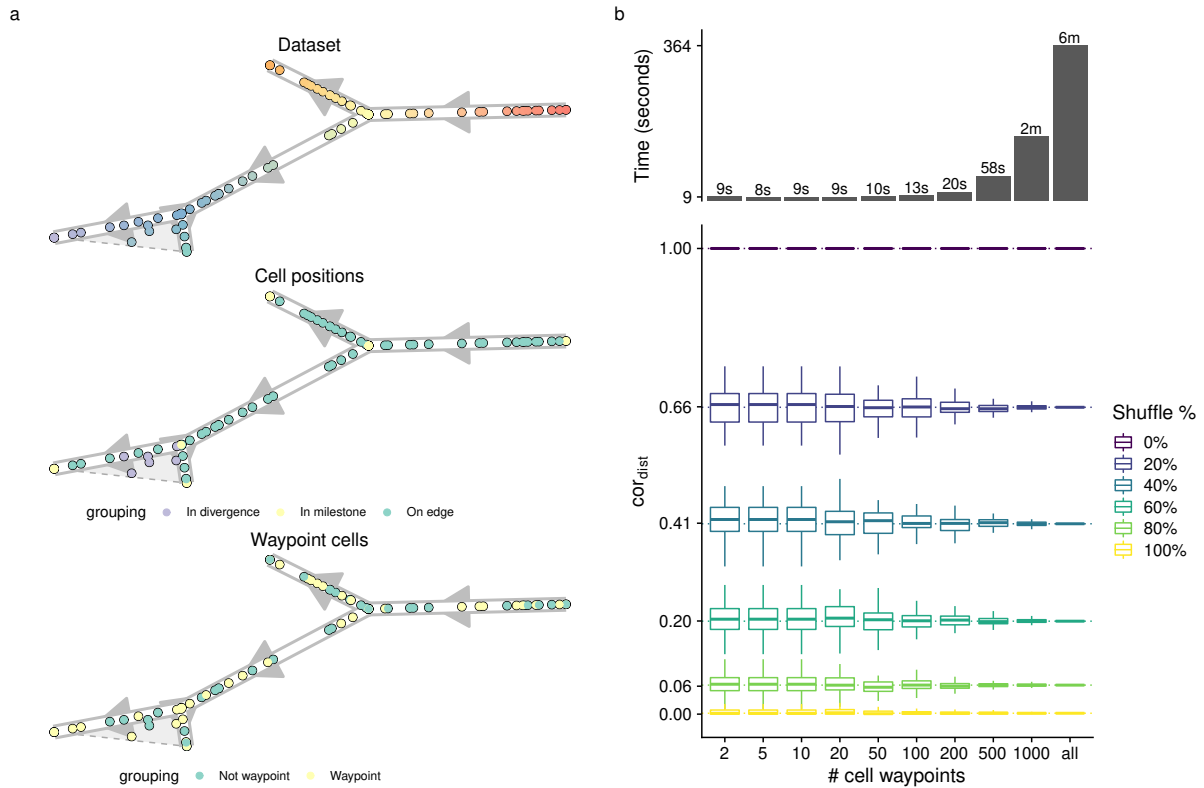


Figure 3.16: Determination of cell waypoints a) Illustration of the stratified cell sampling using an example dataset (top). Each milestone, edge between two milestones and region of delayed commitment is seen as a collection of cells (middle), and the number of waypoints (100 in this case) are divided over each of these collection of cells (bottom). b) Accuracy versus time to calculate cor_{dist} . Shown are distributions over 100 random waypoint samples. The upper whisker of the boxplot extends from the hinge (75% percentile) to the largest value, no further than 1.5× the IQR of the hinge. The lower whisker extends from the hinge (25% percentile) to the smallest value, at most 1.5× the IQR of the hinge.

Although the cor_{dist} 's main characteristic is that it looks at the positions of the cells, other features of the trajectory are also (partly) captured. To illustrate this, we used the geodesic distances themselves as input for dimensionality reduction (Figure 3.17) with varying topologies. This reduced space captures the original trajectory structure quite well, including the overall topology and branch lengths.

NMSE_{rf} and NMSE_{lm}: Using the positions of the cells within one trajectory to predict the cellular positions in the other trajectory

An alternative approach to detect whether the positions of cells are similar between two trajectories, is to use the positions of one trajectory to predict the positions within the other trajectory. If the cells are at similar positions in the trajectory (relative to its nearby cells), the prediction error should be low.

Specifically, we implemented two metrics which predict the milestone percentages from the reference by using the predicted milestone percentages as features (Figure 3.18). We did this with two regression methods, linear regression (*lm*, using the R *lm* function) and Random Forest (*rf*, implemented in the *ranger* package [75]). In both cases, the accuracy of the prediction was measured using the

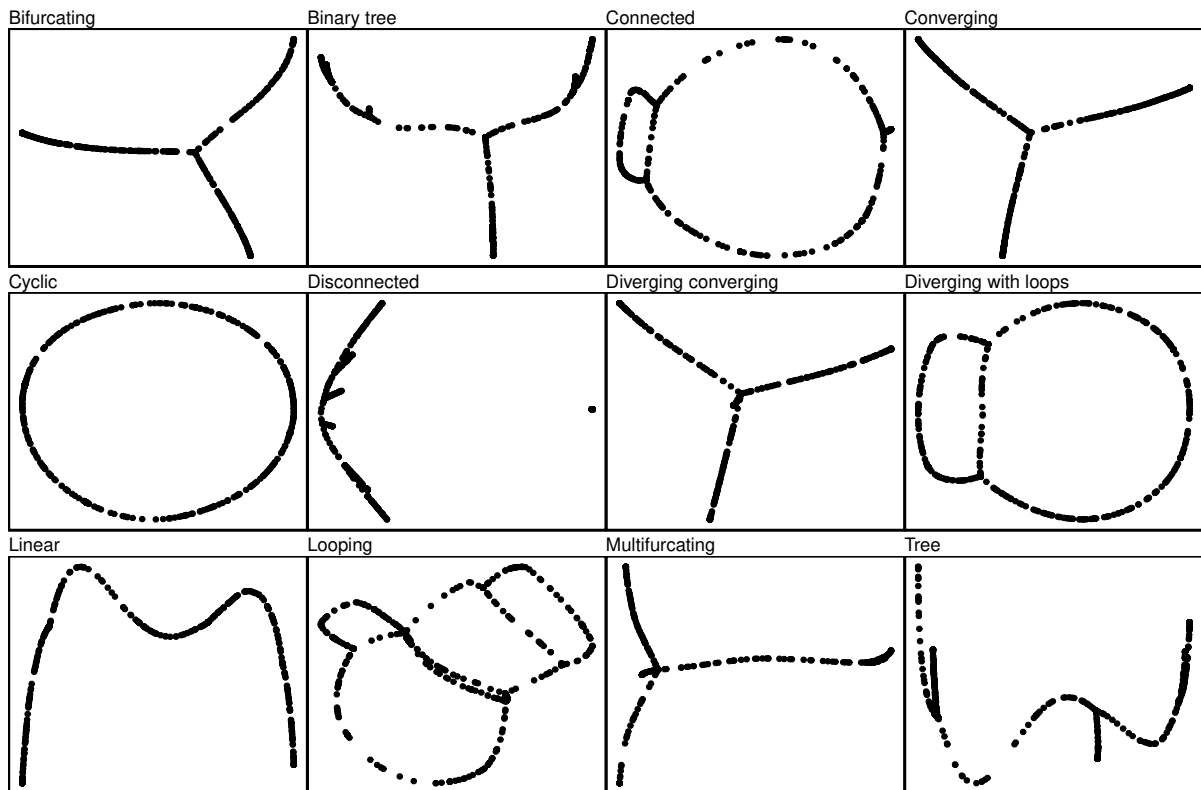


Figure 3.17: Determination of cell waypoints. We generated different toy trajectory datasets with varying topologies and calculated the geodesic distances between all cells within the trajectory. We then used these distances as input for classical multidimensional scaling. This shows that the geodesic distances do not only contain information regarding the cell's positions, but also information on the lengths and wiring of the topology.

Mean Squared error (*MSE*), in the case of Random forest we used the out-of-bag mean-squared error. Next, we calculated MSE_{worst} equal to the *MSE* when predicting all milestone percentages as the average. We used this to calculate the normalised mean squared error as $NMSE = 1 - \frac{MSE}{MSE_{worst}}$. We created a regression model for every milestone in the gold standard, and averaged the *NMSE* values to finally obtain the $NMSE_{rf}$ and $NMSE_{lm}$ scores.

***cor_{features}* and *wcor_{features}*: The accuracy of dynamical differentially expressed features/genes.**

Although most metrics described above already assess some aspects directly relevant to the user, such as whether the method is good at finding the right topology, these metrics do not assess the quality of downstream analyses and hypotheses which can be generated from these models.

Perhaps the main advantage of studying cellular dynamic processes using single-cell -omics data is that the dynamics of gene expression can be studied for the whole transcriptome. This can be used to construct other models such as dynamic regulatory networks and gene expression modules. Such analyses rely on a "good-enough" cellular ordering, so that it can be used to identify dynamical differentially expressed genes.

To calculate the *cor_{features}* we used Random forest regression to rank all the features according to their importance in predicting the positions of cells in the trajectory. More specifically, we first calculated the geodesic distances for each cell to all milestones in the trajectory. Next, we trained a Random Forest regression model (implemented in the R *ranger* package [75], <https://github.com/imbs-hl/ranger>) to predict these distances for each milestone, based on the expression of genes within each cell. We

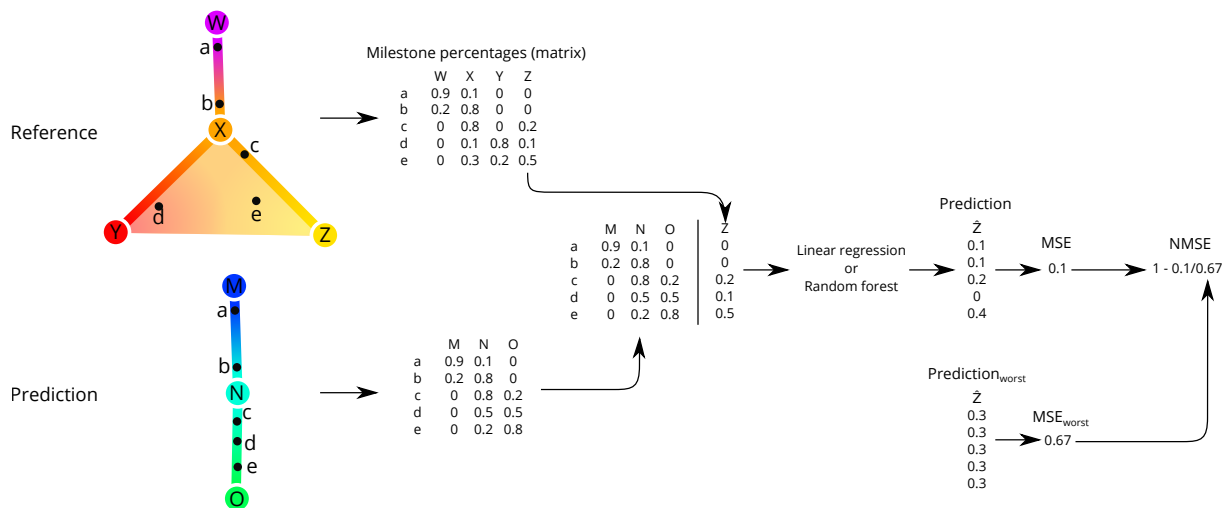


Figure 3.18: The calculation of $NMSE_{im}$ distances on a small example trajectory. The milestone percentages of the reference are predicted based on the milestone percentages of the prediction, using regression models such as linear regression or random forests. The predicted trajectory is then scored by comparing the mean-squared error (MSE) of this regression model with the baseline MSE where the prediction is the average milestone percentage.

then extracted feature importances using the Mean Decrease in Impurity (importance = ‘impurity’ parameter of the ranger function), as illustrated in Figure 3.19. The overall importance of a feature (gene) was then equal to the mean importance over all milestones. Finally, we compared the two rankings by calculating the Pearson correlation, with values between -1 and 0 clipped to 0.

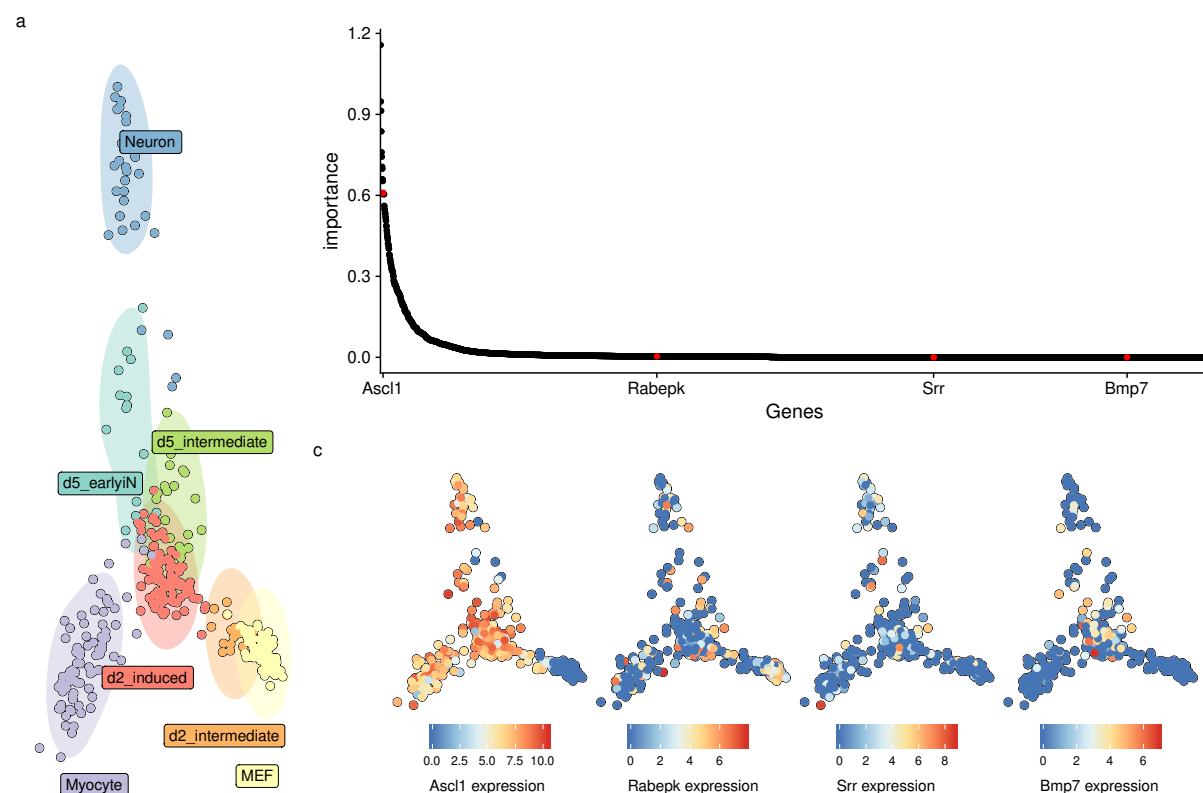


Figure 3.19: An illustration of ranking features based on their importance in a trajectory. (a) A MDS dimensionality reduction of a real dataset in which mouse embryonic fibroblasts (MEF) differentiate into Neurons and Myocytes. (b) The ranking of feature importances from high to low. The majority of features have a very low importance. (c) Some examples, which were also highlighted in b. Higher features in the ranking are clearly specific to certain parts of the trajectory, while features lower on the ranking have a more dispersed expression pattern.

Random forest regression has two main hyperparameters. The number of trees to be fitted (`num_tree` parameter) was fixed to 10000 to provide accurate and stable estimates of the feature importance (Figure 3.20). The number of features on which can be split (`mtre` parameter) was set to 1% of all available features (instead of the default square-root of the number of features), as to make sure that predictive but highly correlated features, omnipresent in transcriptomics data, are not suppressed in the ranking.

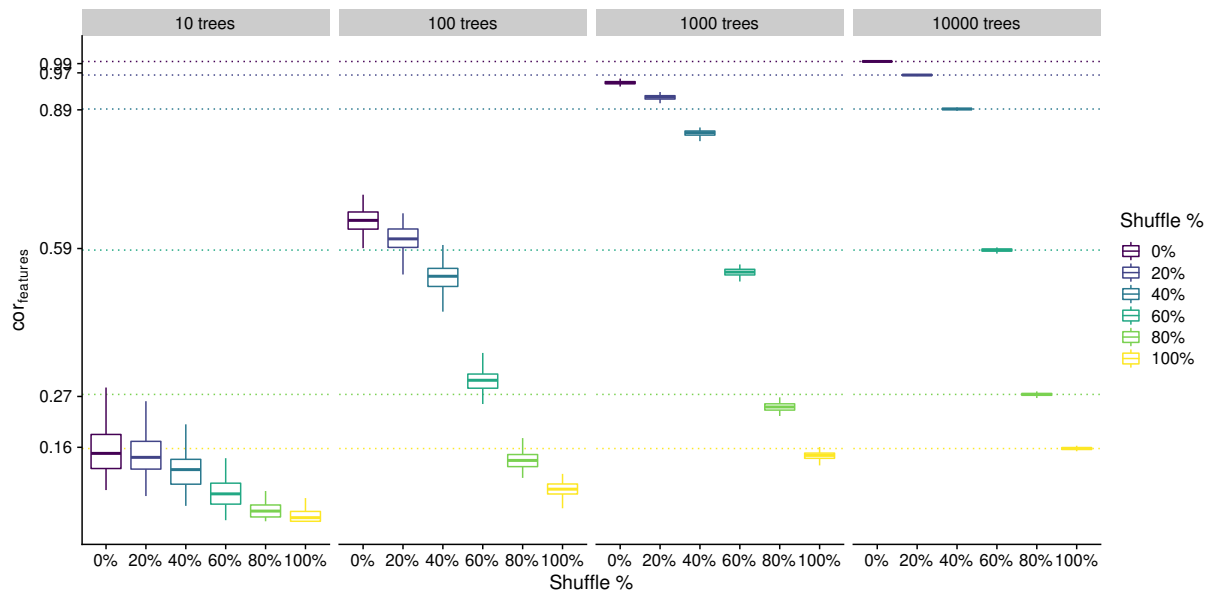


Figure 3.20: Effect of the number of trees parameter on the accuracy and variability of the $cor_{features}$. We used the dataset from Figure 3.19 and calculated the $cor_{features}$ after shuffling a percentage of cells.

For most datasets, only a limited number of features will be differentially expressed in the trajectory. For example, in the dataset used in Figure 3.20 only the top 10%-20% show a clear pattern of differential expression. The correlation will weight each of these features equally, and will therefore give more weight to the bottom, irrelevant features. To prioritise the top differentially expressed features, we also implemented the $wcor_{features}$, which will weight the correlation using the feature importance scores in the reference so that the top features have relatively more impact on the score (Figure 3.21).

3.5.2 Metric conformity

Although most metrics described in the previous section make sense intuitively, this does not necessarily mean that these metrics are robust and will generate reasonable results when used for benchmarking. This is because different methods and datasets will all lead to a varied set of trajectory models:

- Real datasets have all cells grouped onto milestones
- Some methods place all cells in a region of delayed commitment, others never generate a region of delayed commitment
- Some methods always return a linear trajectory, even if a bifurcation is present in the data
- Some methods filter cells

A good metric, especially a good overall metric, should work in all these circumstances. To test this, we designed a set of rules to which a good metric should conform, and assessed empirically whether

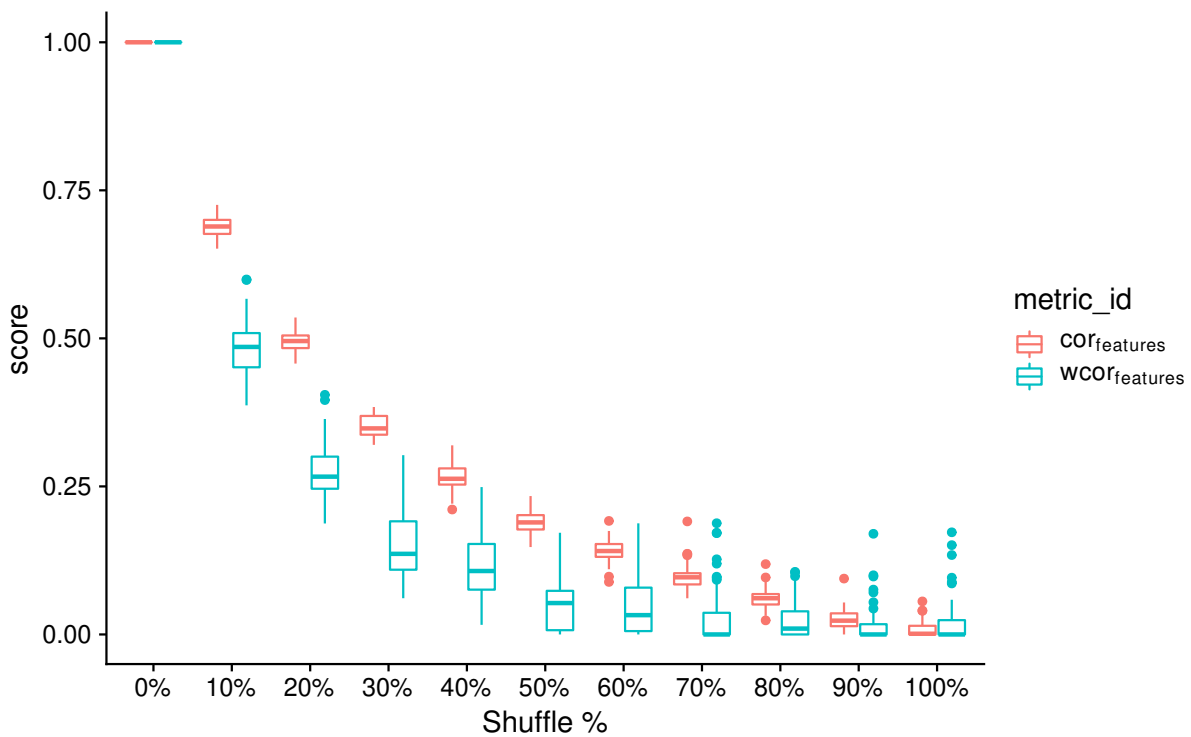


Figure 3.21: Effect of weighting the features based on their feature importance in the reference. We used the same dataset as in Figure 3.19, and calculated the $\text{cor}_{\text{features}}$ after shuffling a percentage of cells.

a metric conforms to these rules.

We generated a panel of toy datasets (using our `dyntoy` package, <https://github.com/dynverse/dyntoy>) with all possible combinations of:

- # cells: 10, 20, 50, 100, 200, 500
- # features: 200
- topologies: linear, bifurcation, multifurcating, tree, cycle, connected graph and disconnected graph
- Whether cells are placed on the milestones (as in real data) or on the edges/regions of delayed commitment between the milestones (as in synthetic data)

We then perturbed the trajectories in these datasets in certain ways, and tested whether the scores follow an expected pattern. An overview of the conformity of every metric is first given in Table 3.2. The individual rules and metric behaviour are discussed in the Supplementary Material that can be found at <https://www.nature.com/articles/s41587-019-0071-9#Sec34>.

3.5.3 Score aggregation

To rank the methods, we need to aggregate on two levels: across **datasets** and across specific/application metrics to calculate an **overall metric**.

Table 3.2: Overview of whether a particular metric conforms to a particular rule

name	cof_{dist}	$NMSE_{rf}$	$NMSE_{lm}$	$edgeflip$	HIM	isomorphic	$cof_{features}$	$wcof_{features}$	$F1_{branches}$	$F1_{milestones}$	$mean_{geometric}$
Same score on identity	✓	✗	✓	✓	✓	✓	✓	✗	✓	✓	✓
Local cell shuffling	✓	✓	✓	✗	✗	✗	✓	✓	✗	✓	✓
Edge shuffling	✓	✓	✓	✗	✗	✗	✓	✓	✓	✓	✓
Local and global cell shuffling	✓	✓	✓	✗	✗	✗	✓	✓	✓	✓	✓
Changing positions locally and/or globally	✓	✓	✓	✗	✗	✗	✓	✓	✗	✗	✓
Cell filtering	✓	✓	✓	✗	✗	✗	✓	✓	✓	✓	✓
Removing divergence regions	✓	✓	✓	✗	✗	✗	✓	✓	✗	✓	✓
Move cells to start milestone	✓	✓	✓	✗	✗	✗	✓	✓	✗	✓	✓
Move cells to closest milestone	✓	✓	✓	✗	✗	✗	✓	✓	✗	✓	✓
Length shuffling	✓	✗	✓	✗	✓	✗	✗	✗	✗	✓	✓
Cells into small subedges	✗	✓	✗	✓	✓	✓	✓	✗	✓	✓	✓
New leaf edges	✓	✓	✗	✓	✓	✓	✗	✗	✓	✓	✓
New connecting edges	✓	✓	✗	✓	✓	✓	✓	✓	✓	✓	✓
Changing topology and cell position	✗	✗	✗	✗	✗	✗	✗	✗	✗	✗	✓
Bifurcation merging	✓	✗	✓	✓	✓	✓	✓	✓	✓	✓	✓
Bifurcation merging and changing cell positions	✓	✓	✓	✗	✗	✗	✓	✓	✓	✓	✓
Bifurcation concatenation	✓	✗	✓	✓	✓	✓	✓	✓	✓	✓	✓
Cycle breaking	✓	✗	✓	✓	✓	✓	✓	✓	✗	✓	✓
Linear joining	✓	✓	✓	✓	✓	✓	✓	✓	✗	✓	✓
Linear splitting	✓	✓	✓	✓	✓	✓	✓	✓	✓	✓	✓
Change of topology	✓	✗	✗	✓	✓	✓	✓	✓	✗	✓	✓
Cells on milestones vs edges	✓	✓	✓	✓	✓	✓	✓	✓	✓	✓	✓

Aggregating over datasets

When combining different datasets, it is important that the biases in the datasets does not influence the overall score. In our study, we define three such biases, although there are potentially many more:

- **Difficulty of the datasets** Some datasets are more difficult than others. This can have various reasons, such as the complexity of the topology, the amount of biological and technical noise, or the dimensions of the data. It is important that a small increase in performance on a more difficult dataset has an equal impact on the final score as a large increase in performance on easier datasets.
- **Dataset sources** It is much easier to generate synthetic datasets than real datasets, and this bias is reflected in our set of datasets. However, given their higher biological relevance, real datasets should be given at least equal importance than synthetic datasets.
- **Trajectory types** There are many more linear and disconnected real datasets, and only a limited number of tree or graph datasets. This imbalance is there because historically most datasets have been linear datasets, and because it is easy to create disconnected datasets by combining different datasets. However, this imbalance in trajectory types does not necessarily reflect the general importance of that trajectory type.

We designed an aggregation scheme which tries to prevent these biases from influencing the ranking of the methods.

The difficulty of a dataset can easily have an impact on how much weight the dataset gets in an overall ranking. We illustrate this with a simple example in Figure 3.22. One method consistently performs well on both the easy and the difficult datasets. But because the differences are small in the difficult datasets, the mean would not give this method a high score. Meanwhile, a variable method which

does not perform well on the difficult dataset gets the highest score, because it scored so high on the easier dataset.

To avoid this bias, we normalise the scores of each dataset by first scaling and centering to $\mu = 0$ and $\sigma = 1$, and then moving the score values back to $[0, 1]$ by applying the unit normal density distribution function. This results in scores which are comparable across different datasets (Figure 3.22). In contrast to other possible normalisation techniques, this will still retain some information on the relative difference between the scores, which would have been lost when using the ranks for normalisation. An example of this normalisation, which will also be used in the subsequent aggregation steps, can be seen in Figure 3.23.

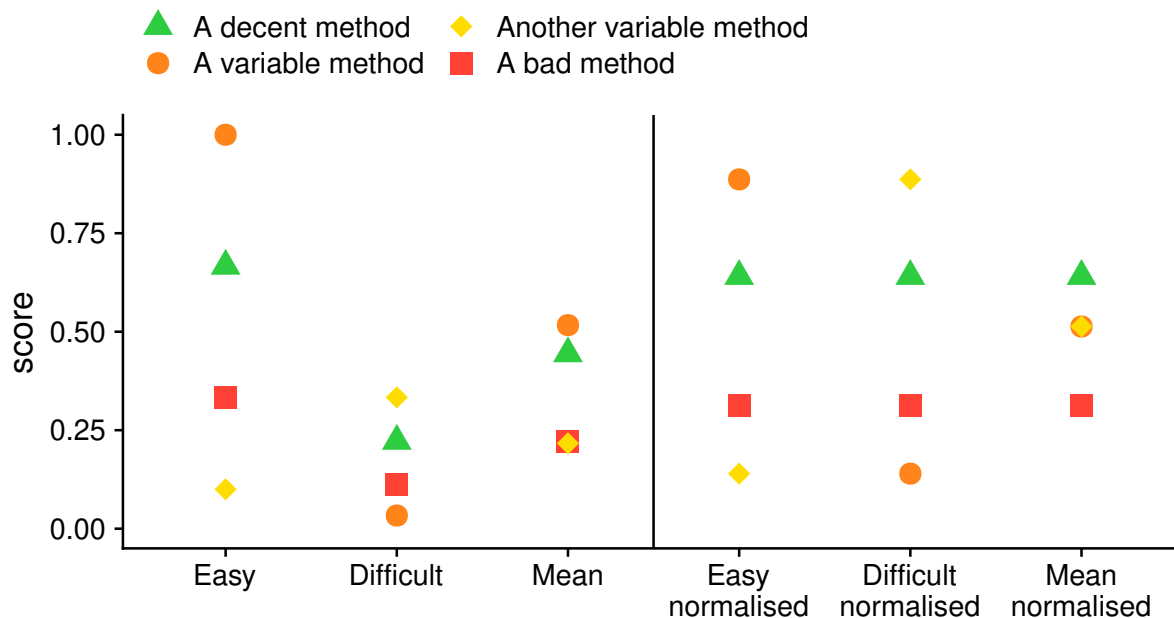


Figure 3.22: An illustration of how the difficulty of a dataset can influence the overall ranking. A decent method, which consistently ranks high on an easy and difficult dataset, does not get a high score when averaging. On the other hand, a method which ranks high on the easy dataset, but very low on the difficult dataset does get a high score on average. After normalising the scores (right), this problem disappears.

For each dataset						Normalised					
Dataset id	Trajectory type	Dataset source	Method id	Metric X	Metric Y	Dataset id	Trajectory type	Dataset source	Method id	Metric X normalised	Metric Y normalised
A	linear	real/gold	a	0.15	0.10	A	linear	real/gold	a	0.14	0.41
			b	0.30	0.05				b	0.55	0.19
			c	0.40	0.20				c	0.82	0.86
B	linear	real/gold	a	0.10	0.00	B	linear	real/gold	a	0.14	0.14
			b	0.25	0.05				b	0.55	0.57
			c	0.35	0.08				c	0.82	0.82
C	linear	real/silver	a	0.25	0.10	C	linear	real/silver	a	0.21	0.19
			b	0.40	0.20				b	0.37	0.41
			c	0.85	0.40				c	0.87	0.86
D	bifurcation	real/gold	a	0.20	0.15	D	bifurcation	real/gold	a	0.14	0.14
			b	0.50	0.60				b	0.55	0.60
			c	0.70	0.80				c	0.82	0.80
E	bifurcation	real/silver	a	0.80	0.90	E	bifurcation	real/silver	a	0.28	0.16
			b	0.90	0.95				b	0.88	0.50
			c	0.80	1.00				c	0.28	0.84

Figure 3.23: An example of the normalisation procedure. Shown are some results of a benchmarking procedure, where every row contains the scores of a particular method (red shading) on a particular dataset (blue shading), with a trajectory type (green shading) and dataset source (orange shading).

After normalisation, we aggregate step by step the scores from different datasets. We first aggregate

the datasets with the same dataset source and trajectory type using an arithmetic mean of their scores (Figure 3.24a). Next, the scores are averaged over different dataset sources, using a arithmetic mean which was weighted based on how much the synthetic and silver scores correlated with the real gold scores (Figure 3.24b). Finally, the scores are aggregated over the different trajectory types again using a arithmetic mean (Figure 3.24c).

Overall metrics

Undoubtedly, a single optimal overall metric does not exist for trajectories, as different users may have different priorities:

- A user may be primarily interested in defining the correct topology, and only use the cellular ordering when the topology is correct
- A user may be less interested in how the cells are ordered within a branch, but primarily in which cells are in which branches
- A user may already know the topology, and may be primarily interested in finding good features related to a particular branching point
- ...

Each of these scenarios would require a combinations of *specific* and *application* metrics with different weights. To provide an “overall” ranking of the metrics, which is impartial for the scenarios described above, we therefore chose a metric which weighs every aspect of the trajectory equally:

- Its **ordering**, using the cor_{dist}
- Its **branch assignment**, using the $F1_{branches}$
- Its **topology**, using the HIM
- The accuracy of **differentially expressed features**, using the $wcor_{features}$

Next, we considered three different ways of averaging different scores: the arithmetic mean, geometric mean and harmonic mean. Each of these types of mean have different use cases. The harmonic mean is most appropriate when the scores would all have a common denominator (as is the case for the *Recovery* and *Relevance* described earlier). The arithmetic mean would be most appropriate when all the metrics have the same range. For our use case, the geometric mean is the most appropriate, because it is low if one of the values is low. For example, this means that if a method is not good at inferring the correct topology, it will get a low overall score, even if it performs better at all other scores. This ensures that a high score will only be reached if a prediction has a good ordering, branch assignment, topology, and set of differentially expressed features.

The final overall score (Figure 3.25) for a method was thus defined as:

$$Overall = mean_{geometric} = \sqrt[4]{cor_{dist} \times F1_{branches} \times HIM \times wcor_{features}}$$

We do however want to stress that different use cases will require a different overall score to order the methods. Such a context-dependent ranking of all methods is provided through the dynguidelines app (<http://guidelines.dynverse.org>).

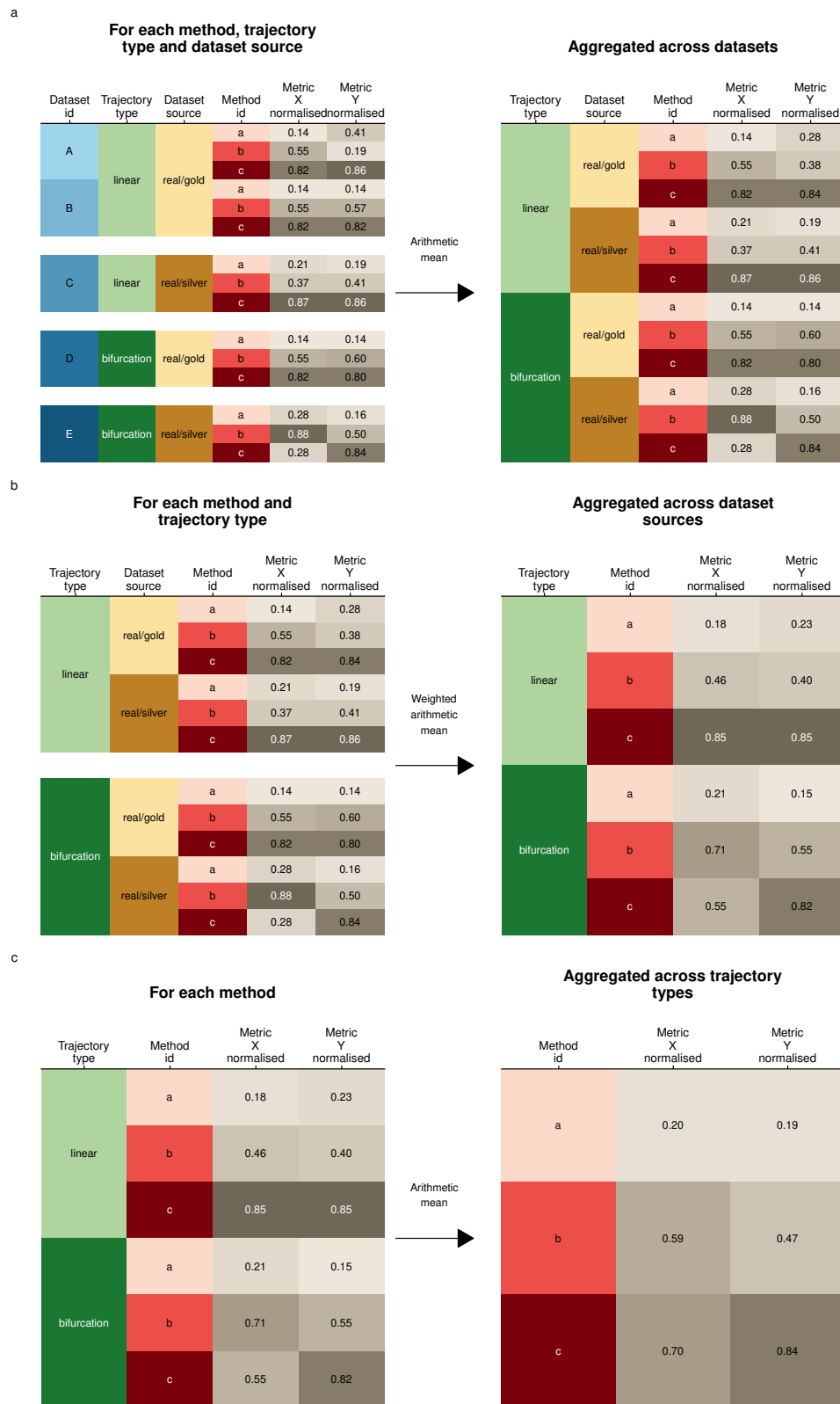


Figure 3.24: An example of the aggregation procedure. In consecutive steps we aggregated across (a) different datasets with the same source and trajectory type, (b) different dataset sources with the same trajectory type (weighted for the correlation of the dataset source with the real gold dataset source) and (c) all trajectory types.

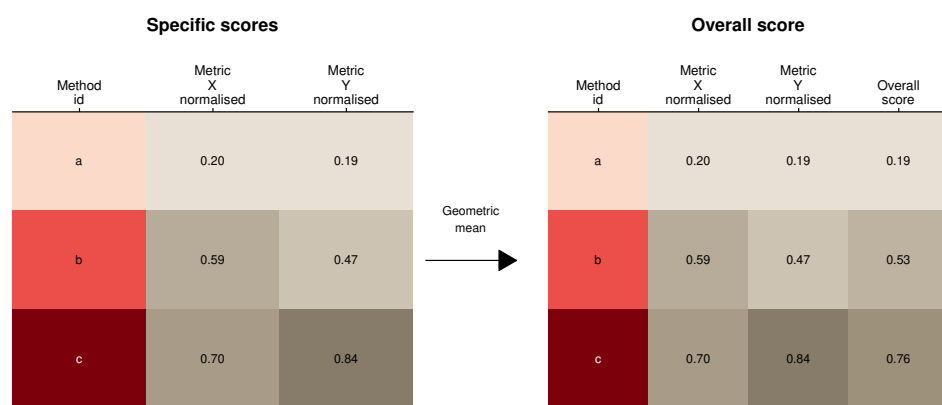


Figure 3.25: An example of the averaging procedure. For each method, we calculated the geometric mean between its normalised and aggregated scores

3.6 References

- [1] Amos Tanay and Aviv Regev. "Scaling Single-Cell Genomics from Phenomenology to Mechanism". In: *Nature* 541.7637 (Jan. 2017), nature21350. ISSN: 1476-4687. DOI: [10.1038/nature21350](https://doi.org/10.1038/nature21350).
- [2] Martin Etzrodt, Max Endele, and Timm Schroeder. "Quantitative Single-Cell Approaches to Stem Cell Research". In: *Cell Stem Cell* 15.5 (2014), pp. 546–558.
- [3] Cole Trapnell. "Defining Cell Types and States with Single-Cell Genomics". In: *Genome Research* 25.10 (2015), pp. 1491–1498. ISSN: 15495469. DOI: [10.1101/gr.190595.115](https://doi.org/10.1101/gr.190595.115). pmid: [26430159](#).
- [4] Robrecht Cannoodt, Wouter Saelens, and Yvan Saeys. "Computational Methods for Trajectory Inference from Single-Cell Transcriptomics". In: *European Journal of Immunology* 46.11 (Nov. 1, 2016), pp. 2496–2506. ISSN: 1521-4141. DOI: [10.1002/eji.201646347](https://doi.org/10.1002/eji.201646347).
- [5] Kevin R Moon et al. "Manifold Learning-Based Methods for Analyzing Single-Cell RNA-Sequencing Data". In: *Current Opinion in Systems Biology*. \$\\backslash\$textbullet{} Future of Systems Biology\$\\backslash\$textbullet{} Genomics and Epigenomics 7 (Feb. 2018), pp. 36–46. ISSN: 2452-3100. DOI: [10.1016/j.coisb.2017.12.008](https://doi.org/10.1016/j.coisb.2017.12.008).
- [6] Zehua Liu et al. "Reconstructing Cell Cycle Pseudo Time-Series via Single-Cell Transcriptome Data". In: *Nature Communications* 8.1 (June 2017), p. 22. ISSN: 2041-1723. DOI: [10.1038/s41467-017-00039-z](https://doi.org/10.1038/s41467-017-00039-z).
- [7] F Alexander Wolf et al. "Graph Abstraction Reconciles Clustering with Trajectory Inference through a Topology Preserving Map of Single Cells". In: *bioRxiv* (Oct. 2017), p. 208819. DOI: [10.1101/208819](https://doi.org/10.1101/208819).
- [8] Andreas Schlitzer et al. "Identification of cDC1- and cDC2-Committed DC Progenitors Reveals Early Lineage Priming at the Common DC Progenitor Stage in the Bone Marrow". In: *Nature Immunology* 16.7 (July 2015), pp. 718–728. ISSN: 1529-2916. DOI: [10.1038/ni.3200](https://doi.org/10.1038/ni.3200).
- [9] Lars Velten et al. "Human Haematopoietic Stem Cell Lineage Commitment Is a Continuous Process". In: *Nature Cell Biology* 19.4 (Apr. 2017), pp. 271–281. ISSN: 1476-4679. DOI: [10.1038/ncb3493](https://doi.org/10.1038/ncb3493).
- [10] Peter See et al. "Mapping the Human DC Lineage through the Integration of High-Dimensional Techniques". In: *Science* 356.6342 (June 2017), eaag3009. ISSN: 0036-8075, 1095-9203. DOI: [10.1126/science.aag3009](https://doi.org/10.1126/science.aag3009). pmid: [28473638](#).
- [11] Sara Aibar et al. "SCENIC: Single-Cell Regulatory Network Inference and Clustering". In: *Nature Methods* (Oct. 2017). ISSN: 1548-7091. DOI: [10.1038/nmeth.4463](https://doi.org/10.1038/nmeth.4463).
- [12] Aviv Regev et al. "The Human Cell Atlas". In: *eLife* 6 (Dec. 2017). ISSN: 2050084X. DOI: [10.7554/eLife.27041](https://doi.org/10.7554/eLife.27041).
- [13] Xiaoping Han et al. "Mapping the Mouse Cell Atlas by Microwell-Seq". In: *Cell* 172.5 (Feb. 2018), 1091–1107.e17. ISSN: 1097-4172. DOI: [10.1016/j.cell.2018.02.001](https://doi.org/10.1016/j.cell.2018.02.001). pmid: [29474909](#).
- [14] Nicholas Schaum et al. "Single-Cell Transcriptomics of 20 Mouse Organs Creates a Tabula Muris". In: *Nature* 562.7727 (Oct. 2018), pp. 367–372. ISSN: 1476-4687. DOI: [10.1038/s41586-018-0590-4](https://doi.org/10.1038/s41586-018-0590-4).
- [15] Philipp Angerer et al. "Single Cells Make Big Data: New Challenges and Opportunities in Transcriptomics". In: *Current Opinion in Systems Biology*. Big Data Acquisition and Analysis \$\\backslash\$textbullet{} Pharmacology and Drug Discovery 4 (Aug. 2017), pp. 85–91. ISSN: 2452-3100. DOI: [10.1016/j.coisb.2017.07.004](https://doi.org/10.1016/j.coisb.2017.07.004).

- [16] Vincent J Henry et al. "OMICtools: An Informative Directory for Multi-Omic Data Analysis". In: *Database: The Journal of Biological Databases and Curation* 2014 (July 2014). ISSN: 1758-0463. DOI: [10.1093/database/bau069](https://doi.org/10.1093/database/bau069). pmid: 25024350.
- [17] Sean Davis et al. Awesome Single Cell. June 2018. URL: <https://github.com/seandavi/awesome-single-cell>.
- [18] Luke Zappia, Belinda Phipson, and Alicia Oshlack. "Exploring the Single-Cell RNA-Seq Analysis Landscape with the scRNA-Tools Database". In: *bioRxiv* (Oct. 2017), p. 206573. DOI: [10.1101/206573](https://doi.org/10.1101/206573).
- [19] Sean C. Bendall et al. "Single-Cell Trajectory Detection Uncovers Progression and Regulatory Coordination in Human B Cell Development". In: *Cell* 157.3 (2014), pp. 714–725. ISSN: 00928674. DOI: [10.1016/j.cell.2014.04.005](https://doi.org/10.1016/j.cell.2014.04.005).
- [20] Jaehoon Shin et al. "Single-Cell RNA-Seq with Waterfall Reveals Molecular Cascades Underlying Adult Neurogenesis". In: *Cell Stem Cell* 17.3 (Sept. 3, 2015), pp. 360–372. ISSN: 1875-9777. DOI: [10.1016/j.stem.2015.07.013](https://doi.org/10.1016/j.stem.2015.07.013). pmid: 26299571.
- [21] Kieran Campbell and Christopher Yau. "Bayesian Gaussian Process Latent Variable Models for Pseudotime Inference in Single-Cell RNA-Seq Data". In: *bioRxiv* (Sept. 2015), p. 26872. DOI: [10.1101/026872](https://doi.org/10.1101/026872).
- [22] Laleh Haghverdi et al. "Diffusion Pseudotime Robustly Reconstructs Lineage Branching". In: *Nature Methods* 13.10 (Oct. 2016), pp. 845–848. ISSN: 1548-7105. DOI: [10.1038/nmeth.3971](https://doi.org/10.1038/nmeth.3971).
- [23] Manu Setty et al. "Wishbone Identifies Bifurcating Developmental Trajectories from Single-Cell Data". In: *Nat. Biotechnol.* 34 (April June 2016), pp. 1–14. ISSN: 1087-0156. DOI: [10.1038/nbt.3569](https://doi.org/10.1038/nbt.3569). pmid: 27136076.
- [24] Cole Trapnell et al. "The Dynamics and Regulators of Cell Fate Decisions Are Revealed by Pseudotemporal Ordering of Single Cells." In: *Nature biotechnology* 32.4 (Mar. 2014), pp. 381–386. ISSN: 1546-1696. DOI: [10.1038/nbt.2859](https://doi.org/10.1038/nbt.2859). pmid: 24658644.
- [25] Hirotaka Matsumoto, Matsumoto Hirotaka, and Kiryu Hisanori. "SCOUPE: A Probabilistic Model Based on the Ornstein-Uhlenbeck Process to Analyze Single-Cell Expression Data during Differentiation". In: *BMC Bioinformatics* 17.1 (2016).
- [26] Xiaojie Qiu et al. "Reversed Graph Embedding Resolves Complex Single-Cell Trajectories". In: *Nature Methods* 14.10 (Oct. 2017), pp. 979–982. ISSN: 1548-7105. DOI: [10.1038/nmeth.4402](https://doi.org/10.1038/nmeth.4402).
- [27] Kelly Street et al. "Slingshot: Cell Lineage and Pseudotime Inference for Single-Cell Transcriptomics". In: *BMC Genomics* 19.1 (June 2018), p. 477. ISSN: 1471-2164. DOI: [10.1186/s12864-018-4772-0](https://doi.org/10.1186/s12864-018-4772-0).
- [28] Zhicheng Ji and Hongkai Ji. "{TSCAN}: Pseudo-Time Reconstruction and Evaluation in Single-Cell {RNA-Seq} Analysis". In: *Nucleic Acids Res.* (2016).
- [29] Joshua D. Welch, Alexander J. Hartemink, and Jan F. Prins. "SLICER: Inferring Branched, Nonlinear Cellular Trajectories from Single Cell RNA-Seq Data". In: *Genome Biology* 17 (2016), p. 106. ISSN: 1474-760X. DOI: [10.1186/s13059-016-0975-3](https://doi.org/10.1186/s13059-016-0975-3).
- [30] David A DuVerle et al. "CellTree: An R/Bioconductor Package to Infer the Hierarchical Structure of Cell Populations from Single-Cell RNA-Seq Data". In: *BMC Bioinformatics* 17 (Sept. 2016), p. 363. ISSN: 1471-2105. DOI: [10.1186/s12859-016-1175-6](https://doi.org/10.1186/s12859-016-1175-6).
- [31] Tapan Lönnberg et al. "Single-Cell RNA-Seq and Computational Analysis Using Temporal Mixture Modeling Resolves TH1/TFH Fate Bifurcation in Malaria". In: *Science Immunology* 2.9 (Mar. 2017), eaal2192. ISSN: 2470-9468. DOI: [10.1126/sciimmunol.aal2192](https://doi.org/10.1126/sciimmunol.aal2192). pmid: 28345074.
- [32] Kieran R Campbell and Christopher Yau. "Probabilistic Modeling of Bifurcations in Single-Cell Gene Expression Data Using a Bayesian Mixture of Factor Analyzers". In: *Wellcome Open Research* 2 (Mar. 2017), p. 19. ISSN: 2398-502X. DOI: [10.12688/wellcomeopenres.11087.1](https://doi.org/10.12688/wellcomeopenres.11087.1).

- [33] Luyi Tian et al. "scRNA-Seq Mixology: Towards Better Benchmarking of Single Cell RNA-Seq Protocols and Analysis Methods". In: *bioRxiv* (Oct. 2018), p. 433102. DOI: [10.1101/433102](https://doi.org/10.1101/433102).
- [34] Thomas Schaffter, Daniel Marbach, and Dario Floreano. "GeneNetWeaver: In Silico Benchmark Generation and Performance Profiling of Network Inference Methods." In: *Bioinformatics* 27.16 (Aug. 2011), pp. 2263–2270. ISSN: 1367-4811. DOI: [10.1093/bioinformatics/btr373](https://doi.org/10.1093/bioinformatics/btr373). pmid: [21697125](#).
- [35] Luke Zappia, Belinda Phipson, and Alicia Oshlack. "Splatter: Simulation of Single-Cell RNA Sequencing Data". In: *Genome Biology* 18 (Sept. 2017), p. 174. ISSN: 1474-760X. DOI: [10.1186/s13059-017-1305-0](https://doi.org/10.1186/s13059-017-1305-0).
- [36] Valentine Svensson, Roser Vento-Tormo, and Sarah A Teichmann. "Exponential Scaling of Single-Cell RNA-Seq in the Past Decade". In: *Nature Protocols* 13.4 (Apr. 2018), pp. 599–604. ISSN: 1750-2799. DOI: [10.1038/nprot.2017.149](https://doi.org/10.1038/nprot.2017.149).
- [37] Junyue Cao et al. "Joint Profiling of Chromatin Accessibility and Gene Expression in Thousands of Single Cells". In: *Science* (Aug. 2018), eaau0730. ISSN: 0036-8075, 1095-9203. DOI: [10.1126/science.aau0730](https://doi.org/10.1126/science.aau0730). pmid: [30166440](#).
- [38] Natalya Pya and Simon N Wood. "Shape Constrained Additive Models". In: *Statistics and Computing* 25.3 (May 2015), pp. 543–559. ISSN: 1573-1375. DOI: [10.1007/s11222-013-9448-7](https://doi.org/10.1007/s11222-013-9448-7).
- [39] Morgan Taschuk and Greg Wilson. "Ten Simple Rules for Making Research Software More Robust". In: *PLOS Computational Biology* 13.4 (Apr. 2017), e1005412. ISSN: 1553-7358. DOI: [10.1371/journal.pcbi.1005412](https://doi.org/10.1371/journal.pcbi.1005412).
- [40] Serghei Mangul et al. "A Comprehensive Analysis of the Usability and Archival Stability of Omics Computational Tools and Resources". In: *bioRxiv* (Oct. 2018), p. 452532. DOI: [10.1101/452532](https://doi.org/10.1101/452532).
- [41] Greg Wilson et al. "Best Practices for Scientific Computing". In: *PLOS Biology* 12.1 (Jan. 2014), e1001745. ISSN: 1545-7885. DOI: [10.1371/journal.pbio.1001745](https://doi.org/10.1371/journal.pbio.1001745).
- [42] Haydee Artaza et al. "Top 10 Metrics for Life Science Software Good Practices". In: *F1000Research* 5 (Aug. 2016), p. 2000. ISSN: 2046-1402. DOI: [10.12688/f1000research.9206.1](https://doi.org/10.12688/f1000research.9206.1).
- [43] Jeff Lee. *Rpackages: R Package Development - the Leek Group Way!* Dec. 2017. URL: <https://github.com/jtleek/rpackages>.
- [44] Hadley Wickham. *R Packages: Organize, Test, Document, and Share Your Code*. O'Reilly Media, Inc., Mar. 26, 2015. 201 pp. ISBN: 978-1-4919-1056-6.
- [45] Luis Bastiao Silva et al. "General Guidelines for Biomedical Software Development". In: *F1000Research* 6 (July 2017). ISSN: 2046-1402. DOI: [10.12688/f1000research.10750.2](https://doi.org/10.12688/f1000research.10750.2). pmid: [28443186](#).
- [46] Rafael C Jiménez et al. "Four Simple Recommendations to Encourage Best Practices in Research Software". In: *F1000Research* 6 (June 2017). ISSN: 2046-1402. DOI: [10.12688/f1000research.11407.1](https://doi.org/10.12688/f1000research.11407.1). pmid: [28751965](#).
- [47] Mehran Karimzadeh and Michael M. Hoffman. "Top Considerations for Creating Bioinformatics Software Documentation". In: *Briefings in Bioinformatics* 19.4 (July 20, 2018), pp. 693–699. ISSN: 1467-5463. DOI: [10.1093/bib/bbw134](https://doi.org/10.1093/bib/bbw134).
- [48] Alex Anderson. *Writing Great Scientific Code*. Oct. 2016. URL: http://alexanderganderson.github.io/code/2016/10/12/coding_tips.html.
- [49] Brett K Beaulieu-Jones and Casey S Greene. "Reproducibility of Computational Workflows Is Automated Using Continuous Analysis". In: *Nature Biotechnology* 35.4 (Mar. 2017), nbt.3780. ISSN: 1546-1696. DOI: [10.1038/nbt.3780](https://doi.org/10.1038/nbt.3780).
- [50] Vincent Driessens. *A Successful Git Branching Model*. Jan. 2010. URL: <http://nvie.com/posts/a-successful-git-branching-model/>.

- [51] Anne-Laure Boulesteix. "Ten Simple Rules for Reducing Overoptimistic Reporting in Methodological Computational Research". In: *PLOS Computational Biology* 11.4 (Apr. 2015), e1004191. ISSN: 1553-7358. DOI: [10.1371/journal.pcbi.1004191](https://doi.org/10.1371/journal.pcbi.1004191).
- [52] Jean Francois Puget. *Green Dice Are Loaded (Welcome to p-Hacking)*. Mar. 2016. URL: https://www.ibm.com/developerworks/community/blogs/jfp/entry/Green_dice_are_loaded_welcome_to_p_hacking.
- [53] Frank Gannon. "The Essential Role of Peer Review". In: *EMBO Reports* 2.9 (Sept. 2001), p. 743. ISSN: 1469-221X. DOI: [10.1093/embo-reports/kve188](https://doi.org/10.1093/embo-reports/kve188). pmid: [11559578](#).
- [54] Melinda Baldwin. "In Referees We Trust?" In: *Physics Today* 70.2 (Feb. 2017), pp. 44–49. ISSN: 0031-9228. DOI: [10.1063/PT.3.3463](https://doi.org/10.1063/PT.3.3463).
- [55] Mohamed Radhouene Aniba, Olivier Poch, and Julie D Thompson. "Issues in Bioinformatics Benchmarking: The Case Study of Multiple Sequence Alignment". In: *Nucleic Acids Research* 38.21 (Nov. 2010), pp. 7353–7363. ISSN: 0305-1048. DOI: [10.1093/nar/gkq625](https://doi.org/10.1093/nar/gkq625). pmid: [20639539](#).
- [56] Monika Jelizarow et al. "Over-Optimism in Bioinformatics: An Illustration". In: *Bioinformatics* 26.16 (Aug. 2010), pp. 1990–1998. ISSN: 1367-4803. DOI: [10.1093/bioinformatics/btq323](https://doi.org/10.1093/bioinformatics/btq323).
- [57] Wouter Saelens, Robrecht Cannoodt, and Yvan Saeys. "A Comprehensive Evaluation of Module Detection Methods for Gene Expression Data". In: *Nature Communications* 9.1 (Mar. 2018), p. 1090. ISSN: 2041-1723. DOI: [10.1038/s41467-018-03424-4](https://doi.org/10.1038/s41467-018-03424-4).
- [58] Gioele La Manno et al. "RNA Velocity of Single Cells". In: *Nature* 560.7719 (Aug. 2018), pp. 494–498. ISSN: 1476-4687. DOI: [10.1038/s41586-018-0414-6](https://doi.org/10.1038/s41586-018-0414-6).
- [59] Raquel Norel, John Jeremy Rice, and Gustavo Stolovitzky. "The Self-Assessment Trap: Can We All Be Better than Average?" In: *Molecular systems biology* 7.1 (2011), p. 537. ISSN: 1744-4292. DOI: [10.1038/msb.2011.70](https://doi.org/10.1038/msb.2011.70). pmid: [21988833](#).
- [60] Anthony Gitter. *Single-Cell RNA-Seq Pseudotime Estimation Algorithm*. June 2018. URL: <https://github.com/agitter/single-cell-pseudotime>.
- [61] Tsukasa Kouno et al. "Temporal Dynamics and Transcriptional Control Using Single-Cell Gene Expression Analysis". In: *Genome Biol.* 14.10 (2013), R118.
- [62] Chun Zeng et al. "Pseudotemporal Ordering of Single Cells Reveals Metabolic Control of Postnatal β Cell Proliferation". In: *Cell Metabolism* 25.5 (May 2017), 1160–1175.e11. ISSN: 15504131. DOI: [10.1016/j.cmet.2017.04.014](https://doi.org/10.1016/j.cmet.2017.04.014).
- [63] Nikolaos Papadopoulos, Rodrigo Gonzalo Parra, and Johannes Soeding. "PROSSTT: Probabilistic Simulation of Single-Cell RNA-Seq Data for Complex Differentiation Processes". In: *bioRxiv* (Jan. 2018), p. 256941. DOI: [10.1101/256941](https://doi.org/10.1101/256941).
- [64] Daniel Marbach et al. "Wisdom of Crowds for Robust Gene Network Inference". In: *Nature methods* 9.8 (July 2012), pp. 796–804. ISSN: 1548-7091. DOI: [10.1038/nmeth.2016](https://doi.org/10.1038/nmeth.2016). pmid: [22796662](#).
- [65] Heping Xu et al. "Regulation of Bifurcating {B} Cell Trajectories by Mutual Antagonism between Transcription Factors {IRF4} and {IRF8} ". In: *Nat. Immunol.* 16.12 (Dec. 2015), pp. 1274–1281.
- [66] Thomas Graf and Tariq Enver. "Forcing Cells to Change Lineages". In: *Nature* 462.7273 (Dec. 2009), p. 587. ISSN: 1476-4687. DOI: [10.1038/nature08533](https://doi.org/10.1038/nature08533).
- [67] Jin Wang et al. "Quantifying the Waddington Landscape and Biological Paths for Development and Differentiation". In: *Proceedings of the National Academy of Sciences* 108.20 (May 2011), pp. 8257–8262. ISSN: 0027-8424, 1091-6490. DOI: [10.1073/pnas.1017017108](https://doi.org/10.1073/pnas.1017017108). pmid: [21536909](#).
- [68] James E Ferrell. "Bistability, Bifurcations, and Waddington's Epigenetic Landscape". In: *Current Biology* 22.11 (June 2012), R458–R466. ISSN: 0960-9822. DOI: [10.1016/j.cub.2012.03.045](https://doi.org/10.1016/j.cub.2012.03.045).

- [69] Nir Yosef et al. "Dynamic Regulatory Network Controlling {TH17} Cell Differentiation". In: *Nature* 496.7446 (2013), pp. 461–468.
- [70] Daniel Marbach et al. "Tissue-Specific Regulatory Circuits Reveal Variable Modular Perturbations across Complex Diseases". In: *Nature Methods* 13.4 (Apr. 2016), p. 366. ISSN: 1548-7105. DOI: [10.1038/nmeth.3799](https://doi.org/10.1038/nmeth.3799).
- [71] Toni Giorgino. "Computing and Visualizing Dynamic Time Warping Alignments in R: The Dtw Package". In: *Journal of Statistical Software* 7 (Sept. 2009). DOI: [10.18637/jss.v031.i07](https://doi.org/10.18637/jss.v031.i07).
- [72] Paolo Tormene et al. "Matching Incomplete Time Series with Dynamic Time Warping: An Algorithm and an Application to Post-Stroke Rehabilitation". In: *Artificial Intelligence in Medicine* 45.1 (Jan. 2009), pp. 11–34. ISSN: 0933-3657. DOI: [10.1016/j.artmed.2008.11.007](https://doi.org/10.1016/j.artmed.2008.11.007).
- [73] Aaron T L Lun, Davis J McCarthy, and John C Marioni. "A Step-by-Step Workflow for Low-Level Analysis of Single-Cell RNA-Seq Data with Bioconductor". In: *F1000Research* 5 (Oct. 2016), p. 2122. ISSN: 2046-1402. DOI: [10.12688/f1000research.9501.2](https://doi.org/10.12688/f1000research.9501.2).
- [74] G Jurman et al. "The HIM Glocal Metric and Kernel for Network Comparison and Classification". In: *2015 IEEE International Conference on Data Science and Advanced Analytics (DSAA)*. Oct. 2015, pp. 1–10. DOI: [10.1109/DSAA.2015.7344816](https://doi.org/10.1109/DSAA.2015.7344816).
- [75] Marvin N Wright and Andreas Ziegler. "Ranger: A Fast Implementation of Random Forests for High Dimensional Data in C++ and R". In: *Journal of Statistical Software* 77.1 (Mar. 2017). DOI: [10.18637/jss.v077.i01](https://doi.org/10.18637/jss.v077.i01).
- [76] T Junnila and P Kaski. "Engineering an Efficient Canonical Labeling Tool for Large and Sparse Graphs". In: *2007 Proceedings of the Ninth Workshop on Algorithm Engineering and Experiments (ALENEX)*. Proceedings. Society for Industrial and Applied Mathematics, Jan. 2007, pp. 135–149. DOI: [10.1137/1.9781611972870.13](https://doi.org/10.1137/1.9781611972870.13).
- [77] Laura Bahiense et al. "The Maximum Common Edge Subgraph Problem: A Polyhedral Investigation". In: *Discrete Applied Mathematics. V Latin American Algorithms, Graphs, and Optimization Symposium* \backslashtextemdash{} Gramado, Brazil, 2009 160.18 (Dec. 2012), pp. 2523–2541. ISSN: 0166-218X. DOI: [10.1016/j.dam.2012.01.026](https://doi.org/10.1016/j.dam.2012.01.026).
- [78] Edward R Dougherty. "Validation of Gene Regulatory Networks: Scientific and Inferential". In: *Briefings in Bioinformatics* 12.3 (May 2011), pp. 245–252. ISSN: 1477-4054. DOI: [10.1093/bib/bbq078](https://doi.org/10.1093/bib/bbq078). pmid: [21183477](#).
- [79] Mads Ipsen and Alexander S Mikhailov. "Evolutionary Reconstruction of Networks". In: *Physical Review. E, Statistical, Nonlinear, and Soft Matter Physics* 66 (4 Pt 2 Oct. 2002), p. 46109. ISSN: 1539-3755. DOI: [10.1103/PhysRevE.66.046109](https://doi.org/10.1103/PhysRevE.66.046109). pmid: [12443261](#).

CHAPTER 4

Paper 3: A toolkit for inferring and interpreting trajectories

Abstract

Purpose: Recent technological advances allow studying dynamic processes by computationally ordering single-cell omics profiles along a trajectory. Since 2014, at least 75 tools for trajectory inference have been developed. For end-users, however, these methods are difficult to execute and compare, mainly due to high variability in input/output data structures, software requirements, and programming interfaces.

Results: We developed `dyno`, a toolkit for inferring, visualising and interpreting single-cell trajectories, giving access to more than 50 TI methods. `dyno` provides downstream analyses such as visualising the trajectory with dot-plots or heatmaps, automated labelling using gene sets, automated inference of the directionality, and detecting genes that are differentially expressed along the trajectory.

Conclusion: By providing a uniform interface for executing and visualising trajectories of 50 methods, `dyno` allows inferring and comparing trajectories for a much broader audience than previously possible.

Publication status

Manuscript in preparation.

Cannoodt R*, Saelens W*, and Saeys Y.

* Equal contribution

Author contributions

- **R.C.** and **W.S.** designed the project.
- **R.C.** and **W.S.** implemented software packages.
- **R.C.** and **W.S.** wrote the original manuscript.
- **Y.S.** supervised the project.

4

4.1 Introduction

Recent technological advances allow unbiased investigation of cellular dynamic processes in a high-throughput manner [1, 2]. Trajectory inference (TI) methods aim to give insight into a dynamic process by inferring a trajectory from omics profiles of cells in which the dynamic process takes place [3]. In a recent study, we benchmarked 45 TI methods in terms of their accuracy, scalability, stability, and robustness [4]. We construct a set of guidelines to help end-users select an appropriate TI method for their dataset of interest. However, executing and comparing multiple methods remains challenging, due to high variability in input/output data structures, software requirements, and programming interfaces.

We developed `dyno`, a toolkit to easily infer, visualise and interpret single-cell trajectories. The user can select the most optimal set of TI methods based on characteristics of the dataset and user preferences. More than 50 TI methods can easily be run within a common interface, and the outputs thereof are converted into a common format. `dyno` provides downstream analysis such as: visualising a trajectory in a low-dimensional space or a heatmap, detecting genes differentially expressed at different stages of the trajectory, comparing multiple trajectories in a common dimensionality reduction, and manipulating the trajectory such as adding directionality or labelling different cell stages.

4.2 Results

This section will present the various components in the `dyno` workflow (Figure 4.1).

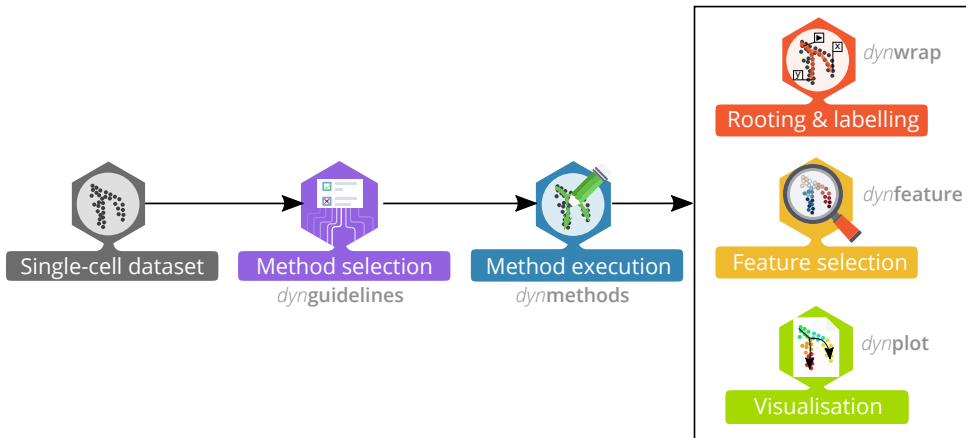


Figure 4.1: The `dyno` workflow for inferring, visualising and interpreting single-cell trajectories. `dynguidelines` allows you to choose a suitable TI method for your dataset of interest. `dynmethods` contains wrappers for 'r `dynmethods::methods`' `dynwrap` provides main functionality for (pre/post-)processing trajectory data structures. `dynfeature` calculates gene importance scores based on a trajectory. `dynplot` provides visualisation tools for trajectories, including scatterplots and heatmaps.

4.2.1 Preparing the dataset

In order to use your dataset of interest, you will first need to wrap it in a `dynwrap` object. We will use a commonly used dataset of 392 mouse embryonic fibroblasts (MEF) undergoing direct reprogramming to induced neuronal cells [5]. By wrapping the counts information and possible prior information (e.g.

known cell types, a start cell, time course information) into a `dynwrap` object, the dataset can be used as input for the various `dyno` components.

4.2.2 Selecting the best methods for a dataset

We performed a comparative study of 45 trajectory inference methods [4]. We evaluated each method in terms of four main aspects:

- **Accuracy:** How similar is the inferred trajectory to the “true” (or “expected”) trajectory in the data. We used several metrics in order to assess similarity in pairwise cellular ordering and also the similarity in topology of the trajectories. We used both real datasets – which has the highest biological relevance – and synthetic datasets – which allow to push methods to their limits more easily.
- **Scalability:** How long the method takes to run and how much memory it consumes. This mainly depends on the dimensions of the input data, i.e. the number of cells and features.
- **Stability:** How stable the results are when rerunning the method with slightly different input data.
- **Usability:** The quality of the corresponding documentation, software package, and manuscript. We assessed how easy it is to run the method, whether the software adheres to good software development practices, and whether the manuscript follows good scientific practices. We reviewed ‘good practices’ literature and created a ‘consensus’ score-sheet of good practices, and filled in to what extent each method adhered to each of the good practices.

We found a high diversity in method performance, and that not many methods perform well across the board. The performance of a method depended on many factors, mainly the dimensions of the data and the kind of trajectory present in the data. Based on this, we developed an interactive Shiny app which can be used to explore the results and select an optimal set of methods for a particular analysis (Figure~4.2).

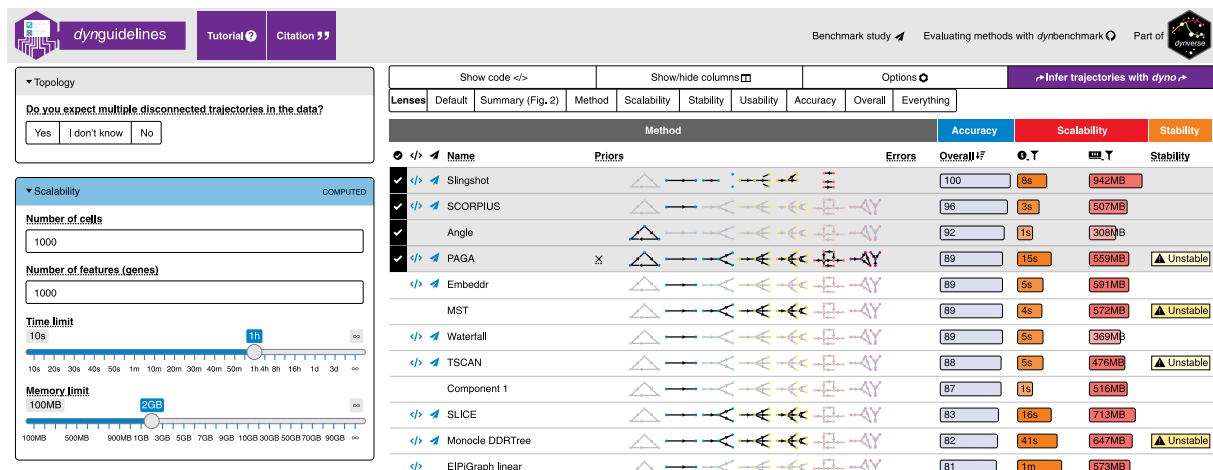


Figure 4.2: A static screenshot of the dynguidelines Shiny interface.

4.2.3 Inferring trajectories

There are over 50 TI methods available as part of `dynmethods`, and executing a TI method on a dataset of interest is as simple as running just one command. Behind the screens, `dyno` will save the dataset,

Table 4.1: The minimum amount of information to define a trajectory.

Milestone network:				Cell progressions:			
from	to	length	directed	cell_id	from	to	percentage
5	1	13.828399	TRUE	1_iN1_C04	2	3	0.3508990
1	2	4.853443	TRUE	1_iN1_C05	2	3	0.5287099
2	3	11.325468	TRUE	1_iN1_C07	1	2	0.1953806
2	4	14.022826	TRUE	1_iN1_C08	2	3	0.8589863
				1_iN1_C09	1	2	0.9076217
				1_iN1_C10	1	2	0.4170644
				1_iN1_C11	2	3	0.7316277
				1_iN1_C12	1	2	0.7108862
				1_iN1_C13	1	2	0.0644059
				1_iN1_C14	1	2	0.7178277
							...

Table 4.2: Possible prior information accepted or required by TI methods.

Name	Description	Type
Start cell(s)	One or more start cell identifiers	soft
End cell(s)	One or more end cell identifiers	soft
# end states	The number of end states	soft
# start states	The number of start states	soft
# leaves	The number of leaves	soft
Cell clustering	Named character vector linking the cell identifiers to different states/branches	hard
# states	Number of states/branches, including start, end and intermediary states	soft
State network	Dataframe containing the known network between states/branches. Contains a from and to column	hard
Time course (continuous)	Named numeric vector linking the cell ids to time points	hard
Time course (discrete)	Named numeric vector linking the cell ids to time course points	hard
Marker genes	Genes/features known to be important in the dynamic process	soft

prior information and parameters as an H5 file and execute a container containing the desired TI method. This ensures that the TI method will not have any issues due to software compatibilities on the host environment. The first time a TI method is run, it will automatically download the corresponding container from Docker Hub.

We inferred a trajectory on the dataset of mouse embryonic fibroblasts using the Slingshot [6] approach. The outputted model contains the main information on the trajectory, namely the milestone network and cell progressions (Table 4.1). These data are hard to interpret manually. Luckily, dyno provides many different visualisation functions for interpreting trajectories.

4.2.4 Execution details

Prior information: The method will error if it requires some prior information that is not already provided in the dataset. Take note that the stronger the assumed priors for a given method, the more biased the output will be (Table 4.2).

Reproducibility: When using this framework for analysing real data, remember to set the seed to ensure reproducibility.

Multiple executions: Often it is useful to run multiple methods and/or use multiple datasets. While you can easily parallelise this yourself, we provide a helper function which integrates well with our visualisation functions.

Errors: Some methods can generate errors which are beyond our control. To know what and where a method generated an error, remember to turn on the verbosity.

Command-line: Each method is also executable from command-line using the Docker container. Check out the help documentation by running a TI method container without extra arguments.

4.2.5 Visualising trajectories

The most common way to visualise a trajectory is to plot it on a dimensionality reduction of the cells (Figure 4.3A). Often (but not always), a TI method will already output a dimensionality reduction itself, which was used to construct the trajectory. `dynplot` will use this dimensionality reduction if available, otherwise it will calculate a dimensionality reduction under the hood. You can also supply it with your own dimensionality reduction. In this case, the trajectory will be *projected* onto this dimensionality reduction (Figure 4.3B). On this plot, you can colour the cells using various layers of information (Figure 4.4): cell ordering, cell grouping, feature expression, and pseudotime.

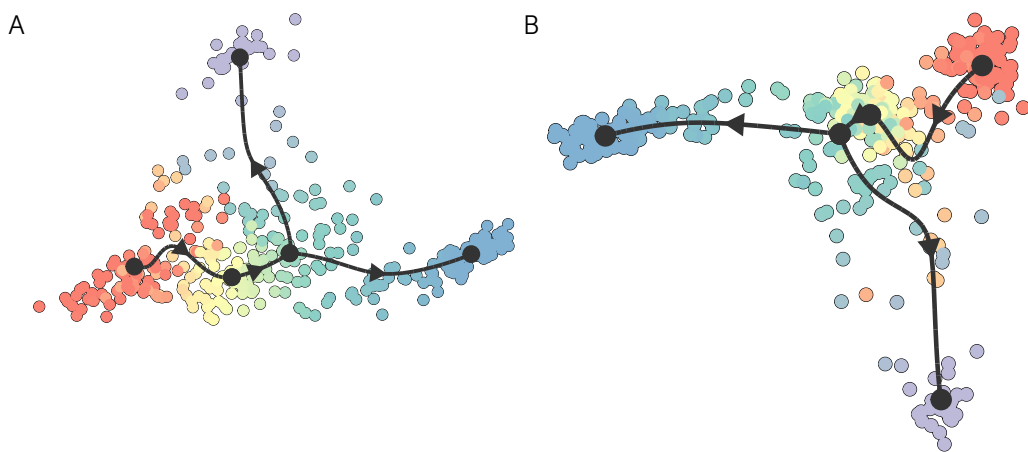


Figure 4.3: **A:** Often, the TI method provides its own dimensionality reduction for the trajectory, which will be plotted by default. This is a visualisation for Slingshot executed on MEF cells from the previous example. **B:** Alternatively, you can provide your own dimensionality reduction, and the trajectory will be projected to it. In this example the Slingshot trajectory is projected to a UMAP dimensionality reduction.

Various layout and colouring options: To visualise a trajectory, it is good practice to take into account what the purpose and intended message of the visualisation is (Figure 4.5). The cells and trajectory can be positioned to place more emphasis on the topology of the inferred trajectory, or on the cellular heterogeneity between the cells, that the trajectory might or might not have been able to detect. Cells and trajectory can be coloured according to the topology of the trajectory, according to gene expression, or a custom input vector of values.

Visualising many genes along a trajectory: A one-dimensional visualisation is especially useful if you combine it with a heatmap (Figure 4.6).

Comparing multiple trajectories: Visualising each method with their own dimensionality reduction can make it hard to interpret to what extend the methods agree/disagree with each-other (Figure 4.7A). Different trajectories become noticeably more comparable when projected to a common dimensionality reduction (Figure 4.7B).

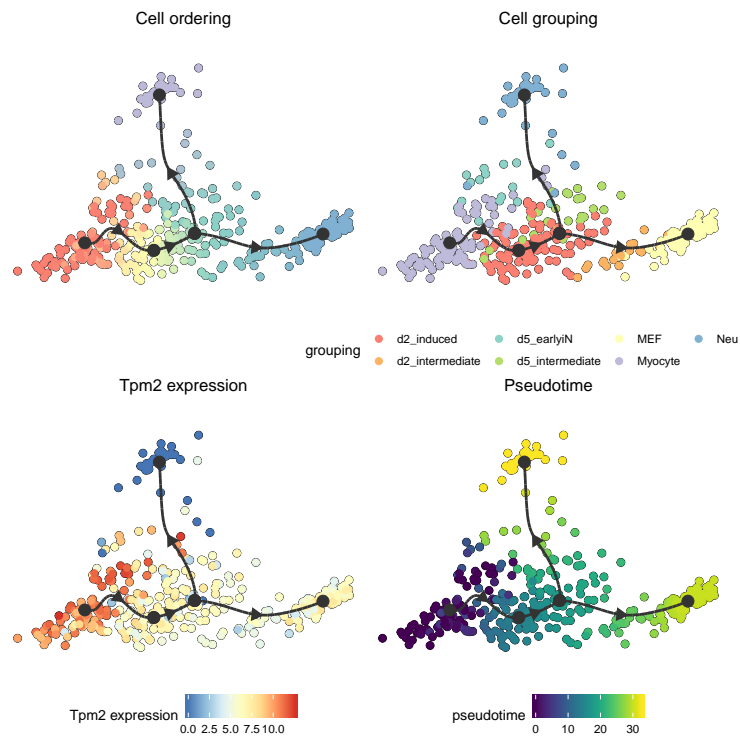


Figure 4.4: Cell ordering: Cells are coloured by their proximity to the different milestones. **Cell grouping:** A given character vector mapping a cell to a group. **Feature expression:** Colour by the expression levels of a particular gene. **Pseudotime:** The distance to a particular root milestone.

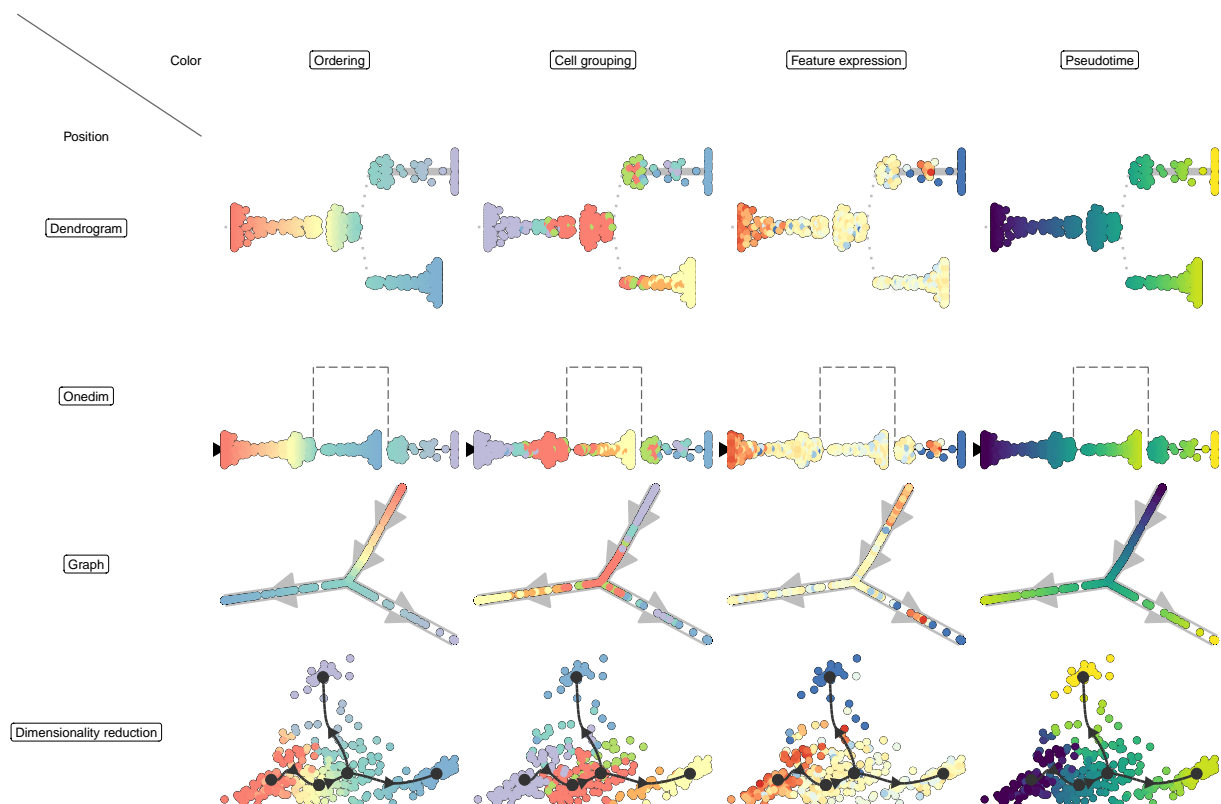


Figure 4.5: Overview of the different combinations of positioning and colouring options, demonstrated on the output of Slingshot.

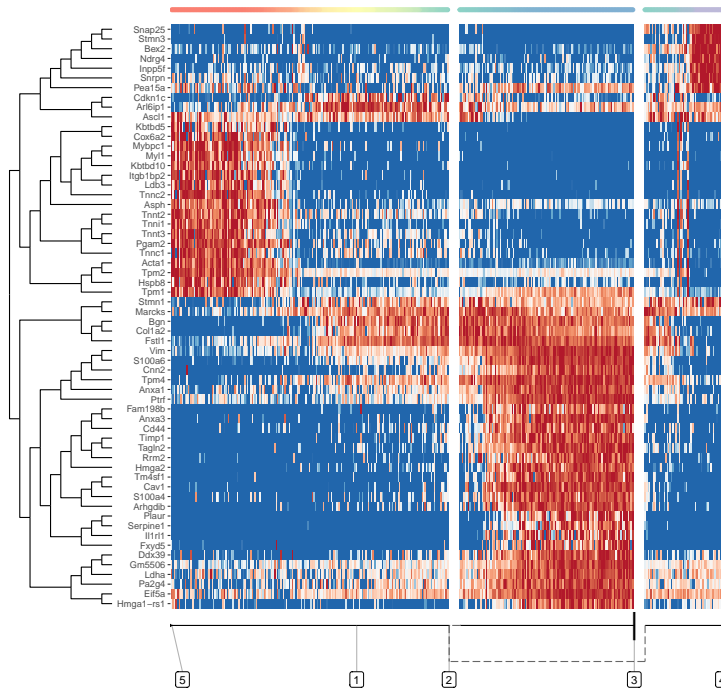


Figure 4.6: Selecting relevant features for this heatmap is discussed in a later section. By default, features will be selected that best explain the main differences over the whole trajectory.

4.2.6 Manipulating the trajectory

dyno allows manipulating trajectories by simplifying, rooting and annotating them.

Simplifying linear segments: Intermediate milestones can be removed by simplifying the trajectory (Figure 4.8A).

Rooting: Most TI methods return undirected trajectories. We provide two ways of rooting a trajectory, namely by manually specifying the root milestone, or by specifying highly expressed marker genes. After rooting, all other edges will point away from the root (Figure 4.8B).

Annotating the trajectory

Similar as with rooting, annotating the trajectory by renaming the milestones can be done either manually, or with given highly expressed gene sets (Figure 4.8C).

4.2.7 Differentially expressed genes along the trajectory

Compared to differential expression between clusters of cells, defining differential expression on trajectories is not so straightforward. What constitutes a trajectory differentially expressed gene?

- A gene that is uniquely expressed in a particular branch?
- A gene that changes at a branching point?
- A gene that changes along pseudotime?

dynfeature allows you to find these different kinds of differential expression in a trajectory. It first defines a particular variable that needs to be predicted (for example, whether a cell is present in a

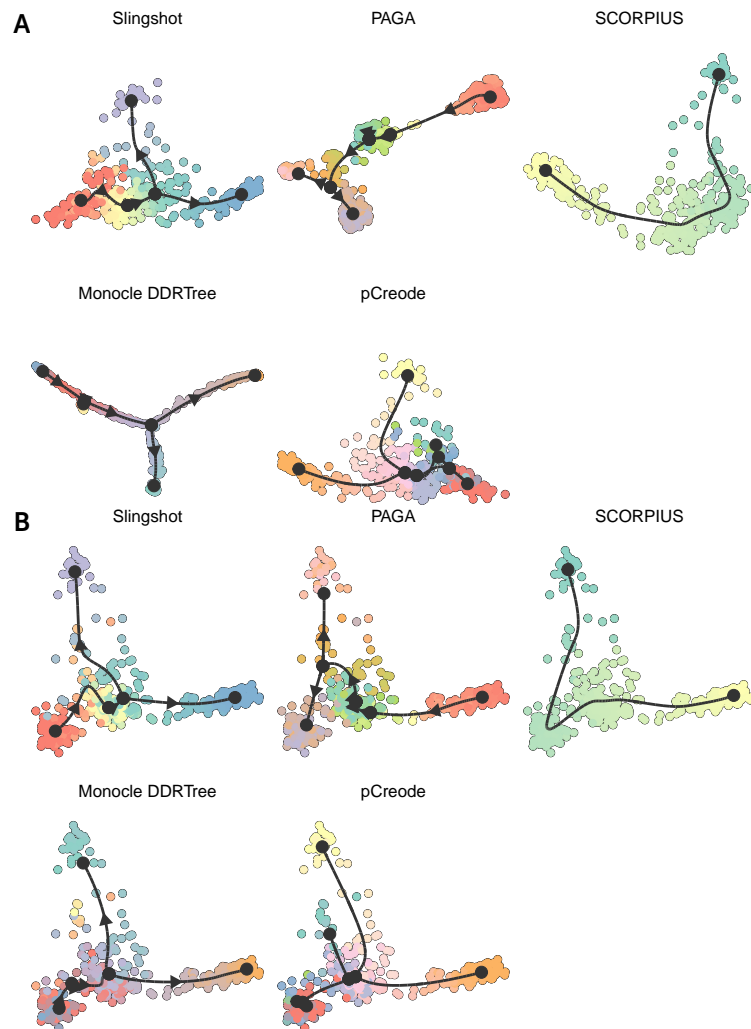


Figure 4.7: **A:** Comparing outputs of multiple TI methods is tedious when they are each visualised using their own visualisation method of interest. **B:** In contrast, by projecting each output to the same dimensionality reduction, the methods become immediately visually comparable.

branch or not), and ranks each gene based on their predictive capability with respect to that variable. This section reviews the types of feature selection supported by `dynfeature`.

Lineage / transition marker genes: We can identify genes that are specifically upregulated or downregulated at a specific branch (Figure 4.9).

Milestone marker genes We can identify genes that are specifically upregulated or downregulated at a particular milestone (Figure 4.10).

Marker genes for the trajectory as a whole We can identify genes that change in function of the ordering of a part of the trajectory (Figure 4.11).

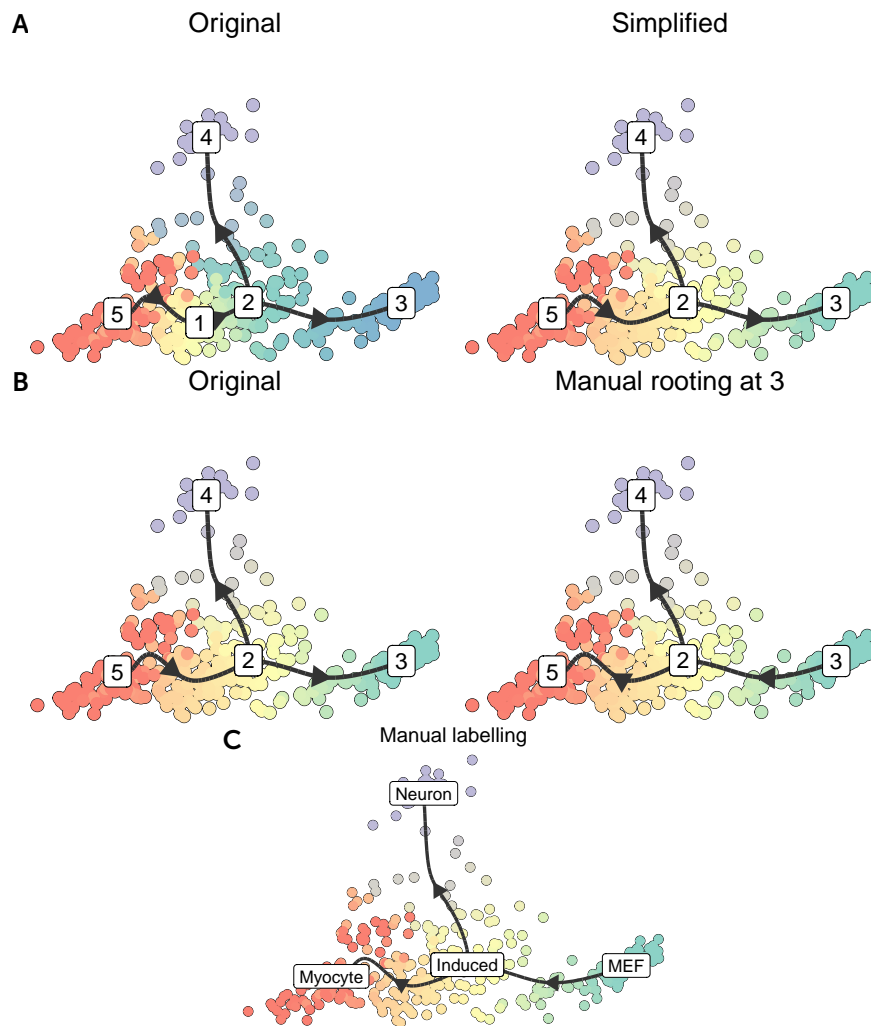


Figure 4.8: **A:** Simplification of the trajectory. **B:** Rooting the trajectory. **C:** Labelling the trajectory.

4.3 Discussion

With *dyno*, we provide a feature-complete toolbox for inferring, visualising and annotating trajectory data. In this work, we demonstrated its usefulness by applying all of its visualisation and manipulation functionality on a particular dataset.

Alternative modalities such as ATAC-Seq or cytometry data are not yet supported, although it is possible to simply include this data as expression and counts. RNA velocity [7] would be particularly useful, as it would allow rooting the directory without any further input from the user.

We are also planning to implement additional tools for interpreting the trajectories, such as alignment and differential expression. While the feature importance tools are incredibly useful towards interpreting trajectories, they do not yet provide a statistical ground to find features which are significantly differentially expressed. In addition, depending on the size of the dataset and of the predicted trajectory, it might take a long time to compute.

feature_id	from	to	importance
Cav1	3	2	3.289198
S100a6	3	2	2.942703
1810020D17Rik	2	5	2.822247
Tagln2	3	2	2.763266
Bex2	2	4	2.672312
Anxa3	3	2	2.630013
Tm4sf1	3	2	2.547472
Vim	3	2	2.431169
Hmga2	3	2	2.376114
Rrm2	3	2	2.346754

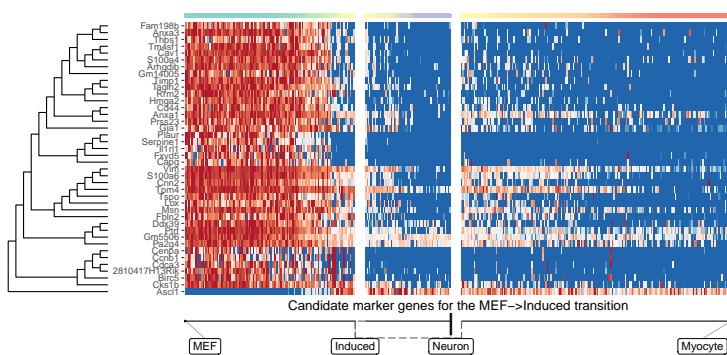


Figure 4.9: Candidate markers genes for the MEF → transition.

milestone_id	feature_id	importance
2	S100a6	2.654416
2	Cav1	2.567051
2	Tagln2	2.501074
2	Fam198b	2.334142
2	Timp1	2.056474
2	Anxa3	2.009431
2	Tm4sf1	1.982274
2	Vim	1.833045
2	Bex2	1.738471
2	Rrm2	1.678349

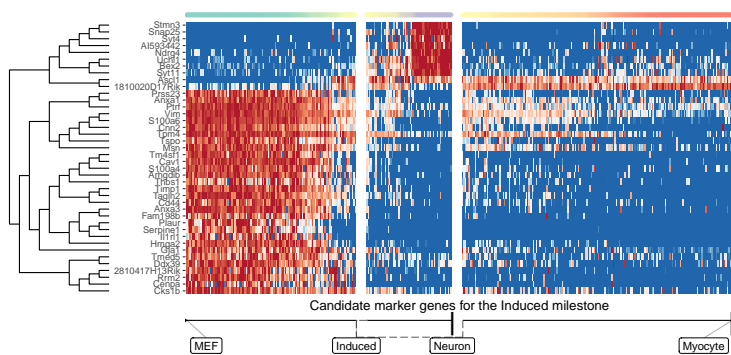


Figure 4.10: Candidate markers genes for the 'induced' milestone.

feature_id	importance
Tpm2	0.4539798
Tagln2	0.3364078
Vim	0.3319566
Plaur	0.3252199
Cav1	0.3224918
Hmga2	0.3189412
Ptrf	0.3180152
Tnnc2	0.3092800
Acta1	0.3087145
Myl1	0.3014400

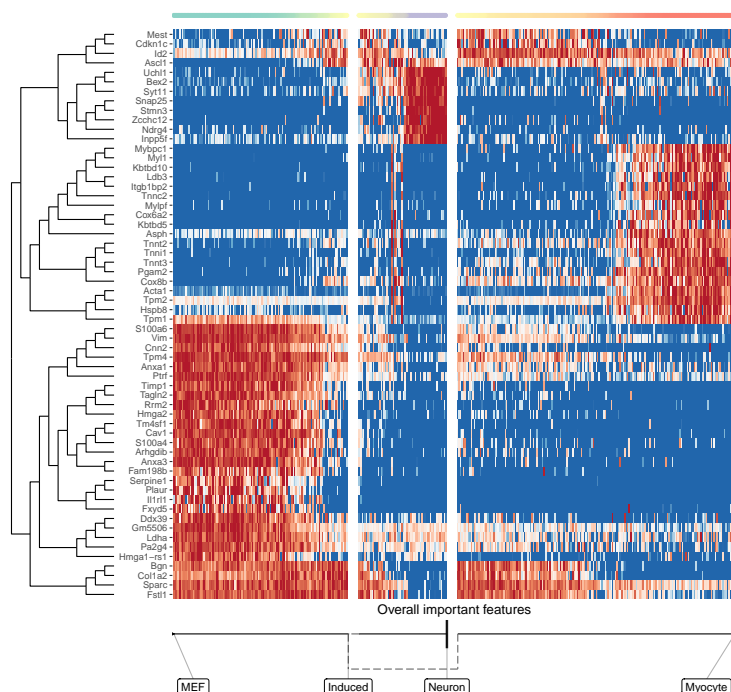


Figure 4.11: Candidate markers genes for the overall trajectory.

4.4 References

- [1] Amos Tanay and Aviv Regev. "Scaling Single-Cell Genomics from Phenomenology to Mechanism". In: *Nature* 541.7637 (Jan. 2017), nature21350. ISSN: 1476-4687. DOI: [10.1038/nature21350](https://doi.org/10.1038/nature21350).
- [2] Martin Etzrodt, Max Endele, and Timm Schroeder. "Quantitative Single-Cell Approaches to Stem Cell Research". In: *Cell Stem Cell* 15.5 (2014), pp. 546–558.
- [3] Robrecht Cannoodt, Wouter Saelens, and Yvan Saeys. "Computational Methods for Trajectory Inference from Single-Cell Transcriptomics". In: *European Journal of Immunology* 46.11 (Nov. 1, 2016), pp. 2496–2506. ISSN: 1521-4141. DOI: [10.1002/eji.201646347](https://doi.org/10.1002/eji.201646347).
- [4] Wouter Saelens et al. "A Comparison of Single-Cell Trajectory Inference Methods". In: *Nature Biotechnology* 37 (May 2019). ISSN: 15461696. DOI: [10.1038/s41587-019-0071-9](https://doi.org/10.1038/s41587-019-0071-9).
- [5] Barbara Treutlein et al. "Dissecting Direct Reprogramming from Fibroblast to Neuron Using Single-Cell RNA-Seq". In: *Nature* 534.7607 (2016), pp. 391–395.
- [6] Kelly Street et al. "Slingshot: Cell Lineage and Pseudotime Inference for Single-Cell Transcriptomics". In: *BMC Genomics* 19.1 (June 2018), p. 477. ISSN: 1471-2164. DOI: [10.1186/s12864-018-4772-0](https://doi.org/10.1186/s12864-018-4772-0).
- [7] Goele La Manno et al. "RNA Velocity of Single Cells". In: *Nature* 560.7719 (Aug. 2018), pp. 494–498. ISSN: 1476-4687. DOI: [10.1038/s41586-018-0414-6](https://doi.org/10.1038/s41586-018-0414-6).

CHAPTER 5

Paper 4: Fast, accurate, and robust single-cell pseudotime

Abstract

Purpose: Recent advances in single-cell RNA-sequencing allow modelling progression of single cells along a dynamic process of interest as a trajectory. While already more than 75 trajectory inference methods have been developed, comprehensive benchmarking demonstrated that pseudotemporal ordering cells robustly is still a challenging task.

Results: SCORPIUS is a trajectory inference method specialised in pseudotemporally ordering single-cell profiles. Applying SCORPIUS to a large collection of datasets shows that it consistently produces more accurate and robust trajectories in comparison to state-of-the-art trajectory inference methods. We used SCORPIUS to generate novel hypotheses regarding dendritic cell development, which were subsequently validated *in vivo*.

Conclusion: By providing a robust and accurate toolkit for inferring linear trajectories, we aim to make pseudotime analysis as easy-to-use and prevalent as other types of analysis such as differential expression and gene set enrichment.

Publication status

Published in bioRxiv 079509; doi:10.1101/241587; 019-0071-9.

Revised manuscript in preparation.

Cannoot R, Saelens W, Sichien D, Tavernier S, Janssens S, Guilliams M, Lambrecht B, De Preter K, and Saeys Y.

Author contributions

- **R.C.** and Y.S. designed the study.
 - **R.C.** and W.S. benchmarks and analysed the data.
 - S.T. and S.D. generated experimental data.
 - **R.C.** implemented the SCORPIUS software package.
 - **R.C.** wrote the original manuscript.
 - **R.C.**, J.S., G.M., L.B., K.D.P., and Y.S. reviewed and edited the manuscript.
 - K.D.P. and Y.S. supervised the project.

5.1 Introduction

Technological advancements in single-cell omics allow studying a dynamic process in a high-throughput manner. This raises concerns regarding biological fundamentals, such as how to define cell types or transitions between them [1, 2]. Trajectory inference (TI) methods aim to give insight into a dynamic process by inferring a trajectory from omics profiles of cells in which the dynamic process takes place [3].

In linear TI, also sometimes called pseudotemporal ordering, the user assumes that the dynamic process of interest is linear and is interested how gene expression changes along the dynamic process. Linear TI is special case of generalised TI which should be easier to tackle since topology is fixed. However, a recent benchmarking study showed that even linear TI is a non-trivial task [4], with most TI methods not capable of producing accurate models for many linear datasets.

In this work, we explain the workings of SCORPIUS, a toolbox specialised in inferring and interpreting linear trajectories. We show that SCORPIUS obtains higher accuracy scores on linear datasets in comparison to state-of-the-art TI methods. Finally, we demonstrate its usage by extracting novel findings from an existing single-cell omics dataset containing developing dendritic cells [5].

5.2 Results

In essence, SCORPIUS reduces the dimensionality of the dataset using Multi-Dimensional Scaling (MDS) [6], and derives a smooth curve that goes through the middle of the dataset using principal curves [7] (Figure 5.1A). However, both MDS and principal curves scale poorly with respect to the number of cells in the dataset, so these were adapted to scale linearly instead (See Methods). In addition, SCORPIUS produces a heatmap of the genes which are strongly up- or downregulated in function of the pseudotemporal ordering (Figure 5.1B). The genes are prioritised using the Random Forest feature importance score [8]. By clustering the genes into sets of coexpressed genes, the user can more easily reason about the functional aspect of the different gene modules.

Examples of other (linear and non-linear) TI methods illustrate common sources of low-accuracy predictions in linear TI (Figure 5.1C), namely the inference of false positive branches or incorrect pseudotemporal orderings.

5.2.1 SCORPIUS outperforms existing TI tools in inferring linear trajectories

In the TI method benchmark, SCORPIUS outperforms all other TI methods in inferring accurate models for datasets containing a linear trajectory [4]. Out of 45 TI methods – of which 14 were linear TI methods – SCORPIUS was the only method capable of producing top-scoring predictions on more than 50% of datasets containing linear trajectories (Figure 5.2A). Overall, SCORPIUS obtained the highest mean accuracy score on linear datasets, and was also one of the top ranked methods in terms of scalability, stability, and usability (Figure 5.2B).

We evaluated the gain in execution time due to optimisations made in the dimensionality reduction and the smoothing of the principal curve. In classical MDS, a square distance matrix between all cells is calculated. In Landmark MDS (LMDS), only the distances between a randomly selected set of landmarks and all other cells needs to be computed, reducing the execution time of the dimensionality

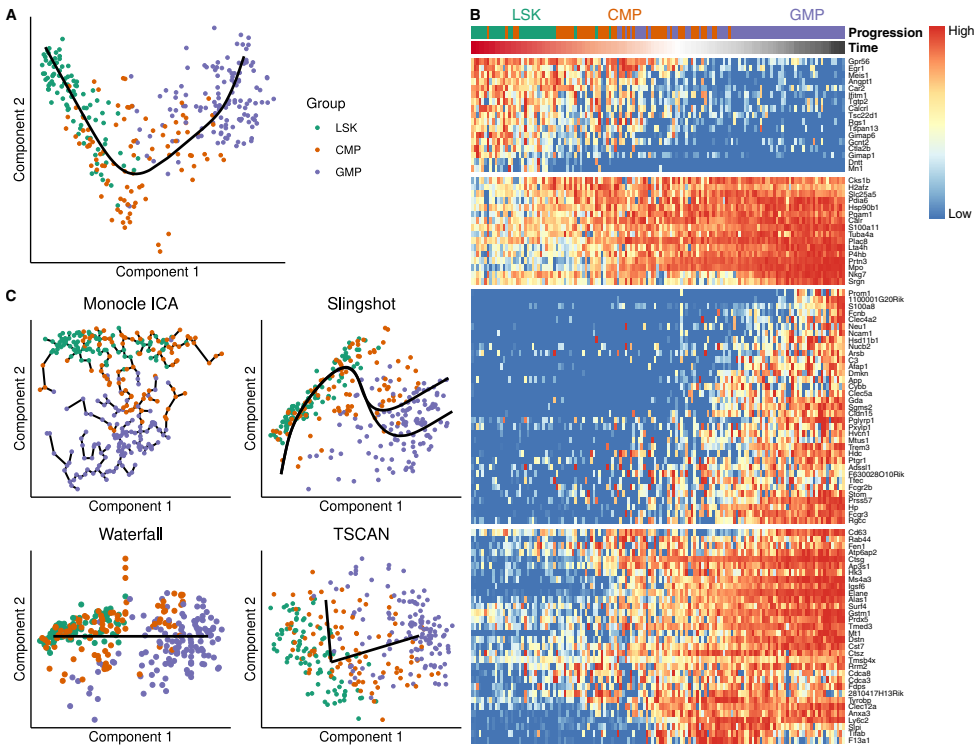


Figure 5.1: **A:** SCORPIUS derives a smooth curve that passes through the middle of the dataset. **B:** Prioritising genes in function of the pseudotemporal ordering allows easier interpretation of the dynamic process at hand. **C:** Low accuracy predictions are a result of false positive branches or incorrect pseudotemporally orderings.

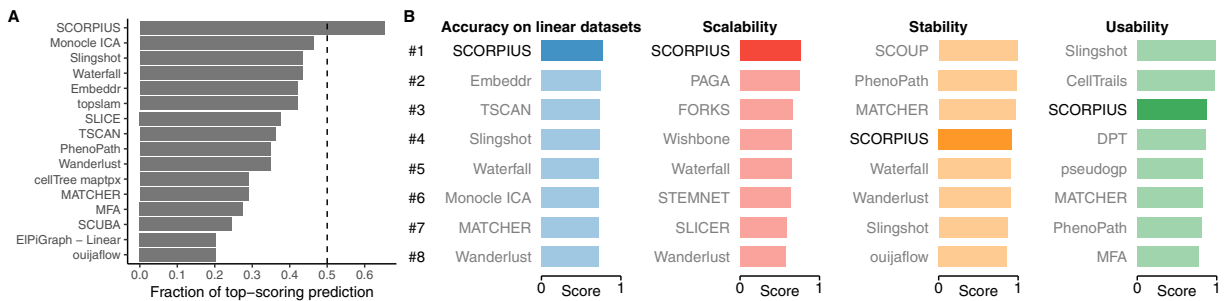


Figure 5.2: SCORPIUS outperforms 44 TI methods in inferring linear trajectories. **A:** It is the only method to produce top-scoring predictions on more than 50% of linear datasets. A predicted model is considered top-scoring if its accuracy is larger than 95% of the maximum accuracy obtained by any method on the same dataset. **B:** SCORPIUS ranks highly in all other categories: scalability, stability and usability. The scalability experiments were performed by upsampling a toy dataset and measuring the execution time and memory usage of each method. Stability experiments were performed by running each method multiple times on subsampled datasets and calculating the similarities between results. The usability of each method was determined by defining a list of good scientific and programming practices and determining to what extent each of these methods adhered to each aspect.

reduction significantly (Figure 5.3A). In the standard principal curves algorithm, a curve consisting of $n - 1$ segments is iteratively smoothed with respect to the positions of n cells. By approximating the principal curve between iterations using a fixed number of segments (e.g. 100), again the execution time of the principal curve algorithm is reduced significantly (Figure 5.3B).

5.2.2 Functional modules in dendritic cell development

Applying SCORPIUS to a dataset of dendritic cell (DC) progenitors [5] reveals several sets of functional modules which are up- and down-regulated during development. DC progenitors are derived from

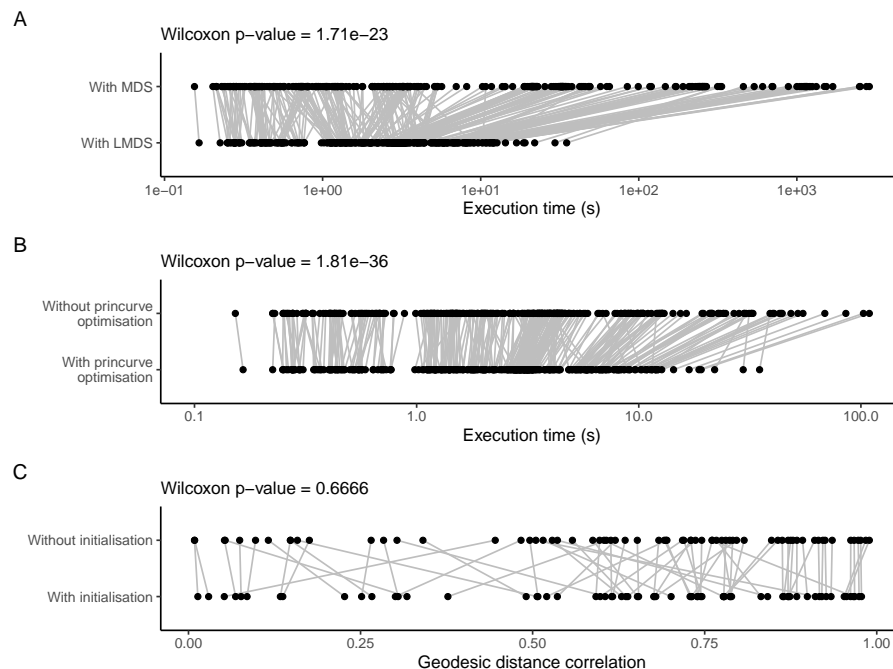


Figure 5.3: Comparison of the effect of different optimisations made in SCORPIUS. The optimisations in the dimensionality reduction (**A**) and principal curves (**B**) steps significantly reduce the execution times of SCORPIUS. Initialising the principal curve does not yield significant improvements on the accuracy of the predicted trajectory (**C**).

hematopoietic stem cells in the bone marrow, and transition through multiple cellular states before becoming fully developed DCs [9]. The dataset contains 57 Monocyte and Dendritic cell Progenitors (MDPs), 95 Common Dendritic cell Progenitors (CDPs) and 96 Pre-Dendritic Cells (PreDCs). SCORPIUS correctly orders the cells with regard to their differentiation status, as indicated by comparing the inferred trajectory with the known transition states (Figure 5.4A).

In order to predict which genes are involved in DC development, SCORPIUS computes the importance value of the genes with respect to the pseudotemporal ordering and selects the top genes for further visualisation. Clustering the genes into gene modules allows to discover similar gene regulation patterns and gene functionality along the pseudotime (Figure 5.4C). In this dataset, modules 1 to 3 are downregulated during the development, while modules 4 to 6 are upregulated, indicating that as part of development the cells lose some functionality but gain others.

The gene expression changes shown in modules 1 to 3 are very gradual and mainly contain genes involved in early hematopoiesis or parallel hematopoietic lineage branches (module 1 and 2), and protein synthesis (module 3). These expression patterns of modules 1 and 2 are expected; as a DC progenitor develops into a DC, it will lose expression of genes associated with pluripotency. In addition, the protein synthesis rate has been shown to gradually decrease during granulocyte and B-cell development [11]. Module 3 suggests that an analogous process exists during DC development. We quantified the protein synthesis rate of murine bone marrow cells *in vivo* by intraperitoneally injecting O-propargyl-puromycin (OP-Puro). While the OP-Puro fluorescence intensities varied across the five individual mice, the relative fluorescence levels are very similar across replicates (Figure 5.4C) and show that indeed protein synthesis rates initially increase during early hematopoiesis but subsequently decrease during DC development.

While module 4 contains mostly genes that are already known to be involved in dendritic cell de-

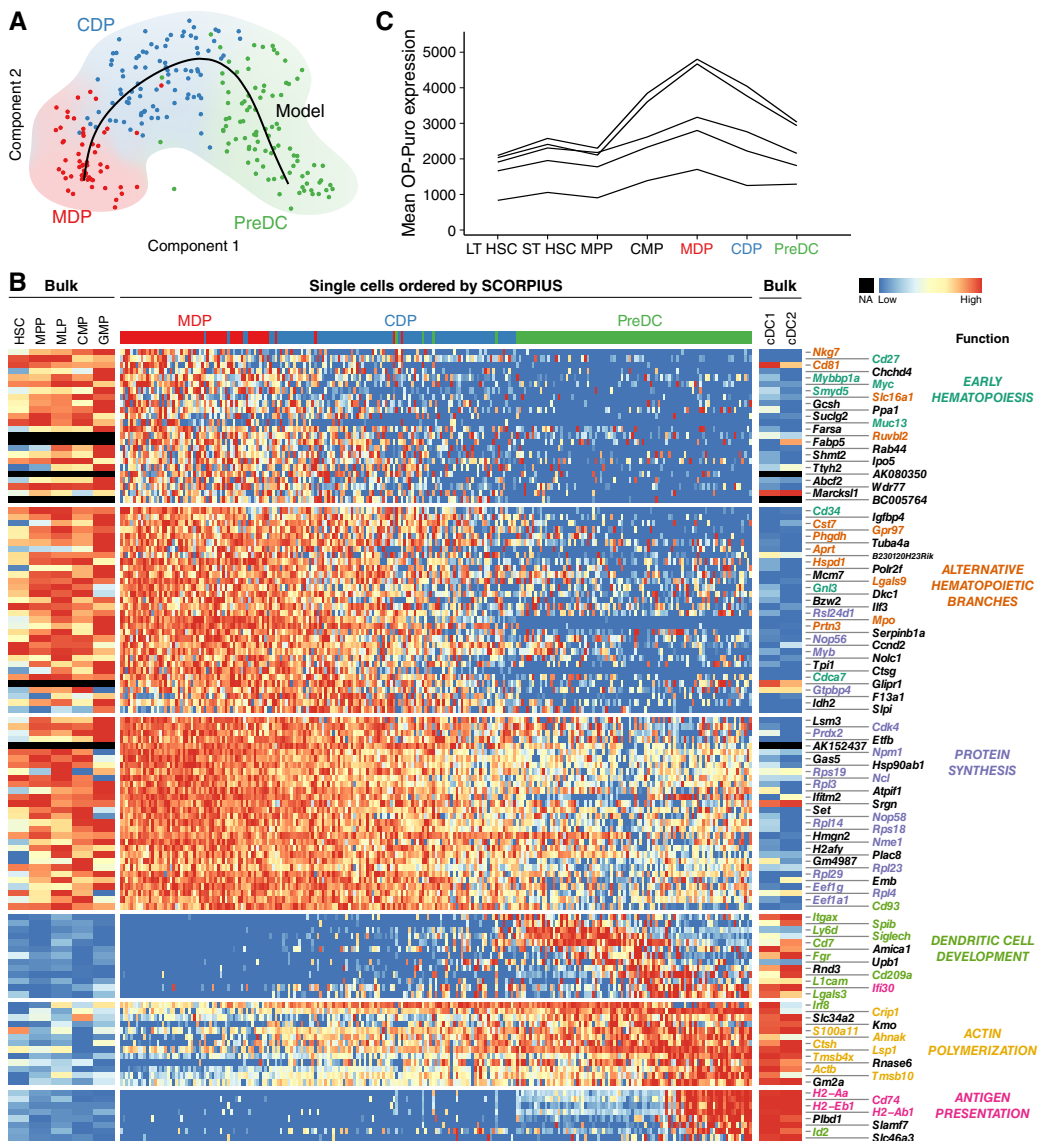


Figure 5.4: SCORPIUS sheds new, data-driven light on dendritic cell development. **A:** SCORPIUS creates an accurate model for DC development from scRNA-seq data. **B:** These genes are clustered into six gene modules. Each module is responsible for different aspects of DC development. Bulk microarray expression for up- and downstream stages of dendritic cell development [10] shows that the gene expression patterns uncovered by SCORPIUS are replicable in other datasets. **C:** In line with the decreasing transcript expression levels of protein translation genes, decreasing OP-Puro fluorescence levels indicates that the protein synthesis rate of preDCs progressively decreases during DC development.

development, it nicely demonstrates the added benefit of pseudotemporal ordering as it possible to distinguish which genes are upregulated first. Module 5 and 6 capture essential functionality of DCs: actin polymerisation plays a crucial role in determining a DC's morphology, migratory behaviour, and antigen internalisation (module 5, [12, 13]), and presenting antigens is one of the core responsibilities of a DC (module 6, [14]).

5.3 Discussion

SCORPIUS is a significant milestone in accurately modelling a multi-stage progression of a dynamic process using single-cell omics datasets. It provides a complete pipeline for inferring, visualising and

interpreting linear trajectories. While linear TI is a simpler case of generalised TI, we showed that it is still a challenging task, as most TI methods generally are not capable of deriving accurate pseudotemporal orderings on linear datasets. SCORPIUS outperforms the 44 other TI methods included in the benchmark in terms of accuracy and stability, and is amongst the top performing methods in terms of stability and usability.

5.4 Methods

SCORPIUS consists of three main steps: dimensionality reduction, trajectory modelling, and feature importance (Figure 5.5). The respective main algorithms for these steps are Multi-Dimensional Scaling (MDS) [6], Principal Curves [7], and Random Forests [8]. However, scRNA-seq datasets can have very high dimensionality (e.g. 100'000 cells and 10'000 features) but are typically very sparse (only 10% of values are non-zero). Each of these steps require modifications in order to be scaleable to large datasets (Sections 5.4.1-5.4.4).

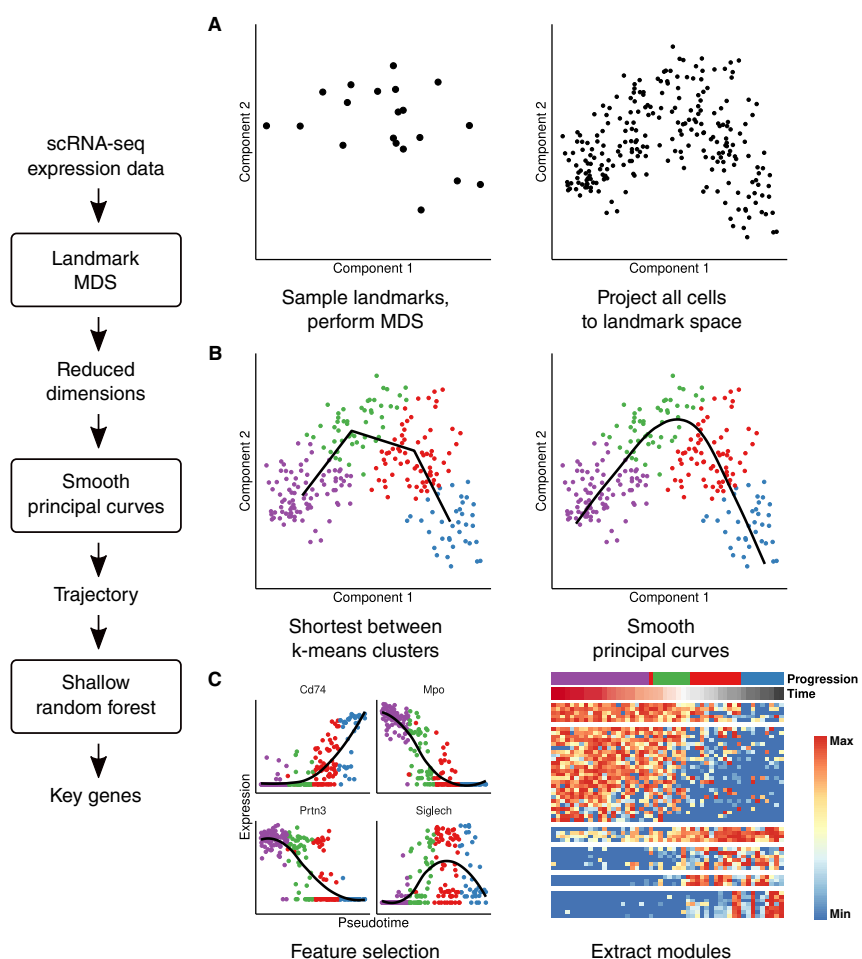


Figure 5.5: SCORPIUS consists of three main steps. **A:** Landmark MDS reduces the dimensionality of a small set of randomly sampled cells called landmarks. Afterwards, all other cells are projected to the landmark space. **B:** Smooth principal curves are used to pseudotemporally order the cells. The principal curve is initialised by connecting k -means clusters to improve robustness. **C:** Shallow random forests prioritise which genes best explain the pseudotemporal ordering.

5.4.1 Sparse Spearman Rank Correlation

Before dimensionality reduction, the distance between two cells x and y is calculated as the Spearman distance for tied ranks (Equation 5.1).

$$\text{dist}(x, y) = \frac{1}{2} - \frac{\text{cov}(\vec{r}_x, \vec{r}_y)}{2 \times \text{sd}(\vec{r}_x) \times \text{sd}(\vec{r}_y)} \quad (5.1)$$

with \vec{r}_x = The rank of the expression values of x ,

$\text{cov}(x, y)$ = The covariance between x and y ,

$\text{sd}(x)$ = The standard deviation of x .

The expression matrix is sparse, however, and computing the rank \vec{r}_x of a gene X would result in a non-sparse vector. Instead, a transformed rank s_X is computed (Equation 5.2) such that $\text{cov}(\vec{r}_x, \vec{r}_y) = \text{cov}(\vec{s}_x, \vec{s}_y)$ and $\text{sd}(\vec{r}_x) = \text{sd}(\vec{s}_x)$. In practice, the expression values are strictly non-negative, but this solution generalises to matrices where negative values are allowed. Calculating the covariance and standard deviation of sparse vectors is relatively trivial.

$$s_{x,g} = \begin{cases} 0 & \text{if } E_{x,g} = 0 \\ r_{x,g} - N_x + (T_{x,g} + Z_x)/2 & \text{if } E_{x,g} > 0 \\ r_{x,g} - N_x + (T_{x,g} - Z_x)/2 & \text{if } E_{x,g} < 0 \end{cases} \quad (5.2)$$

with $E_{x,g}$ = the expression value of gene g in cell x

$r_{x,g}$ = the rank of $E_{x,g}$ in \vec{E}_x

N_x = the number of negative values in \vec{E}_x ,

Z_x = the number of zero values in \vec{E}_x ,

$T_{x,g}$ = the number of values equal to $E_{x,g}$ in \vec{E}_x ,

The distance can be computed using the `calculate_distance()` function from the CRAN package `dynutils`. This function is a wrapper for calculating the transformed rank on a sparse matrix, and calculating the Pearson correlation using `proxyC`.

5.4.2 Landmark Multi-Dimensional Scaling

Landmark MDS [15] is an extension of classical Torgerson MDS [6]. Classical MDS requires the computation of the distance matrix between all pairs of cells, which does not scale well to large datasets. Instead, Landmark MDS only computes the pairwise distances between a small set of landmark cells (which should be representative of the whole population), and project all other cells to the landmark space. Landmark MDS is computed using the `lmds()` function from the CRAN package `lmds`.

5.4.3 Approximated Principal Curves

A principal curve is a smooth one-dimensional curve that passes through the middle of the dimensionality reduction [7]. To best fit the data, the curve is first initialised by k -means clustering the data into k clusters and calculating the shortest path going through each of the cluster centres. The curve

is then iteratively refined by smoothing the coordinates curve in function of the distance from the start, and then orthogonally projecting all cells to the curve. The next iteration uses the curve defined by the segments spanned between the projections of the cells. The distance of a cell from the start of the curve is called its pseudotime.

In the original implementation of the principal curves algorithm, the curve would consist of $N - 1$ segments for a dataset containing N cells; thus the algorithm would not scale well to large datasets. After the smoothing step, a simplification of the curve has been added such that the curve is approximated by a fixed number of segments. The principal curve algorithm is implemented in the `principal_curve()` function from the CRAN package `princurve`.

5.4.4 Gene Importances

Gene importances are calculated by training a Random Forest [16] to predict the pseudotime values from the expression values in the dataset. The algorithm intrinsically computes a feature importance score which ranks the genes in terms of how well a feature is able to predict the pseudotime values. For computing the gene importance values, the `ranger()` function from the CRAN package `ranger` is used [17].

5.4.5 Datasets and benchmark results

The results of the benchmark analysis were obtained directly from the benchmark of 45 Tl methods [4], available at github.com/dynverse/dynbenchmark_results. The accuracy, scalability, stability and usability metrics are described by Saelens et al. [4]. All datasets were obtained from a repository of single-cell omics datasets containing a trajectory hosted on Zenodo record number 1443566 [18].

5.4.6 Measurement of protein synthesis

O-Propargyl Puromycin (Jena Bioscience - NU-931-5) was dissolved in DMSO, further diluted in PBS (10 mg mL^{-1}) and injected intraperitoneally (50mg/kg mouse weight). 1 hour after injection mice were euthanized by cervical dislocation and hind bones were collected. Bone marrow cells were obtained by crushing of bones with pestle and mortar and subsequent lysis of red blood cells. The remaining cells were filtered through a $70 \mu\text{m}$ mesh and resuspended in a Ca^{2+} and Mg^{2+} free phosphate buffered solution (PBS; Gibco). Viable cell numbers were assessed with a FACS Verse (BD Biosciences).

7×10^6 cells were stained with mixtures of antibodies directed against cell surface markers. Each staining lasted approximately 30 min and was performed on ice protected from direct light. Monoclonal antibodies labeled with fluorochromes or biotin recognizing following surface markers were used: CD3 (145-2C11; Tonbo), TCRb (H57-597; BD Pharmingen), CD4 (RM4-5; eBioscience), CD8a (53-6.7; BD Pharmingen), CD19 (1D3; Tonbo), CD45R (RA3-6B2; BD-Pharmingen), TER119 (TER119; eBioscience), Ly-6G (1A8; BD-Pharmingen), NK1.1 (PK136; eBioscience), F4/80 (BM8; eBioscience), CD11c (N418; eBioscience), MHCII (M5/114.15.2; eBioscience), CD135 (A2F10; eBioscience), CD172a (P84; eBioscience), CD45 (30-F11; eBioscience), SiglecH (eBio440c; eBioscience), Ly-6C (HK1.4; eBioscience), CD115 (AFS98; eBioscience), CD117 (2B8; eBioscience), CD127 (SB/199; BD-Pharmingen), Ly-6A/E (D7; eBioscience), CD34(RAM34; eBioscience), CD11b (M1/70; BD Pharmingen). Viable cells were discriminated by the use of the fixable viability dye eFluor506 or eFluor786 (eBioscience).

Next, cells were fixed and permeabilized using the FoxP3 Fixation/Permeabilization kit (eBioscience, 00-5521-00). For OP-Puro labeling, Azide-AF647 is chemically linked to OP-Puro through a copper-catalyzed azide–alkyne cycloaddition. In short, 2.5 µM azide-AF647 (Invitrogen, A10277) is dissolved in the Click-iT Cell Reaction Buffer (Invitrogen, C10269) containing 400 µM CuSO₄. Immediately after preparation, cells are incubated with this mixture on room temperature. After 10 min incubation, the reaction is quenched by addition of PBS supplemented with 5% heat-inactivated fetal calf serum (FCS; Sigma) and 5 mM EDTA (Lonza; 51234). Cells are washed twice to remove unbound azide-AF647. A Fortessa X20 (BD Biosciences) was used for data acquisition and data was analyzed using FlowJo 10 (LLC).

5.4.7 Code availability

SCORPIUS is available as an open source software package on [CRAN](#). All code used in this study is made publicly available at github.com/rcannood/scorpius_analysis.

5.5 References

- [1] Martin Etzrodt, Max Endele, and Timm Schroeder. "Quantitative Single-Cell Approaches to Stem Cell Research". In: *Cell Stem Cell* 15.5 (2014), pp. 546–558.
- [2] Amos Tanay and Aviv Regev. "Scaling Single-Cell Genomics from Phenomenology to Mechanism". In: *Nature* 541.7637 (Jan. 2017), nature21350. ISSN: 1476-4687. DOI: [10.1038/nature21350](https://doi.org/10.1038/nature21350).
- [3] Robrecht Cannoodt, Wouter Saelens, and Yvan Saeys. "Computational Methods for Trajectory Inference from Single-Cell Transcriptomics". In: *European Journal of Immunology* 46.11 (Nov. 1, 2016), pp. 2496–2506. ISSN: 1521-4141. DOI: [10.1002/eji.201646347](https://doi.org/10.1002/eji.201646347).
- [4] Wouter Saelens et al. "A Comparison of Single-Cell Trajectory Inference Methods". In: *Nature Biotechnology* 37 (May 2019). ISSN: 15461696. DOI: [10.1038/s41587-019-0071-9](https://doi.org/10.1038/s41587-019-0071-9).
- [5] Andreas Schlitzer et al. "Identification of cDC1- and cDC2-Committed DC Progenitors Reveals Early Lineage Priming at the Common DC Progenitor Stage in the Bone Marrow". In: *Nature Immunology* 16.7 (July 2015), pp. 718–728. ISSN: 1529-2916. DOI: [10.1038/ni.3200](https://doi.org/10.1038/ni.3200).
- [6] Warren S Torgerson. *Theory and Methods of Scaling*. John Wiley & Sons, 1958.
- [7] Trevor Hastie and Werner Stuetzle. "Principal Curves". In: *Journal of the American Statistical Association* 84.406 (1989), pp. 502–516. ISSN: 01621459. DOI: [10.2307/2289936](https://doi.org/10.2307/2289936).
- [8] Leo Breiman. "Random Forests". In: *Machine Learning* 45 (2001), pp. 5–32.
- [9] Miriam Merad et al. "The Dendritic Cell Lineage: Ontogeny and Function of Dendritic Cells and Their Subsets in the Steady State and the Inflamed Setting." In: *Annual review of immunology* 31 (2013), pp. 563–604. ISSN: 1545-3278. DOI: [10.1146/annurev-immunol-020711-074950](https://doi.org/10.1146/annurev-immunol-020711-074950). pmid: [23516985](#).
- [10] Jennifer C Miller et al. "Deciphering the Transcriptional Network of the Dendritic Cell Lineage". In: *Nature Immunology* 13.9 (2012), pp. 888–899. ISSN: 1529-2908. DOI: [10.1038/ni.2370](https://doi.org/10.1038/ni.2370). pmid: [22797772](#).
- [11] Robert A J Signer et al. "Haematopoietic Stem Cells Require a Highly Regulated Protein Synthesis Rate." In: *Nature* 509.7498 (2014), pp. 49–54. ISSN: 1476-4687. DOI: [10.1038/nature13035](https://doi.org/10.1038/nature13035). pmid: [24670665](#).
- [12] Pablo Vargas et al. "Innate Control of Actin Nucleation Determines Two Distinct Migration Behaviours in Dendritic Cells." In: *Nature cell biology* 18.1 (2016), pp. 43–53. ISSN: 1476-4679. DOI: [10.1038/ncb3284](https://doi.org/10.1038/ncb3284). pmid: [26641718](#).
- [13] Zhenzhen Liu and Paul A. Roche. "Macropinocytosis in Phagocytes: Regulation of MHC Class-II-Restricted Antigen Presentation in Dendritic Cells". In: *Frontiers in Physiology* 6 (JAN 2015), pp. 1–6. ISSN: 1664042X. DOI: [10.3389/fphys.2015.00001](https://doi.org/10.3389/fphys.2015.00001). pmid: [25688210](#).
- [14] Ralph M Steinman. "The Dendritic Cell System". In: (1991), pp. 203–208.
- [15] Vin de Silva and Joshua B Tenenbaum. "Sparse Multidimensional Scaling Using Landmark Points". In: *Technical report, Stanford University* (2004), p. 41.
- [16] L Breiman et al. *Classification and Regression Trees*. Wadsworth Publishing Company, 1984.
- [17] Marvin N Wright and Andreas Ziegler. "Ranger: A Fast Implementation of Random Forests for High Dimensional Data in C++ and R". In: *Journal of Statistical Software* 77.1 (Mar. 2017). DOI: [10.18637/jss.v077.i01](https://doi.org/10.18637/jss.v077.i01).
- [18] Robrecht Cannoodt et al. "Single-Cell -Omics Datasets Containing a Trajectory". In: Zenodo (Oct. 2018). DOI: [10.5281/zenodo.1211532](https://doi.org/10.5281/zenodo.1211532).

CHAPTER 6

Paper 5: Inferring single cell regulatory networks

Abstract

Purpose: ...

Results: ...

Conclusion: ...

Publication status

Manuscript in preparation.

Cannoodt R, Saeys Y*, and De Preter K*.

* Equal contribution

Author contributions

- **R.C.**, K.D.P., and Y.S. designed the study.
- **R.C.** performed the experiments and analysed the data.
- **R.C.** implemented the bred software package.
- **R.C.** wrote the original manuscript.
- **R.C.**, K.D.P., and Y.S. reviewed and edited the manuscript.
- K.D.P. and Y.S. supervised the project.

6.1 Introduction

One of the central cellular processes underlying development is transcriptional regulation. During development, changes in transcription factor activity induce chromatin modifications, chromatin remodelling and ultimately a differential recruitment of the basal transcriptional machinery [1]. Modelling the dynamics of gene regulation is therefore essential to better understand why a cellular dynamic processes progresses through several steps, and what goes wrong in the case of disease.

The dynamics of gene regulation has classically been studied using time series data [2]. When dynamic processes progress asynchronously, such as in hematopoiesis, time series data are usually obtained by sorting different transition states and assessing bulk gene expression and transcription factor binding within the population [3, 4, 5, 6]. Alternatively, time series data can also be generated by synchronizing the dynamic process between cells. However, issues with time-resolution, heterogeneity and good *in vivo* synchronization models can often limit the predictive power of the dynamic models of gene regulation which can be constructed [2].

One of the main advantages of single-cell transcriptomics is the ability to quantify the exact cellular state of thousands of cells per experiment. The intercellular heterogeneity caused by naturally occurring biological stochasticity [7] can be exploited to predict regulatory interactions between transcription factors (TFs) and their target genes. The computational tools that infer gene regulatory networks (GRNs) from omics datasets are called network inference (NI) methods.

Several studies have highlighted how some regulatory interactions can be very dynamic while others show evidence of being static during consecutive developmental stages [8, 9]. Since regulatory interactions are context-dependent [10], attempting to create an accurate model of those processes by inferring a static regulatory network may have limited relevance. Case-wise NI methods¹ avoid predicting a static GRN and instead infer one GRN per cell (or per sample, for bulk omics data).

In order to compute a case-wise GRN for a single sample, Kuijzer et al. [11] and Liu et al. [12] employ similar strategies, namely by computing the difference of computing a static GRN for all the cases, and computing a static GRN for all the cases minus one. Since this procedure needs to be repeated for every case in the dataset, and because NI methods are already amongst the most computationally intensive analyses to perform on omics data, this methodology is not applicable for large omics datasets. Another case-wise NI method, SCENIC [13] infers case-wise GRNs by first inferring a static GRN using GENIE3 [14]. GENIE3 is a static NI method which uses Random Forests [15] feature importance scores to prioritise candidate regulators for a particular target gene. SCENIC then post-processes the static GRN to determine whether an interaction is enriched for particular cases, resulting in a case-wise GRN. In short, while several case-wise NI methods thus already exist, their implementation consisted of post-processing a static GRN to arrive at a case-wise GRN.

In this work, we introduce `bred`, the first ‘true’ case-wise NI method. For each interaction in the inferred case-wise GRN, `bred` predicts both the regulatory strength and its effect. The case-wise GRNs – or ‘case-wise regulomes’ – can be analysed analogously to transcriptomics data; for example by clustering samples, inferring trajectories, or finding differentially activated regions. We demonstrate `bred` by applying it to a single-cell dataset of 22'122 hematopoietic cells from the Tabula Muris project [16], and to a collection of 14'963 bulk omics samples from The Cancer Genome Atlas project [17].

¹Case-wise NI is sometimes also called sample-specific NI or case-specific NI.

6.2 Results

6.2.1 Hematopoietic cells from Tabula Muris

From the Tabula Muris [16] project, we selected all cells involved in some part of the hematopoietic lineage tree. We computed case-wise GRNs between 22'122 remaining single cells, for the 2000 most variable target genes and a subset of transcription factors as regulators.

To summarise the similarity in GRNs across cases, we first visualise a dimensionality reduction of the case-wise GRNs, where every dot represents a single GRN (Figure 6.1A). The dimensionality reduction was computed by applying Fruchterman-Reingold [18] on the k -nearest-neighbour (k NN) graph of the case-wise GRN vectors. On the same k NN graph, the cells were clustered using the Louvain [19] clustering algorithm, and the clusters were labelled using prior information from Tabula Muris. For each cluster, we retained the 50 interactions with the highest mean importance scores (Figure 6.1B). In the visualisation, each node represents a gene, each edge an interaction, and the colour represents which cluster this interaction belongs to.

For the most part, clusters that are proximate in the dimensionality reduction (Figure 6.1A) are also closely connected in the GRN network view (Figure 6.1B). Notably, interactions from the different B cell clusters are almost not connected amongst each-other, while in the dimensionality reduction they're very proximate. Retaining more edges could result in the different B cells being connected in the GRN network view.

At the centre of the network lie many strongly connected interactions which are not specific for any particular cluster, but instead are common to almost all of the clusters. These are likely housekeeping genes or genes involved in key hematopoietic processes.

6.2.2 The Cancer Genome Atlas

We included all available RNA-seq profiles from The Cancer Genome Atlas. In total, we computed case-wise GRNs for 14'963 tumour samples from 50 sub-projects, including 44 different cancer entities. Clusters of case-wise GRNs were relabelled by the project they originate from, or by the cell types or organs the samples originate from.

Most groups of interactions are highly specific to just one cancer type. Samples from the CPTAC project were split into two groups, clustering together with LUAD (lung adenocarcinoma) and kidney carcinoma samples. According to the meta-information of CPTAC profiles, these samples consist of lung, kidney, and uterus adenocarcinomas, explaining the split in CPTAC samples.

6.3 Discussion

The `bred` algorithm is a novel approach for directly computing case-wise GRNs for single-cell omics and bulk omics profiles alike. We applied the method to 22'122 hematopoietic cells and 14'963 cancer profiles, showing that interactions are often grouped together in modules specific for certain cell types, tissue types, or cancer types.

In this work, we only applied clustering methods to the case-specific ‘regulome profiles’, but other types of computational methods can be used to annotate and explore case-specific GRNs, such as

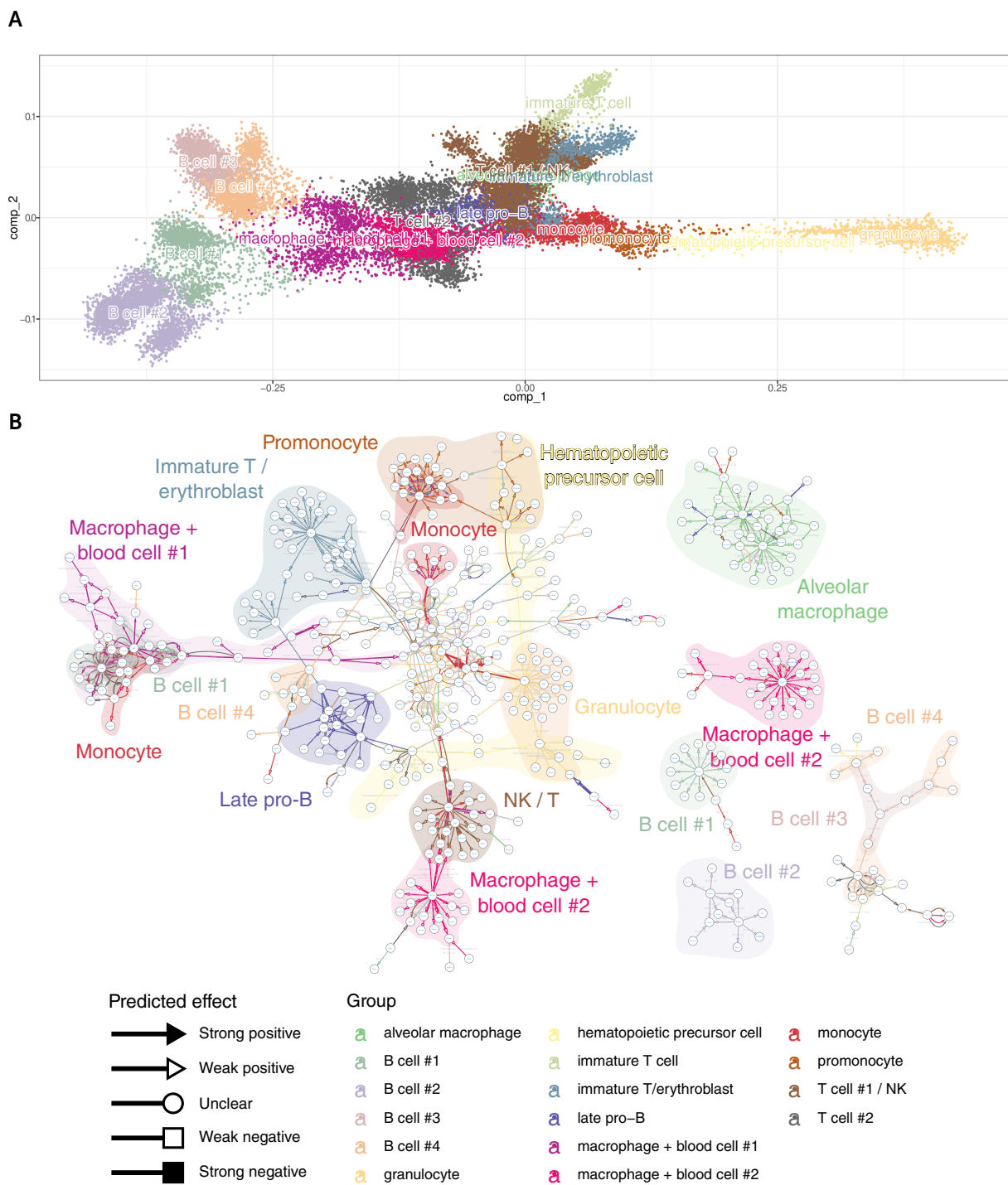


Figure 6.1: 22'122 case-wise GRNs of hematopoietic cells from the Tabula Muris project. A: Each dot in this dimensionality reduction corresponds to the GRN of a single cell. The dimensionality of the cell-specific regulome matrix was reduced using Fruchterman-Reingold and were clustered using Louvain clustering, after which the clusters were relabelled using the meta information from Tabula Muris. **B:** Per cluster, the 50 interactions with the highest mean importance score are visualised.

trajectory inference and differential expression.

Going forward, we will provide further functional validation of the results generated by bred, as well as benchmark the algorithm against various real and *in silico* datasets.

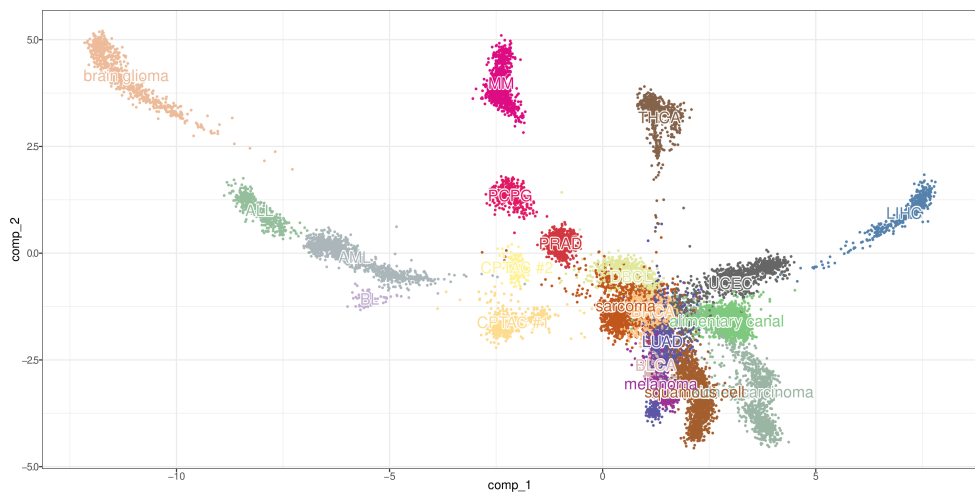
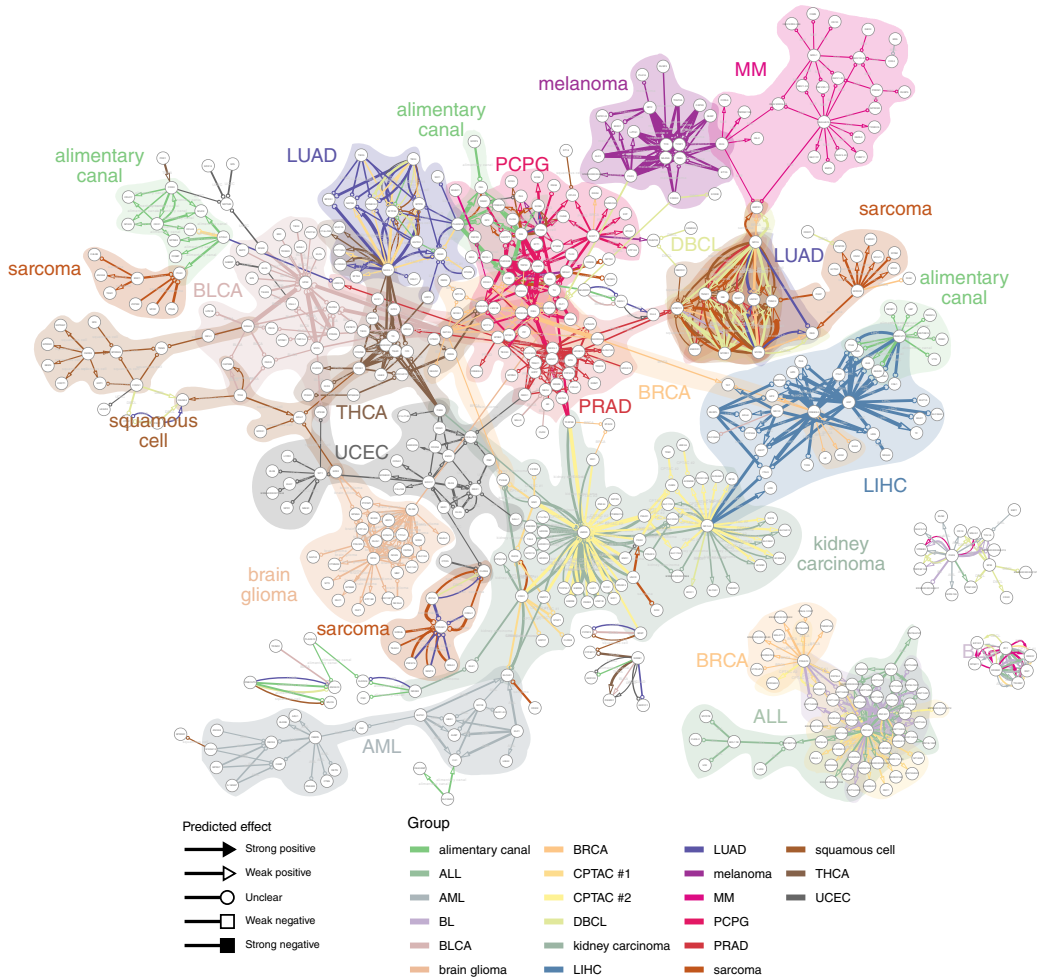
A**B**

Figure 6.2: 14'963 case-wise GRNs of cancer bulk profiles from The Cancer Genome Atlas project. A: The different profiles are visualised and clustered according to their regulomic similarities. **B:** Visualisation of the strongest interactions per cluster shows both pathways distinct to particular cancer entities as well as pathways common to multiple cancer entities.

6.4 Methods

6.4.1 Inferring case-wise GRNs

The task of inferring a static GRN (Figure 6.3A) can be reduced to a simpler problem, namely: for every target T , predict which of the potential regulators R_i regulate T (Figure 6.3B). This simplification allowed GENIE3 [14] to use Random Forest's [15] feature importance scores for inferring GRNs. Namely, a Random Forest is trained to predict the expression of a target gene of interest from the expression of potential regulators. The resulting Random Forest inherently allows to extract a feature importance score by observing the effect of each regulator in making a good prediction for the target expression. As in GENIE3, the target expression is first scaled to normalise feature importance scores across different targets.

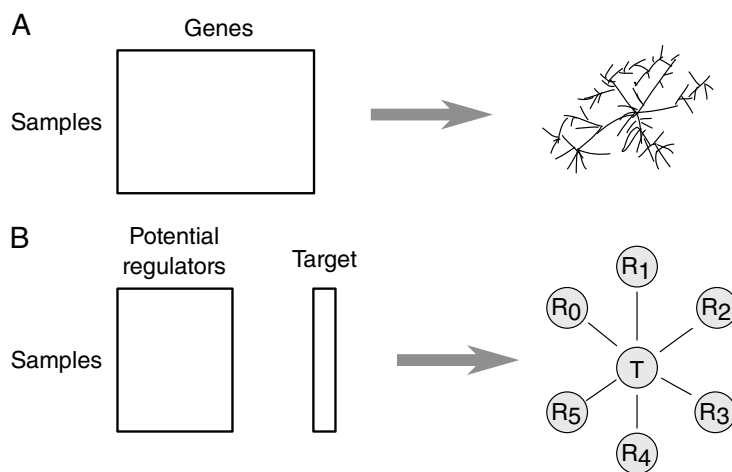


Figure 6.3: **A:** Inferring a gene regulatory network from an omics dataset can be reduced to a simpler problem. **B:** Given the expression of a target of interest and a set of potential regulators, predict which regulators regulate the target gene.

We make the same simplification in order to build case-wise GRNs, also using Random Forests to compute the feature importance scores. A Random Forest consists of K trees, each of which produces feature importance scores, and the feature importance scores of a forest is simply the mean feature importance scores of each of the trees.

Computing the case-wise feature importances of a tree consists of the following 8 steps (Figure 6.4). The 'randomness' of a Random Forest is due to only using a subset of the samples in the dataset in order to build a single decision tree. The samples are split into two groups, the 'in-bag' data and the 'out-of-bag' data (Figure 6.4A). A decision tree [20] is trained on the in-bag expression of the potential regulators in trying to predict the in-bag target gene expression (Figure 6.4B). The target expression of the out-of-bag samples is predicted using the decision tree (Figure 6.4C), and the squared error between the real and target expression is computed (Figure 6.4D). For each sample in the out-of-bag set, this vector represents how well the decision tree was able to predict the expression of the target gene.

The next few steps are repeated for every potential regulator R_i . Within the out-of-bag samples, the expression of R_i is randomly shuffled. The target expression of the out-of-bag samples is again calculated (Figure 6.4F), as well as the squared error between the real target expression and the predicted expression is calculated (Figure 6.4G). The importance of regulator R_i for an out-of-bag sample S_j is

defined as the increase in squared error between the predicted target expression and the real target expression, after perturbing the expression of R_i (Figure 6.4H).

Steps F-G are repeated for every potential regulator R_i . By aggregating all of the feature importance scores over all the samples, regulators and targets, we obtain an M -by- N -by- P tensor².

A moderately-sized dataset could contain $M = 10'000$ samples, $N = 2'000$ regulators, and $P = 10'000$ target genes. Due to memory constraints, only interactions with an average importance value (across all samples) higher than a minimum threshold are retained.

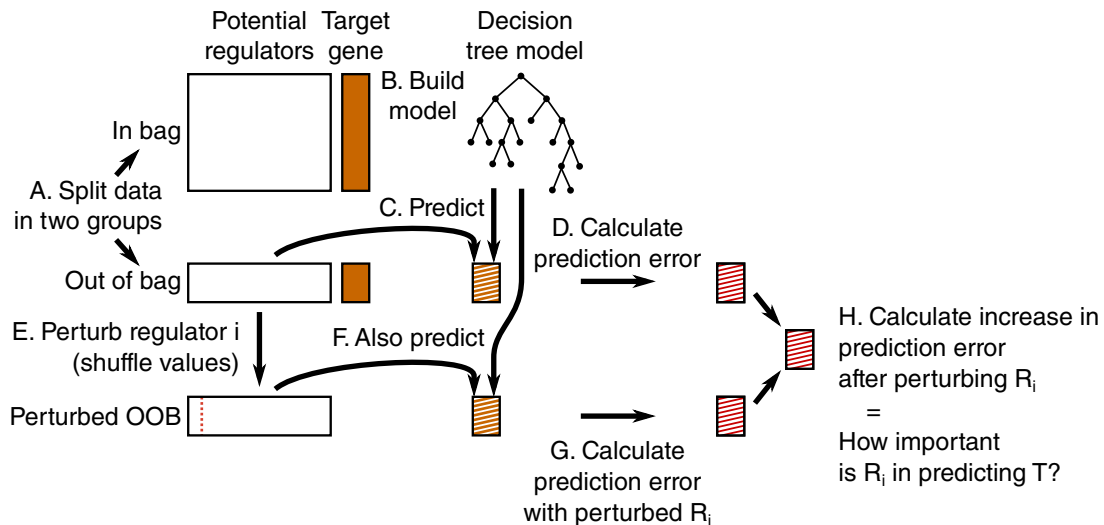


Figure 6.4: Calculating the feature importance score for one decision tree and one target consists of 8 distinct steps. **A:** Randomly split the data into two groups, the in-bag data and the out-of-bag data. **B:** The in-bag data is used to train a decision tree to try to predict the expression of the target gene from the expression values of the regulators. **C:** The decision tree is used to predict the gene expression of the target gene of the out-of-bag samples. **D:** Sample-specific squared error values are computed. **E:** Repeat steps E-H for every regulator R_i . Perturb the expression of regulator R_i in the out-of-bag samples. **F:** Again predict the gene expression of the target gene with the perturbed expression values. **G:** Again compute the sample-specific squared error values. **H:** The difference between the prediction error on the perturbed dataset versus the prediction error on the unperturbed is the importance in R_i in predicting T

To compute the case-wise GRNs, we implemented the abovementioned methodology in C++ in a modified version of the `ranger` R/C++ package [21].

6.4.2 Predicting the effect of an interaction

To predict the effect of a potential regulator R_i on a target gene T for a given tree, the Pearson correlation is calculated between the difference in regulator expression (before and after shuffling the values), and the difference in target expression prediction.

$$\text{effect}(R_i \rightarrow T) = \text{cor}(x, y),$$

with $x = \text{expr_shuffled}[:, R_i] - \text{expr}[:, R_i]$,

and $y = \text{predict(tree, expr_shuffled)} - \text{predict(tree, expr)}$.

The Pearson correlation between two variables x and y is usually defined as shown in Equation 6.1.

²This is the origin of the name of the method, "breed".

Computing r_{xy} for each (regulator, target) pairs, across all trees, would require storing large amounts of data.

$$r_{xy} = \frac{\sum_{i=1}^n (x_i - \bar{x}) \times (y_i - \bar{y})}{\sqrt{\sum_{i=1}^n (x_i - \bar{x})^2} \times \sqrt{\sum_{i=1}^n (y_i - \bar{y})^2}} \quad (6.1)$$

However, by rearranging the formula, it can be defined as Equation 6.2.

$$r_{xy} = \frac{\sum (x_i \times y_i) - \sum x \times \sum y/n}{\sqrt{(\sum x_i^2 - (\sum x)^2/n)} \times \sqrt{(\sum y_i^2 - (\sum y)^2/n)}} \quad (6.2)$$

For every regulator R_i during a perturbation in a given tree, only 6 values need to be stored, namely $A = \sum x_i$, $B = \sum y_i$, $C = n$, $D = \sum x_i \times y_i$, $E = \sum x_i \times x_i$, and $F = \sum y_i \times y_i$.

For every (regulator, target) pair, these values are summed, and the r_{xy} is calculated as shown in Equation 6.3.

$$r_{xy} = \frac{D - A \times B/C}{\sqrt{(E - A^2/C)} \times \sqrt{(F - B^2/C)}} \quad (6.3)$$

The following cutoffs were used to determine the effect.

- Strong negative: $r_{xy} < -0.4$
- Weak negative: $-0.4 \leq r_{xy} < -0.2$
- Unclear: $-0.2 \leq r_{xy} \leq 0.2$
- Weak positive: $0.2 < r_{xy} \leq 0.4$
- Strong positive: $0.4 < r_{xy}$

6.4.3 Clustering of case-wise GRNs

To perform downstream analysis on the cases, first a k -nearest neighbour (k NN) graph of the cases is computed. In order for the k NN graph to better emphasise similarities in GRNs rather than absolute euclidean distances, we first reduce the dimensionality of the case-by-interaction matrix to case-by-20 matrix using Landmark Multi-Dimensional Scaling [22] with a Spearman rank distance metric.

Next, KD-trees are used to calculate the k NN graph efficiently. The cases in the dataset are visualised and clustered using the Fruchterman-Reingold [18] and Louvain clustering [19], respectively.

The following R packages provided implementations for each of these algorithms: lmds, RANN, igraph [23].

6.4.4 Visualising clustered GRNs

After Louvain clustering, the interactions of the 50 interactions with highest mean importance per cluster are retained. These interactions are visualised in Cytoscape [24], in which nodes depict genes, edges depict predicted regulatory interactions, coloured according to which cluster they are predicted for. The shape of the arrow denotes the predicted effect of the regulatory interaction.

6.5 References

- [1] Antoine Coulon et al. "Eukaryotic Transcriptional Dynamics: From Single Molecules to Cell Populations". In: *Nature Reviews Genetics* 14 (July 9, 2013), p. 572. DOI: [10.1038/nrg3484](https://doi.org/10.1038/nrg3484).
- [2] Ziv Bar-Joseph, Anthony Gitter, and Itamar Simon. "Studying and Modelling Dynamic Biological Processes Using Time-Series Gene Expression Data". In: *Nat. Rev. Genet.* 13.8 (Aug. 2012), pp. 552–564.
- [3] Noa Novershtern et al. "Densely Interconnected Transcriptional Circuits Control Cell States in Human Hematopoiesis". In: *Cell* 144.2 (2011), pp. 296–309.
- [4] Gillian May et al. "Dynamic Analysis of Gene Expression and Genome-Wide Transcription Factor Binding during Lineage Specification of Multipotent Progenitors". In: *Cell Stem Cell* 13.6 (2013), pp. 754–768.
- [5] Vladimir Jovic et al. "Identification of Transcriptional Regulators in the Mouse Immune System". In: *Nat. Immunol.* 14.6 (2013), pp. 633–643. DOI: [10.1038/ni.2587](https://doi.org/10.1038/ni.2587).Identification.
- [6] Debbie K Goode et al. "Dynamic Gene Regulatory Networks Drive Hematopoietic Specification and Differentiation". In: *Dev. Cell* 36.5 (2016), pp. 572–587.
- [7] Olivia Padovan-Merhar and Arjun Raj. "Using Variability in Gene Expression as a Tool for Studying Gene Regulation". In: *Wiley Interdisciplinary Reviews. Systems Biology and Medicine* 5.6 (Nov. 2013), pp. 751–759. ISSN: 1939-005X. DOI: [10.1002/wsbm.1243](https://doi.org/10.1002/wsbm.1243). pmid: [23996796](#).
- [8] Victoria Moignard et al. "Characterization of Transcriptional Networks in Blood Stem and Progenitor Cells Using High-Throughput Single-Cell Gene Expression Analysis". In: *Nat. Cell Biol.* 15.4 (Apr. 2013), pp. 363–372.
- [9] Cristina Pina et al. "Single-Cell Network Analysis Identifies DDIT3 as a Nodal Lineage Regulator in Hematopoiesis". In: *Cell reports* 11.10 (2015), pp. 1503–1510. ISSN: 2211-1247. DOI: [10.1016/j.celrep.2015.05.016](https://doi.org/10.1016/j.celrep.2015.05.016). pmid: [26051941](#).
- [10] Balázs Papp and Stephen Oliver. "Genome-Wide Analysis of the Context-Dependence of Regulatory Networks". In: *Genome Biology* 6.2 (Jan. 27, 2005), p. 206. ISSN: 1474-760X. DOI: [10.1186/gb-2005-6-2-206](https://doi.org/10.1186/gb-2005-6-2-206).
- [11] Marieke Lydia Kuijjer et al. "Estimating Sample-Specific Regulatory Networks". In: *iScience* 14 (Mar. 28, 2019), pp. 226–240. ISSN: 2589-0042. DOI: [10.1016/j.isci.2019.03.021](https://doi.org/10.1016/j.isci.2019.03.021). pmid: [30981959](#).
- [12] Xiaoping Liu et al. "Personalized Characterization of Diseases Using Sample-Specific Networks". In: *Nucleic Acids Research* 44.22 (2016), e164–e164. ISSN: 0305-1048. DOI: [10.1093/nar/gkw772](https://doi.org/10.1093/nar/gkw772). pmid: [27596597](#).
- [13] Sara Aibar et al. "SCENIC: Single-Cell Regulatory Network Inference and Clustering". In: *Nature Methods* (Oct. 2017). ISSN: 1548-7091. DOI: [10.1038/nmeth.4463](https://doi.org/10.1038/nmeth.4463).
- [14] VÂN ANH HUYNH-THU et al. "Inferring Regulatory Networks from Expression Data Using Tree-Based Methods". In: *PLoS ONE* 5.9 (Jan. 2010), e12776. ISSN: 1932-6203. DOI: [10.1371/journal.pone.0012776](https://doi.org/10.1371/journal.pone.0012776). pmid: [20927193](#).
- [15] Leo Breiman. "Random Forests". In: *Machine Learning* 45 (2001), pp. 5–32.
- [16] Nicholas Schaum et al. "Single-Cell Transcriptomics of 20 Mouse Organs Creates a Tabula Muris". In: *Nature* 562.7727 (Oct. 2018), pp. 367–372. ISSN: 1476-4687. DOI: [10.1038/s41586-018-0590-4](https://doi.org/10.1038/s41586-018-0590-4).
- [17] John N Weinstein et al. "The Cancer Genome Atlas Pan-Cancer Analysis Project." In: *Nature genetics* 45.10 (Oct. 2013), pp. 1113–20. ISSN: 1546-1718. DOI: [10.1038/ng.2764](https://doi.org/10.1038/ng.2764). pmid: [24071849](#).

- [18] Thomas M. J. Fruchterman and Edward M. Reingold. "Graph Drawing by Force-Directed Placement". In: *Software: Practice and Experience* 21.11 (1991), pp. 1129–1164. ISSN: 1097-024X. DOI: [10.1002/spe.4380211102](https://doi.org/10.1002/spe.4380211102).
- [19] Vincent D Blondel et al. "Fast Unfolding of Communities in Large Networks". In: *Journal of Statistical Mechanics: Theory and Experiment* 2008.10 (Oct. 9, 2008), P10008. ISSN: 1742-5468. DOI: [10.1088/1742-5468/2008/10/p10008](https://doi.org/10.1088/1742-5468/2008/10/p10008).
- [20] L Breiman et al. *Classification and Regression Trees*. Wadsworth Publishing Company, 1984.
- [21] Marvin N Wright and Andreas Ziegler. "Ranger: A Fast Implementation of Random Forests for High Dimensional Data in C++ and R". In: *Journal of Statistical Software* 77.1 (Mar. 2017). DOI: [10.18637/jss.v077.i01](https://doi.org/10.18637/jss.v077.i01).
- [22] Seunghak Lee and Seungjin Choi. "Landmark MDS Ensemble". In: *Pattern Recognition* 42.9 (Sept. 2009), pp. 2045–2053. ISSN: 00313203. DOI: [10.1016/j.patcog.2008.11.039](https://doi.org/10.1016/j.patcog.2008.11.039).
- [23] Gabor Csardi and Tamas Nepusz. "The Igraph Software Package for Complex Network Research". In: *InterJournal, Complex Systems* 1695.5 (2006), pp. 1–9.
- [24] Paul Shannon et al. "Cytoscape: A Software Environment for Integrated Models of Biomolecular Interaction Networks". In: *Genome Research* 13.11 (Nov. 1, 2003), pp. 2498–2504. DOI: [10.1101/gr.1239303](https://doi.org/10.1101/gr.1239303).

CHAPTER 7

Paper 6: Optimising regulatory networks

Abstract

Purpose: Graphlets are small network patterns that can be counted in order to characterise the structure of a network (topology). As part of a topology optimisation process, graphlet counts are used to iteratively modify a network in order to achieve certain topological properties. Up until now, however, graphlets were not suited as a metric for performing topology optimisation; when millions of minor changes are made to the network structure it becomes computationally intractable to recalculate all the graphlet counts for each of the edge modifications.

Results: IncGraph calculates the differences in graphlet counts with respect to the network in its previous state. IncGraph reduces the execution time by several orders of magnitude when compared to recounting the graphlet counts from scratch at every iteration. We demonstrate the usefulness of this approach optimising gene regulatory networks using a graphlet-based fitness score.

Conclusion: IncGraph is able to quickly quantify the topological impact of small changes to a network, which opens novel research opportunities to study changes in topologies in evolving or online networks, or develop graphlet-based criteria for topology optimisation.

Publication status

Published in PLOS ONE 13, 4 (2018). doi:[10.1371/journal.pone.0195997](https://doi.org/10.1371/journal.pone.0195997).

Cannoodt R, Ruysinck J, Ramon J, De Preter K, and Saeys Y.

Author contributions

- **R.C.**, Jo.R., Ja.R., and Y.S. designed the study.
- **R.C.**, Jo.R., and Ja.R. performed the experiments and analysed the data.
- **R.C.** implemented the incgraph software package.
- **R.C.** wrote the original manuscript.
- **R.C.**, Jo.R., Ja.R., K.D.P., and Y.S. reviewed and edited the manuscript.
- Jo.R., K.D.P. and Y.S. supervised the project.

7.1 Introduction

7

Even the simplest of living organisms already consist of complex biochemical networks which must be able to respond to a variety of stressful conditions in order to survive. An organism can be characterised using numerous interaction networks, including gene regulation, metabolic, signalling, and protein-protein interaction. The advent of high-throughput profiling methods (e.g. microarrays and RNA sequencing) have allowed to observe the molecular contents of a cell, which in turn have enabled computational network inference methods to reverse engineer the biochemical interaction networks [1]. Improving the accuracy of inferred networks has been a long-standing challenge, but the development of ever more sophisticated algorithms and community-wide benchmarking studies have resulted in significant progress [2, 3, 4, 5].

Several recent developments involve incorporating topological priors, either to guide the inference process [6] or post-process the network [7]. A common prior is that biological networks are highly modular [8], as they consist of multiple collections of functionally or physically linked molecules [9, 10]. At the lowest level, each module is made up out of biochemical interactions arranged in small topological patterns, which act as fundamental building blocks [11].

Graphlets [12] are one of the tools which could be used to add a topological prior to a biological network. Graphlets are small connected subnetworks which can be counted to identify which low-level topological patterns are present in a network. By comparing how topologically similar a predicted network is to what would be expected of a true biological network, a predicted network can be optimised in order to obtain a better topology.

By counting the number of occurrences of each of the different graphlets (Fig 7.1A) touching a specific node, one can characterise the topology surrounding it. The graphlet counts of a network can be represented as a matrix with one row for each of the nodes and one column for each of the graphlets (Fig 7.1B). An orbit represents a class of isomorphic (i.e. resulting in the same structure) positions of nodes within a graphlet (Fig 7.1A, coloured in red). Both graphlets and orbits have been used extensively for predicting the properties of nodes such as protein functionality [13, 14, 15] and gene oncogenicity [16], by performing network alignment [17, 18] or using them as a similarity measure in machine learning tasks [19, 20].

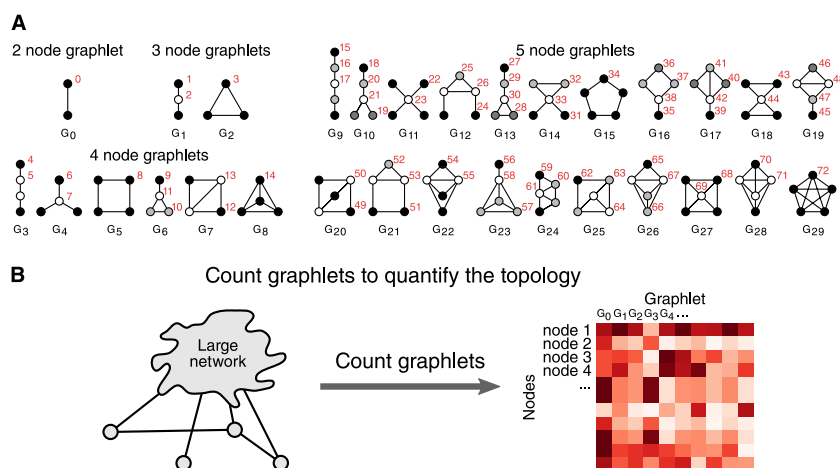


Figure 7.1: Graphlet counting in a network characterises its local topologies. (A) In total, there are 30 different graphlets containing 2 to 5 nodes, ranging from G_0 to G_{29} . Orbita are an extension of graphlets which also take into account the position of a node within a graphlet. The 73 different orbits are coloured in red. (B) By counting the occurrences of these graphlets in the network, the local topology surrounding a node can be quantified.

In this work, we focus on optimising gene regulatory networks by incorporating a topological prior as part of a topology optimisation process. We seek to optimise a predicted network by iteratively modifying the network and accepting modifications that lead to topological properties that resemble better those of true biological networks.

However, using graphlets to perform topology optimisation was hitherto not possible. Calculating the graphlet counts using the most state-of-the-art graphlet counting of a moderately sized gene regulatory network already has an execution time of about five seconds (*E. coli*, ~ 3000 genes, ~ 10000 interactions, up to graphlets up to 5 nodes). While this computational time poses no issue for regular static networks, recalculating all graphlet counts for every network modification made as part of a topology optimisation is computationally intractable. For example, performing 100'000 iterations of topology optimisation on a similarly sized network and calculating the topological impact of 10 possible edge modification at each iteration, already results in a computational time of about 12 days. Graphlet-based topology optimisation thus quickly becomes infeasible for larger networks.

When adding or removing an edge to a large network, the number of altered graphlets is much smaller than the total number of graphlets in the network. It could therefore be much more efficient to iterate over and count all the graphlets that have been added or removed as a result of the edge modification, than it is to recalculate the graphlet counts from scratch.

Eppstein et al. introduced data structures and algorithms for updating the counts of size-three [21] and size-four [22] subgraphs in a dynamic setting. The data structures were determined such that the amortised time is $O(h)$ and $O(h^2)$, respectively, where h is the h-index of the network [23].

We developed IncGraph, an alternative algorithm and implementation for performing incremental counting of graphlets up to size five. We show empirically that IncGraph is several orders of magnitude faster at calculating the differences in graphlet counts in comparison to non-incremental counting approaches. In addition, we demonstrate the practical applicability by developing a graphlet-based optimisation criterion for biological networks.

7.2 Materials and methods

Assume a network G of which the graphlet counts C_G are known. C_G is an n -by- m matrix, with n the number of vertices in the network, $m = 73$ is the number of different orbits, and where $C_G[i, j]$ is the number of times node i is part of a graphlet at orbit O_j . Further assume that one edge has either been added or removed from G , resulting in G' , at which point the counts $C_{G'}$ need to be observed. If multiple edges have been modified, the method described below can be repeated for each edge individually.

7.2.1 Incremental graphlet counting

As stated earlier, recalculating the graphlet counts for each modification made to the network quickly becomes computationally intractable for larger network sizes. However, as the differences in topology between G and G' are small, it is instead possible to calculate the differences in graphlet counts $\Delta_{G,G'}$ instead. This is much more efficient to calculate, as only the neighbourhood of the modified edges needs to be explored. $C_{G'}$ can thus be calculated as $C_{G'} = C_G + \Delta_{G,G'}$.

The differences in graphlet counts $\Delta_{G,G'}$ are calculated by iterating recursively over the neighbours surrounding each of the modified edges (Fig 7.8). Several strategies are used in order to calculate

$\Delta_{G,G'}$ as efficiently as possible (Fig 7.2). (A) The delta matrix is calculated separately for each modified edge. Since the edge already contains two out of five nodes and any modified graphlet is a connected subgraph, the neighbourhood of this edge only needs to be explored up to depth 3 in order to iterate over all modified graphlets. (B) We propose a lookup table to look up the graphlet index of each node of a given subgraph. By weighting each possible edge in a 5-node graphlet, the sum of the edges of a subgraph can be used to easily look up the corresponding graphlet index. (C) During the recursive iteration of the neighbourhood, the same combination of nodes is never visited twice. (D) As the network can be relatively large, the adjacency matrix is binary compressed in order to save memory. One integer requires 4 bytes and contains the adjacency boolean values of 32 edges, whereas otherwise 32 booleans would require 32 bytes. For example, 1GB of memory is large enough to store a compressed adjacency matrix of 92681 nodes. If the network contains too many nodes to fit a compressed adjacency matrix into the memory, a list of sets containing each node's neighbours is used instead.

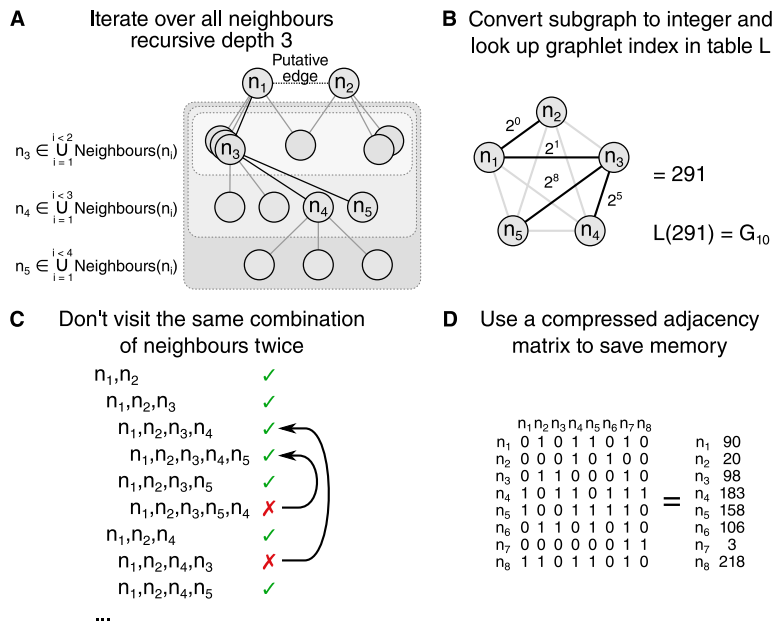


Figure 7.2: Several strategies are employed in order to reduce time and memory consumption. (A) Only the depth 3 neighbourhood of each modified edge needs to be explored in order to have visited all modified five-node graphlets. (B) A lookup table can be used to easily look up the graphlet index of a subgraph, by weighing each edge in a 5-node subgraph by a power of 2. (C) The same combination of five nodes is never repeated, as to avoid counting the same graphlet multiple times. (D) The adjacency matrix of the network is compressed in order to reduce memory usage.

IncGraph supports counting graphlets and orbits of subgraphs up to five nodes in undirected networks. By modifying the lookup table, the method can be easily extended to directed graphlets or larger-node graphlets, or limited to only a selection of graphlets. This allows for variations of the typical graphlets to be studied in an incremental setting.

7.2.2 Timing experiments

We compared the execution time needed to calculate the graphlet counts in iteratively modified networks between our method and a state-of-the-art non-incremental algorithm, Orca [24]. Orca is a heavily optimised algorithm for counting 5-node graphlets in static networks, and outperforms all other static graphlet counting algorithms by an order of magnitude [24].

The timing experiments were performed by generating networks from 3 different network models, making modifications to those networks while still adhering to the network model, and measuring the execution times taken for both approaches to calculate the new graphlet counts (Fig 7.3).

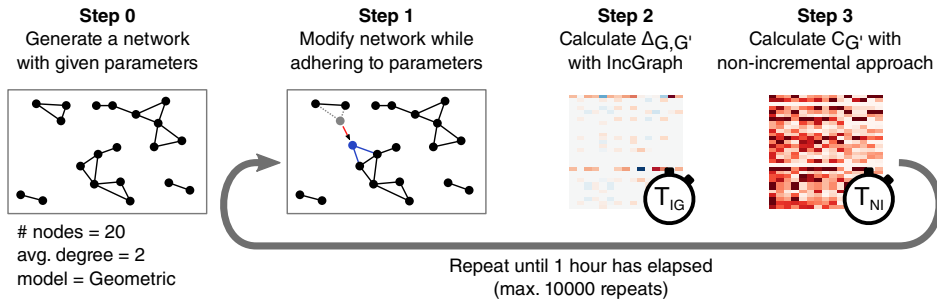


Figure 7.3: Static network model generators were modified to generate dynamic networks. Three network models were used: Barabási-Albert [25], Erdős-Rényi [26], and Geometric [27]. These models were adapted to generate evolving networks instead (Figs 7.9, 7.10, and 7.11). Each model generates an initial network according to the static network model it is based on, and a list of network modifications (removing an edge from or adding an edge to the network). These network modifications are made such that at any given time point in the evolving network, it is likely that the network at its current state could have been generated by the original static network model.

The network models were based on three static network models: Barabási-Albert [25], Erdős-Rényi [26], and Geometric [27]. These models were adapted to generate evolving networks instead (Figs 7.9, 7.10, and 7.11). Each model generates an initial network according to the static network model it is based on, and a list of network modifications (removing an edge from or adding an edge to the network). These network modifications are made such that at any given time point in the evolving network, it is likely that the network at its current state could have been generated by the original static network model.

Networks were generated with varying network models, between 1000 and 16000 nodes, node degrees between 2 and 64, and 10000 time points. We measured the time needed to calculate the delta matrix at random time points until 1 hour has passed. All timings experiments were carried out on Intel(R) Xeon(R) CPU E5-2665 @ 2.40GHz processors, with one thread per processor. The generation of networks with higher node counts or degrees was constrained by the execution time of the network generators, not by IncGraph. All data and scripts are made available at github.com/rcaffo/IncGraph-scripts.

7.2.3 Gene regulatory network optimisation experiments

We demonstrate the usefulness of IncGraph by using a simple graphlet-based metric to optimise gene regulatory networks. One of the striking differences between real and predicted gene regulatory networks is that the predicted networks contain highly connected subnetworks, which contain high amounts of false positives. We determine a penalty score such that predicted networks containing graphlets with many redundant edges will be penalised in comparison to very sparse networks.

The *redundancy penalty* (Fig 7.4A) of a network is defined as the sum of occurrences of each graphlet multiplied by the redundancy associated with each individual graphlet. The redundancy of a graphlet is the number of edges that can be removed without disconnecting the nodes from one another. By using the redundancy penalty score, we aim to improve the gene regulatory network (Fig 7.4B).

The topology optimisation procedure uses an empty network as initialisation and grows the network by selecting interactions iteratively. Each iteration, the top $k = 100$ highest ranked interactions that

are not currently part of the network are evaluated, and the highest ranked interaction passing the redundancy criterion is selected (Fig 7.4C). This procedure is repeated until a predefined amount of time has passed. As the aim of this experiment is not to obtain the highest performing topology optimisation method, parameter optimisation of k has not been performed and is considered to be outside the scope of this work.

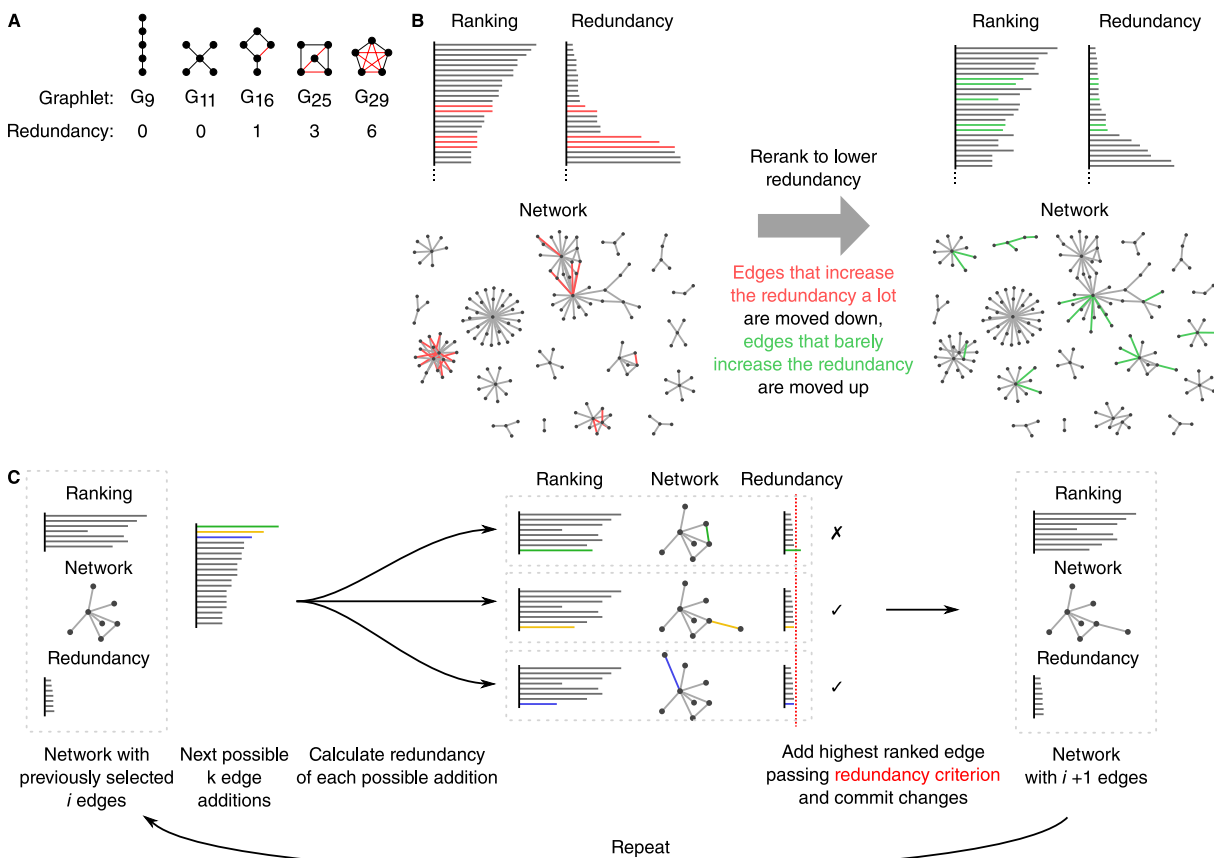


Figure 7.4: Predicted gene regulatory networks of model organisms are optimised to reduce the false positive rate. A) The number of redundant edges in each graphlet are counted. B) The network is optimised in order to obtain a lower redundancy over time. Two networks are shown, one before and one after the optimisation procedure. Edges coloured in red have been removed from the network after optimisation, green edges have been added. C) Starting from an empty network, the interactions are modified by iteratively evaluating the increase in redundancy of the next k interactions, and adding the first edge for which its redundancy is less than the 90th percentile redundancy.

We optimised gene regulatory networks of *E. coli* and *S. cerevisiae*. The predicted networks were generated using the network inference method GENIE3 [28] with default parameters. Gene expression data was obtained from COLOMBOS [29] and GEO [30], respectively. The predicted networks and the optimised versions thereof were compared against respective lists of known gene regulatory interactions [31, 32].

7.3 Results and discussion

The contributions of this work are twofold. Firstly, we propose a new method for incrementally calculating the differences in graphlet counts in changing graphs, and show that it is orders of magnitude faster than non-incremental approaches. Secondly, we demonstrate its applicability by optimising a predicted gene regulatory network in order to reduce the false positive rate therein.

7.3.1 Execution time is reduced by orders of magnitude

Timing experiments show that IncGraph is significantly faster in calculating the delta matrix in comparison to calculating the graphlet counts from scratch at each iteration (Fig 7.5). The observed speedup ratios between IncGraph and the non-incremental approach Orca ranges from about $50\times$ to $10000\times$. The speedup ratio increases as the network size increases. For larger networks, IncGraph can thus calculate the delta matrices of 10000 edge modifications while the non-incremental approach calculates one graphlet count matrix.

Surprisingly, IncGraph obtains higher execution times for networks with 5657 nodes than for networks with 8000 nodes. One possible explanation is that the size of the data structures containing those networks are particularly favourable in avoiding cache misses. Confirmation of this explanation, however, would require further investigation.

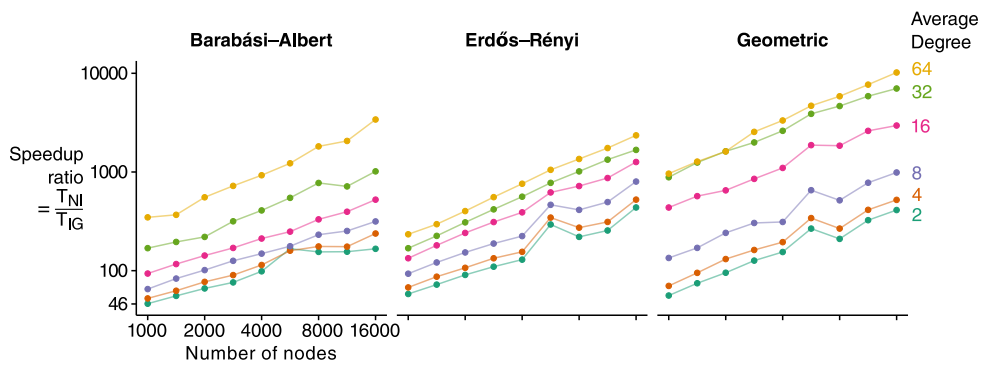


Figure 7.5: IncGraph is significantly faster than non-incremental approaches. For small networks, the execution time of IncGraph T_{IG} is already 50 times less than that of non-incremental approaches T_{NI} . This ratio increases even further for networks with higher numbers of nodes or higher average degrees.

Comparing the execution time of IncGraph to the h-index of the networks indicates that the amortised time of IncGraph could be $O(h^3)$ (Fig 7.7). This is in line with the amortised times $O(h)$ and $O(h^2)$ of the algorithm described by Eppstein et al. [22] for counting three-size and four-size subgraphs respectively.

7.3.2 IncGraph allows for better regulatory network optimisation

We implemented a graphlet-based optimisation algorithm for improving the false positive rate of the predicted gene regulatory networks of *E. coli* and *S. cerevisiae*. After reranking the regulatory interactions, the F1 score of the first 1000 interactions had increased by 7.6% and 2.2% respectively (Fig 7.6A). The obtained speedup of about $15\text{--}30\times$ (Fig 7.6B) is in line with the experiments on *in silico* networks. Namely, for the *E. coli* network at 9618 interactions and 889 nodes (average degree = 10.8), a speedup of about $30\times$ was obtained. Similarly, for the *S. cerevisiae* network at 8013 interactions and 1254 nodes (average degree = 6.4), a speedup of about $15\times$ was obtained. These speedups are in the same order of magnitude of similarly sized networks (1000 nodes and 8000 interactions) generated with a Barabási-Albert model, with a speedup of $65\times$. This is to be expected, as such networks share the same scale-free property that gene regulatory networks have.

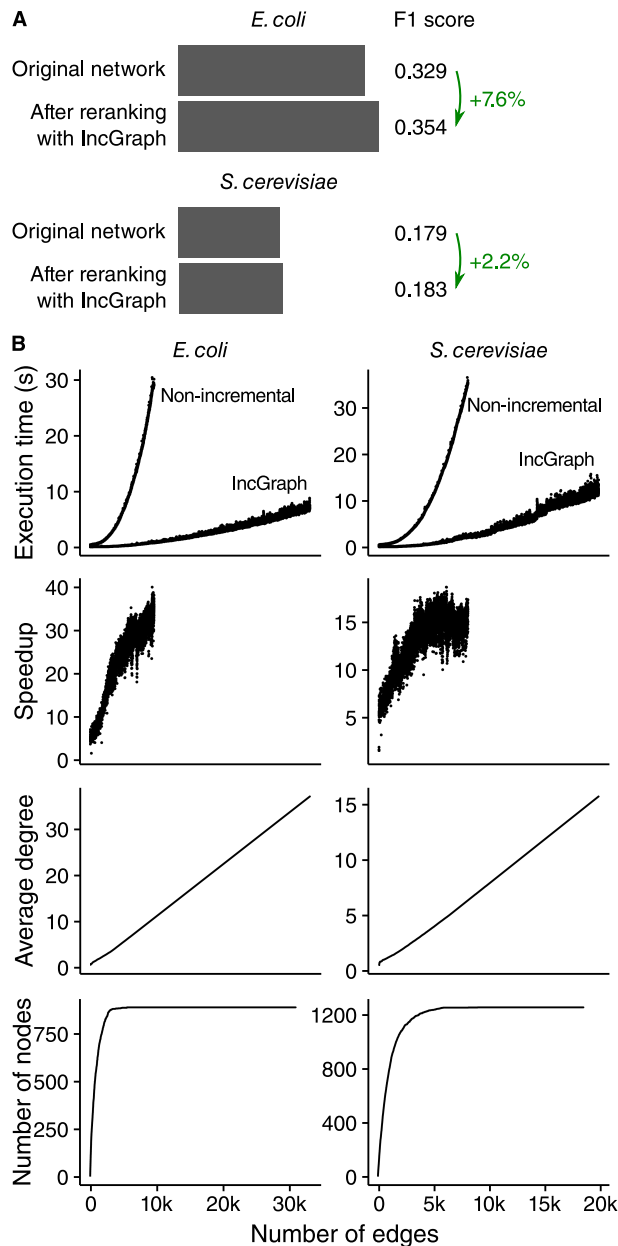


Figure 7.6: A simple graphlet-based scoring method improves predicted regulatory networks. (A) The F1 score was calculated by calculating the harmonic mean of the AUROC and AUPR scores of the first 1000 interactions. (B) IncGraph is significantly faster than the non-incremental approach. Note that for each interaction added to the network, the graphlet counts of 100 putative interactions were evaluated.

7.4 Conclusion

Many improvements over the past few years have resulted in efficient graphlet counting algorithms, even for large static networks. However, needing to perform the simplest of tasks tens of thousands of times quickly becomes computationally intractable. As such, recalculating the graphlet counts of a network after each of the many network modification is infeasible.

This study introduces a method for calculating the differences in graphlet (and orbit) counts, which we call incremental graphlet counting or IncGraph for short. We show that IncGraph is at least 10–100 times faster than non-incremental methods for networks of moderate size, and that the speedup ratio increases even further for larger networks. To demonstrate the applicability of IncGraph, we

optimised a predicted gene regulatory network by enumerating over the ranked edges and observing the graphlet counts of several candidate edges before deciding which edge to add to the network.

IncGraph enables graphlet-based metrics to characterize online networks, e.g. in order to track certain network patterns over time, as a similarity measure in a machine learning task, or as a criterion in a topology optimisation.

7.5 Supporting information

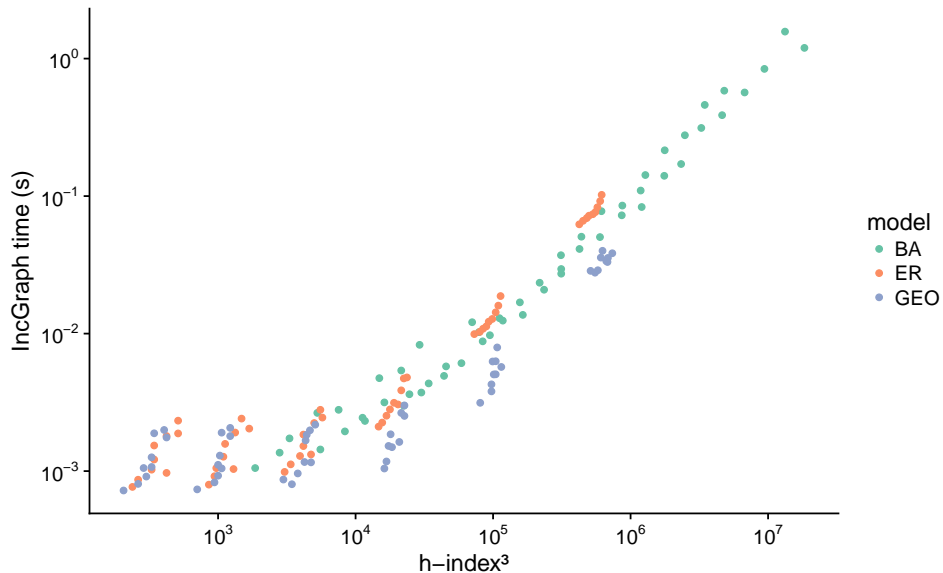


Figure 7.7: Empirical measurements show a strong relation between the execution time of IncGraph and the h-index cubed of the network it was applied to. This is in line with the findings by Eppstein et al., where counting 3-size subgraphs has an amortised time of $O(h)$ and counting 4-size subgraphs has an amortised time of $O(h^2)$.

```

function CalculateDelta(Network  $G'$ , Node  $n_0$ , Node  $n_1$ )
     $\triangleright$  Assuming an edge  $(n_0, n_1)$  has just been added or removed from  $G'$ 
     $\Delta^- \leftarrow \text{Matrix}(\text{NumNodes}(G), 73)$        $\triangleright$  For storing the orbit counts of the removed graphlets
     $\Delta^+ \leftarrow \text{Matrix}(\text{NumNodes}(G), 73)$        $\triangleright$  For storing the orbit counts of the added graphlets
     $B_0 = \{n_0, n_1\}$                                  $\triangleright$  A blacklist of nodes not to visit anymore
     $e = (n_0, n_1)$                                  $\triangleright$  Different name for the edge
    if  $e \in N'$  then
         $(m^-, m^+) = (0, 1)$                        $\triangleright$  In other words,  $m^- = 1$  iff  $e \in N$  and  $m^+ = 1$  iff  $e \in N'$ 
    else
         $(m^-, m^+) = (1, 0)$ 
    end if
     $x_0 = 0$ 
     $(\Delta^+, \Delta^-) = \text{CountOrbits}(\Delta^+, \Delta^-, (n_0, n_1), x_0, m^-, m^+)$        $\triangleright$  Update delta matrices for current
    nodes
    for  $n_2 \in \bigcup_{i \in \{0,1\}} \text{Neighbours}(n_i)$  do
        if  $n_2 \notin B_0$  then
             $B_0 = \{n_2\} \cup B_0$                        $\triangleright$  Add  $n_2$  to blacklist  $B_0$ 
             $x_1 = x_0 + W(G', (n_0, n_2), 1) + W(G', (n_1, n_2), 2)$        $\triangleright$  Calculate edge weights for current
            nodes
             $(\Delta^+, \Delta^-) = \text{CountOrbits}(\Delta^+, \Delta^-, (n_0, n_1, n_2), x_1, m^-, m^+)$ 
             $B_1 = B_0$                                  $\triangleright$  Make a copy for the next iteration depth
            for  $n_3 \in \bigcup_{i \in \{0,1,2\}} \text{Neighbours}(n_i)$  do
                if  $n_3 \notin B_1$  then
                     $B_1 = \{n_3\} \cup B_1$ 
                     $x_2 = x_1 + W(G', (n_0, n_3), 3) + W(G', (n_1, n_3), 4) + W(G', (n_2, n_3), 5)$ 
                     $(\Delta^+, \Delta^-) = \text{CountOrbits}(\Delta^+, \Delta^-, (n_0, n_1, n_2, n_3), x_2, m^-, m^+)$ 
                     $B_2 = B_1$ 
                    for  $n_4 \in \bigcup_{i \in \{0,1,2,3\}} \text{Neighbours}(n_i)$  do
                        if  $n_4 \notin B_2$  then
                             $B_2 = \{n_4\} \cup B_2$ 
                             $x_3 = x_2 + \sum_{i \in \{0,1,2,3\}} W(G', (n_i, n_4), i + 6)$ 
                             $(\Delta^+, \Delta^-) = \text{CountOrbits}(\Delta^+, \Delta^-, (n_0, n_1, n_2, n_3, n_4), x_3, m^-, m^+)$ 
                        end if
                    end for
                end if
            end for
        end if
    end for
end function

function CountOrbits( $\Delta^+$ ,  $\Delta^-$ , Nodes  $S$ , Edgeweights  $x$ , Modifier  $m^-$ , Modifier  $m^+$ )
     $L^- = L[x + m^-]$                                  $\triangleright$  Look up the orbits of the subgraph induced by  $S$  in  $N$ 
     $\Delta^-[S, L^-] += 1$                                  $\triangleright$  Increment orbit counts of nodes  $S$  at positions  $L^-$  in  $\Delta^-$ 
     $L^+ = L[x + m^+]$                                  $\triangleright$  Look up the orbits of the subgraph induced by  $S$  in  $N'$ 
     $\Delta^+[S, L^+] += 1$                                  $\triangleright$  Increment orbit counts of nodes  $S$  at positions  $L^+$  in  $\Delta^+$ 
    return  $(\Delta^-, \Delta^+)$ 
end function

function W(Network  $G$ , Edge  $e$ , Exponent  $i$ )
    return  $e \in \text{Edges}(G) ? 2^i : 0$                    $\triangleright$  Return  $2^i$  if  $G$  contains edge  $e$ 
end function

```

Figure 7.8: Pseudocode of IncGraph. IncGraph calculates $\Delta_{G,G'}$ using a strict branch-and-bound strategy.

```

function BarabasiAlbert(number of nodes  $n$ , degree  $d$ ,
    number of operations  $o$ , offset exponent  $x = 1$ )
     $D \leftarrow \text{Rep}(0, n)$                                  $\triangleright$  All nodes start with 0 degree
     $T \leftarrow \text{Rep}(\{\}, n)$                              $\triangleright$  List of targets of each node
     $S \leftarrow \text{Rep}(\{\}, n)$                              $\triangleright$  List of sources of each node
     $O \leftarrow ()$                                       $\triangleright$  Variable to store the generated operations in
procedure AddEdge(node  $i$ , node  $j$ , add as operation  $b$ )
     $D[i] \leftarrow D[i] + 1; D[j] \leftarrow D[j] + 1$            $\triangleright$  Update degrees
     $T[i] \leftarrow T[i] \cup \{j\}; S[j] \leftarrow S[j] \cup \{i\}$        $\triangleright$  Update targets and sources
    if  $b$  then
         $O \leftarrow O + (\text{ADD}, (i, j))$ 
    end if
end procedure
procedure RemoveEdge(node  $i$ , node  $j$ , add as operation  $b$ )
     $D[i] \leftarrow D[i] - 1; D[j] \leftarrow D[j] - 1$            $\triangleright$  Update degrees
     $T[i] \leftarrow T[i] \setminus \{j\}; S[j] \leftarrow S[j] \setminus \{i\}$        $\triangleright$  Update targets and sources
    if  $b$  then
         $O \leftarrow O + (\text{REM}, (i, j))$ 
    end if
end procedure
procedure AddNode(node  $i$ , add as operations  $b$ )
     $C \leftarrow \{j \mid 0 \leq j < i \wedge j \notin S[i]\}$            $\triangleright$  Select candidate neighbours
     $W \leftarrow (D[C] / \sum D[C])^x$                           $\triangleright$  Calculate weights for preferred attachment
     $X \leftarrow \text{sample } d \text{ neighbours from } C \text{ with weights } W$ 
    for  $j \in X$  do
        AddEdge( $i, j, b$ )
    end for
end procedure
procedure RemoveNode(node  $i$ , add as operations  $b$ )
    while  $|T[i]| > 0$  do
         $j \leftarrow \text{Head}(T[i], 1)$ 
        RemoveEdge( $i, j, b$ )
    end while
end procedure
for  $i \in \{1..m\}$  do
    for  $j \in \{0..i-1\}$  do
        AddEdge( $i, j, \text{false}$ )
    end for
end for
for  $i \in \{m+1..n-1\}$  do
    AddNode( $i, \text{false}$ )                                      $\triangleright$  Start with  $m+1$  complete graph
end for
 $G_0 \leftarrow \{(i, j) \mid i \in \{0..n-1\} \wedge j \in N[i]\}$            $\triangleright$  Initial network
while  $|O| < o$  do
     $i \leftarrow \text{Sample 1 index from } \{0..n-1\}$ 
    RemoveNode( $i, \text{true}$ )
    AddNode( $i, \text{true}$ )
end while
 $O \leftarrow \text{Head}(O, o)$                                           $\triangleright$  Modify network until  $O$  is sufficiently large
return  $(N_0, O)$                                                $\triangleright$  Return the initial network and  $o$  operations
end function

```

Figure 7.9: Pseudo code for generating an evolving Barabási-Albert (BA) network. It first generates a BA network, and then generates o operations such that at any time point, the network is or very closely resembles a BA network.

```

function ErdosRenyi(number of nodes  $n$ , number of edges  $e$ , number of operations  $o$ )
     $P \leftarrow \{(i, j) \mid i \in \{1..n-1\} \wedge j \in \{0..i-1\}\}$                                  $\triangleright$  All possible interactions
     $N_0 \leftarrow \text{Sample } e \text{ edges from } P$ 
     $N_c \leftarrow N_0$ 
    while  $|O| < o$  do
         $e_a \leftarrow \text{Sample 1 edge from } P \setminus N_c$ 
         $e_r \leftarrow \text{Sample 1 edge from } N_c$ 
         $N_c \leftarrow (N_c \setminus e_r) \cup \{e_a\}$ 
         $O \leftarrow O + ((\text{ADD}, e_a), (\text{REM}, e_r))$ 
    end while
     $O \leftarrow \text{Head}(O, o)$ 
    return  $(N_0, O)$                                  $\triangleright$  Return the initial geometric network and  $o$  operations
end function

```

Figure 7.10: Pseudo code for generating an evolving Erdős–Rényi (ER) network. It first generates an ER network, and then generates o operations such that at any time point, the network is or very closely resembles an ER network.

```

function Geometric(number of nodes  $n$ , number of edges  $e$ ,
                    number of operations  $o$ , number of dimensions  $d = 3$ )
     $P \leftarrow \text{Sample } n \text{ points from a multivariate continuous uniform distribution } U_d((0, 1)^d)$ 
     $D \leftarrow \text{Calculate distance matrix from } P$ 
     $N_0 \leftarrow \text{Head}(\text{ArgSort}(\text{LowerTriangle}(D)), e)$                                  $\triangleright$  Initial network
     $N_p \leftarrow N_0$ 
     $O \leftarrow ()$                                  $\triangleright$  Variable to store the generated operations in
    while  $|O| < o$  do                                 $\triangleright$  Modify network until  $O$  is sufficiently large
         $i \leftarrow \text{Sample 1 index from } \{0..n-1\}$ 
         $P[i] \leftarrow \text{Sample 1 point from a } U_d((0, 1)^d)$                                  $\triangleright$  Give node  $i$  a new location
         $D[i, :] \leftarrow D[:, i] \leftarrow \text{Calculate new distances between node } i \text{ and all other nodes}$        $\triangleright$  New network
         $N_c \leftarrow \text{Head}(\text{ArgSort}(\text{LowerTriangle}(D)), e)$                                  $\triangleright$  Gather added edges
         $O_a \leftarrow \{(\text{ADD}, e) \mid e \notin E(N_p) \wedge e \in E(N_c)\}$ 
         $O_r \leftarrow \{(\text{REM}, e) \mid e \in E(N_p) \wedge e \notin E(N_c)\}$                                  $\triangleright$  Gather removed edges
         $O \leftarrow O + \text{Shuffle}(O_a + O_r)$                                  $\triangleright$  Append new operations to  $O$ 
         $N_p \leftarrow N_c$ 
    end while
     $O \leftarrow \text{Head}(O, o)$ 
    return  $(N_0, O)$                                  $\triangleright$  Return the initial geometric network and  $o$  operations
end function

```

Figure 7.11: Pseudo code for generating an evolving geometric network. It first generates a geometric network, and then generates o operations such that at any time point, the network is or very closely resembles a geometric network.

7.6 References

- [1] R. Albert. "Network Inference, Analysis, and Modeling in Systems Biology". In: *the Plant Cell Online* 19.11 (2007), pp. 3327–3338. issn: 1040-4651. doi: [10.1105/tpc.107.054700](https://doi.org/10.1105/tpc.107.054700). pmid: [18055607](https://pubmed.ncbi.nlm.nih.gov/18055607/).
- [2] Daniel Marbach et al. "Revealing Strengths and Weaknesses of Methods for Gene Network Inference". In: *Proceedings of the National Academy of Sciences* 107.14 (Apr. 2010), pp. 6286–6291. issn: 1091-6490. doi: [10.1073/pnas.0913357107](https://doi.org/10.1073/pnas.0913357107). pmid: [20308593](https://pubmed.ncbi.nlm.nih.gov/20308593/).
- [3] Varun Narendra et al. "A Comprehensive Assessment of Methods for De-Novo Reverse-Engineering of Genome-Scale Regulatory Networks". In: *Genomics* 97.1 (2011), pp. 7–18. issn: 08887543. doi: [10.1016/j.ygeno.2010.10.003](https://doi.org/10.1016/j.ygeno.2010.10.003). pmid: [20951196](https://pubmed.ncbi.nlm.nih.gov/20951196/).
- [4] Daniel Marbach et al. "Wisdom of Crowds for Robust Gene Network Inference". In: *Nature methods* 9.8 (July 2012), pp. 796–804. issn: 1548-7091. doi: [10.1038/nmeth.2016](https://doi.org/10.1038/nmeth.2016). pmid: [22796662](https://pubmed.ncbi.nlm.nih.gov/22796662/).
- [5] Tarmo Äijö and Richard Bonneau. "Biophysically Motivated Regulatory Network Inference: Progress and Prospects". In: *Human Heredity* 81.2 (2017), pp. 62–77. issn: 14230062. doi: [10.1159/000446614](https://doi.org/10.1159/000446614). pmid: [28076866](https://pubmed.ncbi.nlm.nih.gov/28076866/).
- [6] Fabricio M. Lopes et al. "A Feature Selection Technique for Inference of Graphs from Their Known Topological Properties: Revealing Scale-Free Gene Regulatory Networks". In: *Information Sciences* 272 (2014), pp. 1–15. issn: 00200255. doi: [10.1016/j.ins.2014.02.096](https://doi.org/10.1016/j.ins.2014.02.096).
- [7] Joeri Ruyssinck et al. "Netter: Re-Ranking Gene Network Inference Predictions Using Structural Network Properties." In: *BMC Bioinformatics* 17.1 (2016), p. 76. issn: 1471-2105. doi: [10.1186/s12859-016-0913-0](https://doi.org/10.1186/s12859-016-0913-0). pmid: [26862054](https://pubmed.ncbi.nlm.nih.gov/26862054/).
- [8] Alexander W Rives and Timothy Galitski. "Modular Organization of Cellular Networks." In: *Proceedings of the National Academy of Sciences of the United States of America* 100.3 (2003), pp. 1128–33. issn: 0027-8424. doi: [10.1073/pnas.0237338100](https://doi.org/10.1073/pnas.0237338100). pmid: [12538875](https://pubmed.ncbi.nlm.nih.gov/12538875/).
- [9] L H Hartwell et al. "From Molecular to Modular Cell Biology." In: *Nature* 402 (6761 Suppl 1999), pp. C47–C52. issn: 0028-0836. doi: [10.1038/35011540](https://doi.org/10.1038/35011540). pmid: [10591225](https://pubmed.ncbi.nlm.nih.gov/10591225/).
- [10] a Barabasi et al. "Network Biology: Understanding the Cell's Functional Organization." In: *Nature reviews. Genetics* 5.2 (Feb. 2004), pp. 101–13. issn: 1471-0056. doi: [10.1038/nrg1272](https://doi.org/10.1038/nrg1272). pmid: [14735121](https://pubmed.ncbi.nlm.nih.gov/14735121/).
- [11] R Milo et al. "Network Motifs: Simple Building Blocks of Complex Networks." In: *Science (New York, N.Y.)* 298.2002 (2002), pp. 824–827. issn: 00368075. doi: [10.1126/science.298.5594.824](https://doi.org/10.1126/science.298.5594.824). pmid: [12399590](https://pubmed.ncbi.nlm.nih.gov/12399590/).
- [12] N Przulj et al. "Modeling Interactome: Scale-Free or Geometric?" In: *Bioinformatics (Oxford, England)* 20.18 (Dec. 2004), pp. 3508–15. issn: 1367-4803. doi: [10.1093/bioinformatics/bth436](https://doi.org/10.1093/bioinformatics/bth436). pmid: [15284103](https://pubmed.ncbi.nlm.nih.gov/15284103/).
- [13] Tijana Milenković and Nataša Pržulj. "Uncovering Biological Network Function via Graphlet Degree Signatures". In: *Cancer Informatics* 6 (Jan. 1, 2008), CIN.S680. issn: 1176-9351. doi: [10.4137/CIN.S680](https://doi.org/10.4137/CIN.S680).
- [14] Cortnie Guerrero et al. "Characterization of the Proteasome Interaction Network Using a QTAX-Based Tag-Team Strategy and Protein Interaction Network Analysis." In: *Proceedings of the National Academy of Sciences of the United States of America* 105.36 (2008), pp. 13333–13338. issn: 0027-8424. doi: [10.1073/pnas.0801870105](https://doi.org/10.1073/pnas.0801870105). pmid: [18757749](https://pubmed.ncbi.nlm.nih.gov/18757749/).

- [15] Omkar Singh, Kunal Sawariya, and Polamarasetty Aparoy. "Graphlet Signature-Based Scoring Method to Estimate Protein-Ligand Binding Affinity." In: *Royal Society open science* 1.4 (2014), p. 140306. issn: 2054-5703. doi: [10.1098/rsos.140306](https://doi.org/10.1098/rsos.140306). pmid: [26064572](#).
- [16] Tijana Milenković et al. "Optimal Network Alignment with Graphlet Degree Vectors". In: *Cancer Informatics* 9 (Jan. 1, 2010), CIN.S4744. issn: 1176-9351. doi: [10.4137/CIN.S4744](https://doi.org/10.4137/CIN.S4744).
- [17] Oleksii Kuchaiev et al. "Topological Network Alignment Uncovers Biological Function and Phylogeny." In: *Journal of the Royal Society, Interface / the Royal Society* 7.50 (2010), pp. 1341–1354. issn: 1742-5662. doi: [10.1098/rsif.2010.0063](https://doi.org/10.1098/rsif.2010.0063). pmid: [20236959](#).
- [18] Tijana Milenković, Han Zhao, and Fazle E. Faisal. "Global Network Alignment in the Context of Aging". In: *Proceedings of the International Conference on Bioinformatics, Computational Biology and Biomedical Informatics*. BCB'13. New York, NY, USA: ACM, 2013, 23:23–23:32. isbn: 978-1-4503-2434-2. doi: [10.1145/2506583.2508968](https://doi.org/10.1145/2506583.2508968).
- [19] Nino Shervashidze et al. "Efficient Graphlet Kernels for Large Graph Comparison". In: *Proceedings of the Twelfth International Conference on Artificial Intelligence and Statistics*. Ed. by David van Dyk and Max Welling. Vol. 5. Proceedings of Machine Learning Research. Hilton Clearwater Beach Resort, Clearwater Beach, Florida USA: PMLR, Apr. 16–18, 2009, pp. 488–495. url: <http://proceedings.mlr.press/v5/shervashidze09a.html>.
- [20] Vladimir Vacic et al. "Graphlet Kernels for Prediction of Functional Residues in Protein Structures." In: *Journal of computational biology : a journal of computational molecular cell biology* 17.1 (2010), pp. 55–72. issn: 1557-8666. doi: [10.1089/cmb.2009.0029](https://doi.org/10.1089/cmb.2009.0029). pmid: [20078397](#).
- [21] David Eppstein and Emma S. Spiro. "The H-Index of a Graph and Its Application to Dynamic Subgraph Statistics". In: *Lecture Notes in Computer Science (Including Subseries Lecture Notes in Artificial Intelligence and Lecture Notes in Bioinformatics)*. Vol. 5664 LNCS. Springer-Verlag, 2009, pp. 278–289. isbn: 3-642-03366-0. doi: [10.1007/978-3-642-03367-4_25](https://doi.org/10.1007/978-3-642-03367-4_25).
- [22] David Eppstein et al. "Extended Dynamic Subgraph Statistics Using H-Index Parameterized Data Structures". In: *Theoretical Computer Science* 447 (Aug. 2012), pp. 44–52. issn: 03043975. doi: [10.1016/j.tcs.2011.11.034](https://doi.org/10.1016/j.tcs.2011.11.034).
- [23] J E Hirsch. "An Index to Quantify an Individual's Scientific Research Output". In: *Proceedings of the National Academy of Sciences of the United States of America* 102.46 (Nov. 2005), pp. 16569–72. issn: 0027-8424. doi: [10.1073/pnas.0507655102](https://doi.org/10.1073/pnas.0507655102). pmid: [16275915](#).
- [24] Tomaž Hočevar and Janez Demšar. "A Combinatorial Approach to Graphlet Counting." In: *Bioinformatics (Oxford, England)* 30.4 (Feb. 2014), pp. 559–65. issn: 1367-4811. doi: [10.1093/bioinformatics/btt717](https://doi.org/10.1093/bioinformatics/btt717). pmid: [24336411](#).
- [25] Réka Albert and Albert Laszlo Barabasi. "Statistical Mechanics of Complex Networks". In: *Reviews of Modern Physics* 74 (January 2002), pp. 47–97. issn: 1478-3967. doi: [10.1088/1478-3967/1/3/006](https://doi.org/10.1088/1478-3967/1/3/006). pmid: [16204838](#).
- [26] P. Erdős and A Rényi. "On Random Graphs". In: *Publicationes Mathematicae* 6 (1959), pp. 290–297. issn: 00029947. doi: [10.2307/1999405](https://doi.org/10.2307/1999405). pmid: [1205592](#).
- [27] M J B Appel and R P Russo. "The Minimum Vertex Degree of a Graph on Uniform Points in $[0,1]^d$ ". In: *Adv. in Appl. Probab.* 29.3 (1997), pp. 582–594. issn: 00018678.
- [28] VÂN ANH HUYNH-THU et al. "Inferring Regulatory Networks from Expression Data Using Tree-Based Methods". In: *PLoS ONE* 5.9 (Jan. 2010), e12776. issn: 1932-6203. doi: [10.1371/journal.pone.0012776](https://doi.org/10.1371/journal.pone.0012776). pmid: [20927193](#).
- [29] Marco Moretto et al. "COLOMBOS v3.0: Leveraging Gene Expression Compendia for Cross-Species Analyses". In: *Nucleic Acids Research* 44.D1 (2016), pp. D620–D623. issn: 13624962. doi: [10.1093/nar/gkv1251](https://doi.org/10.1093/nar/gkv1251). pmid: [26586805](#).

- [30] R. Edgar. "Gene Expression Omnibus: NCBI Gene Expression and Hybridization Array Data Repository". In: *Nucleic Acids Research* 30.1 (2002), pp. 207–210. issn: 13624962. doi: [10.1093/nar/30.1.207](https://doi.org/10.1093/nar/30.1.207). pmid: [11752295](https://pubmed.ncbi.nlm.nih.gov/11752295/).
- [31] Socorro Gama-Castro et al. "RegulonDB Version 9.0: High-Level Integration of Gene Regulation, Coexpression, Motif Clustering and Beyond". In: *Nucleic Acids Research* 44.D1 (2016), pp. D133–D143. issn: 13624962. doi: [10.1093/nar/gkv1156](https://doi.org/10.1093/nar/gkv1156). pmid: [26527724](https://pubmed.ncbi.nlm.nih.gov/26527724/).
- [32] Sisi Ma et al. "De-Novo Learning of Genome-Scale Regulatory Networks in *S. Cerevisiae*". In: *PLoS ONE* 9.9 (2014). issn: 19326203. doi: [10.1371/journal.pone.0106479](https://doi.org/10.1371/journal.pone.0106479). pmid: [25215507](https://pubmed.ncbi.nlm.nih.gov/25215507/).

CHAPTER 8

Paper 7: Self-assessment in trajectory inference

Abstract

Purpose: A brief of 75 articles of trajectory tools reveals that only 37% of works contain a quantitative self-assessment. While self-assessments are universally biased in favour of the authors, it is dangerous to publish a computational tool without quantitatively demonstrating its performance compared to state-of-the-art methods.

Results: We hypothesise that low self-assessment rates are primarily caused by a lack of a standardised problem definition, readily available benchmarking datasets, and suitable metrics. We elaborate on these causal reasons and provide viable solutions for performing benchmarks more easily.

Conclusion: With this perspective, we hope to address the elephant in the room, and provide developers of trajectory inference methods with the necessary tools for performing benchmarking software quantitatively.

Publication status

Manuscript in preparation.

Cannoodt R.

Author contributions

- **R.C.** designed the study.
- **R.C.** surveyed 75 manuscripts from literature and analysed the data.
- **R.C.** wrote the original manuscript.

8.1 Introduction

Many articles introducing novel trajectory inference (TI) tools lack a quantitative assessment of the accuracy of the method. Instead, they rely on anecdotal evidence to demonstrate their added value. A brief review of 75 articles reveals that only about 37% of articles contain a self-assessment (Figure 8.1A,B). Peer-reviewed articles fared even worse, self-assessing in only 35% of cases ($n=55$), whereas articles first published as a pre-print self-assess in 44% of cases ($n=39$).

The number of datasets used and methods compared against is also below expectations (Figure 8.1C,D). Only three TI articles feature a comparison of at least 5 methods using 5 datasets or more [1, 2, 3]. In comparison, our recent benchmark of TI methods evaluated the performance 45 TI methods on 110 real and 229 synthetic datasets [4].

While self-assessments are universally biased in favour of the authors [5] (intentionally or not), it is dangerous and unusual to publish a computational tool without quantitatively demonstrating its performance compared to state-of-the-art methods. Indeed, our comparison demonstrated that most methods perform worse than a few baseline methods constructed by combining simple off-the-shelf algorithms such as PCA, k -means and MST.

In this perspective, we hypothesise that low self-assessment rates are primarily caused by a lack of a standardised problem definition, readily available benchmarking datasets, and suitable metrics. We elaborate on these causal reasons and provide viable solutions for performing TI benchmarks more easily.

8.2 Problem definition

One main reason why benchmarking TI methods is difficult is due to there being slight variations of the problem a method is attempting to solve (Figure 8.2A). For example, a method might infer linear or cyclic trajectories, or predict the probability of a cell ending up in one of several end states.

As a result, it becomes harder to discover similar methods to compare against, as certain articles might only show up with search terms such as “pseudotemporal ordering”, “lineage trees” or “fate bias”. For the discoverability of a new TI method, it is therefore essential to use the term “trajectory inference”, or at least list it as one of the keywords.

A more significant and harder to solve problem is that the data formats produced by different methods varies greatly. This makes visualising and comparing multiple trajectories difficult, as different output types cannot be compared directly. The most commonly used and generalised format is one where cells are positioned along a set of edges connecting milestones (“Regular TI”, Figure 8.2A). By adding an extension to regular TI to allow for cells to be part of three or more cellular states, thereby a cell to delay its commitment toward a particular end state (Figure 8.2B). By adding this extension, all TI subtypes can easily be converted into the common format. In practice, this format consists of two data structures: the milestone network specify transition between cell states, and the cell progressions specify how far along each cell has progressed along a transition (Figure 8.2C). In addition, regions of delayed commitment need to be specified, if any (Figure 8.2D).

In our comparison of TI methods, we implemented conversions in `dynwrap` [6]. Each TI method was wrapped into a Docker container with a common command-line interface, returning output in the common output. Using this standardised format allows developing reusable software for visualising

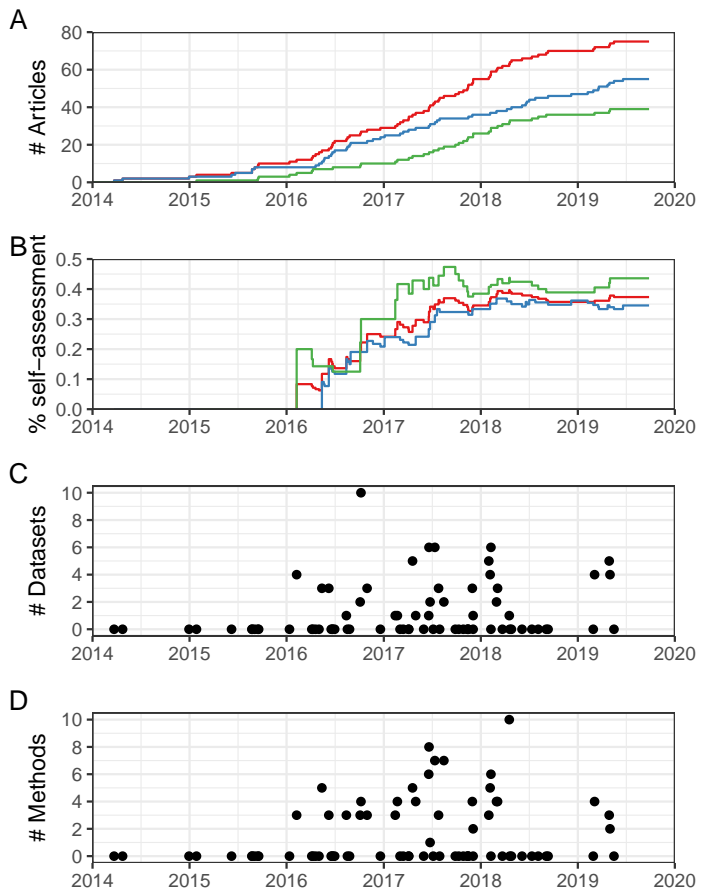


Figure 8.1: Less than half of all TI articles perform quantitative self-assessment. **A:** Since 2016, the number of TI articles has been increasing rapidly. Note that TI methods with both a pre-print and a peer-reviewed article only count once in the overall tally. **B:** Less than 50% of articles feature a self-assessment. Peer-reviewed articles self-assess only in 34% of cases. **C:** The number of datasets used in each benchmark is low. **D:** The number of methods (including itself) evaluated is low.

and comparing trajectories from different TI methods. Readers developing their own TI method can plug their method into our framework by wrapping it in a container.

8.3 Benchmarking datasets

Another hurdle in benchmarking trajectory inference methods is collecting datasets to benchmark against. Before 2018, there were only a handful of datasets containing complex trajectories (Figure 8.3).

When real data is scarce, synthetic data is often used to evaluate computational methods, either standalone ($n=5$) or to complement real data ($n=7$). Most synthetic data is generated by the authors themselves ($n=7$), whereas some reuse datasets generated by others ($n=3$) or use one of the readily available simulators ($n=2$). To avoid introducing self-assessment bias in a benchmark, it is recommended to use readily available simulators if they fit the requirements. Examples are dyntoy [4], dyngen [7], splatter [8], and PROSSTT [9].

Benefits of synthetic data are that they offer more control over the data characteristics and that they can be generated in large quantities. This allows evaluating the performance of a method in function

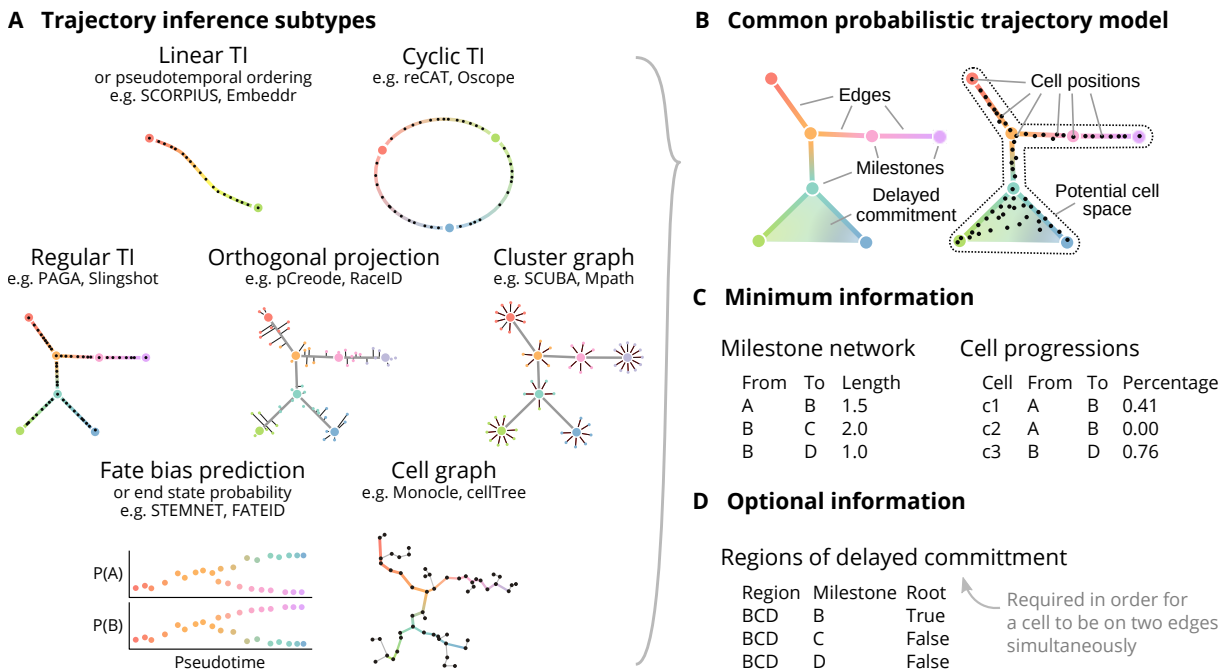


Figure 8.2: Different forms of trajectory inference. **A:** All TI methods can be categorised into one of seven subtypes in terms of its produced output [4]. **B:** Each of these can be translated into a common format, allowing easier comparison of multiple trajectories. **C:** The minimum information required to describe a trajectory in this way is the milestone network – representing transitions between cellular states – and the cell progressions – representing the positions of cells along the transitions. **D:** Optionally, regions of delayed commitment can be defined. A region of delayed commitment contain multiple transitions starting from the same milestone. This allows a TI method to assign probabilities on how likely a cell is part of one of these transitions.

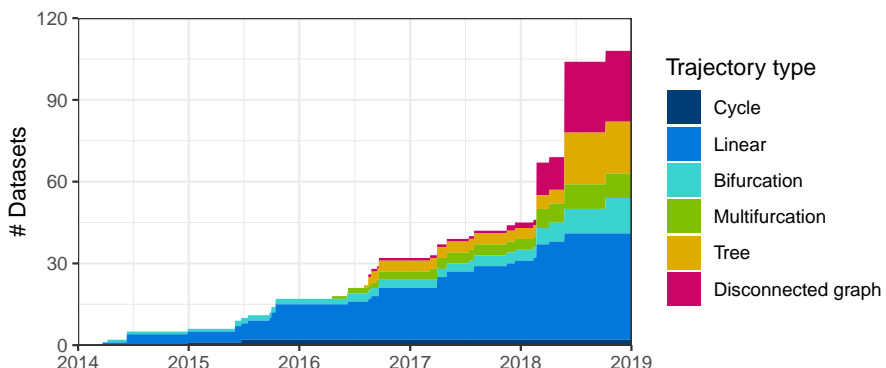


Figure 8.3: An overview collection of real TI benchmarking datasets in function of their publication date and the topology of the trajectory. These datasets are readily available on Zenodo [10].

of a changing parameter (e.g. dataset size or noise levels), which provides information on how well the method will work on real datasets.

A common counterargument of synthetic data is that they generate unrealistic datasets and thus provide no additional value in evaluating a method. In contrast, we argue that a good set of synthetic datasets should allow benchmarkers to verify that a method should *at least* work well on the synthetic datasets, but good performance on synthetic datasets does not guarantee good performance on real datasets.

Most authors use mainly real datasets to evaluate their method (82%, n=23), though only a few use more than four datasets (n=4). By now, already hundreds of suitable real datasets are available from GEO and ArrayExpress (Figure 8.3). Downloading and pre-processing them requires a significant time

investment, but by processing the datasets once and storing them in a single repository they can be reused for multiple purposes. Mixture control experiments [11] and lineage tracing [12] are particularly useful in this context.

Readers are welcome to reuse (and extend) the 110 real and 229 synthetic datasets used in our comparison of TI methods [4]. The datasets are hosted on Zenodo [10] and the scripts to process them on GitHub¹. Note that the ground truths of the datasets are represented using the common data structure format in the previous section.

8.4 Metrics

To evaluate a TI method, a quantitative metric is needed to compare the predicted trajectory to the ground truth trajectory. No off-the-shelf metrics exist for comparing complex multilayered data structures such as trajectories to each other. To get around this problem, most benchmarks repurpose metrics from other domains (Figure 8.4A).

For example, most benchmarks ($n=25$) compare the linear pseudotime ordering of a trajectory with ground-truth information such as time of sampling, quite often by calculating the Pearson correlation. This is a good approach for comparing linear trajectories but is not suitable as a metric for comparing non-linear trajectories (e.g. by calculating the distance from one endpoint of the trajectory), as this metric does not capture any differences in topology between the two trajectories (Figure 8.4B). Several other benchmarks ($n=5$) use a metric typically used to compare a clustering method, by comparing a cell's assignment to the transitions of the trajectory to ground-truth information such as the cell's cell type. While this will provide some information on whether cells are grouped correctly in comparison to the ground-truth, it also does not capture topological differences between trajectories (Figure 8.4C).

Only few evaluated the robustness of a method by comparing multiple executions of the same method [13, 14, 1, 15] ($n=4$). Computing the robustness does not replace the necessity of a relevant metric that captures whether a predicted trajectory resembles the ground truth – that is, a TI method can robustly make incorrect predictions and obtain high robustness scores. In one instance, an internal metric is used to quantify the smoothness of gene expression along the pseudotime [16] – the idea being that a good TI method would order cells such that gene expression is smooth along the pseudotime.

In our comparison of TI methods [4], we use a metric called the *geodesic correlation*. Here, two trajectories are compared by calculating the geodesic distances between pairs of cells and comparing those distance values using a Pearson correlation. Note not all pairwise distances are evaluated in this way, or the metric would not scale well to larger datasets. We also use the Hamming-Ipsen-Mikhailov (HIM) distance [17] to compare the topology of two trajectories.

In Supplementary Note 1 of our comparison of TI methods, we describe and illustrate 10 different metrics, including the geodesic correlation metric, the HIM distance, and several clustering and internal metrics. We constructed 26 test cases (similar to Figure 8.4B,C) to assess whether a metric is capable of capturing the desired information. We found that the geodesic distance passes nearly all of the test cases, using the geometric mean of different metrics performs much better. Implementations of these metrics are available in `dyneval` [6].

¹github.com/dynverse/dynbenchmark/tree/master/scripts/01-datasets

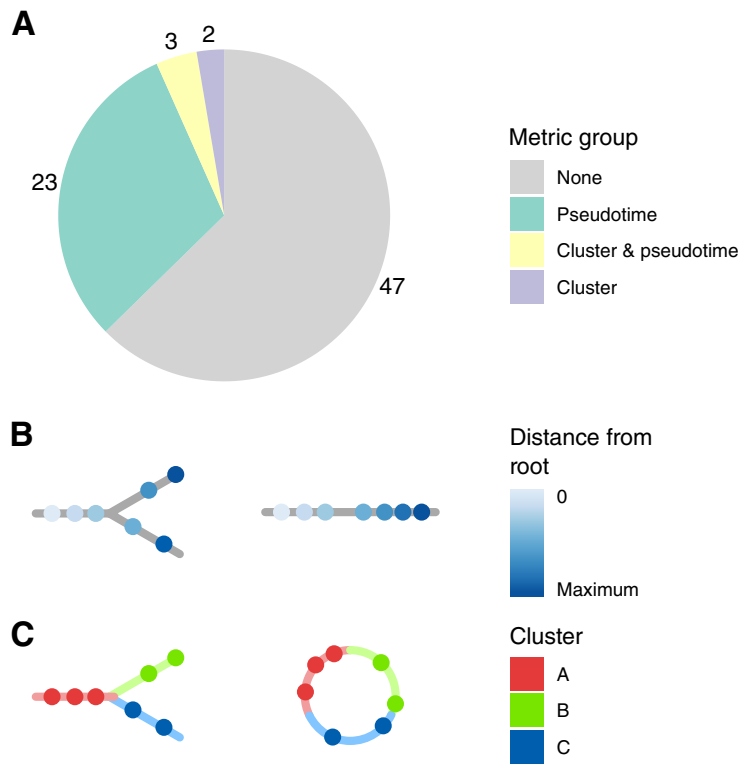


Figure 8.4: **A:** Without any off-the-shelf metrics to use for evaluating TI methods, authors use metrics from other domains. **B:** Comparing these two trajectories using a pseudotime metric (e.g. Pearson correlation) would return a perfect score, even though these two trajectories are clearly different. **C:** Comparing these two trajectories using a clustering metric (e.g. ARI) would also return a perfect score, even though these two trajectories are clearly different.

8.5 Guidelines for performing self-assessments

Articles introducing novel trajectory inference methods have unfortunately been plagued by low self-assessment rates. Most articles passing peer-review do not provide quantitative evidence that their method performs well. In the previous sections, we show that this is most likely caused by differing problem statements making methods hard to compare and a lack of benchmarking datasets and relevant metrics. We provide the reader with viable solutions to each of the problems, to be able to benchmark their method with ease.

We wish to leave the reader with a ‘Hippocratic oath for method developers’ (Figure 8.5). We hope this will inspire authors of new TI methods to benchmark their method, so that we can cross the 50% threshold of benchmarked methods, and beyond.

- In developing a new computational tool, I swear to fulfil, to the best of my ability, the following items:
- I will write software that works reliably but fails gracefully when it does not.
- I will assert that my method produces accurate and reproducible results.
- I will validate the performance of my tool with previously unseen data from third-party sources.
- I will use suitable quantitative performance metrics. If possible, I use multiple metrics to avoid overfitting.
- I will compare the performance to relevant methods.
- I will report positive achievements of my method, but also be critical of it, and discuss areas in which it performs suboptimally.
- I will write unit tests to ensure that each component in my tool works as intended. If the tool produces unexpected errors when tested on various edge cases, my tool will be perceived as dysfunctional by others.
- I will follow reproducible research best practices, by making code and data publicly available.

Figure 8.5: A hippocratic oath for computational method developers. Inspired by Laplante [18] and lists of guidelines for benchmarking [5, 19]

Table 8.1: Trajectory inference method metadata.

ID	Pre-print date	Publication date	Methods compared	Metrics used	Datasets used	Ref.
monocle1		2014-03-23				[20]
wanderlust		2014-04-24				[21]
scuba		2014-12-30				[22]
sincell	2015-01-27	2015-06-22				[23]
nbor		2015-06-08				[24]
oscope		2015-08-24				[25]
cycler		2015-08-24				[26]
waterfall		2015-09-03				[27]
gpseudotime	2015-09-15					[28]
embeddr		2015-09-18				[29]
eclair	2016-01-12	2016-05-20	dpt, wishbone, monocle1	pseudotime_correlation, robustness_unknown	moignard, klein, paul, synthetic_dpt	[30]
dpt	2016-02-08	2016-08-29				[31]
pseudogp	2016-04-05	2016-11-21				[32]
slicer	2016-04-09	2016-05-23				[33]
scell		2016-04-19				[34]
wishbone		2016-05-02				[35]
tscan		2016-05-13	monocle1, tscan, waterfall, scuba, wanderlust	pseudotime_pos	trapnell, amit, shin	
scoup		2016-06-08	scoup, monocle1, tscan	pseudotime_pis	kouno, moignard, shalek	[36]
delorean		2016-06-17				[37]
raceid_stemid		2016-06-21				[38]
ouja	2016-06-23					[39]
mpath		2016-06-30				[40]
celltree		2016-08-13	monocle1, tscan, celltree	pseudotime_unknown	trapnell	[41]
wavecrest		2016-08-17				[42]
stemnet		2016-08-25				[43]
scimitar	2016-10-04	2017-01-04	scimitar, monocle1, wanderlust	pseudotime_correlation	synthetic_scimitar, synthetic_scimitar	[44]
scorpius	2016-10-07		scorpius, wanderlust, monocle1, waterfall	pseudotime_cos, robustness_cva	schlitzer, buettner, shalek, shalek, trapnell, kowalczyk, kowalczyk, kowalczyk, kowalczyk	[44]
scent		2016-10-30	scent, slice, stemid	pseudotime_wilcox, pseudotime_auc	chu, trapnell, treutlein	[45]
slice		2016-12-19				[46]
topslam	2017-02-13		monocle1, wishbone, topslam	pseudotime_correlation	synthetic_topslam	[47]
monocle2	2017-02-21	2017-07-20	monocle1, monocle2, dpt, wishbone	pseudotime_correlation, branch_ari	paul	[48]
gpfates		2017-03-03				[49]
mfa		2017-03-15				[50]
tasic		2017-04-04				[51]
somsc	2017-04-05					[52]
slingshot	2017-04-19	2018-06-19	slingshot, monocle1, monocle2, dpt, tscan	pseudotime_correlation	synthetic_splatter, synthetic_splatter, synthetic_splatter, synthetic_splatter	[53]
sctda		2017-05-01	sctda, wishbone, slicer, dpt	pseudotime_correlation	synthetic_sctda	[54]
uncurl		2017-05-31				[55]
recat		2017-06-19	recat, scuba, monocle1, tscan, wishbone, dpt	pseudotime_correlation, time_custom	buettner	[56]
forks	2017-06-20		forks, monocle2, scuba, tscan, waterfall, dpt	pseudotime_correlation, robustness_stddev	windram, deng, guo, klein, amit, petropoulos	[1]
matcher		2017-06-24			angelmueller, synthetic_matcher	[57]
phenopath	2017-07-06	2018-06-23				[58]
hopland		2017-07-12	hopland, wanderlust, monocle1, topslam, scuba, wishbone, dpt	pseudotime_correlation	guo, deng, yan, amit, islam, synthetic_topslam	[2]
soptsc	2017-07-26	2019-06-20	soptsc, monocle2, dpt	pseudotime_correlation	guo, klein, shalek	[59]
pba		2017-07-30				[60]
brgps	2017-08-15		brgps, grandprix, monocle2, scuba, slicer, tscan, wishbone	pseudotime_correlation	guo, guo	[61]
wot		2017-09-27	2019-02-07			[62]
treetop		2017-10-10				[63]
paga		2017-10-27	2019-03-19			[64]
fateid		2017-11-11				[65]
psuedodynamics		2017-11-14				[66]
precode		2017-11-15				[67]
icpsc		2017-11-30	icpsc, wishbone, monocle2, dpt	pseudotime_correlation	sun, trapnell, yao	[68]
grandprix	2017-12-03	2018-07-02	delorean, grandprix	pseudotime_correlation	windram	[69]
cshmm		2017-12-03				[70]
calista		2018-01-31	monocle2, calista, dpt	pseudotime_correlation	moignard, bargaje, treutlein, chu, synthetic_calista	[71]
scepath		2018-02-05	scepath, monocle1, monocle2, tscan, dpt	pseudotime_correlation, robustness_correlation	yan, treutlein, trapnell	[15]
merlot	2018-02-08		merlot, dpt, slicer, monocle2, slingshot, tscan	branch_mi, pseudotime_correlation	paul, guo, velten, synthetic_prosstt, synthetic_prosstt, synthetic_splatter	[3]
gpseudorank	2018-02-08	2018-07-25	monocle2, dpt, wishbone, waterfall	internal_autocorrelation	paul, olsson	[72]
cellrouter		2018-03-01			petropoulos, synthetic_phate, synthetic_topslam	[16]
densitypath	2018-03-05	2018-12-07	monocle2, wishbone, dpt, densitypath	branch_ari, pseudotime_correlation		[73]
topographer		2018-03-23				[74]
stream		2018-04-18	stream, sctda, wishbone, slicer, monocle2, dpt, tscan, scuba, mpath, gpfates	pseudotime_correlation	synthetic_sctda	[75]
eligraph		2018-04-20				[76]
urd		2018-04-26				[77]
celltrails		2018-06-05				[78]
ddd	2018-07-12					[79]
palantir	2018-08-05	2019-03-21				[80]
confess		2018-09-04				[81]
graphhdp		2018-09-11				[82]
monocle3		2019-02-28				[83]
gpseudoclust	2019-03-05		gpseudoclust, monocle2, delorian, slicer	cluster_ari, cluster_fmi, cluster_nmi	sasagawa, shalek, synthetic_gpseudoclust, synthetic_gpseudoclust	[84]
psupertime	2019-04-29		monocle2, slingshot, psupertime	pseudotime_correlation	enge, qu, petropoulos, li, treutlein	[85]
cyclum	2019-05-02		cyclum, recat	cluster_accuracy	buettnner, mcdavid, mcdavid, mcdavid	[86]
sinova		2019-05-17				[87]

8.6 References

- [1] Mayank Sharma et al. "FORKS: Finding Orderings Robustly Using K-Means and Steiner Trees". In: *bioRxiv* (June 2017), p. 132811. doi: [10.1101/132811](https://doi.org/10.1101/132811).
- [2] Jing Guo and Jie Zheng. "HopLand: Single-Cell Pseudotime Recovery Using Continuous Hopfield Network-Based Modeling of Waddington's Epigenetic Landscape". In: *Bioinformatics* 33.14 (July 2017), pp. i102–i109. issn: 1367-4803. doi: [10.1093/bioinformatics/btx232](https://doi.org/10.1093/bioinformatics/btx232).
- [3] R Gonzalo Parra et al. "Reconstructing Complex Lineage Trees from scRNA-Seq Data Using MERLoT". In: *bioRxiv* (Feb. 2018), p. 261768. doi: [10.1101/261768](https://doi.org/10.1101/261768).
- [4] Wouter Saelens et al. "A Comparison of Single-Cell Trajectory Inference Methods". In: *Nature Biotechnology* 37 (May 2019). issn: 15461696. doi: [10.1038/s41587-019-0071-9](https://doi.org/10.1038/s41587-019-0071-9).
- [5] Raquel Norel, John Jeremy Rice, and Gustavo Stolovitzky. "The Self-Assessment Trap: Can We All Be Better than Average?" In: *Molecular systems biology* 7.1 (2011), p. 537. issn: 1744-4292. doi: [10.1038/msb.2011.70](https://doi.org/10.1038/msb.2011.70). pmid: [21988833](#).
- [6] Robrecht Cannoodt, Wouter Saelens, and Yvan Saeys. "Dyno: A Toolkit for Inferring and Interpreting Trajectories". In: *In preparation* (Sept. 2019).
- [7] Robrecht Cannoodt, Wouter Saelens, and Yvan Saeys. "Dyngen: Benchmarking with *in Silico* Single Cells". In: *In preparation* (Sept. 2019).
- [8] Luke Zappia, Belinda Phipson, and Alicia Oshlack. "Splatter: Simulation of Single-Cell RNA Sequencing Data". In: *Genome Biology* 18 (Sept. 2017), p. 174. issn: 1474-760X. doi: [10.1186/s13059-017-1305-0](https://doi.org/10.1186/s13059-017-1305-0).
- [9] Nikolaos Papadopoulos, Rodrigo Gonzalo Parra, and Johannes Soeding. "PROSSTT: Probabilistic Simulation of Single-Cell RNA-Seq Data for Complex Differentiation Processes". In: *bioRxiv* (Jan. 2018), p. 256941. doi: [10.1101/256941](https://doi.org/10.1101/256941).
- [10] Robrecht Cannoodt et al. "Single-Cell -Omics Datasets Containing a Trajectory". In: *Zenodo* (Oct. 2018). doi: [10.5281/zenodo.1211532](https://doi.org/10.5281/zenodo.1211532).
- [11] Luyi Tian et al. "Benchmarking Single Cell RNA-Sequencing Analysis Pipelines Using Mixture Control Experiments". In: *Nature Methods* 16.6 (June 2019), pp. 479–487. issn: 1548-7105. doi: [10.1038/s41592-019-0425-8](https://doi.org/10.1038/s41592-019-0425-8). pmid: [31133762](#).
- [12] Caleb Weinreb et al. "Lineage Tracing on Transcriptional Landscapes Links State to Fate during Differentiation". In: *bioRxiv* (Dec. 1, 2018), p. 467886. doi: [10.1101/467886](https://doi.org/10.1101/467886).
- [13] Laleh Haghverdi et al. "Diffusion Pseudotime Robustly Reconstructs Lineage Branching". In: *Nature Methods* 13.10 (Oct. 2016), pp. 845–848. issn: 1548-7105. doi: [10.1038/nmeth.3971](https://doi.org/10.1038/nmeth.3971).
- [14] Robrecht Cannoodt et al. "SCORPIUS Improves Trajectory Inference and Identifies Novel Modules in Dendritic Cell Development". In: (Oct. 2016). doi: [10.1101/079509](https://doi.org/10.1101/079509).
- [15] Suoqin Jin et al. "scEpath: Energy Landscape-Based Inference of Transition Probabilities and Cellular Trajectories from Single-Cell Transcriptomic Data". In: *Bioinformatics (Oxford, England)* (Feb. 2018). issn: 1367-4811. doi: [10.1093/bioinformatics/bty058](https://doi.org/10.1093/bioinformatics/bty058). pmid: [29415263](#).
- [16] Edroaldo Lummertz da Rocha et al. "Reconstruction of Complex Single-Cell Trajectories Using CellRouter". In: *Nature Communications* 9.1 (Mar. 1, 2018), p. 892. issn: 2041-1723. doi: [10.1038/s41467-018-03214-y](https://doi.org/10.1038/s41467-018-03214-y).
- [17] G Jurman et al. "The HIM Glocal Metric and Kernel for Network Comparison and Classification". In: *2015 IEEE International Conference on Data Science and Advanced Analytics (DSAA)*. Oct. 2015, pp. 1–10. doi: [10.1109/DSAA.2015.7344816](https://doi.org/10.1109/DSAA.2015.7344816).
- [18] Phillip A Laplante. "First, Do No Harm: A Hippocratic Oath for Software Developers". In: *Queue* 2.4 (2004), p. 14.

- [19] Lukas M. Weber et al. "Essential Guidelines for Computational Method Benchmarking". In: *Genome Biology* 20.1 (June 20, 2019), p. 125. issn: 1474-760X. doi: [10.1186/s13059-019-1738-8](https://doi.org/10.1186/s13059-019-1738-8).
- [20] Cole Trapnell et al. "The Dynamics and Regulators of Cell Fate Decisions Are Revealed by Pseudotemporal Ordering of Single Cells." In: *Nature biotechnology* 32.4 (Mar. 2014), pp. 381–386. issn: 1546-1696. doi: [10.1038/nbt.2859](https://doi.org/10.1038/nbt.2859). pmid: [24658644](#).
- [21] Sean C. Bendall et al. "Single-Cell Trajectory Detection Uncovers Progression and Regulatory Coordination in Human B Cell Development". In: *Cell* 157.3 (2014), pp. 714–725. issn: 00928674. doi: [10.1016/j.cell.2014.04.005](https://doi.org/10.1016/j.cell.2014.04.005).
- [22] Eugenio Marco et al. "Bifurcation Analysis of Single-Cell Gene Expression Data Reveals Epigenetic Landscape". In: *Proc. Natl. Acad. Sci. U. S. A.* 111.52 (2014), E5643–50.
- [23] Miguel Juliá et al. "Sincell : An {R/Bioconductor} Package for Statistical Assessment of Cell-State Hierarchies from Single-Cell {RNA-Seq}: Fig. 1". In: *Bioinformatics* 31.20 (2015), pp. 3380–3382.
- [24] Andreas Schlitzer et al. "Identification of cDC1- and cDC2-Committed DC Progenitors Reveals Early Lineage Priming at the Common DC Progenitor Stage in the Bone Marrow". In: *Nature Immunology* 16.7 (July 2015), pp. 718–728. issn: 1529-2916. doi: [10.1038/ni.3200](https://doi.org/10.1038/ni.3200).
- [25] Ning Leng et al. "Oscope Identifies Oscillatory Genes in Unynchronized Single Cell RNA-Seq Experiments". In: *Submitted* 12.10 (2015). issn: 1548-7091. doi: [10.1038/nmeth.3549](https://doi.org/10.1038/nmeth.3549). pmid: [26301841](#).
- [26] Gabriele Gut et al. "Trajectories of Cell-Cycle Progression from Fixed Cell Populations". In: *Nature Methods* 12.10 (2015), pp. 951–954. issn: 1548-7091. doi: [10.1038/nmeth.3545](https://doi.org/10.1038/nmeth.3545).
- [27] Jaehoon Shin et al. "Single-Cell RNA-Seq with Waterfall Reveals Molecular Cascades Underlying Adult Neurogenesis". In: *Cell Stem Cell* 17.3 (Sept. 3, 2015), pp. 360–372. issn: 1875-9777. doi: [10.1016/j.stem.2015.07.013](https://doi.org/10.1016/j.stem.2015.07.013). pmid: [26299571](#).
- [28] Kieran Campbell and Christopher Yau. "Bayesian Gaussian Process Latent Variable Models for Pseudotime Inference in Single-Cell RNA-Seq Data". In: *bioRxiv* (Sept. 2015), p. 26872. doi: [10.1101/026872](https://doi.org/10.1101/026872).
- [29] Kieran Campbell, Chris P Ponting, and Caleb Webber. "Laplacian Eigenmaps and Principal Curves for High Resolution Pseudotemporal Ordering of Single-Cell RNA-Seq Profiles". In: *bioRxiv* (Sept. 2015), p. 027219. doi: [10.1101/027219](https://doi.org/10.1101/027219).
- [30] Gregory Giecold et al. "Robust Lineage Reconstruction from High-Dimensional Single-Cell Data". In: *Nucleic Acids Research* 44.14 (Aug. 2016), e122–e122. issn: 0305-1048. doi: [10.1093/nar/gkw452](https://doi.org/10.1093/nar/gkw452).
- [31] Kieran R Campbell and Christopher Yau. "Order Under Uncertainty: Robust Differential Expression Analysis Using Probabilistic Models for Pseudotime Inference". In: *PLOS Computational Biology* 12.11 (Nov. 2016), e1005212. issn: 1553-7358. doi: [10.1371/journal.pcbi.1005212](https://doi.org/10.1371/journal.pcbi.1005212).
- [32] Joshua D. Welch, Alexander J. Hartemink, and Jan F. Prins. "SLICER: Inferring Branched, Nonlinear Cellular Trajectories from Single Cell RNA-Seq Data". In: *Genome Biology* 17 (2016), p. 106. issn: 1474-760X. doi: [10.1186/s13059-016-0975-3](https://doi.org/10.1186/s13059-016-0975-3).
- [33] Aaron Diaz et al. "SCell: Integrated Analysis of Single-Cell RNA-Seq Data". In: *Bioinformatics* 32.14 (July 2016), pp. 2219–2220. issn: 1367-4803. doi: [10.1093/bioinformatics/btw201](https://doi.org/10.1093/bioinformatics/btw201).
- [34] Manu Setty et al. "Wishbone Identifies Bifurcating Developmental Trajectories from Single-Cell Data". In: *Nat. Biotechnol.* 34 (April June 2016), pp. 1–14. issn: 1087-0156. doi: [10.1038/nbt.3569](https://doi.org/10.1038/nbt.3569). pmid: [27136076](#).
- [35] Zhicheng Ji and Hongkai Ji. "{TSCAN}: Pseudo-Time Reconstruction and Evaluation in Single-Cell {RNA-Seq} Analysis". In: *Nucleic Acids Res.* (2016).

- [36] Hirotaka Matsumoto, Matsumoto Hirotaka, and Kiryu Hisanori. "SCOUPE: A Probabilistic Model Based on the Ornstein-Uhlenbeck Process to Analyze Single-Cell Expression Data during Differentiation". In: *BMC Bioinformatics* 17.1 (2016).
- [37] John E Reid and Lorenz Wernisch. "Pseudotime Estimation: Deconfounding Single Cell Time Series". In: *Bioinformatics* 32.19 (Oct. 2016), pp. 2973–2980. issn: 1367-4803. doi: [10.1093/bioinformatics/btw372](https://doi.org/10.1093/bioinformatics/btw372).
- [38] Dominic Grün et al. "De Novo Prediction of Stem Cell Identity Using Single-Cell Transcriptome Data". In: *Cell Stem Cell* 19.2 (Aug. 2016), pp. 266–277. issn: 1934-5909. doi: [10.1016/j.stem.2016.05.010](https://doi.org/10.1016/j.stem.2016.05.010).
- [39] Kieran R Campbell and Christopher Yau. "A Descriptive Marker Gene Approach to Single-Cell Pseudotime Inference". In: *bioRxiv* (Nov. 2017), p. 60442. doi: [10.1101/060442](https://doi.org/10.1101/060442).
- [40] Jinmiao Chen et al. "Mpath Maps Multi-Branching Single-Cell Trajectories Revealing Progenitor Cell Progression during Development". In: *Nature Communications* 7 (June 2016), p. 11988. issn: 2041-1723. doi: [10.1038/ncomms11988](https://doi.org/10.1038/ncomms11988).
- [41] David A DuVerle et al. "CellTree: An R/Bioconductor Package to Infer the Hierarchical Structure of Cell Populations from Single-Cell RNA-Seq Data". In: *BMC Bioinformatics* 17 (Sept. 2016), p. 363. issn: 1471-2105. doi: [10.1186/s12859-016-1175-6](https://doi.org/10.1186/s12859-016-1175-6).
- [42] Li-Fang Chu et al. "Single-Cell RNA-Seq Reveals Novel Regulators of Human Embryonic Stem Cell Differentiation to Definitive Endoderm". In: *Genome Biology* 17 (Aug. 2016), p. 173. issn: 1474-760X. doi: [10.1186/s13059-016-1033-x](https://doi.org/10.1186/s13059-016-1033-x).
- [43] Lars Velten et al. "Human Haematopoietic Stem Cell Lineage Commitment Is a Continuous Process". In: *Nature Cell Biology* 19.4 (Apr. 2017), pp. 271–281. issn: 1476-4679. doi: [10.1038/ncb3493](https://doi.org/10.1038/ncb3493).
- [44] Pablo Cordero and Joshua M Stuart. "Tracing Co-Regulatory Network Dynamics in Noisy Single-Cell Transcriptome Trajectories". In: *Pacific Symposium on Biocomputing. Pacific Symposium on Biocomputing* 22 (2017), pp. 576–587. issn: 2335-6936. doi: [10.1142/9789813207813_0053](https://doi.org/10.1142/9789813207813_0053). pmid: [27897008](#).
- [45] Andrew E Teschendorff and Tariq Enver. "Single-Cell Entropy for Accurate Estimation of Differentiation Potency from a Cell's Transcriptome". In: *Nature Communications* 8 (June 2017), p. 15599. issn: 2041-1723. doi: [10.1038/ncomms15599](https://doi.org/10.1038/ncomms15599).
- [46] Minzhe Guo et al. "SLICE: Determining Cell Differentiation and Lineage Based on Single Cell Entropy". In: *Nucleic Acids Research* 45.7 (Apr. 2017), e54–e54. issn: 0305-1048. doi: [10.1093/nar/gkw1278](https://doi.org/10.1093/nar/gkw1278).
- [47] Max Zwiessele and Neil D Lawrence. "Topslam: Waddington Landscape Recovery for Single Cell Experiments". In: *bioRxiv* (Feb. 2017), p. 57778. doi: [10.1101/057778](https://doi.org/10.1101/057778).
- [48] Xiaojie Qiu et al. "Reversed Graph Embedding Resolves Complex Single-Cell Trajectories". In: *Nature Methods* 14.10 (Oct. 2017), pp. 979–982. issn: 1548-7105. doi: [10.1038/nmeth.4402](https://doi.org/10.1038/nmeth.4402).
- [49] Tapio Lönnberg et al. "Single-Cell RNA-Seq and Computational Analysis Using Temporal Mixture Modeling Resolves TH1/TFH Fate Bifurcation in Malaria". In: *Science Immunology* 2.9 (Mar. 2017), eaal2192. issn: 2470-9468. doi: [10.1126/sciimmunol.aal2192](https://doi.org/10.1126/sciimmunol.aal2192). pmid: [28345074](#).
- [50] Kieran R Campbell and Christopher Yau. "Probabilistic Modeling of Bifurcations in Single-Cell Gene Expression Data Using a Bayesian Mixture of Factor Analyzers". In: *Wellcome Open Research* 2 (Mar. 2017), p. 19. issn: 2398-502X. doi: [10.12688/wellcomeopenres.11087.1](https://doi.org/10.12688/wellcomeopenres.11087.1).
- [51] Sabrina Rashid, Darrell N Kotton, and Ziv Bar-Joseph. "TASIC: Determining Branching Models from Time Series Single Cell Data". In: *Bioinformatics* 33.16 (Aug. 2017), pp. 2504–2512. issn: 1367-4803. doi: [10.1093/bioinformatics/btx173](https://doi.org/10.1093/bioinformatics/btx173). pmid: [28379537](#).

- [52] Tao Peng and Qing Nie. "SOMSC: Self-Organization-Map for High-Dimensional Single-Cell Data of Cellular States and Their Transitions". In: *bioRxiv* (Aug. 2017), p. 124693. doi: [10.1101/124693](https://doi.org/10.1101/124693).
- [53] Kelly Street et al. "Slingshot: Cell Lineage and Pseudotime Inference for Single-Cell Transcriptomics". In: *BMC Genomics* 19.1 (June 2018), p. 477. issn: 1471-2164. doi: [10.1186/s12864-018-4772-0](https://doi.org/10.1186/s12864-018-4772-0).
- [54] Abbas H Rizvi et al. "Single-Cell Topological RNA-Seq Analysis Reveals Insights into Cellular Differentiation and Development". In: *Nature Biotechnology* 35.6 (June 2017), pp. 551–560. issn: 1546-1696. doi: [10.1038/nbt.3854](https://doi.org/10.1038/nbt.3854).
- [55] Sumit Mukherjee et al. "Scalable Preprocessing for Sparse scRNA-Seq Data Exploiting Prior Knowledge". In: *bioRxiv* (Mar. 2018), p. 142398. doi: [10.1101/142398](https://doi.org/10.1101/142398).
- [56] Zehua Liu et al. "Reconstructing Cell Cycle Pseudo Time-Series via Single-Cell Transcriptome Data". In: *Nature Communications* 8.1 (June 2017), p. 22. issn: 2041-1723. doi: [10.1038/s41467-017-00039-z](https://doi.org/10.1038/s41467-017-00039-z).
- [57] Joshua D Welch, Alexander J Hartemink, and Jan F Prins. "MATCHER: Manifold Alignment Reveals Correspondence between Single Cell Transcriptome and Epigenome Dynamics". In: *Genome Biology* 18 (July 2017), p. 138. issn: 1474-760X. doi: [10.1186/s13059-017-1269-0](https://doi.org/10.1186/s13059-017-1269-0).
- [58] Kieran Campbell and Christopher Yau. "Uncovering Genomic Trajectories with Heterogeneous Genetic and Environmental Backgrounds across Single-Cells and Populations". In: *bioRxiv* (July 2017), p. 159913. doi: [10.1101/159913](https://doi.org/10.1101/159913).
- [59] Shuxiong Wang et al. "Cell Lineage and Communication Network Inference via Optimization for Single-Cell Transcriptomics". In: *Nucleic Acids Research* 47.11 (Mar. 29, 2019), e66–e66. issn: 0305-1048. doi: [10.1093/nar/gkz204](https://doi.org/10.1093/nar/gkz204).
- [60] Caleb Weinreb et al. "Fundamental Limits on Dynamic Inference from Single-Cell Snapshots". In: *Proceedings of the National Academy of Sciences* (Feb. 2018), p. 201714723. issn: 0027-8424, 1091-6490. doi: [10.1073/pnas.1714723115](https://doi.org/10.1073/pnas.1714723115). pmid: [29463712](#).
- [61] Christopher Andrew Penfold et al. "Nonparametric Bayesian Inference of Transcriptional Branching and Recombination Identifies Regulators of Early Human Germ Cell Development". In: *bioRxiv* (Sept. 2017), p. 167684. doi: [10.1101/167684](https://doi.org/10.1101/167684).
- [62] Geoffrey Schiebinger et al. "Optimal-Transport Analysis of Single-Cell Gene Expression Identifies Developmental Trajectories in Reprogramming". In: *Cell* 176.4 (Feb. 7, 2019), 928–943.e22. issn: 0092-8674. doi: [10.1016/j.cell.2019.01.006](https://doi.org/10.1016/j.cell.2019.01.006).
- [63] Will Macnair et al. "Tree-Ensemble Analysis Tests for Presence of Multifurcations in Single Cell Data". In: *bioRxiv* (Oct. 2017), p. 200923. doi: [10.1101/200923](https://doi.org/10.1101/200923).
- [64] F Alexander Wolf et al. "Graph Abstraction Reconciles Clustering with Trajectory Inference through a Topology Preserving Map of Single Cells". In: *bioRxiv* (Oct. 2017), p. 208819. doi: [10.1101/208819](https://doi.org/10.1101/208819).
- [65] Josip S Herman, Sagar, and Dominic Grün. "FatelD Infers Cell Fate Bias in Multipotent Progenitors from Single-Cell RNA-Seq Data". In: *Nature Methods* (Apr. 2018). issn: 1548-7105. doi: [10.1038/nmeth.4662](https://doi.org/10.1038/nmeth.4662).
- [66] David S. Fischer et al. "Beyond Pseudotime: Following T-Cell Maturation in Single-Cell RNAseq Time Series". In: *bioRxiv* (Jan. 1, 2017), p. 219188. doi: [10.1101/219188](https://doi.org/10.1101/219188).
- [67] Charles A Herring et al. "Unsupervised Trajectory Analysis of Single-Cell RNA-Seq and Imaging Data Reveals Alternative Tuft Cell Origins in the Gut". In: *Cell Systems* 6.1 (Jan. 2018), 37–51.e9. issn: 2405-4712. doi: [10.1016/j.cels.2017.10.012](https://doi.org/10.1016/j.cels.2017.10.012).

- [68] Na Sun et al. "Inference of Differentiation Time for Single Cell Transcriptomes Using Cell Population Reference Data". In: *Nature Communications* 8.1 (Nov. 2017), p. 1856. issn: 2041-1723. doi: [10.1038/s41467-017-01860-2](https://doi.org/10.1038/s41467-017-01860-2).
- [69] Sumon Ahmed, Magnus Rattray, and Alexis Boukouvalas. "GrandPrix: Scaling up the Bayesian GPLVM for Single-Cell Data". In: *bioRxiv* (Dec. 2017), p. 227843. doi: [10.1101/227843](https://doi.org/10.1101/227843).
- [70] Chieh Lin and Ziv Bar-Joseph. "Continuous-State HMMs for Modeling Time-Series Single-Cell RNA-Seq Data". In: *Bioinformatics* (btz296 Apr. 30, 2019). issn: 1367-4803. doi: [10.1093/bioinformatics/btz296](https://doi.org/10.1093/bioinformatics/btz296).
- [71] Nan Papili Gao, Thomas Hartmann, and Rudiyanto Gunawan. "CALISTA: Clustering And Lineage Inference in Single-Cell Transcriptional Analysis". In: *bioRxiv* (Jan. 2018), p. 257550. doi: [10.1101/257550](https://doi.org/10.1101/257550).
- [72] Magdalena E Strauß, John E Reid, and Lorenz Wernisch. "GPseudoRank: A Permutation Sampler for Single Cell Orderings". In: *Bioinformatics* 35.4 (Feb. 15, 2019), pp. 611–618. issn: 1367-4803. doi: [10.1093/bioinformatics/bty664](https://doi.org/10.1093/bioinformatics/bty664).
- [73] Ziwei Chen et al. "DensityPath: An Algorithm to Visualize and Reconstruct Cell State-Transition Path on Density Landscape for Single-Cell RNA Sequencing Data". In: *Bioinformatics* 35.15 (Dec. 7, 2018), pp. 2593–2601. issn: 1367-4803. doi: [10.1093/bioinformatics/bty1009](https://doi.org/10.1093/bioinformatics/bty1009).
- [74] Jiajun Zhang and Tianshou Zhou. "Topographer Reveals Stochastic Dynamics of Cell Fate Decisions from Single-Cell RNA-Seq Data". In: *bioRxiv* (Jan. 2018), p. 251207. doi: [10.1101/251207](https://doi.org/10.1101/251207).
- [75] Huidong Chen et al. "Single-Cell Trajectories Reconstruction, Exploration and Mapping of Omics Data with STREAM". In: *Nature Communications* 10.1 (Apr. 23, 2019), p. 1903. issn: 2041-1723. doi: [10.1038/s41467-019-09670-4](https://doi.org/10.1038/s41467-019-09670-4).
- [76] Luca Albergante et al. "Robust And Scalable Learning Of Complex Dataset Topologies Via Elpigraph". In: (Apr. 20, 2018). arXiv: [1804.07580 \[cs, q-bio, stat\]](https://arxiv.org/abs/1804.07580). url: <http://arxiv.org/abs/1804.07580> (visited on 09/21/2019).
- [77] Jeffrey A. Farrell et al. "Single-Cell Reconstruction of Developmental Trajectories during Zebrafish Embryogenesis". In: *Science* 360.6392 (June 1, 2018), eaar3131. doi: [10.1126/science.aar3131](https://doi.org/10.1126/science.aar3131).
- [78] Daniel C. Ellwanger et al. "Transcriptional Dynamics of Hair-Bundle Morphogenesis Revealed with CellTrails". In: *Cell Reports* 23.10 (June 5, 2018), 2901–2914.e13. issn: 2211-1247. doi: [10.1016/j.celrep.2018.05.002](https://doi.org/10.1016/j.celrep.2018.05.002).
- [79] Jake P. Taylor-King, Asbjørn N. Riseth, and Manfred Claassen. "Dynamic Distribution Decomposition for Single-Cell Snapshot Time Series Identifies Subpopulations and Trajectories during iPSC Reprogramming". In: *bioRxiv* (Jan. 1, 2018), p. 367789. doi: [10.1101/367789](https://doi.org/10.1101/367789).
- [80] Manu Setty et al. "Characterization of Cell Fate Probabilities in Single-Cell Data with Palantir". In: *Nature Biotechnology* 37.4 (Apr. 1, 2019), pp. 451–460. issn: 1546-1696. doi: [10.1038/s41587-019-0068-4](https://doi.org/10.1038/s41587-019-0068-4).
- [81] Efthymios Motakis and Diana H.P. Low. "CONFESS: Fluorescence-Based Single-Cell Ordering in R". In: *bioRxiv* (Jan. 1, 2018), p. 407932. doi: [10.1101/407932](https://doi.org/10.1101/407932).
- [82] Fabrizio Costa, Dominic Grün, and Rolf Backofen. "GraphDDP: A Graph-Embedding Approach to Detect Differentiation Pathways in Single-Cell-Data Using Prior Class Knowledge". In: *Nature Communications* 9.1 (Sept. 11, 2018), p. 3685. issn: 2041-1723. doi: [10.1038/s41467-018-05988-7](https://doi.org/10.1038/s41467-018-05988-7).
- [83] Junyue Cao et al. "The Single-Cell Transcriptional Landscape of Mammalian Organogenesis". In: *Nature* 566.7745 (Feb. 1, 2019), pp. 496–502. issn: 1476-4687. doi: [10.1038/s41586-019-0969-x](https://doi.org/10.1038/s41586-019-0969-x).

- [84] Magdalena E Strauss et al. "GPseudoClust: Deconvolution of Shared Pseudo-Profiles at Single-Cell Resolution". In: *bioRxiv* (Jan. 1, 2019), p. 567115. doi: [10.1101/567115](https://doi.org/10.1101/567115).
- [85] Will Macnair and Manfred Claassen. "Psupertime: Supervised Pseudotime Inference for Single Cell RNA-Seq Data with Sequential Labels". In: *bioRxiv* (Jan. 1, 2019), p. 622001. doi: [10.1101/622001](https://doi.org/10.1101/622001).
- [86] Shaoheng Liang et al. "Latent Periodic Process Inference from Single-Cell RNA-Seq Data". In: *bioRxiv* (Jan. 1, 2019), p. 625566. doi: [10.1101/625566](https://doi.org/10.1101/625566).
- [87] Junxiang Li et al. "Systematic Reconstruction of Molecular Cascades Regulating GP Development Using Single-Cell RNA-Seq". In: *Cell Reports* 15.7 (May 17, 2016), pp. 1467–1480. issn: 2211-1247. doi: [10.1016/j.celrep.2016.04.043](https://doi.org/10.1016/j.celrep.2016.04.043).

CHAPTER 9

Paper 8: Essential guidelines for computational method benchmarking

Abstract

Purpose: In computational biology and other sciences, researchers are frequently faced with a choice between several computational methods for performing data analyses. Benchmarking studies aim to rigorously compare the performance of different methods using well-characterized benchmark datasets, to determine the strengths of each method or to provide recommendations regarding suitable choices of methods for an analysis. However, benchmarking studies must be carefully designed and implemented to provide accurate, unbiased, and informative results.

Results: Here, we summarise key practical guidelines and recommendations for performing high-quality benchmarking analyses, based on our experiences in computational biology. Our review spans the full pipeline of benchmarking, from defining the scope to best practices for reproducibility. This includes crucial questions regarding design and evaluation principles.

Conclusion: With this review, we aim to guide computational researchers in avoiding common pitfalls in designing, performing, and interpreting benchmarks.

Publication status

Published in Genome Biology 20, 125 (2019). doi:[10.1186/s13059-019-1738-8](https://doi.org/10.1186/s13059-019-1738-8).

Weber LM, Saelens W, **Cannoodt R**, Soneson C, Hapfelmeier A, Gardner PP, Boulesteix A, Saeyns Y, and Robinson MD

Author contributions

- L.M.W. proposed the project and drafted the manuscript.
- W.S., **R.C.**, C.S., A.H., P.P.G., A.L.B., Y.S., and M.D.R. contributed ideas and references and contributed to drafting of the manuscript.
- Y.S. and M.D.R. supervised the project.

9.1 Introduction

Many fields of computational research are characterized by a growing number of available methods for data analysis. For example, at the time of writing, almost 400 methods are available for analysing data from single-cell RNA-sequencing experiments [1]. For experimental researchers and method users, this represents both an opportunity and a challenge, since method choice can significantly affect conclusions.

Benchmarking studies are carried out by computational researchers to compare the performance of different methods, using reference datasets and a range of evaluation criteria. Benchmarks may be performed by authors of new methods to demonstrate performance improvements or other advantages; by independent groups interested in systematically comparing existing methods; or organized as community challenges. Neutral benchmarking studies, i.e., those performed independently of new method development by authors without any perceived bias, and with a focus on the comparison itself, are especially valuable for the research community [2, 3].

From our experience conducting benchmarking studies in computational biology, we have learned several key lessons that we aim to synthesize in this review. A number of previous reviews have addressed this topic from a range of perspectives, including: overall commentaries and recommendations on benchmarking design [2, 4, 5, 6, 7, 8, 9]; surveys of design practices followed by existing benchmarks [7]; the importance of neutral benchmarking studies [3]; principles for the design of real-data benchmarking studies [10, 11] and simulation studies [12]; the incorporation of meta-analysis techniques into benchmarking [13, 14, 15, 16]; the organization and role of community challenges [17, 18]; and discussions on benchmarking design for specific types of methods [19, 20]. More generally, benchmarking may be viewed as a form of meta-research [21].

Our aim is to complement previous reviews by providing a summary of essential guidelines for designing, performing, and interpreting benchmarks. While all guidelines are essential for a truly excellent benchmark, some are more fundamental than others. Our target audience consists of computational researchers who are interested in performing a benchmarking study, or who have already begun one. Our review spans the full pipeline of benchmarking, from defining the scope to best practices for reproducibility. This includes crucial questions regarding design and evaluation principles: for example, using rankings according to evaluation metrics to identify a set of high-performing methods, and then highlighting different strengths and trade-offs among these.

9.2 Ten essential guidelines

The review is structured as a series of guidelines (Figure 9.1), each explained in detail in the following sections. We use examples from computational biology; however, we expect that most arguments apply equally to other fields. We hope that these guidelines will continue the discussion on benchmarking design, as well as assisting computational researchers to design and implement rigorous, informative, and unbiased benchmarking analyses.

9.2.1 Defining the purpose and scope

The purpose and scope of a benchmark should be clearly defined at the beginning of the study, and will fundamentally guide the design and implementation. In general, we can define three broad types

1. Define the purpose and scope of the benchmark.
2. Include all relevant methods.
3. Select (or design) representative dataset.
4. Choose appropriate parameter values and software versions.
5. Evaluate methods according to key quantitative performance metrics.
6. Evaluate secondary measures including computational requirements, user-friendliness, installation procedures, and documentation quality.
7. Interpret results and provide recommendations from both user and method developer perspectives.
8. Publish results in an accessible format
9. Design the benchmark to enable future extensions.
10. Follow reproducible research best practices, by making code and data publicly available.

Figure 9.1: Summary of the guidelines as a set of recommendations. Each recommendation is discussed in more detail in the corresponding section in the text.

of benchmarking studies: (i) those by method developers, to demonstrate the merits of their approach (e.g. [22, 23, 24, 25, 26]); (ii) neutral studies performed to systematically compare methods for a certain analysis, either conducted directly by an independent group (e.g. [27, 28, 29, 30, 31, 32, 33, 34, 35, 36, 37, 38]) or in collaboration with method authors (e.g. [39]); or (iii) those organized in the form of a community challenge, such as those from the DREAM [40, 41, 42, 43, 44], FlowCAP [45, 46], CASP [47, 48], CAMI [49], Assemblathon [50, 51], MAQC/SEQC [52, 53, 54], and GA4GH [55] consortia.

A neutral benchmark or community challenge should be as comprehensive as possible, although for any benchmark there will be trade-offs in terms of available resources. To minimize perceived bias, a research group conducting a neutral benchmark should be approximately equally familiar with all included methods, reflecting typical usage of the methods by independent researchers [3]. Alternatively, the group could include the original method authors, so that each method is evaluated under optimal conditions; methods whose authors decline to take part should be reported. In either case, bias due to focusing attention on particular methods should be avoided – for example, when tuning parameters or fixing bugs. Strategies to avoid these types of biases, such as the use of blinding, have been previously proposed [10].

By contrast, when introducing a new method, the focus of the benchmark will be on evaluating the relative merits of the new method. This may be sufficiently achieved with a less extensive benchmark, for example, by comparing against a smaller set of state-of-the-art and baseline methods. However, the benchmark must still be carefully designed to avoid disadvantaging any methods; for example, extensively tuning parameters for the new method while using default parameters for competing methods would result in a biased representation. Some advantages of a new method may fall outside the scope of a benchmark; for example, a new method may enable more flexible analyses than previous methods (e.g. beyond two-group comparisons in differential analyses [22]).

Finally, results should be summarized in the context of the original purpose of the benchmark. A neutral benchmark or community challenge should provide clear guidelines for method users, and highlight weaknesses in current methods so that these can be addressed by method developers. On the other hand, benchmarks performed to introduce a new method should discuss what the new method offers compared with the current state-of-the-art, such as discoveries that would otherwise not be possible.

9.2.2 Selection of methods

The selection of methods to include in the benchmark will be guided by the purpose and scope of the study. A neutral benchmark should include all available methods for a certain type of analysis. In this case, the publication describing the benchmark will also function as a review of the literature; a summary table describing the methods is a key output (e.g. Figure 2 in [27] or Table 1 in [31]). Alternatively, it may make sense to include only a subset of methods, by defining inclusion criteria: for example, all methods that (i) provide freely available software implementations, (ii) are available for commonly used operating systems, and (iii) can successfully be installed without errors following a reasonable amount of trouble-shooting. Such criteria should be chosen without favouring any methods, and exclusion of any widely used methods should be justified. A useful strategy can be to involve method authors within the process, since they may provide additional details on optimal usage. In addition, community involvement can lead to new collaborations and inspire future method development. However, the overall neutrality and balance of the resulting research team should be maintained. Finally, if the benchmark is organized as a community challenge, the selection of methods will be determined by the participants. In this case, it is important to communicate the initiative widely – for example, through an established network such as DREAM challenges. However, some authors may choose not to participate; a summary table documenting non-included methods should be provided in this case.

When developing a new method, it is generally sufficient to select a representative subset of existing methods to compare against. For example, this could consist of the current best-performing methods (if known), a simple baseline method, and any methods that are widely used. The selection of competing methods should ensure an accurate and unbiased assessment of the relative merits of the new approach, compared with the current state-of-the-art. In fast-moving fields, for a truly excellent benchmark, method developers should be prepared to update their benchmarks or design them to easily allow extensions as new methods emerge.

9.2.3 Selection (or design) of datasets

The selection of reference datasets is a critical design choice. If suitable publicly accessible datasets cannot be found, they will need to be generated or constructed, either experimentally or by simulation. Including a variety of datasets ensures that methods can be evaluated under a wide range of conditions. In general, reference datasets can be grouped into two main categories: simulated (or synthetic) and real (or experimental).

Simulated data have the advantage that a known true signal (or ground truth) can easily be introduced; for example, whether a gene is differentially expressed. Quantitative performance metrics measuring the ability to recover the known truth can then be calculated. However, it is important to demonstrate that simulations accurately reflect relevant properties of real data, by inspecting empirical summaries of both simulated and real datasets (e.g. using automated tools [56]). The set of empirical summaries to use is context-specific; for example, for single-cell RNA-sequencing, drop-out profiles and dispersion-mean relationships should be compared [29]; for DNA methylation, correlation patterns among neighbouring CpG sites should be investigated [57]; for comparing mapping algorithms, error profiles of the sequencing platforms should be considered [58]. Simplified simulations can also be useful, to evaluate a new method under a basic scenario, or to systematically test aspects such as scalability and stability. However, overly simplistic simulations should be avoided, since these will not provide useful information on performance. A further advantage of simulated data is that it is possi-

ble to generate as much data as required; for example, to study variability and draw statistically valid conclusions.

Experimental data often do not contain a ground truth, making it difficult to calculate performance metrics. Instead, methods may be evaluated by comparing them against each other (e.g. overlap between sets of detected differential features [23]), or against a current widely accepted method or gold standard (e.g. manual gating to define cell populations in high-dimensional cytometry [31, 45], or fluorescence *in situ* hybridization to validate absolute copy number predictions [6]). In the context of supervised learning, the response variable to be predicted is known in the manually labelled training and test data. However, individual datasets should not be overused, and using the same dataset for both method development and evaluation should be avoided, due to the risk of overfitting and overly optimistic results [59, 60]. In some cases, it is also possible to design experimental datasets containing a ground truth. Examples include: (i) spiking in synthetic RNA molecules at known relative concentrations [61] in RNA-sequencing experiments (e.g. [54, 62]), (ii) large-scale validation of gene expression measurements by quantitative polymerase chain reaction (e.g. [54]), (iii) using genes located on sex chromosomes as a proxy for silencing of DNA methylation status (e.g. [26, 63]), (iv) using fluorescence-activated cell sorting to sort cells into known sub-populations prior to single-cell RNA-sequencing (e.g. [29, 64, 65]), or (v) mixing different cell lines to create pseudo-cells [66]. However, it may be difficult to ensure that the ground truth represents an appropriate level of variability – for example, the variability of spiked-in material, or whether method performance on cell line data is relevant to out-bred populations. Alternatively, experimental datasets may be evaluated qualitatively, for example, by judging whether each method can recover previous discoveries, although this strategy relies on the validity of previous results.

A further technique is to design semi-simulated datasets that combine real experimental data with an *in silico* (i.e., computational) spike-in signal; for example, by combining cells or genes from null (e.g. healthy) samples with a subset of cells or genes from samples expected to contain a true differential signal (examples include [22, 67, 68]). This strategy can create datasets with more realistic levels of variability and correlation, together with a ground truth.

Overall, there is no perfect reference dataset, and the selection of appropriate datasets will involve trade-offs, for example, regarding the level of complexity. Both simulated and experimental data should not be too simple (e.g. two of the datasets in the FlowCAP-II challenge [45] gave perfect performance for several algorithms) or too difficult (e.g. for the third dataset in FlowCAP-II, no algorithms performed well); in these situations, it can be impossible to distinguish performance. In some cases, individual datasets have also been found to be unrepresentative, leading to over-optimistic or otherwise biased assessment of methods (e.g. [69]). Overall, the key to truly excellent benchmarking is diversity of evaluations, i.e., using a range of metrics and datasets that span the range of those that might be encountered in practice, so that performance estimates can be credibly extrapolated.

9.2.4 Parameters and software versions

Parameter settings can have a crucial impact on performance. Some methods have a large number of parameters, and tuning parameters to optimal values can require significant effort and expertise. For a neutral benchmark, a range of parameter values should ideally be considered for each method, although trade-offs need to be considered regarding available time and computational resources. Importantly, the selection of parameter values should comply with the neutrality principle, i.e., certain methods should not be favoured over others through more extensive parameter tuning.

There are three major strategies for choosing parameters. The first (and simplest) is to use default values for all parameters. Default parameters may be adequate for many methods, although this is difficult to judge in advance. While this strategy may be viewed as too simplistic for some neutral benchmarks, it reflects typical usage. We used default parameters in several neutral benchmarks where we were interested in performance for untrained users [27, 70, 71]. In addition, for [27], due to the large number of methods and datasets, total runtime was already around a week using 192 processor cores, necessitating judgement in the scope of parameter tuning. The second strategy is to choose parameters based on previous experience or published values. This relies on familiarity with the methods and the literature, reflecting usage by expert users. The third strategy is to use a systematic or automated parameter tuning procedure – for example, a grid search across ranges of values for multiple parameters or techniques such as cross-validation (e.g. [30]). The strategies may also be combined, for example, by setting non-critical parameters to default values and performing a grid search for key parameters. Regardless, neutrality should be maintained: comparing methods with the same strategy makes sense, while comparing one method with default parameters against another with extensive tuning makes for an unfair comparison.

For benchmarks performed to introduce a new method, comparing against a single set of optimal parameter values for competing methods is often sufficient; these values may be selected during initial exploratory work or by consulting documentation. However, as outlined above, bias may be introduced by tuning the parameters of the new method more extensively. The parameter selection strategy should be transparently discussed during the interpretation of the results, to avoid the risk of over-optimistic reporting due to expending more researcher degrees of freedom on the new method [5, 72].

Software versions can also influence results, especially if updates include major changes to methodology (e.g. [73]). Final results should generally be based on the latest available versions, which may require re-running some methods if updates become available during the course of a benchmark.

9.2.5 Evaluation criteria: key quantitative performance metrics

Evaluation of methods will rely on one or more quantitative performance metrics (Figure 9.2A). The choice of metric depends on the type of method and data. For example, for classification tasks with a ground truth, metrics include the true positive rate (TPR; sensitivity or recall), false positive rate (FPR; 1 - specificity), and false discovery rate (FDR). For clustering tasks, common metrics include the F1 score, adjusted Rand index, normalized mutual information, precision, and recall; some of these can be calculated at the cluster level as well as averaged (and optionally weighted) across clusters (e.g. these metrics were used to evaluate clustering methods in our own work [28, 31] and by others [33, 45, 74]). Several of these metrics can also be compared visually to capture the trade-off between sensitivity and specificity, for example, using receiver operating characteristic (ROC) curves (TPR versus FPR), TPR versus FDR curves, or precision-recall (PR) curves (Figure 9.2B). For imbalanced datasets, PR curves have been shown to be more informative than ROC curves [75, 76]. These visual metrics can also be summarized as a single number, such as area under the ROC or PR curve; examples from our work include [22, 29]. In addition to the trade-off between sensitivity and specificity, a methods operating point' is important; in particular, whether the threshold used (e.g. 5% FDR) is calibrated to achieve the specified error rate. We often overlay this onto TPR-FDR curves by filled or open circles (e.g. Figure 9.2B, generated using the iCOBRA package [77]); examples from our work include [22, 23, 25, 78].

For methods with continuous-valued output (e.g. effect sizes or abundance estimates), metrics in-

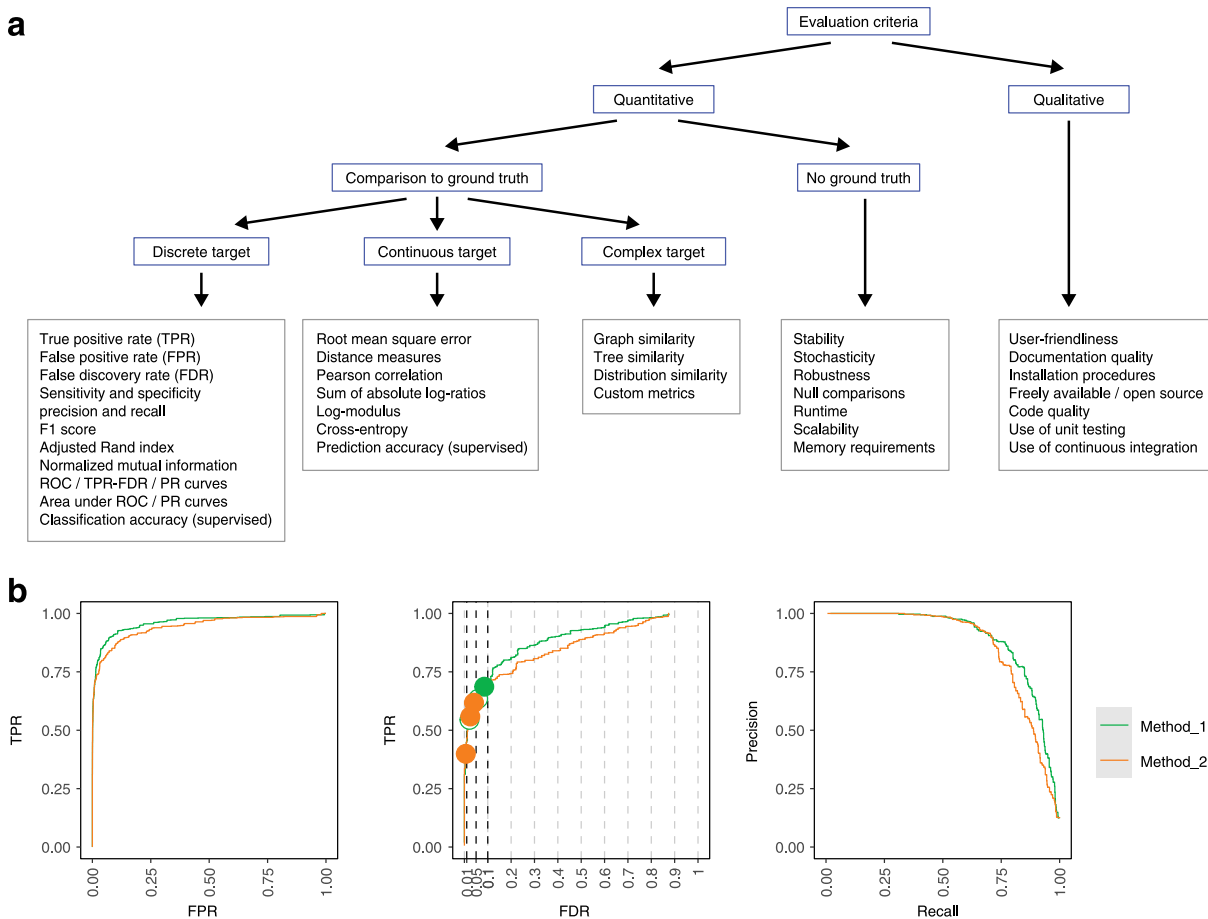


Figure 9.2: Summary and examples of performance metrics. **A:** Schematic overview of classes of frequently used performance metrics, including examples (*boxes outlined in gray*). **B:** Examples of popular visualizations of quantitative performance metrics for classification methods, using reference datasets with a ground truth. ROC curves (*left*). TPR versus FDR curves (*centre*); circles represent observed TPR and FDR at typical FDR thresholds of 1, 5, and 10%, with filled circles indicating observed FDR lower than or equal to the imposed threshold. PR curves (*right*). Visualizations were generated using iCOBRA R/Bioconductor package [77]. *FDR* false discovery rate, *FPR* false positive rate, *PR* precision-recall, *ROC* receiver operating characteristic, *TPR* true positive rate

clude the root mean square error, distance measures, Pearson correlation, sum of absolute log-ratios, log-modulus, and cross-entropy. As above, the choice of metric depends on the type of method and data (e.g. [41, 79] used correlation, while [48] used root mean square deviation). Further classes of methods include those generating graphs, phylogenetic trees, overlapping clusters, or distributions; these require more complex metrics. In some cases, custom metrics may need to be developed (e.g. we defined new metrics for topologies of developmental trajectories in [27]). When designing custom metrics, it is important to assess their reliability across a range of prediction values (e.g. [80, 81]). For some metrics, it may also be useful to assess uncertainty, for example, via confidence intervals. In the context of supervised learning, classification or prediction accuracy can be evaluated by cross-validation, bootstrapping, or on a separate test dataset (e.g. [13, 46]). In this case, procedures to split data into training and test sets should be appropriate for the data structure and the prediction task at hand (e.g. leaving out whole samples or chromosomes [82]).

Additional metrics that do not rely on a ground truth include measures of stability, stochasticity, and robustness. These measures may be quantified by running methods multiple times using different inputs or sub-sampled data (e.g. we observed substantial variability in performance for some methods in [29, 31]). Missing values may occur if a method does not return any values for a certain metric, for

example, due to a failure to converge or other computational issues such as excessive runtime or memory requirements (e.g. [27, 29, 31]). Fall-back solutions such as imputation may be considered in this case [83], although these should be transparently reported. For non-deterministic methods (e.g. with random starts or stochastic optimization), variability in performance when using different random seeds or sub-sampled data should be characterized. Null comparisons can be constructed by randomizing group labels such that datasets do not contain any true signal, which can provide information on error rates (e.g. [22, 25, 26]). However, these must be designed carefully to avoid confounding by batch or population structure, and to avoid strong within-group batch effects that are not accounted for.

For most benchmarks, multiple metrics will be relevant. Focusing on a single metric can give an incomplete view: methods may not be directly comparable if they are designed for different tasks, and different users may be interested in different aspects of performance. Therefore, a crucial design decision is whether to focus on an overall ranking, for example, by combining or weighting multiple metrics. In general, it is unlikely that a single method will perform best across all metrics, and performance differences between top-ranked methods for individual metrics can be small. Therefore, a good strategy is to use rankings from multiple metrics to identify a set of consistently high-performing methods, and then highlight the different strengths of these methods. For example, in [31], we identified methods that gave good clustering performance, and then highlighted differences in run-times among these. In several studies, we have presented results in the form of a graphical summary of performance according to multiple criteria (examples include Figure 3 in [27] and Figure 5 in [29] from our work; and Figure 2 in [39] and Figure 6 in [32] from other authors). Identifying methods that consistently under-perform can also be useful, to allow readers to avoid these.

9.2.6 Evaluation criteria: secondary measures

In addition to the key quantitative performance metrics, methods should also be evaluated according to secondary measures, including runtime, scalability, and other computational requirements, as well as qualitative aspects such as user-friendliness, installation procedures, code quality, and documentation quality (Figure 9.2A). From the user perspective, the final choice of method may involve trade-offs according to these measures: an adequately performing method may be preferable to a top-performing method that is especially difficult to use.

In our experience, run-times and scalability can vary enormously between methods (e.g. in our work, run-times for cytometry clustering algorithms [31] and meta-genome analysis tools [79] ranged across multiple orders of magnitude for the same datasets). Similarly, memory and other computational requirements can vary widely. Run-times and scalability may be investigated systematically, for example, by varying the number of cells or genes in a single-cell RNA-sequencing dataset [28, 29]. In many cases, there is a trade-off between performance and computational requirements. In practice, if computational requirements for a top-performing method are prohibitive, then a different method may be preferred by some users.

User-friendliness, installation procedures, and documentation quality can also be highly variable [84, 85]. Streamlined installation procedures can be ensured by distributing the method via standard package repositories, such as CRAN and Bioconductor for R, or PyPI for Python. Alternative options include GitHub and other code repositories or institutional websites; however, these options do not provide users with the same guarantees regarding reliability and documentation quality. Availability across multiple operating systems and within popular programming languages for data analysis is also impor-

tant. Availability of graphical user interfaces can further extend accessibility, although graphical-only methods hinder reproducibility and are thus difficult to include in a systematic benchmark.

For many users, freely available and open source software will be preferred, since it is more broadly accessible and can be adapted by experienced users. From the developer perspective, code quality and use of software development best practices, such as unit testing and continuous integration, are also important. Similarly, adherence to commonly used data formats (e.g. GFF/GTF files for genomic features, BAM/SAM files for sequence alignment data, or FCS files for flow or mass cytometry data) greatly improves accessibility and extensibility.

High-quality documentation is critical, including help pages and tutorials. Ideally, all code examples in the documentation should be continually tested, for example, as Bioconductor does, or through continuous integration.

9.2.7 Interpretation, guidelines, and recommendations

For a truly excellent benchmark, results must be clearly interpreted from the perspective of the intended audience. For method users, results should be summarized in the form of recommendations. An overall ranking of methods (or separate rankings for multiple evaluation criteria) can provide a useful overview. However, as mentioned above, some methods may not be directly comparable (e.g. since they are designed for different tasks), and different users may be interested in different aspects of performance. In addition, it is unlikely that there will be a clear winner across all criteria, and performance differences between top-ranked methods can be small. Therefore, an informative strategy is to use the rankings to identify a set of high-performing methods, and to highlight the different strengths and trade-offs among these methods. The interpretation may also involve biological or other domain knowledge to establish the scientific relevance of differences in performance. Importantly, neutrality principles should be preserved during the interpretation.

For method developers, the conclusions may include guidelines for possible future development of methods. By assisting method developers to focus their research efforts, high-quality benchmarks can have significant impact on the progress of methodological research.

Limitations of the benchmark should be transparently discussed. For example, in [27] we used default parameters for all methods, while in [31] our datasets relied on manually gated reference cell populations as the ground truth. Without a thorough discussion of limitations, a benchmark runs the risk of misleading readers; in extreme cases, this may even harm the broader research field by guiding research efforts in the wrong directions.

9.2.8 Publication and reporting of results

The publication and reporting strategy should emphasize clarity and accessibility. Visualizations summarizing multiple performance metrics can be highly informative for method users (examples include Figure 3 in [27] and Figure 5 in [29] from our own work; as well as Figure 6 in [32]). Summary tables are also useful as a reference (e.g. [31, 45]). Additional visualizations, such as flow charts to guide the choice of method for different analyses, are a helpful way to engage the reader (e.g. Figure 5 in [27]).

For extensive benchmarks, online resources enable readers to interactively explore the results (examples from our work include [27, 31], which allow users to filter metrics and datasets). Figure 3 displays an example of an interactive website from one of our benchmarks [27], which facilitates exploration

of results and assists users with choosing a suitable method. While trade-offs should be considered in terms of the amount of work required, these efforts are likely to have significant benefit for the community.

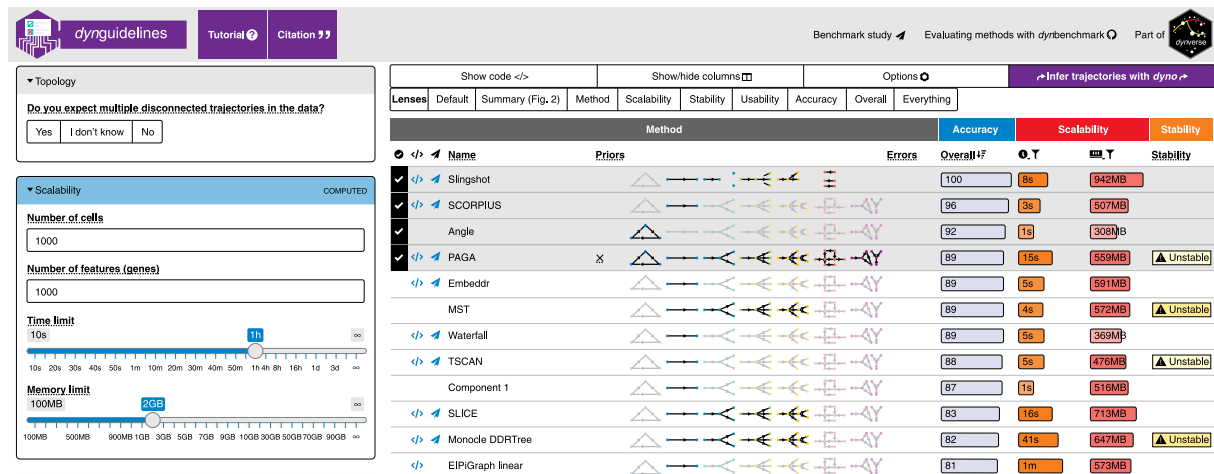


Figure 9.3: Example of an interactive website allowing users to explore the results of one of our benchmarking studies [27]. This website was created using the Shiny framework in R.

In most cases, results will be published in a peer-reviewed article. For a neutral benchmark, the benchmark will be the main focus of the paper. For a benchmark to introduce a new method, the results will form one part of the exposition. We highly recommend publishing a preprint prior to peer review (e.g. on bioRxiv or arXiv) to speed up distribution of results, broaden accessibility, and solicit additional feedback. In particular, direct consultation with method authors can generate highly useful feedback (examples from our work are described in the acknowledgements in [79, 86]). Finally, at publication time, considering open access options will further broaden accessibility.

9.2.9 Enabling future extensions

Since new methods are continually emerging [1], benchmarks can quickly become out of date. To avoid this, a truly excellent benchmark should be extensible. For example, creating public repositories containing code and data allows other researchers to build on the results to include new methods or datasets, or to try different parameter settings or pre-processing procedures (examples from our work include [27, 28, 29, 30, 31]). In addition to raw data and code, it is useful to distribute pre-processed and/or results data (examples include [28, 29, 77] from our work and [74, 87, 88] from others), especially for computationally intensive benchmarks. This may be combined with an interactive website, where users can upload results from a new method, to be included in an updated comparison either automatically or by the original authors (e.g. [35, 89, 90]). Continuous benchmarks, which are continually updated, are especially convenient (e.g. [91]), but may require significant additional effort.

9.2.10 Reproducible research best practices

Reproducibility of research findings has become an increasing concern in numerous areas of study [92]. In computational sciences, reproducibility of code and data analyses has been recognized as a useful minimum standard that enables other researchers to verify analyses [93]. Access to code and data has previously enabled method developers to uncover potential errors in published benchmarks due to suboptimal usage of methods [73, 94, 95]. Journal publication policies can play a crucial role

in encouraging authors to follow these practices [96]; experience shows that statements that code and data are available on request are often insufficient [97]. In the context of benchmarking, code and data availability also provides further benefits: for method users, code repositories serve as a source of annotated code to run methods and build analysis pipelines, while for developers, code repositories can act as a prototype for future method development work.

Parameter values (including random seeds) and software versions should be clearly reported to ensure complete reproducibility. For methods that are run using scripts, these will be recorded within the scripts. In R, the command `sessionInfo()` gives a complete summary of package versions, the version of R, and the operating system. For methods only available via graphical interfaces, parameters and versions must be recorded manually. Reproducible workflow frameworks, such as the Galaxy platform [98], can also be helpful. A summary table or spreadsheet of parameter values and software versions can be published as supplementary information along with the publication describing the benchmark (e.g. Supporting Information Table S1 in our study [31]).

Automated workflow management tools and specialized tools for organizing benchmarks provide sophisticated options for setting up benchmarks and creating a reproducible record, including software environments, package versions, and parameter values. Examples include `SummarizedBenchmark` [99], `DataPackageR` [100], `workflowr` [101], and `Dynamic Statistical Comparisons` [102]. Some tools (e.g. `workflowr`) also provide streamlined options for publishing results online. In machine learning, OpenML provides a platform to organize and share benchmarks [103]. More general tools for managing computational workflows, including `Snakemake` [104], `Make`, `Bioconda` [105], and `conda`, can be customized to capture setup information. Containerization tools such as Docker and Singularity may be used to encapsulate a software environment for each method, preserving the package version as well as dependency packages and the operating system, and facilitating distribution of methods to end users (e.g. in our study [27]). Best practices from software development are also useful, including unit testing and continuous integration.

Many free online resources are available for sharing code and data, including GitHub and Bitbucket, repositories for specific data types (e.g. `ArrayExpress` [106], the `Gene Expression Omnibus` [107], and `FlowRepository` [108]), and more general data repositories (e.g. figshare, Dryad, Zenodo, Bioconductor ExperimentHub, and Mendeley Data). Customized resources (examples from our work include [29, 77]) can be designed when additional flexibility is needed. Several repositories allow the creation of digital object identifiers (DOIs) for code or data objects. In general, preference should be given to publicly funded repositories, which provide greater guarantees for long-term archival stability [84, 85].

An extensive literature exists on best practices for reproducible computational research (e.g. [109]). Some practices (e.g. containerization) may involve significant additional work; however, in our experience, almost all efforts in this area prove useful, especially by facilitating later extensions by ourselves or other researchers.

9.3 Discussion

In this review, we have described a set of key principles for designing a high-quality computational benchmark. In our view, elements of all of these principles are essential. However, we have also emphasized that any benchmark will involve trade-offs, due to limited expertise and resources, and that some principles are less central to the evaluation. Table 9.1 provides a summary of examples of

key trade-offs and pitfalls related to benchmarking, along with our judgement of how truly essential each principle is.

Table 9.1: Summary of our views regarding how essential each principle is for a truly excellent benchmark, along with examples of key trade-offs and potential pitfalls relating to each principle. The higher the number of plus signs, the more central the principle is to the evaluation.

Principle	How essential	Trade-offs	Potential pitfalls
1. Defining the purpose and score	+++	How comprehensive the benchmark should be	Scope too broad: too much work given available resources Scope too narrow: unrepresentative and possibly misleading results
2. Selection of methods	+++	Number of methods to include	Excluding key methods
3. Selection (or design) of datasets	+++	Number and types of datasets to include	Subjectivity in the choice of datasets: e.g. selecting datasets that are unrepresentative of real-world applications Too few datasets or simulation scenarios Overly simplistic simulations
4. Parameter and software versions	++	Amount of parameter tuning	Extensive parameter tuning for some methods while using default parameters for others (e.g. competing methods)
5. Evaluation criteria: key quantitative performance metrics	+++	Number and types of performance metrics	Subjectivity in the choice of metrics: e.g. selecting metrics that do not translate to real-world performance Metrics that give over-optimistic estimates of performance Methods may not be directly comparable according to individual metrics (e.g. if methods are designed for different tasks)
6. Evaluation criteria: secondary measures	++	Number and types of performance metrics	Subjectivity of qualitative measures such as user-friendliness, installation procedures, and documentation quality Subjectivity in relative weighting between multiple metrics Measures such as runtime and scalability depend on processor speed and memory
7. Interpretation, guidelines, and recommendations	++	Generality versus specificity of recommendations	Performance differences between top-ranked methods may be minor Different readers may be interested in different aspects of performance
8. Publication and reporting of results	+	Amount of resources to dedicate to building online resources	Online resources may not be accessible (or may no longer run) several years later
9. Enabling future extensions	++	Amount of resources to dedicate to ensuring extensibility	Selection of methods or datasets for future extensions may be unrepresentative (e.g. due to requests from method authors)
10. Reproducible research best practices	++	Amount of resources to dedicate to reproducibility	Some tools may not be compatible or accessible several years later

A number of potential pitfalls may arise from benchmarking studies (Table 9.1). For example, subjectivity in the choice of datasets or evaluation metrics could bias the results. In particular, a benchmark that relies on unrepresentative data or metrics that do not translate to real-world scenarios may be misleading by showing poor performance for methods that otherwise perform well. This could harm method users, who may select an inappropriate method for their analyses, as well as method developers, who may be discouraged from pursuing promising methodological approaches. In extreme cases, this could negatively affect the research field by influencing the direction of research efforts. A thorough discussion of the limitations of a benchmark can help avoid these issues. Over the longer term, critical evaluations of published benchmarks, so-called meta-benchmarks, will also be informative [10, 13, 14].

Well-designed benchmarking studies provide highly valuable information for users and developers of computational methods, but require careful consideration of a number of important design principles.

In this review, we have discussed a series of guidelines for rigorous benchmarking design and implementation, based on our experiences in computational biology. We hope these guidelines will assist computational researchers to design high-quality, informative benchmarks, which will contribute to scientific advances through informed selection of methods by users and targeting of research efforts by developers.

9.4 References

- [1] Luke Zappia, Belinda Phipson, and Alicia Oshlack. "Exploring the Single-Cell RNA-Seq Analysis Landscape with the scRNA-Tools Database". In: *PLOS Computational Biology* 14.6 (June 2018), e1006245. issn: 1553-7358. doi: [10.1371/journal.pcbi.1006245](https://doi.org/10.1371/journal.pcbi.1006245).
- [2] Anne-Laure Boulesteix et al. "On the Necessity and Design of Studies Comparing Statistical Methods". In: *Biometrical Journal* 60.1 (2018), pp. 216–218. issn: 1521-4036. doi: [10.1002/bimj.201700129](https://doi.org/10.1002/bimj.201700129).
- [3] Anne-Laure Boulesteix, Sabine Lauer, and Manuel J. A. Eugster. "A Plea for Neutral Comparison Studies in Computational Sciences". In: *PLoS One* 8.4 (2013), e61562. issn: 1932-6203. doi: [10.1371/journal.pone.0061562](https://doi.org/10.1371/journal.pone.0061562). pmid: 23637855.
- [4] Bjoern Peters et al. "Putting Benchmarks in Their Rightful Place: The Heart of Computational Biology". In: *PLoS computational biology* 14.11 (Nov. 2018), e1006494. issn: 1553-7358. doi: [10.1371/journal.pcbi.1006494](https://doi.org/10.1371/journal.pcbi.1006494). pmid: 30408027.
- [5] Anne-Laure Boulesteix. "Ten Simple Rules for Reducing Overoptimistic Reporting in Methodological Computational Research". In: *PLOS Computational Biology* 11.4 (Apr. 2015), e1004191. issn: 1553-7358. doi: [10.1371/journal.pcbi.1004191](https://doi.org/10.1371/journal.pcbi.1004191).
- [6] Siyuan Zheng. "Benchmarking: Contexts and Details Matter". In: *Genome Biology* 18.1 (May 7, 2017), p. 129. issn: 1474-760X. doi: [10.1186/s13059-017-1258-3](https://doi.org/10.1186/s13059-017-1258-3). pmid: 28679434.
- [7] Serghei Mangul et al. "Systematic Benchmarking of Omics Computational Tools". In: *Nature Communications* 10.1 (Mar. 27, 2019), p. 1393. issn: 2041-1723. doi: [10.1038/s41467-019-09406-4](https://doi.org/10.1038/s41467-019-09406-4). pmid: 30918265.
- [8] Raquel Norel, John Jeremy Rice, and Gustavo Stolovitzky. "The Self-Assessment Trap: Can We All Be Better than Average?" In: *Molecular systems biology* 7.1 (2011), p. 537. issn: 1744-4292. doi: [10.1038/msb.2011.70](https://doi.org/10.1038/msb.2011.70). pmid: 21988833.
- [9] Mohamed Radhouene Aniba, Olivier Poch, and Julie D Thompson. "Issues in Bioinformatics Benchmarking: The Case Study of Multiple Sequence Alignment". In: *Nucleic Acids Research* 38.21 (Nov. 2010), pp. 7353–7363. issn: 0305-1048. doi: [10.1093/nar/gkq625](https://doi.org/10.1093/nar/gkq625). pmid: 20639539.
- [10] Anne-Laure Boulesteix, Rory Wilson, and Alexander Hapfelmeier. "Towards Evidence-Based Computational Statistics: Lessons from Clinical Research on the Role and Design of Real-Data Benchmark Studies". In: *BMC medical research methodology* 17.1 (Sept. 9, 2017), p. 138. issn: 1471-2288. doi: [10.1186/s12874-017-0417-2](https://doi.org/10.1186/s12874-017-0417-2). pmid: 28888225.
- [11] Anne-Laure Boulesteix et al. "A Statistical Framework for Hypothesis Testing in Real Data Comparison Studies". In: *The American Statistician* 69.3 (July 3, 2015), pp. 201–212. issn: 0003-1305. doi: [10.1080/00031305.2015.1005128](https://doi.org/10.1080/00031305.2015.1005128).
- [12] Tim P. Morris, Ian R. White, and Michael J. Crowther. "Using Simulation Studies to Evaluate Statistical Methods". In: *Statistics in Medicine* 38.11 (May 20, 2019), pp. 2074–2102. issn: 1097-0258. doi: [10.1002/sim.8086](https://doi.org/10.1002/sim.8086). pmid: 30652356.
- [13] Paul P. Gardner et al. "Identifying Accurate Metagenome and Amplicon Software via a Meta-Analysis of Sequence to Taxonomy Benchmarking Studies". In: *PeerJ* 7 (2019), e6160. issn: 2167-8359. doi: [10.7717/peerj.6160](https://doi.org/10.7717/peerj.6160). pmid: 30631651.
- [14] Paul P. Gardner et al. "A Meta-Analysis of Bioinformatics Software Benchmarks Reveals That Publication-Bias Unduly Influences Software Accuracy". In: *bioRxiv* (Jan. 2, 2017), p. 092205. doi: [10.1101/092205](https://doi.org/10.1101/092205).

- [15] Evangelos Evangelou and John P. A. Ioannidis. "Meta-Analysis Methods for Genome-Wide Association Studies and Beyond". In: *Nature Reviews. Genetics* 14.6 (June 2013), pp. 379–389. issn: 1471-0064. doi: [10.1038/nrg3472](https://doi.org/10.1038/nrg3472). pmid: [23657481](#).
- [16] Fangxin Hong and Rainer Breitling. "A Comparison of Meta-Analysis Methods for Detecting Differentially Expressed Genes in Microarray Experiments". In: *Bioinformatics (Oxford, England)* 24.3 (Feb. 1, 2008), pp. 374–382. issn: 1367-4811. doi: [10.1093/bioinformatics/btm620](https://doi.org/10.1093/bioinformatics/btm620). pmid: [18204063](#).
- [17] Paul C. Boutros et al. "Toward Better Benchmarking: Challenge-Based Methods Assessment in Cancer Genomics". In: *Genome Biology* 15.9 (Sept. 17, 2014), p. 462. issn: 1474-760X. doi: [10.1186/s13059-014-0462-7](https://doi.org/10.1186/s13059-014-0462-7). pmid: [25314947](#).
- [18] Iddo Friedberg et al. "Ten Simple Rules for a Community Computational Challenge". In: *PLoS computational biology* 11.4 (Apr. 2015), e1004150. issn: 1553-7358. doi: [10.1371/journal.pcbi.1004150](https://doi.org/10.1371/journal.pcbi.1004150). pmid: [25906249](#).
- [19] Iven Van Mechelen et al. "Benchmarking in Cluster Analysis: A White Paper". In: (Sept. 27, 2018). arXiv: [1809.10496 \[stat\]](https://arxiv.org/abs/1809.10496). url: <http://arxiv.org/abs/1809.10496> (visited on 09/19/2019).
- [20] Alexandre Angers-Loustau et al. "The Challenges of Designing a Benchmark Strategy for Bioinformatics Pipelines in the Identification of Antimicrobial Resistance Determinants Using next Generation Sequencing Technologies". In: *F1000Research* 7 (Dec. 7, 2018), p. 459. issn: 2046-1402. doi: [10.12688/f1000research.14509.2](https://doi.org/10.12688/f1000research.14509.2).
- [21] John P. A. Ioannidis. "Meta-Research: Why Research on Research Matters". In: *PLoS biology* 16.3 (Mar. 2018), e2005468. issn: 1545-7885. doi: [10.1371/journal.pbio.2005468](https://doi.org/10.1371/journal.pbio.2005468). pmid: [29534060](#).
- [22] Lukas M. Weber et al. "Diffcyt: Differential Discovery in High-Dimensional Cytometry via High-Resolution Clustering". In: *Communications Biology* 2 (2019), p. 183. issn: 2399-3642. doi: [10.1038/s42003-019-0415-5](https://doi.org/10.1038/s42003-019-0415-5). pmid: [31098416](#).
- [23] Małgorzata Nowicka and Mark D. Robinson. "DRIMSeq: A Dirichlet-Multinomial Framework for Multivariate Count Outcomes in Genomics". In: *F1000Research* 5 (2016), p. 1356. issn: 2046-1402. doi: [10.12688/f1000research.8900.2](https://doi.org/10.12688/f1000research.8900.2). pmid: [28105305](#).
- [24] Jacob H. Levine et al. "Data-Driven Phenotypic Dissection of AML Reveals Progenitor-like Cells That Correlate with Prognosis". In: *Cell* 162.1 (July 2, 2015), pp. 184–197. issn: 1097-4172. doi: [10.1016/j.cell.2015.05.047](https://doi.org/10.1016/j.cell.2015.05.047). pmid: [26095251](#).
- [25] Xiaobei Zhou, Helen Lindsay, and Mark D. Robinson. "Robustly Detecting Differential Expression in RNA Sequencing Data Using Observation Weights". In: *Nucleic Acids Research* 42.11 (June 2014), e91. issn: 1362-4962. doi: [10.1093/nar/gku310](https://doi.org/10.1093/nar/gku310). pmid: [24753412](#).
- [26] Charity W. Law et al. "Voom: Precision Weights Unlock Linear Model Analysis Tools for RNA-Seq Read Counts". In: *Genome Biology* 15.2 (Feb. 3, 2014), R29. issn: 1474-760X. doi: [10.1186/gb-2014-15-2-r29](https://doi.org/10.1186/gb-2014-15-2-r29). pmid: [24485249](#).
- [27] Wouter Saelens et al. "A Comparison of Single-Cell Trajectory Inference Methods". In: *Nature Biotechnology* 37 (May 2019). issn: 15461696. doi: [10.1038/s41587-019-0071-9](https://doi.org/10.1038/s41587-019-0071-9).
- [28] Angelo Duò, Mark D. Robinson, and Charlotte Soneson. "A Systematic Performance Evaluation of Clustering Methods for Single-Cell RNA-Seq Data". In: *F1000Research* 7 (2018), p. 1141. issn: 2046-1402. doi: [10.12688/f1000research.15666.2](https://doi.org/10.12688/f1000research.15666.2). pmid: [30271584](#).
- [29] Charlotte Soneson and Mark D. Robinson. "Bias, Robustness and Scalability in Single-Cell Differential Expression Analysis". In: *Nature Methods* 15.4 (Apr. 2018), pp. 255–261. issn: 1548-7105. doi: [10.1038/nmeth.4612](https://doi.org/10.1038/nmeth.4612). pmid: [29481549](#).

- [30] Wouter Saelens, Robrecht Cannoodt, and Yvan Saeys. "A Comprehensive Evaluation of Module Detection Methods for Gene Expression Data". In: *Nature Communications* 9.1 (Mar. 2018), p. 1090. issn: 2041-1723. doi: [10.1038/s41467-018-03424-4](https://doi.org/10.1038/s41467-018-03424-4).
- [31] Lukas M. Weber and Mark D. Robinson. "Comparison of Clustering Methods for High-Dimensional Single-Cell Flow and Mass Cytometry Data". In: *Cytometry Part A* 89.12 (2016), pp. 1084–1096. issn: 1552-4930. doi: [10.1002/cyto.a.23030](https://doi.org/10.1002/cyto.a.23030).
- [32] Keegan Korthauer et al. "A Practical Guide to Methods Controlling False Discoveries in Computational Biology". In: *Genome Biology* 20.1 (Apr. 6, 2019), p. 118. issn: 1474-760X. doi: [10.1186/s13059-019-1716-1](https://doi.org/10.1186/s13059-019-1716-1). pmid: [31164141](#).
- [33] Saskia Freytag et al. "Comparison of Clustering Tools in R for Medium-Sized 10x Genomics Single-Cell RNA-Sequencing Data". In: *F1000Research* 7 (2018), p. 1297. issn: 2046-1402. doi: [10.12688/f1000research.15809.2](https://doi.org/10.12688/f1000research.15809.2). pmid: [30228881](#).
- [34] Giacomo Baruzzo et al. "Simulation-Based Comprehensive Benchmarking of RNA-Seq Aligners". In: *Nature Methods* 14.2 (Feb. 2017), pp. 135–139. issn: 1548-7105. doi: [10.1038/nmeth.4106](https://doi.org/10.1038/nmeth.4106). pmid: [27941783](#).
- [35] Alexander Kanitz et al. "Comparative Assessment of Methods for the Computational Inference of Transcript Isoform Abundance from RNA-Seq Data". In: *Genome Biology* 16 (July 23, 2015), p. 150. issn: 1474-760X. doi: [10.1186/s13059-015-0702-5](https://doi.org/10.1186/s13059-015-0702-5). pmid: [26201343](#).
- [36] Charlotte Soneson and Mauro Delorenzi. "A Comparison of Methods for Differential Expression Analysis of RNA-Seq Data". In: *BMC bioinformatics* 14 (Mar. 9, 2013), p. 91. issn: 1471-2105. doi: [10.1186/1471-2105-14-91](https://doi.org/10.1186/1471-2105-14-91). pmid: [23497356](#).
- [37] Franck Rapaport et al. "Comprehensive Evaluation of Differential Gene Expression Analysis Methods for RNA-Seq Data". In: *Genome Biology* 14.9 (2013), R95. issn: 1474-760X. doi: [10.1186/gb-2013-14-9-r95](https://doi.org/10.1186/gb-2013-14-9-r95). pmid: [24020486](#).
- [38] Marie-Agnès Dillies et al. "A Comprehensive Evaluation of Normalization Methods for Illumina High-Throughput RNA Sequencing Data Analysis". In: *Briefings in Bioinformatics* 14.6 (Nov. 2013), pp. 671–683. issn: 1477-4054. doi: [10.1093/bib/bbs046](https://doi.org/10.1093/bib/bbs046). pmid: [22988256](#).
- [39] Daniel Sage et al. "Quantitative Evaluation of Software Packages for Single-Molecule Localization Microscopy". In: *Nature Methods* 12.8 (Aug. 2015), pp. 717–724. issn: 1548-7105. doi: [10.1038/nmeth.3442](https://doi.org/10.1038/nmeth.3442). pmid: [26076424](#).
- [40] Matthew T. Weirauch et al. "Evaluation of Methods for Modeling Transcription Factor Sequence Specificity". In: *Nature Biotechnology* 31.2 (Feb. 2013), pp. 126–134. issn: 1546-1696. doi: [10.1038/nbt.2486](https://doi.org/10.1038/nbt.2486). pmid: [23354101](#).
- [41] James C. Costello et al. "A Community Effort to Assess and Improve Drug Sensitivity Prediction Algorithms". In: *Nature Biotechnology* 32.12 (Dec. 2014), pp. 1202–1212. issn: 1546-1696. doi: [10.1038/nbt.2877](https://doi.org/10.1038/nbt.2877). pmid: [24880487](#).
- [42] Robert Küffner et al. "Crowdsourced Analysis of Clinical Trial Data to Predict Amyotrophic Lateral Sclerosis Progression". In: *Nature Biotechnology* 33.1 (Jan. 2015), pp. 51–57. issn: 1546-1696. doi: [10.1038/nbt.3051](https://doi.org/10.1038/nbt.3051). pmid: [25362243](#).
- [43] Adam D. Ewing et al. "Combining Tumor Genome Simulation with Crowdsourcing to Benchmark Somatic Single-Nucleotide-Variant Detection". In: *Nature Methods* 12.7 (July 2015), pp. 623–630. issn: 1548-7105. doi: [10.1038/nmeth.3407](https://doi.org/10.1038/nmeth.3407).
- [44] Steven M. Hill et al. "Inferring Causal Molecular Networks: Empirical Assessment through a Community-Based Effort". In: *Nature Methods* 13.4 (Apr. 2016), pp. 310–318. issn: 1548-7105. doi: [10.1038/nmeth.3773](https://doi.org/10.1038/nmeth.3773). pmid: [26901648](#).

- [45] Nima Aghaeepour et al. "Critical Assessment of Automated Flow Cytometry Data Analysis Techniques." In: *Nature methods* 10.3 (Mar. 2013), pp. 228–38. issn: 1548-7105. doi: [10.1038/nmeth.2365](https://doi.org/10.1038/nmeth.2365). pmid: [23396282](https://pubmed.ncbi.nlm.nih.gov/23396282/).
- [46] Nima Aghaeepour et al. "A Benchmark for Evaluation of Algorithms for Identification of Cellular Correlates of Clinical Outcomes". In: *Cytometry Part A* 89.1 (2016), pp. 16–21. issn: 1552-4930. doi: [10.1002/cyto.a.22732](https://doi.org/10.1002/cyto.a.22732).
- [47] John Moult et al. "Critical Assessment of Methods of Protein Structure Prediction (CASP)-Round XII". In: *Proteins* 86 Suppl 1 (Mar. 2018), pp. 7–15. issn: 1097-0134. doi: [10.1002/prot.25415](https://doi.org/10.1002/prot.25415). pmid: [29082672](https://pubmed.ncbi.nlm.nih.gov/29082672/).
- [48] John Moult et al. "Critical Assessment of Methods of Protein Structure Prediction: Progress and New Directions in Round XI". In: *Proteins* 84 Suppl 1 (Sept. 2016), pp. 4–14. issn: 1097-0134. doi: [10.1002/prot.25064](https://doi.org/10.1002/prot.25064). pmid: [27171127](https://pubmed.ncbi.nlm.nih.gov/27171127/).
- [49] Alexander Sczyrba et al. "Critical Assessment of Metagenome Interpretation-a Benchmark of Metagenomics Software". In: *Nature Methods* 14.11 (Nov. 2017), pp. 1063–1071. issn: 1548-7105. doi: [10.1038/nmeth.4458](https://doi.org/10.1038/nmeth.4458). pmid: [28967888](https://pubmed.ncbi.nlm.nih.gov/28967888/).
- [50] Dent Earl et al. "Assemblathon 1: A Competitive Assessment of de Novo Short Read Assembly Methods". In: *Genome Research* 21.12 (Dec. 2011), pp. 2224–2241. issn: 1549-5469. doi: [10.1101/gr.126599.111](https://doi.org/10.1101/gr.126599.111). pmid: [21926179](https://pubmed.ncbi.nlm.nih.gov/21926179/).
- [51] Keith R. Bradnam et al. "Assemblathon 2: Evaluating de Novo Methods of Genome Assembly in Three Vertebrate Species". In: *GigaScience* 2.1 (Dec. 1, 2013). doi: [10.1186/2047-217X-2-10](https://doi.org/10.1186/2047-217X-2-10).
- [52] MAQC Consortium et al. "The MicroArray Quality Control (MAQC) Project Shows Inter- and Intraplatform Reproducibility of Gene Expression Measurements". In: *Nature Biotechnology* 24.9 (Sept. 2006), pp. 1151–1161. issn: 1087-0156. doi: [10.1038/nbt1239](https://doi.org/10.1038/nbt1239). pmid: [16964229](https://pubmed.ncbi.nlm.nih.gov/16964229/).
- [53] Leming Shi et al. "The MicroArray Quality Control (MAQC)-II Study of Common Practices for the Development and Validation of Microarray-Based Predictive Models". In: *Nature Biotechnology* 28.8 (Aug. 2010), pp. 827–838. issn: 1546-1696. doi: [10.1038/nbt.1665](https://doi.org/10.1038/nbt.1665). pmid: [20676074](https://pubmed.ncbi.nlm.nih.gov/20676074/).
- [54] SEQC/MAQC-III Consortium. "A Comprehensive Assessment of RNA-Seq Accuracy, Reproducibility and Information Content by the Sequencing Quality Control Consortium". In: *Nature Biotechnology* 32.9 (Sept. 2014), pp. 903–914. issn: 1546-1696. doi: [10.1038/nbt.2957](https://doi.org/10.1038/nbt.2957). pmid: [25150838](https://pubmed.ncbi.nlm.nih.gov/25150838/).
- [55] Peter Krusche et al. "Best Practices for Benchmarking Germline Small-Variant Calls in Human Genomes". In: *Nature Biotechnology* 37.5 (May 2019), pp. 555–560. issn: 1546-1696. doi: [10.1038/s41587-019-0054-x](https://doi.org/10.1038/s41587-019-0054-x).
- [56] Charlotte Soneson and Mark D. Robinson. "Towards Unified Quality Verification of Synthetic Count Data with countsimQC". In: *Bioinformatics* 34.4 (Feb. 15, 2018), pp. 691–692. issn: 1367-4803. doi: [10.1093/bioinformatics/btx631](https://doi.org/10.1093/bioinformatics/btx631).
- [57] Keegan Korthauer et al. "Detection and Accurate False Discovery Rate Control of Differentially Methylated Regions from Whole Genome Bisulfite Sequencing". In: *Biostatistics (Oxford, England)* 20.3 (Jan. 7, 2019), pp. 367–383. issn: 1468-4357. doi: [10.1093/biostatistics/kxy007](https://doi.org/10.1093/biostatistics/kxy007). pmid: [29481604](https://pubmed.ncbi.nlm.nih.gov/29481604/).
- [58] Séolène Caboche et al. "Comparison of Mapping Algorithms Used in High-Throughput Sequencing: Application to Ion Torrent Data". In: *BMC genomics* 15 (Apr. 5, 2014), p. 264. issn: 1471-2164. doi: [10.1186/1471-2164-15-264](https://doi.org/10.1186/1471-2164-15-264). pmid: [24708189](https://pubmed.ncbi.nlm.nih.gov/24708189/).
- [59] Dominik G. Grimm et al. "The Evaluation of Tools Used to Predict the Impact of Missense Variants Is Hindered by Two Types of Circularity". In: *Human Mutation* 36.5 (May 2015), pp. 513–523. issn: 1059-7794. doi: [10.1002/humu.22768](https://doi.org/10.1002/humu.22768). pmid: [25684150](https://pubmed.ncbi.nlm.nih.gov/25684150/).

- [60] Monika Jelizarow et al. "Over-Optimism in Bioinformatics: An Illustration". In: *Bioinformatics* 26.16 (Aug. 2010), pp. 1990–1998. issn: 1367-4803. doi: [10.1093/bioinformatics/btq323](https://doi.org/10.1093/bioinformatics/btq323).
- [61] Lichun Jiang et al. "Synthetic Spike-in Standards for RNA-Seq Experiments". In: *Genome Research* 21.9 (Sept. 2011), pp. 1543–1551. issn: 1549-5469. doi: [10.1101/gr.121095.111](https://doi.org/10.1101/gr.121095.111). pmid: [21816910](#).
- [62] Daniel R. Garalde et al. "Highly Parallel Direct RNA Sequencing on an Array of Nanopores". In: *Nature Methods* 15.3 (Mar. 2018), pp. 201–206. issn: 1548-7105. doi: [10.1038/nmeth.4577](https://doi.org/10.1038/nmeth.4577). pmid: [29334379](#).
- [63] Fang Fang et al. "Genomic Landscape of Human Allele-Specific DNA Methylation". In: *Proceedings of the National Academy of Sciences of the United States of America* 109.19 (May 8, 2012), pp. 7332–7337. issn: 1091-6490. doi: [10.1073/pnas.1201310109](https://doi.org/10.1073/pnas.1201310109). pmid: [22523239](#).
- [64] Nicholas Schaum et al. "Single-Cell Transcriptomics of 20 Mouse Organs Creates a Tabula Muris". In: *Nature* 562.7727 (Oct. 2018), pp. 367–372. issn: 1476-4687. doi: [10.1038/s41586-018-0590-4](https://doi.org/10.1038/s41586-018-0590-4).
- [65] Grace X. Y. Zheng et al. "Massively Parallel Digital Transcriptional Profiling of Single Cells". In: *Nature Communications* 8 (Jan. 16, 2017), p. 14049. issn: 2041-1723. doi: [10.1038/ncomms14049](https://doi.org/10.1038/ncomms14049). pmid: [28091601](#).
- [66] Luyi Tian et al. "Benchmarking Single Cell RNA-Sequencing Analysis Pipelines Using Mixture Control Experiments". In: *Nature Methods* 16.6 (June 2019), pp. 479–487. issn: 1548-7105. doi: [10.1038/s41592-019-0425-8](https://doi.org/10.1038/s41592-019-0425-8). pmid: [31133762](#).
- [67] Eirini Arvaniti and Manfred Claassen. "Sensitive Detection of Rare Disease-Associated Cell Subsets via Representation Learning". In: *Nature Communications* 8.1 (Apr. 6, 2017), pp. 1–10. issn: 2041-1723. doi: [10.1038/ncomms14825](https://doi.org/10.1038/ncomms14825).
- [68] Guillem Rigaill et al. "Synthetic Data Sets for the Identification of Key Ingredients for RNA-Seq Differential Analysis". In: *Briefings in Bioinformatics* 19.1 (Jan. 1, 2018), pp. 65–76. issn: 1477-4054. doi: [10.1093/bib/bbw092](https://doi.org/10.1093/bib/bbw092). pmid: [27742662](#).
- [69] Benedikt Löwes et al. "The BRaliBase Dent-a Tale of Benchmark Design and Interpretation". In: *Briefings in Bioinformatics* 18.2 (Jan. 3, 2017), pp. 306–311. issn: 1477-4054. doi: [10.1093/bib/bbw022](https://doi.org/10.1093/bib/bbw022). pmid: [26984616](#).
- [70] Raphael Couronné, Philipp Probst, and Anne-Laure Boulesteix. "Random Forest versus Logistic Regression: A Large-Scale Benchmark Experiment". In: *BMC Bioinformatics* 19.1 (July 17, 2018), p. 270. issn: 1471-2105. doi: [10.1186/s12859-018-2264-5](https://doi.org/10.1186/s12859-018-2264-5).
- [71] Jochen Schneider et al. "Mortality Risk for Acute Cholangitis (MAC): A Risk Prediction Model for in-Hospital Mortality in Patients with Acute Cholangitis". In: *BMC gastroenterology* 16 (Feb. 9, 2016), p. 15. issn: 1471-230X. doi: [10.1186/s12876-016-0428-1](https://doi.org/10.1186/s12876-016-0428-1). pmid: [26860903](#).
- [72] Qiwen Hu and Casey S. Greene. "Parameter Tuning Is a Key Part of Dimensionality Reduction via Deep Variational Autoencoders for Single Cell RNA Transcriptomics". In: *Pacific Symposium on Biocomputing. Pacific Symposium on Biocomputing* 24 (2019), pp. 362–373. issn: 2335-6936. pmid: [30963075](#).
- [73] Jorge Vaquero-Garcia, Scott Norton, and Yoseph Barash. "LeafCutter vs. MAJIQ and Comparing Software in the Fast Moving Field of Genomics". In: *bioRxiv* (Nov. 8, 2018), p. 463927. doi: [10.1101/463927](https://doi.org/10.1101/463927).
- [74] Christian Wiwie, Jan Baumbach, and Richard Röttger. "Comparing the Performance of Biomedical Clustering Methods". In: *Nature Methods* 12.11 (Nov. 2015), pp. 1033–1038. issn: 1548-7105. doi: [10.1038/nmeth.3583](https://doi.org/10.1038/nmeth.3583). pmid: [26389570](#).

- [75] Takaya Saito and Marc Rehmsmeier. "The Precision-Recall Plot Is More Informative than the ROC Plot When Evaluating Binary Classifiers on Imbalanced Datasets". In: *PLoS One* 10.3 (2015), e0118432. issn: 1932-6203. doi: [10.1371/journal.pone.0118432](https://doi.org/10.1371/journal.pone.0118432). pmid: 25738806.
- [76] David M. W. Powers. "Visualization of Tradeoff in Evaluation: From Precision-Recall & PN to LIFT, ROC & BIRD". In: (May 3, 2015). arXiv: [1505.00401 \[cs, stat\]](https://arxiv.org/abs/1505.00401). url: <http://arxiv.org/abs/1505.00401> (visited on 09/19/2019).
- [77] Charlotte Soneson and Mark D. Robinson. "iCOBRA: Open, Reproducible, Standardized and Live Method Benchmarking". In: *Nature Methods* 13.4 (Apr. 2016), p. 283. issn: 1548-7105. doi: [10.1038/nmeth.3805](https://doi.org/10.1038/nmeth.3805). pmid: 27027585.
- [78] Charlotte Soneson, Michael I. Love, and Mark D. Robinson. "Differential Analyses for RNA-Seq: Transcript-Level Estimates Improve Gene-Level Inferences". In: *F1000Research* 4 (Feb. 29, 2016). issn: 2046-1402. doi: [10.12688/f1000research.7563.2](https://doi.org/10.12688/f1000research.7563.2). pmid: 26925227.
- [79] Stinus Lindgreen, Karen L. Adair, and Paul P. Gardner. "An Evaluation of the Accuracy and Speed of Metagenome Analysis Tools". In: *Scientific Reports* 6 (Jan. 18, 2016), p. 19233. issn: 2045-2322. doi: [10.1038/srep19233](https://doi.org/10.1038/srep19233). pmid: 26778510.
- [80] Alexey Gurevich et al. "QUAST: Quality Assessment Tool for Genome Assemblies". In: *Bioinformatics (Oxford, England)* 29.8 (Apr. 15, 2013), pp. 1072–1075. issn: 1367-4811. doi: [10.1093/bioinformatics/btt086](https://doi.org/10.1093/bioinformatics/btt086). pmid: 23422339.
- [81] Giuseppe Narzisi and Bud Mishra. "Comparing de Novo Genome Assembly: The Long and Short of It". In: *PLoS One* 6.4 (Apr. 29, 2011), e19175. issn: 1932-6203. doi: [10.1371/journal.pone.0019175](https://doi.org/10.1371/journal.pone.0019175). pmid: 21559467.
- [82] Jacob Schreiber et al. "A Pitfall for Machine Learning Methods Aiming to Predict across Cell Types". In: *bioRxiv* (Jan. 4, 2019), p. 512434. doi: [10.1101/512434](https://doi.org/10.1101/512434).
- [83] Bernd Bischl, Julia Schiffner, and Claus Weihs. "Benchmarking Local Classification Methods". In: *Computational Statistics* 28.6 (Dec. 1, 2013), pp. 2599–2619. issn: 1613-9658. doi: [10.1007/s00180-013-0420-y](https://doi.org/10.1007/s00180-013-0420-y).
- [84] Serghei Mangul et al. "Improving the Usability and Archival Stability of Bioinformatics Software". In: *Genome Biology* 20.1 (Feb. 27, 2019), p. 47. issn: 1474-760X. doi: [10.1186/s13059-019-1649-8](https://doi.org/10.1186/s13059-019-1649-8). pmid: 30813962.
- [85] Serghei Mangul et al. "Challenges and Recommendations to Improve the Installability and Archival Stability of Omics Computational Tools". In: *PLoS biology* 17.6 (June 2019), e3000333. issn: 1545-7885. doi: [10.1371/journal.pbio.3000333](https://doi.org/10.1371/journal.pbio.3000333). pmid: 31220077.
- [86] Eva K. Freyhult, Jonathan P. Bollback, and Paul P. Gardner. "Exploring Genomic Dark Matter: A Critical Assessment of the Performance of Homology Search Methods on Noncoding RNA". In: *Genome Research* 17.1 (Jan. 2007), pp. 117–125. issn: 1088-9051. doi: [10.1101/gr.5890907](https://doi.org/10.1101/gr.5890907). pmid: 17151342.
- [87] Nicholas A. Bokulich et al. "Mockrobiota: A Public Resource for Microbiome Bioinformatics Benchmarking". In: *mSystems* 1.5 (Sept. 2016). issn: 2379-5077. doi: [10.1128/mSystems.00062-16](https://doi.org/10.1128/mSystems.00062-16). pmid: 27822553.
- [88] Shane Ó Conchúir et al. "A Web Resource for Standardized Benchmark Datasets, Metrics, and Rosetta Protocols for Macromolecular Modeling and Design". In: *PLOS ONE* 10.9 (Sept. 2015), e0130433. issn: 1932-6203. doi: [10.1371/journal.pone.0130433](https://doi.org/10.1371/journal.pone.0130433).
- [89] Leslie M. Cope et al. "A Benchmark for Affymetrix GeneChip Expression Measures". In: *Bioinformatics (Oxford, England)* 20.3 (Feb. 12, 2004), pp. 323–331. issn: 1367-4803. doi: [10.1093/bioinformatics/btg410](https://doi.org/10.1093/bioinformatics/btg410). pmid: 14960458.

- [90] Rafael A. Irizarry, Zhijin Wu, and Harris A. Jaffee. "Comparison of Affymetrix GeneChip Expression Measures". In: *Bioinformatics (Oxford, England)* 22.7 (Apr. 1, 2006), pp. 789–794. issn: 1367-4803. doi: [10.1093/bioinformatics/btk046](https://doi.org/10.1093/bioinformatics/btk046). pmid: [16410320](#).
- [91] Michael Barton. *Nucleotides · Genome Assembler Benchmarking*. Oct. 2014. url: <http://nucleotid.es> (visited on 09/20/2019).
- [92] John P. A. Ioannidis. "Why Most Published Research Findings Are False". In: *PLoS medicine* 2.8 (Aug. 2005), e124. issn: 1549-1676. doi: [10.1371/journal.pmed.0020124](https://doi.org/10.1371/journal.pmed.0020124). pmid: [16060722](#).
- [93] Roger D. Peng. "Reproducible Research in Computational Science". In: *Science (New York, N.Y.)* 334.6060 (Dec. 2, 2011), pp. 1226–1227. issn: 1095-9203. doi: [10.1126/science.1213847](https://doi.org/10.1126/science.1213847). pmid: [22144613](#).
- [94] Xiaobei Zhou and Mark D. Robinson. "Do Count-Based Differential Expression Methods Perform Poorly When Genes Are Expressed in Only One Condition?" In: *Genome Biology* 16 (Oct. 8, 2015), p. 222. issn: 1474-760X. doi: [10.1186/s13059-015-0781-3](https://doi.org/10.1186/s13059-015-0781-3). pmid: [26450178](#).
- [95] Xiaobei Zhou, Alicia Oshlack, and Mark D. Robinson. "miRNA-Seq Normalization Comparisons Need Improvement". In: *RNA (New York, N.Y.)* 19.6 (June 2013), pp. 733–734. issn: 1469-9001. doi: [10.1261/rna.037895.112](https://doi.org/10.1261/rna.037895.112). pmid: [23616640](#).
- [96] Benjamin Hofner, Matthias Schmid, and Lutz Edler. "Reproducible Research in Statistics: A Review and Guidelines for the Biometrical Journal". In: *Biometrical Journal. Biometrische Zeitschrift* 58.2 (Mar. 2016), pp. 416–427. issn: 1521-4036. doi: [10.1002/bimj.201500156](https://doi.org/10.1002/bimj.201500156). pmid: [26711717](#).
- [97] Anne-Laure Boulesteix et al. "Making Complex Prediction Rules Applicable for Readers: Current Practice in Random Forest Literature and Recommendations". In: *Biometrical Journal. Biometrische Zeitschrift* 61.5 (Sept. 2019), pp. 1314–1328. issn: 1521-4036. doi: [10.1002/bimj.201700243](https://doi.org/10.1002/bimj.201700243). pmid: [30069934](#).
- [98] Enis Afgan et al. "The Galaxy Platform for Accessible, Reproducible and Collaborative Biomedical Analyses: 2018 Update". In: *Nucleic Acids Research* 46.W1 (Feb. 7, 2018), W537–W544. issn: 1362-4962. doi: [10.1093/nar/gky379](https://doi.org/10.1093/nar/gky379). pmid: [29790989](#).
- [99] Patrick K. Kimes and Alejandro Reyes. "Reproducible and Replicable Comparisons Using SummarizedBenchmark". In: *Bioinformatics (Oxford, England)* 35.1 (Jan. 1, 2019), pp. 137–139. issn: 1367-4811. doi: [10.1093/bioinformatics/bty627](https://doi.org/10.1093/bioinformatics/bty627). pmid: [30016409](#).
- [100] Greg Finak et al. "DataPackageR: Reproducible Data Preprocessing, Standardization and Sharing Using R/Bioconductor for Collaborative Data Analysis". In: *Gates Open Research* 2 (July 10, 2018), p. 31. issn: 2572-4754. doi: [10.12688/gatesopenres.12832.2](https://doi.org/10.12688/gatesopenres.12832.2). pmid: [30234197](#).
- [101] John Blischak, Peter Carbonetto, and Matthew Stephens. *Workflowr: A Framework for Reproducible and Collaborative Data Science*. R package version 1.4.0. 2019. url: <https://CRAN.R-project.org/package=workflowr>.
- [102] G Wang, Matthew Stephens, and Peter Carbonetto. *DSC: Dynamic Statistical Comparisons*. Apr. 2016. url: <https://stephenslab.github.io/dsc-wiki/index.html> (visited on 09/20/2019).
- [103] Joaquin Vanschoren et al. "OpenML: Networked Science in Machine Learning". In: *SIGKDD Explor. Newsl.* 15.2 (June 2014), pp. 49–60. issn: 1931-0145. doi: [10.1145/2641190.2641198](https://doi.org/10.1145/2641190.2641198).
- [104] Johannes Köster and Sven Rahmann. "Snakemake—a Scalable Bioinformatics Workflow Engine". In: *Bioinformatics (Oxford, England)* 28.19 (Oct. 1, 2012), pp. 2520–2522. issn: 1367-4811. doi: [10.1093/bioinformatics/bts480](https://doi.org/10.1093/bioinformatics/bts480). pmid: [22908215](#).
- [105] Björn Grüning et al. "Bioconda: Sustainable and Comprehensive Software Distribution for the Life Sciences". In: *Nature Methods* 15.7 (July 2018), pp. 475–476. issn: 1548-7105. doi: [10.1038/s41592-018-0046-7](https://doi.org/10.1038/s41592-018-0046-7). pmid: [29967506](#).

- [106] Nikolay Kolesnikov et al. "ArrayExpress Update—Simplifying Data Submissions". In: *Nucleic Acids Research* 43 (Database issue Jan. 2015), pp. D1113–1116. issn: 1362-4962. doi: [10.1093/nar/gku1057](https://doi.org/10.1093/nar/gku1057). pmid: [25361974](#).
- [107] Tanya Barrett et al. "NCBI GEO: Archive for Functional Genomics Data Sets—Update". In: *Nucleic Acids Research* 41 (Database issue Jan. 2013), pp. D991–995. issn: 1362-4962. doi: [10.1093/nar/gks1193](https://doi.org/10.1093/nar/gks1193). pmid: [23193258](#).
- [108] Josef Spidlen et al. "FlowRepository: A Resource of Annotated Flow Cytometry Datasets Associated with Peer-Reviewed Publications". In: *Cytometry Part A* 81A.9 (2012), pp. 727–731. issn: 1552-4930. doi: [10.1002/cyto.a.22106](https://doi.org/10.1002/cyto.a.22106).
- [109] Geir Kjetil Sandve et al. "Ten Simple Rules for Reproducible Computational Research". In: *PLoS computational biology* 9.10 (Oct. 2013), e1003285. issn: 1553-7358. doi: [10.1371/journal.pcbi.1003285](https://doi.org/10.1371/journal.pcbi.1003285). pmid: [24204232](#).

CHAPTER 10

Discussion

In this work, we aimed to accelerate scientific progress in the field of single-cell omics by providing and evaluating computational tools. In section 1.3 we proposed a concrete set of objectives this work will attempt to solve. Every chapter respectively tackles one of these research objectives, and each chapter discusses the implications of that part of our research in detail. This chapter reflects on the impact of this work on the field, going over each of the objectives and respective chapters.

10.1 Benchmarking with *in silico* single cells

We developed `dyngen`, a simulator of single cells to benchmark and stress-test computational tools for single-cell omics (Chapter 2). The `dyngen` software supports a selection of existing experimental protocols, and can also simulate experiments that are possible with the current technologies, such as generating omics profiles from the same cell at multiple timepoints. The generated data can help kick-start emerging domains with low data availability more safely by allowing software developers to test their method before numerous datasets become publicly available.

`dyngen` has already been successfully used to evaluate trajectory inference [1], trajectory alignment [2], and network inference [3] methods. Furthermore, we showed that it can also be used to evaluate differential network inference methods, and trajectory alignment methods.

10.2 Comparing 45 trajectory inference methods

Using this simulator and a collection of real datasets, we performed a comparison of 45 TI methods (Chapter 3). Our contributions include writing software to run 45 different error-prone TI methods with a common interface, downloading and processing hundreds of single cell datasets, and developing novel metrics for comparing ground truth and predicted trajectories. With this benchmarking study, we had two clear goals in mind: to help guide users to TI methods that are suitable for their needs, and to provide developers of TI methods with the necessary tools to benchmark their own tool.

We accomplished the first goal by constructing a set of guidelines for end-users to help choose a TI method that is accurate, robust and fit for their application. Since such guidelines were hitherto lacking, they are now commonly disseminated in manuscripts [4, 5], courses [6, 7], and slides shown during keynote caffeine refuelling sessions [8].

For our second goal, it seems too early to tell whether our research had any effect on self-assessments of TI method developers. We did make our pipeline, datasets, metrics, and containerised wrappers of TI methods publicly available for developers to use. However, so far we do not observe an increase in developers performing quantitative benchmarks. We hypothesise causal reasons for this phenomenon and provide solutions in order to spur TI developers to perform more self-assessments (Chapter 8).

10.3 A toolkit to infer, visualise and interpret single-cell trajectories

The previous two works necessitated developing a tool for visualising trajectory data. We extended this implementation into a full toolkit, named `dyno`, for inferring and analysing trajectories (Chapter 4). The toolkit allows performing downstream analyses such as detecting differentially expressed genes

along transitions in the trajectory, annotating the trajectory, and comparing multiple trajectories in a common dimensionality reduction. A major benefit of `dyno` is that it allows utilising any of the 50 TI methods we wrapped as part of the comparison, without having to install dependencies for every TI method separately.

The software packages consist of several subpackages, each with a separate functionality (e.g. `dynplot` visualises trajectories, `dynmethods` provides wrappers for the TI methods). Since most of the packages are currently only hosted on Github, only users familiar with Github have been able to use it. To make `dyno` available to a larger audience, we are publishing each of these packages and developing command-line interfaces for the most important functionalities.

10.4 Fast, accurate, and robust single-cell pseudotime

We developed a TI method, called `SCORPIUS`, specialised in inferring linear trajectories (Chapter 5). Since our comparison of TI methods already lists 30 TI methods that can infer trajectories that are more complex than a linear ordering of cells, why would we need a linear TI method?

Being able to study how cells progress over time is in terms of analysis as fundamental as being able to cluster cells or to identify differentially expressed genes between two groups. We showed that for analysing datasets containing linear trajectories, `SCORPIUS` outperforms all other TI methods tested as part of our TI benchmark.

Despite `SCORPIUS` published on bioRxiv in 2016, discussion and usage of the pre-print has largely been limited to comparing the results of a different (linear) TI methods to those of `SCORPIUS`. Since the pre-print, many improvements have been made to improve the accuracy and robustness of predicted trajectories, to allow scaling up to datasets containing 100'000s of cells, and to providing a more user-friendly interface. Since the beginning of 2019 – before the publication of our benchmark of TI methods – several studies have now reported using `SCORPIUS` as a tool for deriving primary results [9, 10, 11, 12, 13, 14].

10.5 Inferring single cell regulatory networks

We proposed a novel algorithm for inferring case-wise gene regulatory interactions. While we demonstrated the methodology by inferring 22'122 cell-specific GRNs and 14'963 sample-specific GRNs from the Tabula Muris and TCGA projects respectively, further interpretation of these results needs to be performed to further validate the usefulness of the method.

Additional avenues for exploration could involve applying trajectory inference on the case-wise regulome data, and quantitatively evaluating the performance of the algorithm using the `dyngen` simulations.

10.6 Optimising regulatory networks

This project was a spin-off of Netter [15], a tool for reranking GRN predictions using structural network properties. Predicted GRNs often are topologically dissimilar to real networks, and as such, Netter

quantifies the topological properties of a network and makes incremental changes in order to arrive at a network with a 'better' topological profile.

The topological 'profile' of a network was defined as the frequencies of particular topological patterns called 'graphlets'. Keeping track of the frequencies of graphlets during an iterative process proved difficult at first. `incgraph` provides a solution to this problem (Chapter 7) by making assuming that the incremental changes between two different networks are relatively small (less than 100 edge additions/removals). Under this assumption, it is possible to calculate the differences in topological patterns significantly faster in comparison to recomputing the graphlet frequencies from scratch at every iteration.

While `incgraph` solved a very specific and interesting problem, and was eventually published as a peer-reviewed article, it has not succeeded in making a direct impact on scientific research as of yet. Perhaps, at some point, a researcher will come across `incgraph` and find that it exactly solves his or her problem.

10.7 A life without Git, Travis CI, or tidyverse

A significant portion of this work involved developing large software libraries, in a collaborative setting, over a time span of about four years. Since the results of our comparison of 45 TI methods required three years to develop, we were happily forced to develop a system where experiments could be rerun and results could be updated on-the-fly.

We summarised our experiences in the form of a set of guidelines for benchmarking computational tools (Chapter 9). However, these guidelines do not touch upon many aspects of good software development practices that we learned to use in order to bring this thesis to a good end. In particular, I would like to highlight several fundamental (open-source) projects without the likes of which our research would have been simply impossible to perform, namely Git, Travis CI, and the tidyverse.

Git [16] is a code-revision system that allows multiple users to collaborate on developing code and keep track of what changes were made by whom. Since Wouter Saelens and I were often working closely together on a specific part of our software, Git saved us a lot of time by merging together changes developed in parallel. Only in few cases did we need to intervene manually to merge our changes. Additionally, Github.com allowed us not only to collaborate with each-other, but also correspond and collaborate with other software developers from many different research groups, using Github Issues to discuss problems with other researchers, and Github Pull Requests to contribute code to open-source projects.

Together, we published over 20'000 code contributions (commits) across 50+ software packages [17]. Since many of these packages depend on one another, it is inevitable that changes made to one package would break another package. We wrote many, many unit tests (and still too few), and we let these tests automatically be executed on **Travis CI** [18]. This way, when we pushed breaking changes to Github, Travis CI would notify that our commit has resulted in one or more unit tests failing. While sometimes it is a hassle to set up, Travis CI has prevented us countless times from generating faulty results due to a faulty underlying function.

Software bugs can be introduced even by incredibly small, seemingly insignificant changes. The R programming language seems particularly susceptible towards getting trapped by its many pitfalls. However, there are many benefits of using R in bioinformatics research context, such as its extensive

community of statisticians develop packages for the R ecosystem. The **tidyverse** packages [19], developed by the RStudio team and many online contributors, completely transformed my experiences with R from tedious struggles to efficient everyday functional programming.

Honourable mentions go to Linux, Fedora, L^AT_EX, TeXstudio, (R)Markdown, Bash, Sed, Regular expressions, Rocket Chat, for making bioinformatics software development even more fun and enjoyable.

10.8 References

- 10
- [1] Wouter Saelens et al. "A Comparison of Single-Cell Trajectory Inference Methods". In: *Nature Biotechnology* 37 (May 2019). issn: 15461696. doi: [10.1038/s41587-019-0071-9](https://doi.org/10.1038/s41587-019-0071-9).
 - [2] Koen Van den Berge et al. "Trajectory-Based Differential Expression Analysis for Single-Cell Sequencing Data". In: *bioRxiv* (Jan. 1, 2019), p. 623397. doi: [10.1101/623397](https://doi.org/10.1101/623397).
 - [3] Aditya Pratapa et al. "Benchmarking Algorithms for Gene Regulatory Network Inference from Single-Cell Transcriptomic Data". In: *bioRxiv* (June 4, 2019), p. 642926. doi: [10.1101/642926](https://doi.org/10.1101/642926).
 - [4] Atefeh Lafzi et al. "Tutorial: Guidelines for the Experimental Design of Single-Cell RNA Sequencing Studies". In: *Nature Protocols* 13.12 (Dec. 1, 2018), pp. 2742–2757. issn: 1750-2799. doi: [10.1038/s41596-018-0073-y](https://doi.org/10.1038/s41596-018-0073-y).
 - [5] Malte D Luecken and Fabian J Theis. "Current Best Practices in Single-Cell RNA-Seq Analysis: A Tutorial". In: *Molecular Systems Biology* 15.6 (June 1, 2019), e8746. issn: 1744-4292. doi: [10.1525/msb.20188746](https://doi.org/10.1525/msb.20188746).
 - [6] Vladimir Kiselev et al. "Analysis of Single Cell RNA-Seq Data" (Cambridge, UK). May 2, 2019. url: <https://scrnaseq-course.cog.sanger.ac.uk/website/index.html> (visited on 08/22/2019).
 - [7] Liesbet Martens and Niels Vandamme. "Analysis of Single Cell RNA-Seq Data from 10x Genomics" (Ghent). Aug. 29, 2019. url: <https://training.vib.be/analysis-single-cell-rna-seq-data-10x-genomics> (visited on 08/22/2019).
 - [8] Coffee Break during "Analysis of Single Cell RNA-Seq Data 23-24 May 2019" Workshop. In collab. with Vladimir Kiselev. May 23, 2019. url: https://www.youtube.com/watch?v=7dQ_pleDO2Y&t=1h53m14s.
 - [9] Nicolas Damond et al. "A Map of Human Type 1 Diabetes Progression by Imaging Mass Cytometry". In: *Cell Metabolism* 29.3 (Mar. 5, 2019), 755–768.e5. issn: 1550-4131. doi: [10.1016/j.cmet.2018.11.014](https://doi.org/10.1016/j.cmet.2018.11.014).
 - [10] Yang Cheng et al. "Multifactorial Heterogeneity of Virus-Specific T Cells and Association with the Progression of Human Chronic Hepatitis B Infection". In: *Science Immunology* 4.32 (Feb. 8, 2019), eaau6905. issn: 2470-9468. doi: [10.1126/sciimmunol.aau6905](https://doi.org/10.1126/sciimmunol.aau6905). pmid: [30737354](#).
 - [11] Christopher Andrew Tibbitt et al. "Single-Cell RNA Sequencing of the T Helper Cell Response to House Dust Mites Defines a Distinct Gene Expression Signature in Airway Th2 Cells". In: *Immunity* 51.1 (July 16, 2019), 169–184.e5. issn: 1074-7613. doi: [10.1016/j.immuni.2019.05.014](https://doi.org/10.1016/j.immuni.2019.05.014).
 - [12] Hannah Van Hove et al. "A Single-Cell Atlas of Mouse Brain Macrophages Reveals Unique Transcriptional Identities Shaped by Ontogeny and Tissue Environment". In: *Nature Neuroscience* 22.6 (June 2019), pp. 1021–1035. issn: 1546-1726. doi: [10.1038/s41593-019-0393-4](https://doi.org/10.1038/s41593-019-0393-4).
 - [13] Jasper Wouters et al. "Single-Cell Gene Regulatory Network Analysis Reveals New Melanoma Cell States and Transition Trajectories during Phenotype Switching". In: *bioRxiv* (Jan. 1, 2019), p. 715995. doi: [10.1101/715995](https://doi.org/10.1101/715995).
 - [14] Johan Reimegård et al. "Combined mRNA and Protein Single Cell Analysis in a Dynamic Cellular System Using SPARC". In: *bioRxiv* (Jan. 1, 2019), p. 749473. doi: [10.1101/749473](https://doi.org/10.1101/749473).
 - [15] Joeri Ruyssinck et al. "Netter: Re-Ranking Gene Network Inference Predictions Using Structural Network Properties." In: *BMC Bioinformatics* 17.1 (2016), p. 76. issn: 1471-2105. doi: [10.1186/s12859-016-0913-0](https://doi.org/10.1186/s12859-016-0913-0). pmid: [26862054](#).
 - [16] Linus Torvalds and Junio Hamano. *Git: Fast Version Control System*. 2005. url: <http://git-scm.com>.

- [17] *The Development of Dynverse*. Apr. 1, 2019. url: <https://www.youtube.com/watch?v=C42F5Y8kCU0> (visited on 10/14/2019).
- [18] GmbH Travis CI. *Travis CI - Test and Deploy Your Code with Confidence*. 2011. url: <https://travis-ci.org> (visited on 10/14/2019).
- [19] Hadley Wickham. *The Tidy Tools Manifesto*. Nov. 13, 2017. url: <https://cran.r-project.org/web/packages/tidyverse/vignettes/manifesto.html> (visited on 10/14/2019).

APPENDIX A

Curriculum Vitae

A.1 Personalia

Name Robrecht Cannoodt
Date of Birth January 25th, 1990
Place of birth Ghent
Nationality Belgian
Address Kerkstraat 75, 9070 Destelbergen
Email robrecht.cannoodt@gmail.com

A.2 Professional Experience

Ph.D. student in Bioinformatics

Ghent University, Belgium, September 2013 – now

Laboratory assistant (summer job)

Bloedtransfusiecentrum Gent, Belgium, July (2009 – 2012)

A.3 Education

Master of Science in Computer Science Engineering: Software Engineering

Ghent University, Belgium, 2011 – 2013

Bachelors degree in Informatics

Ghent University, Belgium, 2008 – 2011

Bachelors degree in Engineering: Architecture

Ghent University, Belgium, 2007 – 2008

International Baccalaureate

A

International School of Berne, Switzerland, 2002 – 2007

A.4 First-author publications

- **Cannoodt R**, Saelens W, Sichien D, Tavernier S, Janssens S, Guilliams M, Lambrecht B, De Preter K, Saeys Y. SCORPIUS improves trajectory inference and identifies novel modules in dendritic cell development. *bioRxiv* 079509. 2016 Oct.
- **Cannoodt R** *, Saelens W *, Saeys Y. Computational methods for trajectory inference from single-cell transcriptomics. *European journal of immunology*. 2016 Nov;46(11):2496-506.
- **Cannoodt R**, Ruyssinck J, Ramon J, De Preter K, Saeys Y. IncGraph: Incremental graphlet counting for topology optimisation. *PloS one*. 2018 Apr 26;13(4):e0195997.
- Saelens W *, **Cannoodt R** *, Todorov H, Saeys Y. A comparison of single-cell trajectory inference methods. *Nature biotechnology*. 2019 May;37(5):547.

*: Equal contribution.

A.5 Co-author publications

- Decock A, Ongenaert M, **Cannoodt R**, Verniers K, De Wilde B, Laureys G, Van Roy N, Berbegall AP, Bienertova-Vasku J, Bown N, Clément N. Methyl-CpG-binding domain sequencing reveals a prognostic methylation signature in neuroblastoma. *Oncotarget*. 2016 Jan 12;7(2):1960.
- Van Cauwenbergh C, Van Schil K, **Cannoodt R**, Bauwens M, Van Laethem T, De Jaegere S, Steyaert W, Sante T, Menten B, Leroy BP, Coppieters F. arrEYE: a customized platform for high-resolution copy number analysis of coding and noncoding regions of known and candidate retinal dystrophy genes and retinal noncoding RNAs. *Genetics in Medicine*. 2017 Apr;19(4):457.
- Claeys S, Denecker G, **Cannoodt R**, Kumps C, Durinck K, Speleman F, De Preter K. Early and late effects of pharmacological ALK inhibition on the neuroblastoma transcriptome. *Oncotarget*. 2017 Dec 5;8(63):106820.
- Depuydt P, Boeva V, Hocking TD, **Cannoodt R**, Ambros IM, Ambros PF, Asgharzadeh S, Attiyeh EF, Combaret V, Defferrari R, Fischer M. Genomic amplifications and distal 6q loss: novel markers for poor survival in high-risk neuroblastoma patients. *JNCI: Journal of the National Cancer Institute*. 2018 Mar 5;110(10):1084-93.
- Scott CL, T'Jonck W, ..., **Cannoodt R**, Saelens W ..., Guilliams M. The transcription factor ZEB2 is required to maintain the tissue-specific identities of macrophages. *Immunity*. 2018 Aug 21;49(2):312-25.
- Saelens W, **Cannoodt R**, Saeys Y. A comprehensive evaluation of module detection methods for gene expression data. *Nature communications*. 2018 Mar 15;9(1):1090.
- Todorov H, **Cannoodt R**, Saelens W, Saeys Y. Network Inference from Single-Cell Transcriptomic Data. In *Gene Regulatory Networks* 2019 (pp. 235-249). Humana Press, New York, NY..

- Van den Berge K, De Bezieux HR, Street K, Saelens W, **Cannoodt R**, Saeys Y, Dudoit S, Clement L. Trajectory-based differential expression analysis for single-cell sequencing data. *BioRxiv*. 2019 Jan 1:623397.
- Weber LM, Saelens W, **Cannoodt R**, Soneson C, Hafelmeier A, Gardner PP, Boulesteix AL, Saeys Y, Robinson MD. Essential guidelines for computational method benchmarking. *Genome biology*. 2019 Dec;20(1):125.
- Lorenzi L, ..., **Cannoodt R**, ..., Mestdagh P. The RNA-Atlas, a single nucleotide resolution map of the human transcriptome. In preparation.
- Van den Berge K, Roux de Bézieux H, Street K, Saelens W, **Cannoodt R**, Saeys Y, Dudoit S. Trajectory-based differential expression analysis. Submitted to *Nature Communications*.
- Van de Sande B, ..., **Cannoodt R**, ..., Saeys Y, Aerts S. A scalable SCENIC workflow for single-cell gene regulatory network analysis. Submitted to *Nature Protocols*.

A.6 Open-source software

As part of this work, many open-source software packages were created and many others were contributed to (Table A.1).

Packages that were created as part of this work are hosted on Github under the username `rcannoodt`¹ or the `dynverse` organisation². As part of our standard development practices, we automate execution of unit tests and write extensive documentation to ensure the code complies with CRAN policy before submission. We aim to submit all other packages to CRAN as well.

We also helped maintain or extend other packages on Github, CRAN or Bioconductor on which our software depends. This includes speeding up parts of the dependency (`slingshot`), adding new functionality (`devtools`, `ParamHelpers`), fixing bugs (`proxyC`, `rlang`, `monocle`, `splatter`, `slingshot`), becoming a maintainer of orphaned packages (`diffusionMap`, `princurve`, `GillespieSSA`), and extending the documentation (`devtools`, `mlr`, `remotes`). Several of these package receive millions of downloads per year (`devtools`, `remotes`, `rlang`).

A.7 Sources of funding

This study was supported by the Fonds Wetenschappelijk Onderzoek (11Y6218N).

¹<https://github.com/rcannoodt?tab=repositories>

²<https://github.com/dynverse?tab=repositories>

Table A.1: Contributions to open-source software. Following abbreviations denote the relation with respect to the package: *aut* Author, *ctb* Contributor. Yearly download statistics are based on the number of downloads between 2019-08-01 and 2019-10-14. CRAN download statistics are retrieved from the Rstudio CRAN mirror only; other CRAN mirrors do not track download statistics. In addition, many of the dynverse packages have only recently been published on CRAN. For Github repositories, no download statistics could be retrieved.

Name	Role	Host	Downloads per year	Description
babelwhale	aut	CRAN	5810	Interacting with Docker and Singularity containers
diffusionMap	aut	CRAN	30'450	Implements diffusion map method of data parameterization
dynbenchmark	aut	Github		Pipeline for benchmarking trajectory inference methods
dyndimred	aut	CRAN	5535	Applying dimensionality reduction methods
dyneval	aut	Github		Evaluating trajectory inference methods
dynfeature	aut	Github		Calculating feature importance scores from trajectories
dyngen	aut	Github		Simulating single-cell data using gene regulatory networks
dynguidelines	aut	Github		User guidelines for trajectory inference
dynmethods	aut	Github		A collection of wrappers for trajectory inference methods
dyno	aut	Github		A pipeline for inferring, visualising and interpreting trajectories
dynparam	aut	CRAN	3265	Creating meta-information for parameters
dynplot	aut	Github		A simple visualisation library for trajectories
dynplot2	aut	Github		A fully customisable visualisation library for trajectories
dyntoy	aut	Github		Generating simple toy data of cellular differentiation
dynutils	aut	CRAN	13'130	Common functionality for the dynverse packages
dynwrap	aut	CRAN	990	A common format for trajectories
GillespieSSA	aut	CRAN	7880	Gillespie's Stochastic Simulation Algorithm (SSA)
GillespieSSA2	aut	CRAN	4950	Gillespie's Stochastic Simulation Algorithm for Impatient People
gng	aut	Github		Growing Neural Gas implemented in Rcpp
incgraph	aut	CRAN	3565	Incremental graphlet counting for network optimisation
lmds	aut	CRAN	815	Landmark Multi-Dimensional Scaling
princurve	aut	CRAN	29'100	Fits a principal curve in arbitrary dimension
proxyC	aut	CRAN	117'480	Computes proximity in large sparse matrices
qsub	aut	CRAN	3585	Running commands remotely on gridengine clusters
SCORPIUS	aut	CRAN	4520	Inferring developmental chronologies from single-cell RNA sequencing data
badger	ctb	CRAN	6240	Query information and generate badge for using in README
ClusterSignificance	ctb	Bioc	935	Assess if class clusters in dimensionality reduced data representations have a separation different from permuted data
devtools	ctb	CRAN	5'918'700	Tools to make developing R packages easier
merlot	ctb	Github		Reconstructing lineage-tree topologies from scRNA-seq data
mlr	ctb	CRAN	176'330	Machine Learning in R
monocle	ctb	Bioc	34'360	Clustering, differential expression, and trajectory analysis for single-cell RNA-Seq
ParamHelpers	ctb	CRAN	150'775	Helpers for Parameters in Black-Box Optimization, Tuning and Machine Learning
pseudogp	ctb	Github		Probabilistic pseudotime for single-cell RNA-seq
ranger	ctb	CRAN	413'641	A Fast Implementation of Random Forests
Rdimtools	ctb	CRAN	7367	Dimension Reduction and Estimation Methods
remotes	ctb	CRAN	3'944'090	R package installation from remote repositories
rlang	ctb	CRAN	13'269'115	Functions for base types and core R and tidyverse features
SCope	ctb	Github		Visualization of high dimensional single cell data
slingshot	ctb	Bioc	12'085	Tools for ordering single-cell sequencing
splatter	ctb	Bioc	5015	Simple simulation of single-cell RNA sequencing data
URD	ctb	Github		Reconstructing branching trajectories from single-cell RNAseq data
wishbone	ctb	Github		Identify bifurcating developmental trajectories from single-cell data

Acknowledgements
